



EX LIBRIS
UNIVERSITATIS
ALBERTENSIS

The Bruce Peel
Special Collections
Library



Digitized by the Internet Archive
in 2025 with funding from
University of Alberta Library

<https://archive.org/details/0163020055782>

UNIVERSITY OF ALBERTA

Library Release Form

Name of Author: Errol Savio D'Souza
Title of Thesis: Evaluation of the Ultrasonic Technique to Measure
Liquid Penetration in Paper
Degree: Master of Science
Year this Degree Granted: 2003

Permission is hereby granted to the University of Alberta Library to reproduce single copies of this thesis and to lend or sell such copies for private, scholarly or scientific research purposes only.

The author reserves all other publication and other rights in association with the copyright in the thesis, and except as herein before provided, neither the thesis nor any substantial portion thereof may be printed or otherwise reproduced in any material form whatever without the author's prior written permission.

UNIVERSITY OF ALBERTA

Evaluation of the Ultrasonic Technique
to
Measure Liquid Penetration in Paper

by

Errol Savio D'Souza



A thesis submitted to the Faculty of Graduate Studies and Research in partial

fulfillment of the requirements for the degree of

Master of Science

in

Chemical Engineering

Department of Chemical and Materials Engineering

Edmonton, Alberta

Spring, 2003

UNIVERSITY OF ALBERTA

FACULTY OF GRADUATE STUDIES AND RESEARCH

The undersigned certify that they have read, and recommend to the Faculty of Graduate Studies and Research for acceptance, a thesis entitled **Evaluation of the Ultrasonic Technique to Measure Liquid Penetration in Paper** by **Errol Savio D'Souza** in partial fulfillment of the requirements for the degree of **Master of Science in Chemical Engineering**.

ABSTRACT

The objective of this study was to develop a more fundamental understanding of the ultrasonic method for measuring the dynamics of liquid penetration in paper. Several geometrically well-defined rigid porous structures were tested by using probe liquids of varying surface tension. These model structures were also characterised in terms of pore size, porosity, permeability and contact angles. Typical commercial paper grades were tested using swelling and non-swelling probe liquids. The paper grades were characterised using a capillary flow porometer. Results obtained from the ultrasonic method were compared with fundamental capillary penetration theory and other measured characteristics of the different pore structures and paper grades.

The investigations gave good insight into the use of the ultrasonic method and some of its limitations. The parameters tB and $L\%$ from the instrument showed some interesting trends with respect to permeability, pore volume and mean flow pore diameter.

ACKNOWLEDGEMENTS

I would like to take this opportunity to express my sincere gratitude to those involved in making this research study a valuable learning experience for me.

Dr. R. E. Hayes

My MSc Program supervisor, for constant advice and guidance and giving me the opportunity to pursue a graduate degree in Canada.

Dr. J. F. Oliver, Senior Research Scientist, Pulp and Paper, Alberta Research Council:

My MSc research co-supervisor, for ongoing guidance and numerous insightful discussions into liquid-paper interactions during the course of this research project

Frank Tosto, Joyce Chen, Deb Henry - Pulp and Paper Dept, Alberta Research Council

For help in testing of paper physical properties and image analysis work.

Dr. P. Sarkar, Senior Research Scientist, Advanced Ceramics, Alberta Research Council:

For allowing the use of the PMI Capillary Flow Porometer.

Lorne Johanson, Florin Esanu - Advanced Ceramics Dept., Alberta Research Council

For useful inputs in the operation of the PMI Capillary Flow Porometer

Dr. J Masliyah and Dr. Z. Xu

For allowing the use of the Kruss Drop Shape Analysis System and the goniometer

George Braybrook and Don Resultay - Earth and Atmospheric Sciences Dept., University of Alberta

For help in the SEM work.

Richard Cooper, Instrument Technician, Dept of Chemical Engineering

For help with viscosity measurements using the Canon-Fenske viscometer

Financial support received from Natural Sciences and Engineering Research Council of Canada, Alberta Research Council and the Captain Thomas Farrell Greenhalgh Award is also greatly acknowledged.

TABLE OF CONTENTS

List of Tables

List of Figures

Nomenclature

1.0	Introduction	1
1.1	Present Scenario in the Canadian Paper Industry	1
1.2	Significance of the phenomenon of liquid penetration in paper	3
1.3	Research Objectives and Motivation	4
1.4	Research Approach	6
1.5	Thesis Outline	7
2.0	Literature Review	9
3.0	The Ultrasonic Dynamic Liquid Penetration Measurement Method	31
3.1	Brief Overview of Sound Theory	31
3.2	Principle of Operation	34
3.3	Construction and Working	35
3.4	Outputs from the Instrument	38
3.5	Other Aspects	45
4.0	Experimental Work	53
4.1	Model Pore Structures	53
4.2	Commercial Printing Paper Grades and Glass-fibre paper	76
4.3	Pore Structure Characterization	86
4.3.1	Permeability measurements using Variable Head Permeameter	86
4.3.2	Capillary Flow Porometry	94
4.3.3	Thickness Measurements	109
4.3.4	Porosity Measurements	111

4.4	Contact Angle Measurements	113
4.5	Dynamics of Liquid Penetration using Emco DPM -30	124
5.0	Analysis and Discussion	164
5.1	Model Pore Structures	164
5.2	Commercial Paper Grades and Glass-fibre paper	182
6.0	Conclusions and Future Work	186
6.1	Summary and Conclusions	186
6.2	Future Work	190
	References	192
	Appendices	
A	Emco DPM-30 Specifications	201
B	PEG solution viscosity measurements	204
C	Raw data from variable head permeameter experiments	206
D	PMI Capillary flow porometer specifications	218
E	Raw data from contact angle measurements	219
F	Emco - DPM 30 detailed measurement data	229

LIST OF TABLES

Table 2.1:	Brief Chronological Summary of Literature on the use of the Ultrasonic Method	27
Table 4.1	Nuclepore® Membrane Characteristics	60
Table 4.2	Nuclepore® Membrane Specifications	60
Table 4.3	Micro-etch® screen characteristics	74
Table 4.4	Micro-mesh® precision sieve characteristics	75
Table 4.5	Permeability Calculations - Nuclepore® Membranes	92
Table 4.6	Permeability Calculations - Voith Spectra Meshes	93
Table 4.7	Permeability Calculations - Voith Woven Fabrics	93
Table 4.8	Comparison of Characterization Techniques	100
Table 4.9	Summary of Results - Capillary Flow Porometry	103
Table 4.10	PMI - Capillary flow porometry tests with commercial paper grades	105
Table 4.11	Thickness Measurements of various porous samples based on automatic caliper instrument	109
Table 4.12	Porosity - Nuclepore® Membranes	112
Table 4.13	Porosity - Voith Spectra Structures	112
Table 4.14	Porosity - Voith Woven Fabrics	112
Table 4.15	Properties of aq. methanol solutions at 20 °C (CRC Handbook, 1988-89)	113
Table 4.16	Mean Contact Angle Values	116
Table 4.17	Summary of Characterization - Model Pore Structures	122
Table 4.18	Summary of Characterization - Commercial Paper Grades	123
Table 4.19	Test Procedure Summary	125
Table 4.20	Summary - Emco Software generated output parameters for average curves	158
Table 4.21	Summary - Emco output parameters for average curves (corrected)	159

Table 4.22	Summary of error calculations for Emco average results	160
	(a) Nuclepore® Membranes	160
	(b) Spectra Meshes	161
	(c) Voith Fabrics	162
	(d) Commercial Paper Grades	163
Table B.1:	Viscosity measurements for 25% Aq. PEG 35000	204
Table C.1:	Permeameter Experimental Data - Nuclepore Membranes	206
	a) 12 Micron	206
	b) 8 Micron	206
	c) 5 Micron	206
	d) 2 Micron	207
Table C.2:	Permeameter Experimental Data - Voith Spectra Meshes	208
	a) Spectra Q	208
	b) Spectra T	208
	c) Spectra F	208
Table C.3:	Permeameter Experimental Data - Voith Woven Fabrics	209
	a) Voith 1	209
	b) Voith 2	209
	c) Voith 3	209
	d) Voith 4	210
	e) Voith 5	210
	f) Voith 6	210
	g) Voith 7	211
Table E.1:	Contact Angle Measurements-Non-porous Polycarbonate (PC) Membrane	219

	(a) PC-Water	219
	(b) PC-6% Methanol	219
	(c) PC-20% Methanol	219
	(d) PC-40% Methanol	219
	(e) PC-70% Methanol	219
	(f) PC-100% Methanol	219
Table E.2:	Contact angle measurements - Polyvinylpyrrolidone (PVP) coating on a non-porous PC membrane	220
	(a) PVP-Water	220
	(b) PVP-6% Methanol	220
	(c) PVP-20% Methanol	220
	(d) PVP-40% Methanol	220
Table E.3:	Contact Angle Measurements - Nuclepore® 2 micron membrane	221
	(a) Nuclepore 2 μm -Water	221
	(b) Nuclepore 2 μm -6% Methanol	221
	(c) Nuclepore 2 μm -20% Methanol	221
	(d) Nuclepore 2 μm -40% Methanol	221
Table E.4:	Contact Angle Measurements - Nuclepore® 5 micron membrane	222
	(a) Nuclepore 5 μm - Water	222
	(b) Nuclepore 5 μm - 6% Methanol	222
	(c) Nuclepore 5 μm - 20% Methanol	222
	(d) Nuclepore 5 μm - 40% Methanol	222
	(e) Nuclepore 5 μm - 70% Methanol	222
	(f) Nuclepore 5 μm - 100% Methanol	222

Table E. 5:	Contact Angle Measurements - Nuclepore® 8 micron membrane	223
	(a) Nuclepore 8 μm - Water	223
	(b) Nuclepore 8 μm - 6% Methanol	223
	(c) Nuclepore 8 μm - 20% Methanol	223
	(d) Nuclepore 8 μm - 40% Methanol	223
	(e) Nuclepore 8 μm - 70% Methanol	223
	(f) Nuclepore 8 μm - 100% Methanol	223
Table E.6:	Contact Angle Measurements - Nuclepore® 12 micron membrane	224
	(a) Nuclepore 12 μm - Water	224
	(b) Nuclepore 12 μm - 6% Methanol	224
	(c) Nuclepore 12 μm - 20% Methanol	224
	(d) Nuclepore 12 μm - 40% Methanol	224
	(e) Nuclepore 12 μm - 70% Methanol	224
	(f) Nuclepore 12 μm - 100% Methanol	224
Table E.7:	Contact Angle Measurements - Spectra F Mesh	225
	(a) Voith - Spectra F - Water	225
	(b) Voith - Spectra F - 6% Methanol	225
	(c) Voith - Spectra F - 20% Methanol	225
	(d) Voith - Spectra F - 40% Methanol	225
	(e) Voith - Spectra F - 70% Methanol	225
	(f) Voith - Spectra F - 100% Methanol	225
Table E.8:	Contact Angle Measurements - Spectra Q Mesh	226
	(a) Voith - Spectra Q - Water	226
	(b) Voith - Spectra Q - 6% Methanol	226
	(c) Voith - Spectra Q - 20% Methanol	226
	(d) Voith - Spectra Q - 40% Methanol	226

Table E.9:	Contact Angle Measurements - Spectra T Mesh	227
	(a) Voith - Spectra T - Water	227
	(b) Voith - Spectra T - 6% Methanol	227
	(c) Voith - Spectra T - 20% Methanol	227
	(d) Voith - Spectra T - 40% Methanol	227
	(e) Voith - Spectra T - 70% Methanol	227
Table E.10:	Contact angle measurements using manual goniometer with water	228

LIST OF FIGURES

Figure 1.1:	Ink Jet Grade Office Paper (Weyerhaeuser First Choice)- Surface View	8
Figure 1.2:	Cross-Sectional view of a 100% Thermo-Mechanical Pulp Commercial Paper	8
Figure 2.1:	Cobb Test Apparatus	13
Figure 2.2:	Stöckigt Test Sample ("Boat")	13
Figure 2.3:	Bristow Test Principle	14
Figure 2.4:	Bristow 'ideal' absorption curves	15
Figure 2.5:	Schematic Diagram of Ultrasonic attenuation measurement apparatus (Pan, 1985)	17
Figure 2.6:	Schematic Diagram of the apparatus for the ultrasonic measurement of liquid penetration into paper (Pan, 1988)	18
Figure 2.7:	Master Curve of the time dependence of acoustic attenuation (Pan, 1988)	18
Figure 3.1:	Incident, reflected and refracted sound waves	33
Figure 3.2:	Ultrasonic Method Principle of Operation	35
Figure 3.3:	Construction of Emco-DPM 30	35
Figure 3.4:	Schematic Representation of the attenuation before start of penetration (cross-sectional view)	36
Figure 3.5:	Phases of sample immersion	38
Figure 3.6:	Typical output curves for some commercial grade paper samples	38
Figure 3.7:	Emco DPM-30 Measured Parameters	40
Figure 3.8:	Ultrasound transmission in a paper sample during water penetration	44
Figure 3.9:	Absolute Graphs - Different Liquids in Measuring Cell	46

Insert, 1 MHz frequency

Figure 3.10:	Absolute Graphs - Different Materials in Water, 1 MHz frequency	47
Figure 3.11:	Absolute graphs - Same paper grade with different sample holder material and sensor areas, Test liquid - H ₂ O, 2 MHz frequency	47
Figure 3.12:	Standardized graph for Figure 3.10	48
Figure 3.13:	Standardized graph for Figure 3.11	49
Figure 3.14:	Theoretical measuring area and actual measuring area showing 'dark-spots' caused by air bubbles	50
Figure 3.15:	Absolute Graph showing effect of air bubbles on the measurement	50
Figure 3.16:	Standardized Graph (on Maximum) for Figure 3.15	51
Figure 4.1:	Surface View of a 12 micron Nuclepore® Membrane	55
Figure 4.2:	Surface View of a 12 micron Nuclepore® Membrane (Glossy-side)	55
Figure 4.3:	Surface View of a 12 micron Nuclepore® Membrane (Matte-side)	56
Figure 4.4:	Pore detail - 12 micron Nuclepore® membrane (Glossy side)	56
Figure 4.5:	Pore detail - 12 micron Nuclepore® membrane (Matte side)	57
Figure 4.6:	Cross Sectional view of a 12 micron Nuclepore® Membrane	57
Figure 4.7:	Cross Sectional view of an 8 micron Nuclepore® Membrane	58
Figure 4.8:	Cross Sectional view of a 5 micron Nuclepore® Membrane	58
Figure 4.9:	Cross Sectional view of a 2 micron Nuclepore® Membrane	59
Figure 4.10:	(a) Surface View of Voith Spectra Q - Side1	62
	(b) Surface View of Voith Spectra Q - Side 2	62
Figure 4.11:	(a) Surface View of Voith Spectra T - Side1	63
	(b) Surface View of Voith Spectra T - Side2	63
Figure 4.12:	(a) Surface View of Voith Spectra F - Side1	64
	(b) Surface View of Voith Spectra F - Side2	64

Figure 4.13:	(a) Surface View of Voith 1 Fabric - Side 1	66
	(b) Surface View of Voith 1 Fabric - Side 2	66
Figure 4.14:	(a) Surface View of Voith 2 Fabric - Side 1	67
	(b) Surface View of Voith 2 Fabric - Side 2	67
Figure 4.15:	(a) Surface View of Voith 3 Fabric - Side 1	68
	(b) Surface View of Voith 3 Fabric - Side 2	68
Figure 4.16:	(a) Surface View of Voith 4 Fabric - Side 1	69
	(b) Surface View of Voith 4 Fabric - Side 2	69
Figure 4.17:	(a) Surface View of Voith 5 Fabric - Side 1	70
	(b) Surface View of Voith 5 Fabric - Side 2	70
Figure 4.18:	(a) Surface View of Voith 6 Fabric - Side 1	71
	(b) Surface View of Voith 6 Fabric - Side 2	71
Figure 4.19:	(a) Surface View of Voith 7 Fabric - Side 1	72
	(b) Surface View of Voith 7 Fabric - Side 2	72
Figure 4.20:	Surface view of Micro-Etch® screen	73
Figure 4.21:	Surface view of Micro-mesh® precision sieve	74
Figure 4.22:	Commercial Weyerhaeuser First Choice (WFC) 'plain' ink jet grade	77
Figure 4.23:	Commercial Hammermill (H) xerographic color printer grade	78
Figure 4.24:	Commercial Champion 'plain' ink jet (CIJ) grade	79
Figure 4.25:	Commercial Alberta Newsprint Company - Offset newsprint grade (ANC-Off)	80
Figure 4.26:	Commercial Alberta Newsprint Company - Rotogravure newsprint grade (ANC-Roto)	81
Figure 4.27:	Whatman® Glass Fibre Filter Paper Grade- GF/A	82
Figure 4.28:	Whatman® Glass Fibre Filter Paper Grade - GF/B	83
Figure 4.29:	Whatman® Glass Fibre Filter Paper Grade - GF/F	84
Figure 4.30:	Whatman® Phase Separation Filter Paper Grade - 1PS	85
Figure 4.31:	Variable Head Permeameter	88
Figure 4.32	Flow Porometry Operation Principle	95

Figure 4.33:	Pore Size Definition	96
Figure 4.34:	Measured Pore Diameter in Porometry	96
Figure 4.35:	Bubble Point Pressure and Mean Flow Pressure	98
Figure 4.36:	Envelope Surface Area and Total Surface Area	99
Figure 4.37:	Pore Size Distributions for Nuclepore® Membranes	104
Figure 4.38:	Nuclepore® Membranes - Differential Pressure vs. Air flow rate	105
Figure 4.39:	Pore Size Distributions for Commercial Paper Grades	106
Figure 4.40:	Pore Size Distributions for Voith Fabrics	107
Figure 4.41:	Commercial Paper Grades - Differential Pressure vs. Air flow rate	108
Figure 4.42:	Voith Fabrics - Differential Pressure vs. Air flow rate	108
Figure 4.43:	Drop Shape Analysis System	113
Figure 4.44:	Contact Angle Measurements - Smooth non-porous polycarbonate Membrane	117
Figure 4.45:	Contact Angle Measurements - Polyvinylpyrrolidone coating on solid polycarbonate membrane	117
Figure 4.46:	Contact Angle Measurements - Nuclepore® 2 micron membrane	118
Figure 4.47:	Contact Angle Measurements - Nuclepore® 5 micron membrane	118
Figure 4.48:	Contact Angle Measurements - Nuclepore® 8 micron membrane	119
Figure 4.49:	Contact Angle Measurements - Nuclepore® 12micron membrane	119
Figure 4.50:	Contact Angle Measurements - Voith Spectra F Mesh	120
Figure 4.51:	Contact Angle Measurements - Voith - Spectra Q Mesh	120
Figure 4.52:	Contact Angle Measurements - Voith - Spectra T Mesh	121
Figure 4.53:	Nuclepore® 2 micron - 'Untreated' PC membrane with different probe liquids	128

Figure 4.54:	Nuclepore® 2 micron - 'Methanol Treated' PC membrane with different probe liquids	128
Figure 4.55:	(a) Nuclepore® 12 micron - different probe liquids (long time regime)	129
	(b) Nuclepore® 12 micron - different probe liquids (intermediate time regime)	129
	(c) Nuclepore® 12 micron - different probe liquids (short time regime)	130
Figure 4.56:	(a) Nuclepore® 8 micron - different probe liquids (long time regime)	130
	(b) Nuclepore® 8 micron - different probe liquids (intermediate time regime)	131
	(c) Nuclepore® 8 micron - different probe liquids (short time regime)	131
Figure 4.57:	(a) Nuclepore® 5 micron - different probe liquids (long time regime)	132
	(b) Nuclepore® 5 micron - different probe liquids (intermediate time regime)	132
	(c) Nuclepore® 5 micron - different probe liquids (short time regime)	133
Figure 4.58:	(a) Nuclepore® 2 micron - different probe liquids (long time regime)	133
	(b) Nuclepore® 2 micron - different probe liquids (intermediate time regime)	134
	(c) Nuclepore® 2 micron - different probe liquids (short time regime)	134
Figure 4.59:	Different Nuclepore® Membranes - Distilled Water	135
Figure 4.60:	Different Nuclepore® Membranes - 6% Methanol	135
Figure 4.61:	Different Nuclepore® Membranes - 20% Methanol	136
Figure 4.62:	Different Nuclepore® Membranes - 40% Methanol	136
Figure 4.63:	Different Nuclepore® Membranes - 70% Methanol	137

Figure 4.64:	Different Nuclepore® Membranes - 100% Methanol	137
Figure 4.65:	Spectra F - Different Probe Liquids	139
Figure 4.66:	(a) Spectra Q - Different Probe Liquids (Long Time Regime)	139
	(b) Spectra Q - Different Probe Liquids (Short Time Regime)	140
Figure 4.67:	(a) Spectra T - Different Probe Liquids (Long Time Regime)	140
	(b) Spectra T - Different Probe Liquids (Short Time Regime)	141
Figure 4.68:	Different Spectra Meshes - Distilled Water	141
Figure 4.69:	Different Spectra Meshes - 6% methanol solution	142
Figure 4.70:	Different Spectra Meshes - 20% methanol solution	142
Figure 4.71:	Different Spectra Meshes - 40% methanol solution	143
Figure 4.72:	Different Spectra Meshes - 70% methanol solution	143
Figure 4.73:	Different Spectra Meshes - 100% methanol solution	144
Figure 4.74:	Different Spectra Meshes - Distilled water (penetration from both sides of sample)	144
Figure 4.75:	(a) Voith Woven Fabrics - Penetration with water from both sides(Long time regime)	146
	(b) Voith Woven Fabrics - Penetration with water from both sides (Short time regime)	146
Figure 4.76:	(a) Voith Woven Fabrics - Penetration with water from one side (Long time regime)	147
	(b) Voith Woven Fabrics - Penetration with water from one side (Short time regime)	147
Figure 4.77:	Voith Woven Fabrics - Penetration with water from one side (Comparison of Side 1 with Side 2)	148
Figure 4.78:	Micro-Etch® screen samples 6-4-4 and 8-6-2 - Results with penetration of water from one side and both sides	150
Figure 4.79:	Micro-Etch® screen samples 6-4-4 and 8-6-2 - Results with penetration of 6%wt methanol solution from one side	150
Figure 4.80:	Micro-mesh® sieve sample 150 lpi - Results with penetration of water from one side	151

Figure 4.81:	(a) Penetration Dynamics - Different Paper Grades With Water (Short Time Regime)	154
	(b) Penetration Dynamics - Different Paper Grades With Water (Long Time Regime)	154
Figure 4.82:	Penetration Dynamics - Different Paper Grades With Polydimethylsiloxane (Dow Corning 200 ® Fluid)	155
Figure 4.83:	(a) Penetration Dynamics - Glass Fibre Paper With Water	155
	(b) - Penetration Dynamics - Glass Fibre Paper With Water	156
Figure 4.84:	Penetration Dynamics - Glass Fibre Paper With Polydimethylsiloxane (Dow Corning 200 ® Fluid)	156
Figure 5.1:	Dynamics of penetration in Nuclepore® 12 micron based on Lucas-Washburn equation (calculations based on γ, r, θ, μ)	165
Figure 5.2:	Dynamics of penetration in Nuclepore® 12 micron based on Lucas-Washburn equation (calculations based on $\gamma, K, \epsilon, \theta, \mu$)	165
Figure 5.3:	Dynamics of penetration in Spectra Meshes based on Lucas-Washburn equation (calculations based on γ, r, θ, μ)	167
Figure 5.4:	Dynamics of penetration in Spectra Meshes based on Lucas-Washburn equation (calculations based on $\gamma, K, \epsilon, \theta, \mu$)	167
Figure 5.5:	Comparison of Emco parameters 'tB' and 'L%' for Nuclepore® Membranes	171
Figure 5.6:	Nuclepore® Membranes - Porosity and Permeability	171
Figure 5.7:	Nuclepore® Membranes - Derived Characteristics	172
Figure 5.8:	Nuclepore® Membranes - Emco parameters 'tB' and 'L%' for different probe liquids	173
Figure 5.9:	Nuclepore® Membranes - Comparison of Emco parameters with penetration coefficient	175
Figure 5.10:	Comparison of Emco parameters 'tB' and 'L%' for Spectra Meshes	177

Figure 5.11:	Spectra Meshes - Porosity and Permeability	178
Figure 5.12:	Spectra Meshes Derived Characteristics	178
Figure 5.13:	Spectra Meshes - Emco parameters 'tB' and '%L' for different probe liquids	179
Figure 5.14:	Emco parameters 'tB' and 'L%' for Voith Fabrics	181
Figure 5.15:	Voith Fabrics - Other characteristics	182
Figure 5.16:	Emco Parameters for Commercial Paper Grades - Tests with PDMS	183
Figure 5.17:	Emco Parameters for Commercial Paper Grades - Tests with Water	183
Figure 5.18:	Other Measured Characteristics of Commercial Paper grades	184
Figure A.1:	Type 4 Sample Holder	202
Figure A.2:	Type 7 Sample Holder	203
Figure B.1:	Viscosity Plot for 25% Aq. PEG 35000	205
Figure C.1:	Permeameter Experimental Data - Nuclepore Membranes	212
	a) 12 Micron	212
	b) 8 Micron	212
	c) 5 Micron	212
	d) 2 Micron	213
Figure C.2:	Permeameter Experimental Data - Voith Spectra Meshes	214
	a) Spectra Q	214
	b) Spectra T	214
	c) Spectra F	214
Figure C.3:	Permeameter Experimental Data - Voith Woven Fabrics	215
	a) Voith 1	215
	b) Voith 2	215
	c) Voith 3	215

d) Voith 4	216
e) Voith 5	216
f) Voith 6	216
g) Voith 7	217

Figure E.1: Contact angle measurements using manual goniometer with water	228
---	-----

Emco Experimental Data

Figure F.1: Nuclepore® 12 micron - water	229
Figure F.2: Nuclepore® 12 micron - 6% methanol	229
Figure F.3: Nuclepore® 12 micron - 20% methanol	230
Figure F.4: Nuclepore® 12 micron - 40% methanol	230
Figure F.5: Nuclepore® 12 micron - 70% methanol	231
Figure F.6: Nuclepore® 12 micron - 100% methanol	231
Figure F.7: Nuclepore® 8 micron - Water	232
Figure F.8: Nuclepore® 8 micron - 6% methanol	232
Figure F.9: Nuclepore® 8 micron - 20% methanol	233
Figure F.10: Nuclepore® 8 micron - 40% methanol	233
Figure F.11: Nuclepore® 8 micron - 70% methanol	234
Figure F.12: Nuclepore® 8 micron - 100% methanol	234
Figure F.13: Nuclepore® 5 micron - water	235
Figure F.14: Nuclepore® 5 micron - 6% methanol	235
Figure F.15: Nuclepore® 5 micron - 20% methanol	236
Figure F.16: Nuclepore® 5 micron - 40% methanol	236
Figure F.17: Nuclepore® 5 micron - 70% methanol	237
Figure F.18: Nuclepore® 5 micron - 100% methanol	237
Figure F.19: Nuclepore® 2 micron - Water	238
Figure F.20: Nuclepore® 2 micron - 6% methanol	238
Figure F.21: Nuclepore® 2 micron - 20% methanol	239

Figure F.22:	Nuclepore® 2 micron -40% methanol	239
Figure F.23:	Nuclepore® 2 micron - 70% methanol	240
Figure F.24:	Nuclepore® 2 micron - 100% methanol	240
Figure F.25:	Spectra F - Water	241
Figure F.26:	Spectra F - 6% methanol	241
Figure F.27:	Spectra F -20% methanol	242
Figure F.28:	Spectra F - 40% methanol	242
Figure F.29:	Spectra F - 70% methanol	243
Figure F.30:	Spectra F -100% methanol	243
Figure F.31:	Spectra Q - Water	244
Figure F.32:	Spectra Q - 6% methanol	244
Figure F.33:	Spectra Q - 20% methanol	245
Figure F.34:	Spectra Q - 40% methanol	245
Figure F.35:	Spectra Q - 70% methanol	246
Figure F.36:	Spectra Q - 100% methanol	246
Figure F.37:	Spectra T - Water	247
Figure F.38:	Spectra T - 6% methanol	247
Figure F.39:	Spectra T - 20% methanol	248
Figure F.40:	Spectra T -40% methanol	248
Figure F.41:	Spectra T -70% methanol	249
Figure F.42:	Spectra T - 100% methanol	249
Figure F.43:	Voith 1 - 2 sides – water (long time)	250
Figure F.44:	Voith 1 - 2 sides – water (short time)	250
Figure F.45:	Voith 1 - 1 side – water (long time)	251
Figure F.46:	Voith 1 - 1 side - water (short time)	251
Figure F.47:	Voith 2 - 2 sides – water (long time)	252
Figure F.48:	Voith 2 - 2 sides – water (short time)	252
Figure F.49:	Voith 2 –1, 1 side – water (long time)	253
Figure F.50:	Voith 2 –1, 1 side – water (short time)	253
Figure F.51:	Voith 2 –2, 1 side – water (long time)	254
Figure F.52:	Voith 2 –2, 1 side – water (short time)	254

Figure F.53:	Voith 3 - 2 sides – water (long time)	255
Figure F.54:	Voith 3 - 2 sides – water (short time)	255
Figure F.55:	Voith 3 - 1 side – water (long time)	256
Figure F.56:	Voith 3 – 1 side – water (short time)	256
Figure F.57:	Voith 3 – 2 sides – water (long time)	257
Figure F.58:	Voith 3 - 2 sides – water (short time)	257
Figure F.59:	Voith 4 –2 sides-water(long time)	258
Figure F.60:	Voith 4 – 2 sides – water (short time)	258
Figure F.61:	Voith 4 – 1 side – water (long time)	259
Figure F.62:	Voith 5 –2 sides – water(long time)	259
Figure F.63:	Voith 5 – 2 sides – water (short time)	260
Figure F.64:	Voith 5 – 1 side-water (long time)	260
Figure F.65:	Voith 5 – 1 side – water (short time)	261
Figure F.66:	Voith 6 – 2 sides – water (long time)	261
Figure F.67:	Voith 6 – 2 sides – water (short time)	262
Figure F.68:	Voith 6 – 1 side –water (long time)	262
Figure F.69:	Voith 6 – 1 side – water (short time)	263
Figure F.70:	Voith 7 -2 sides –water (long time)	263
Figure F.71:	Voith 7 - 2 sides – water (short time)	264
Figure F.72:	Voith 7 –1, 1 side –water (long time)	264
Figure F.73:	Voith 7 –1, 1 side – water (short time)	265
Figure F.74:	Voith 7 –2, 1 side – water (long time)	265
Figure F.75:	Voith 7 –2, 1 side – water (short time)	266
Figure F.76:	Voith 1 – 2 sides - methanol	266
Figure F.77:	Buckbee Mears 6-4-4 - water (liquid penetration from both sides)	267
Figure F.78:	Buckbee Mears 6-4-4 - water (liquid penetration from one side)	267
Figure F.79:	Buckbee Mears 8-6-2 - water (liquid penetration from one sides)	268
Figure F.80:	Buckbee Mears 8-6-2 - water (liquid penetration from both	268

sides)

Figure F.81:	Alberta Newsprint Company Offset Grade - Water	269
Figure F.82:	Alberta Newsprint Company Offset Grade - PDMS	269
Figure F.83:	Alberta Newsprint Company Roto Grade - Water	270
Figure F.84:	Alberta Newsprint Company Roto Grade - PDMS	270
Figure F.85:	Champion Ink Jet - Water	271
Figure F.86:	Champion Ink Jet - PDMS	271
Figure F.87:	Hammermill Color - Water	272
Figure F.88:	Hammermill Color - PDMS	272
Figure F.89:	Weyerhaeuser First Choice - Water	273
Figure F.90:	Weyerhaeuser First Choice - PDMS	273
Figure F.91:	Glass Fibre Paper (GF/A) - Water	274
Figure F.92:	Glass Fibre Paper (GF/A) - PDMS	274
Figure F.93:	Glass Fibre Paper (GF/B) - Water	275
Figure F.94:	Glass Fibre Paper (GF/B) - PDMS	275
Figure F.95:	Glass Fibre Paper (GF/F) - Water	276
Figure F.96:	Glass Fibre Paper (GF/F) - PDMS	276
Figure F.97:	Phase Separation Filter (1PS) - Water	277
Figure F.98:	Phase Separation Filter (1PS) - PDMS	277

NOMENCLATURE

\overline{E}	= Energy per unit volume, J/m ³
ΔP	= Driving pressure, N/m ²
(S)	= Stockigt sizing degree
A	= Amplitude, m
E	= Bulk Modulus of Elasticity, N/m ²
B	= Length of slot in Bristow test apparatus, m
C	= Concentration of diffusing liquid, mole/m ³
c	= Wave velocity, m/s
C_p	= Gas specific heat capacity at constant pressure, J/kg-K
C_v	= Gas specific heat capacity at constant volume, J/kg-K
D	= Diffusion coefficient, m ² /s
f	= Wave frequency, Hz
F	= Fraction of the amount of penetrant taken up in time 't' relative to the amount taken up in infinite time
h	= Distance travelled by the penetrating liquid or depth of penetration, m
I	= Sound Intensity, W/m ²
K	= Permeability in the direction of flow, m ² or Darcies
K_a	= Absorption coefficient obtained from Bristow test, ml/m ² s ^{1/2}
K_r	= Roughness index obtained from Bristow test, ml/m ²
K_u	= Maximum rate of increase of attenuation in curve from Ultrasonic Wettability Tester
L	= Length of trace produced in Bristow test, m
$L\%$	= Difference between initial transmission and maximum transmission (Emco parameter)
M	= Amount of penetrant, kg
P	= Acoustic Pressure, N/m ²
r	= Capillary radius, m or microns

R	= Intensity Reflection Coefficient
Re	= Reynold's Number
S	= Maximum negative gradient (Emco parameter)
T	= Intensity Transmission Coefficient
t	= Time, s
t_B	= Time at maximum transmission (Emco parameter)
t_u	= Minimum value of attenuation in curve from Ultrasonic Wettability Tester
t_w	= Wetting time obtained from Bristow test, s
V	= Liquid volume, m ³ or ml
Y	= Young's Modulus of Elasticity, N/m ²
Z	= Acoustic impedance, kg/m ² -s

Greek Symbols

ω	= Angular frequency, Hz
α	= Attenuation coefficient
θ	= Contact Angle, degree
ρ	= Density, kg/m ³
η	= Effective system viscosity (related to shear modulus of system), Pa-s
μ	= Liquid viscosity, Pa-s
ε	= Porosity, %
γ	= Surface Tension, N/m
λ	= Wavelength, m
θ_i	= Angle of incidence, degree
θ_r	= Angle of reflection, degree
θ_t	= Angle of transmission, degree

Abbreviations

%Tr	= % Transmission
-----	------------------

AKD	= Alkyl Ketene Dimer
ANC	= Alberta Newsprint Company
CIJ	= Champion Ink Jet
$D_{\max \text{ PSD}}$	= Diameter at maximum pore size distribution
$D_{\text{bubble pt}}$	= Bubble point pore diameter
$D_{\text{mean flow}}$	= Mean flow pore diameter
D_{\min}	= Smallest detected pore diameter
DPM	= Dynamic Penetration Meter
H	= Hammermill
IGT	= Institute for Graphic Technology
JIS	= Japanese Industrial Standard
LWC	= Light Weight Coated
MSP	= Metered Size Press
PC	= Polycarbonate
PDA	= Penetration Dynamics Analyzer
PDMS	= Polydimethylsiloxane
PEG	= Polyethylene glycol
PET	= Polyester Terephthalate
PMI	= Porous Material Inc.
PVP	= Polyvinylpyrrolidone
RH	= Relative humidity
SC	= Super Calendered
TAPPI	= Technical Association of Pulp and Paper Industry
UWT	= Ultrasonic Wettability Tester
WFC	= Weyerhaeuser First Choice

1.0 Introduction

1.1 *Present Scenario in the Canadian and World Paper Industry*

In spite of predictions for the paperless office, demand for paper as a communications medium continues its relentless growth in the 21st century. World demand for paper has doubled in the past 20 years and is predicted to double again by the year 2010 (www.cppa.org/english/future.htm). The annual consumption growth over the next 15 years for paper and board is projected at 2.5 % for developed countries, 5.5 % for developing countries and 3.2 % for the world overall. Shifts in the patterns of paper consumption are however expected. For example, it is expected that the demand for printing paper and value-added papers will increase while the demand for cheaper lower grades will decrease.

It is anticipated that in developing countries, demand for paper products will continue to increase owing to growing literacy rates, population increases and a rising standard of living. In developed countries, the continuing need for a "hard copy" is an indication of a growing demand for paper even as information technology becomes more significant in this century. Indeed, contrary to what was predicted, increase in the use of the Internet has caused an increase in the demand for products being ordered on line such as office printing paper as well as paperboard and speciality packaging grades.

Over 200 million personal printers have been purchased in the past three years. Sales of ink-jet speciality printers designed to print digital photographs, is expected to jump from 2.1 million in 1999 to 6.3 million units in 2003. These are strong indications of the growing demand for speciality paper for a variety of printing applications (CPPA, 2000)

Canada has the world's most competitive paper products industry in terms of exports market, followed by the United States and Scandinavian countries. The

US is the world's highest per capita consumer and the largest importer of paper products, with Canada supplying 75% of US imports of pulp, paper and allied products. The Canadian Pulp and Paper Association annual review for the year 2000 indicates an increase of 2.1 % in overall shipments. The increase in shipments of printing and writing paper was 11.4 % and that of newsprint was 1.2 %. Over the last decade, Canada has doubled its capacity for making value-added printing and writing papers to serve the growing world markets.

Light weight coated (LWC) papers are being viewed as a significant player for meeting the increasing requirements of printing papers for different applications. LWC papers can be broadly referred to as coated groundwood papers that typically contain at least 10 % mechanical pulp. The coating weight for these LWC coated papers is typically 30% of total sheet weight. Demand for LWC paper end-use sectors in North America is dominated by magazines (55%) and catalogues (30%), followed by coupons (7%). Consumption for magazines is expected to hold through to 2010, while that for catalogues is expected to decrease slowly (Habermehl, 1999).

European paper producers have specialised in those grades of coated papers which use a high proportion of mechanical fibre and/or minerals for filling and coating. The European paper industry has become the largest producer and exporter of coated (and uncoated) paper for colour printing with Asia as its largest export region, and the USA its largest single country for exports. The US currently imports around 1.4 million metric tonnes of coated paper, mostly coated mechanical paper, with Canada as the largest source of supply, but with Europe increasing in importance. The European, North American and Japanese markets however are approaching maturity and the real rapid and dynamic growth in coated paper consumption is expected to take place in the developing regions of the world, particularly in Asia and Latin America (Clark, 1999)

Super Calendered (SC) papers are a major competitor to the LWC market. Recent gap former technology in the wet end of the papermaking process has greatly eliminated the "two-sidedness" of paper and resulted in the new SC quality. The debate between SC and LWC papers centres mainly around quality and cost. LWC has advantages of print gloss, stiffness, bulk, opacity, and printability for both offset and rotogravure presses, while SC has advantages of brightness and gloss similar to that of LWC but at a lower price. As manufacturers of both types of paper vie for the market share, the final choice will depend on the consumer.

1.2 *Significance of the phenomenon of liquid penetration in paper*

Liquid absorption properties are an important characteristic of paper. Different grades of paper require various levels of absorptive properties ranging from very absorbent to water resistant depending on the final application. For example:

- Aqueous inks are often used on ink jet and writing papers and for acceptable print quality the paper must have a certain degree of resistance to penetration by water.
- Milk and juice cartons need to be highly water-resistant whereas paper towels, diapers etc need to be highly absorbent.

Of particular importance is the growth and relevance of digital printing papers due to the increased use of personal computers and printers. Liquid absorption represents a critical property in the performance of many printing papers. For ink jet paper grades, the rate of ink absorption into the bulk structure governs surface ink holdout, which in turn affects print quality, ink drying and paper dimensional stability (Oliver 1990).

Penetration is also very significant in the paper coating process. A coating solution essentially consists of an aqueous solution of pigment, binder and other additives. The function of the binder is to hold the coating pigments together after

drying of the coating layer and also to bind the pigments to the basepaper. Excessive transfer of the binder to the basepaper may give weaker coatings and increase the adhesive demand. More significantly, the migration of binder within the coating will affect the coating structure and in adverse situations, cause starvation of adhesive, which results in local weak spots in the coating layer. Aside from altering the coating solution composition, the principal way to control water drainage from the coating is by adjusting the properties of the base sheet. From an industrial production point of view, the Metered size press (MSP) is growing in importance for use in on-line coating, due to good runnability during the coating sequence. In this process the base sheet properties are important for ensuring good print quality.

Rapid improvements in printing and imaging technologies are continuously increasing the demands on print quality performance. Papermakers are constantly faced with challenges of designing paper grades to meet end user requirements. Despite significant improvements in printing paper grades over the past decade, much remains to be learnt and understood in order to develop the right basesheet structure for the desired print quality performance.

1.3 Research Objectives

Characterization methods of the paper basesheet are important for understanding paper-liquid interactions and can help in demarcating subtle differences between key surface and bulk properties of paper (Oliver 2001). Thus, they are an important step in the process of designing a paper grade for a particular application. A recently developed method for characterizing the dynamics of liquid penetration into paper is the ultrasonic-based method.

The main advantage of this method in comparison to older more conventional methods is that the dynamics of penetration can be tracked in real time, using an ultrasonic beam with time resolution in the millisecond range. The test method is simple, quick, less labour intensive and the results obtained are

very reproducible as compared to other test methods such as the Bristow (1967) sizing method and Cobb (1990) test.

However, most of the work reported in literature involving the use of the ultrasonic liquid penetration is of "qualitative" nature. The test method has been applied as a quality control tool for differentiating "good" or "bad" papers. Depending on the grade of paper, the absorption profiles often show several transition regimes and at best serve only as a qualitative guideline for characterising the paper. Correlation of some of the parameters obtained from the method with other test methods has been attempted, but the results have been quite inconclusive. Since the ultrasound method is based on a principle that has not been previously used to measure the penetration of liquids into surfaces, the scientific understanding of its results is still in its infancy.

Moreover, it would be more useful to explore the potential of the ultrasonic method as a "quantitative", rather than a qualitative type of instrument. Comparison of the instrument outputs from the method with fundamental theory of capillary penetration of liquids into porous media, including paper would help in improved prediction of liquid-paper interactions and ultimately the print quality capabilities of the paper. Such a test method that can help to understand the absorption and wetting on paper surfaces would be an invaluable tool to assist papermakers in manufacturing a base paper, which will meet final product performance requirements.

The specific objectives of this thesis are:

- To develop a more fundamental understanding of the ultrasonic test method for measurement of the dynamics of penetration of liquid into a porous substrate/paper.
- To compare the outputs from the method with basic capillary penetration theory applied to porous media/paper and assess the potential of the method as a "quantitative" tool.

1.4 Research Approach

Paper is a network of cellulose fibres forming a complex pore structure. For example, Figure 1.1 shows a top view of an inkjet grade office paper and Figure 1.2 shows a cross-sectional view of a 100% thermo-mechanical pulp newspaper. The complexity of the pore structure of paper can easily be perceived from these images. Cellulose fibres also have the tendency to swell when contacted with polar liquids such as water. This further complicates the phenomenon of liquid penetration into paper.

The approach used in this study to assess the potential of the ultrasonic test method consisted of the following steps

- Identification of several mathematically well defined pore structures of varying porosity, pore size and thickness.
- Testing of the latter model pore structures using suitable probe liquids or penetrants with a range of different surface tensions and viscosities.
- Testing of a variety of commercial paper grades with different pore structures and rigid fibre structures similar to paper (such as glass fibre filter paper) with swelling and non-swelling probe liquids.
- Porosity and permeability measurements for the model pore structures as an independent method of characterization.
- Capillary flow porometry measurements for the various commercial paper grades.
- Analysis and comparison of the results from the ultrasonic test method with capillary penetration theory, porosity, permeability and porometry data.

The information and results obtained from the above approach were used to evaluate the potential of the ultrasonic method for quantitative characterization of liquid penetration dynamics in paper.

1.5 Thesis Outline

The thesis is structured so that the reader can first obtain a good insight into the phenomena of liquid penetration into paper. This area is outlined in Chapter 2 and includes previously completed research work, various applications and available test methods. A detailed description of the set up and principles of the ultrasonic test method follows this section in Chapter 3. Next follows the various experiments conducted with well-characterized model pore structures and commercial paper grades, in Chapter 4. The analysis of these results and relationship with fundamental theory is given in Chapter 5. A summary of the important findings and avenues for further work is given in Chapter 6.

Figure 1.1: Ink Jet Grade Office Paper (Weyerhaeuser First Choice) - Surface view

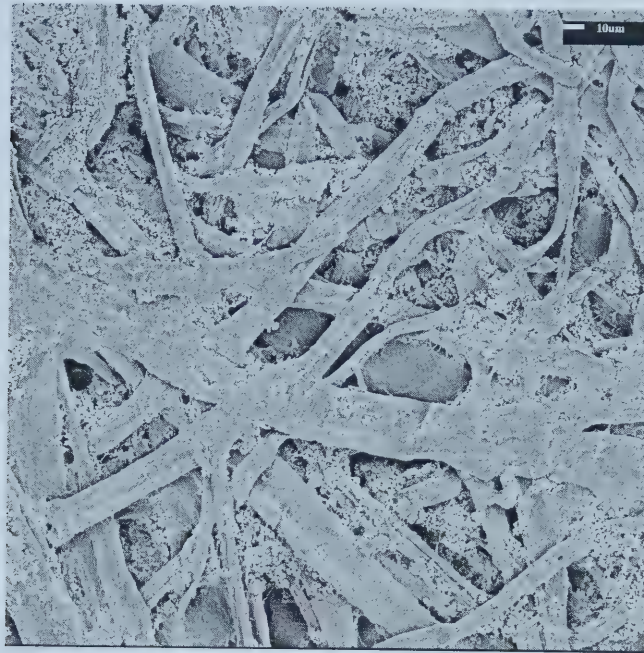


Figure 1.2: Cross-Sectional view of a 100% Thermo-Mechanical Pulp Commercial Paper



→ Cross Direction
(Perpendicular to Machine Direction)

100 μm

2.0 Literature Review

Penetration of liquids into paper

Penetration of liquids into paper has been a topic of much research for the past 30 years. As discussed in the previous chapter, the market driven demand for speciality grade papers has increased the need for a more fundamental understanding of liquid-paper interactions. Penetration of liquids into paper is a complex phenomenon mainly due to the complex random network of fibres in paper and a pore structure that is difficult to characterise. A further complexity is created if the penetrating liquid is aqueous. Cellulose fibres have a high affinity for water and penetration of an aqueous liquid into paper results in swelling of the fibres and modification of the original pore structure. Currently, there are two fundamental approaches for treating penetration of liquids in paper

- 1) Lucas-Washburn Kinetics
- 2) Fickian Diffusion

The Lucas-Washburn equation was developed independently by Lucas (1918) and Washburn (1921) and is the simplest equation to model the rate of capillary penetration into a porous material. It is derived from the Poiseuille equation for laminar flow of a Newtonian liquid through capillaries of circular cross-section by considering that the driving force for flow is the capillary pressure given by the Young-Laplace equation.

The Poiseuille equation can be written as

$$\frac{dh}{dt} = \frac{r^2 \Delta P}{8\mu h} \quad (2.1)$$

where h = distance travelled by the liquid or depth of penetration

r = capillary radius

μ = liquid viscosity

ΔP = differential pressure

The driving pressure from the Young-Laplace equation is given by

$$\Delta P = \frac{2\gamma \cos\theta}{r} \quad (2.2)$$

where γ = surface tension of the liquid

θ = contact angle between the liquid and the capillary wall

Substitution of equation (2.2) in equation (2.1) gives the Lucas-Washburn equation

$$\frac{dh}{dt} = \frac{r\gamma \cos\theta}{4\mu h} \quad (2.3)$$

The integrated form is given as

$$h^2 = \frac{r\gamma \cos\theta}{2\mu} t \quad (2.4)$$

or

$$h = \left(\frac{r\gamma \cos\theta}{2\mu} \right)^{1/2} t^{1/2} \quad (2.5)$$

This equation indicates that for a particular liquid-paper system, the amount of liquid absorbed should be proportional to the square root of time if this model is valid. The application of this equation to paper assumes that the random pore structure of paper can be described as equivalent to a bundle of cylindrical capillaries. It also assumes that the contact angle and the pore structure remains unchanged during the course of penetration. Although this is adequate to some extent for non-aqueous liquids which do not swell paper fibres, its applicability to aqueous liquids leaves much to be desired. An equivalent form of the equation in terms of porosity and permeability can be derived (Hayes, 1999) and is given as

$$h = \left(\frac{4K \gamma \cos\theta}{\varepsilon \mu r} \right)^{1/2} t^{1/2} \quad (2.6)$$

where K = Permeability in the direction of flow, and

ε = Porosity

In the Fickian diffusion approach, penetration is considered analogous to a molecular diffusion process. The properties of the pore system, including fibre swelling effects, and penetrating liquid are incorporated into a diffusion coefficient. Commencing with Fick's second law of diffusion, which is given as

$$\frac{\partial C}{\partial t} = D \frac{\partial^2 C}{\partial x^2} \quad (2.7)$$

where C = concentration of the diffusing liquid

x = distance in direction of diffusion

D = diffusion coefficient

t = time

Hoyland (1977) derived the following equation to describe penetration of an aqueous liquid by diffusion

$$F = \frac{m_t - m_0}{m_\infty - m_0} = \frac{2}{h} \left(\frac{Dt}{\pi} \right)^{1/2} \quad (2.8)$$

where F = fraction of the amount of penetrant taken up in time t relative to the amount taken up at infinite time

m = amount of penetrant present at time 0 , t and ∞

Various attempts have been made to compensate for the deficiencies in the Lucas-Washburn equation. Hoyland (1976) introduced a correction term in the Lucas-Washburn equation to account for fibre swelling. Tollenaar (1967) introduced a tortuosity factor to account for pore size distribution and non-connected pores. Ruoff et al (1959, 1960) developed an interconnected capillary model which was based on chromatography experiments. They also showed that aqueous liquid flow in paper could be modelled on a macroscopic scale Fickian diffusion process, provided that the diffusion coefficient which is unique for every liquid-paper system, can be measured. Marmur (1988) proposed further refinements in modelling penetration in paper, which were experimentally verified more recently by Borhan and Rungta (1993). Marmur's models include

Lucas-Washburn kinetics for radial penetration of liquid and delineation between surface porosity and bulk porosity. In another study Oliver et al (1994) used a diffusion approach for modelling kinetics of penetration into paper and experimentally determined diffusion coefficients of various ink-paper systems from video-microscope studies. In more specific applications Poulin et al (1997) have developed a model based on the Lucas-Washburn equation which takes into account the effect of basepaper permeability on coating penetration.

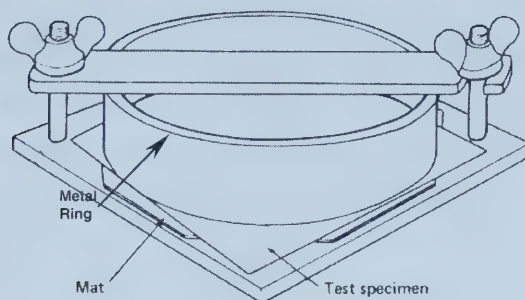
Apart from theoretically derived models, various test methods have also been developed over the years to measure absorption of liquids into paper. The more commonly used methods are described below.

Test Methods

Cobb Test Method

This test method is used for assessing the absorptive properties of paper and was developed by Cobb in 1934. It is a widely accepted and standardised test method (for example TAPPI Test Method T 441 om-90). A sample of paper is clamped between a metal ring and a rubber mat which is supported on a base plate as shown in Figure 2.1. A measured volume of 100 ml of water is poured into the metal ring to give a liquid head of 1 cm. After a predetermined test period, usually 60 seconds, the water is quickly poured out of the ring. Excess water is removed from the sample with blotting paper and a hand roller. The sample is then immediately weighed to obtain the weight of water absorbed. This is a simple test method giving results of good accuracy and reproducibility. However, the disadvantage of this method is that the time period required to practically carry out the test is much longer than typically encountered during industrial processes.

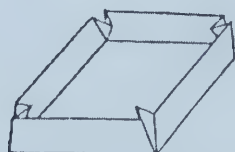
Figure 2.1: Cobb Test Apparatus (Reproduced from Tappi Test Method - T441 om-90)



Stöckigt Sizing Test Method

This method is typically used for measuring the sizing degree (resistance to water) of paper. The paper sample is folded on all four edges to form a "boat" as show in Figure 2.2. The sample is then floated in a solution of 2% ammonium thiocyanate, a drop of 1% ferric chloride is quickly place on the sample and the time taken for three red spots to appear on the paper is noted. This time is recorded as the Stöckigt sizing degree.

Figure 2.2: Stöckigt Test Sample -"Boat" (Reproduced from JIS P8122-1976)

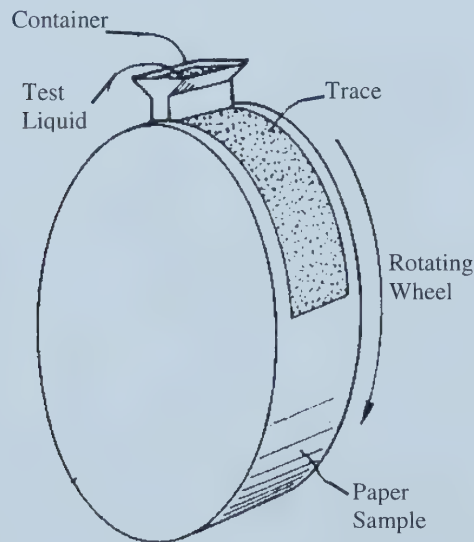


Bristow Test Method

This method was developed by Bristow (1967) to measure liquid absorption into paper during short time intervals. The principle of the apparatus used is shown in Figure 2.3. A strip of paper is affixed to a rotating wheel and allowed to pass under a liquid container which has a rectangular opening. As the

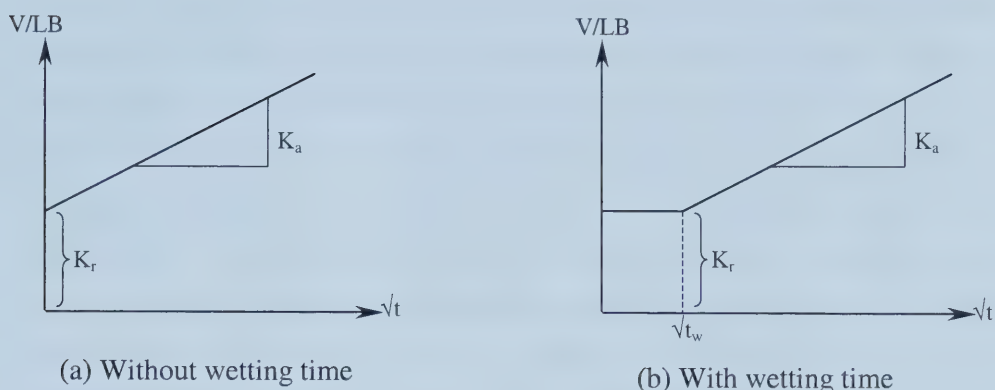
wheel rotates, liquid is transferred to the paper depending upon the speed of rotation and the absorption properties of the paper. A liquid trace is left on the paper and the length of the trace for a certain volume of liquid in the container provides information on the transferred liquid quantity per unit area. A series of measurements is done with different rotation speeds and the quantity of liquid absorbed can be plotted against time. The absorption is calculated as V/LB (ml/m^2), where ' V ' is the liquid volume in the container, ' L ' is the length of the trace produced and ' B ' is the length of the slot.

Figure 2.3: Bristow Test Principle (Reproduced from US Patent 5065620, 1991)



The ideal absorption curves obtained are shown in Figure 2.4. The slope of the line obtained is termed as ' K_a ', the absorption coefficient ($\text{ml}/\text{m}^2\text{s}^{1/2}$). The intercept is termed as ' K_r ', the roughness index (ml/m^2). The wetting time, ' t_w ' is typically observed from tests with water or aqueous solutions.

Figure 2.4: Bristow 'ideal' absorption curves



The Ultrasonic Test method

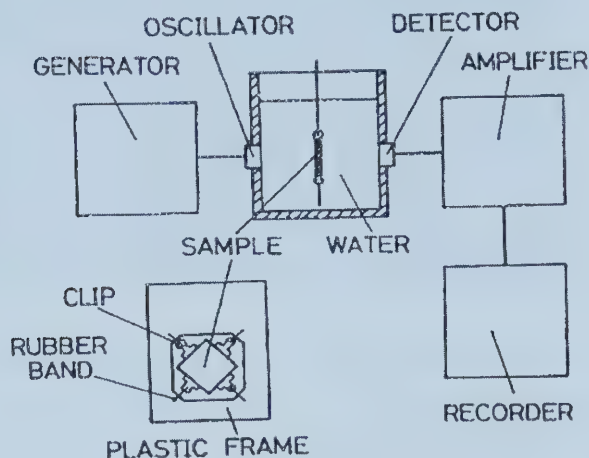
Over the past four decades ultrasound has been widely used in the paper industry for measurement of paper properties. The earliest methods were based on the measurement of the sonic velocity through the media and the factors controlling it were used to measure the strength properties of paper. A good review of the use of ultrasound as a non- destructive method for measuring the strength properties of paper has been given by Waterhouse (1994) and Brodeur (1998). The speed of the sound wave in a material is directly related to its elastic properties. This property can be used to indirectly measure the strength of paper (Craver, 1996). Ultrasound has also been used to measure the thickness (Brodeur, 1994) and orientation of paper (Titus, 1994). The sonic velocity method has also been used to study the water retention properties of coatings (Taylor, 1967) and the absorption of water in paper (Chatterjee, 1971).

More recent methods developed specifically for measuring the wetting and penetration dynamics of liquid penetration of paper are based on the measurement of the attenuation or transmission of an ultrasonic signal, through the paper. The earliest reported work involving the use of such a method is Pan et al (1985a). They used an instrument supplied by Cho-onpa Kogya Co., Tokyo. The method

involved measuring the attenuation of a 2 MHz ultrasonic signal transmitted through paper samples with different degrees of sizing, which were immersed in water. Penetration of the water was from both sides of the sample. Results were obtained as a plot of the percentage attenuation against immersion time. The value of attenuation at 60 min, ' $A(60)$ ' after immersion was chosen as the index of sizing because after this elapsed time the attenuation value for most paper samples was constant. The $A(60)$ values obtained for different papers were compared with the Stockigt sizing degree (S) test (JIS P 8122-1976). Trends obtained in both tests were similar, however reproducibility and accuracy of the results from the ultrasonic method was found to be higher than the Stockigt sizing test. It was also found that the $A(60)$ value was much less dependent on thickness or basis weight (grams/m^2) than S for papers of common thickness (50-100 microns). Further work by Pan et al (1985b) showed that the $A(60)$ values correlated with the degree of sizing and were quite sensitive for very slack sized papers. Their findings also indicated that $A(t)$ was not affected by paper thickness or basis weight in the range of 0.5 – 0.15 mm.

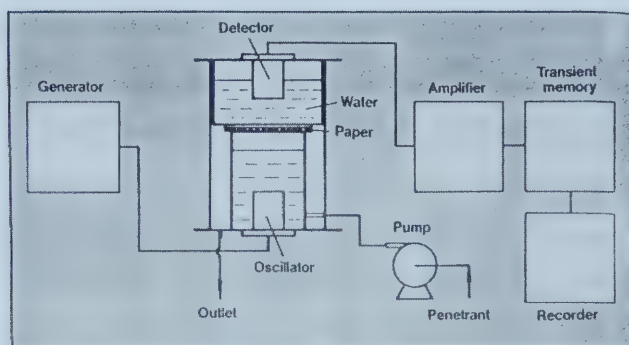
In another study Pan et al (1985c) used an apparatus which was originally developed for measuring the consistency of a particulate slurry and is shown in Figure 2.5. Tests done with solid plate samples showed that a plastic plate attenuated the ultrasonic wave to a much lesser extent than a solid copper plate. When the surfaces of the plates were abraded with sandpaper and then tested, the attenuation increased according to the surface roughness. Other findings in this study were similar to those described by Pan (1988a) viz. the attenuation and the Stockigt sizing value decreased with decrease in sheet thickness. The effect of filler content in the paper was also assessed and was found to have no effect on the attenuation of the ultrasound signal.

Figure 2.5 Schematic Diagram of Ultrasonic attenuation measurement apparatus (Pan, 1985)



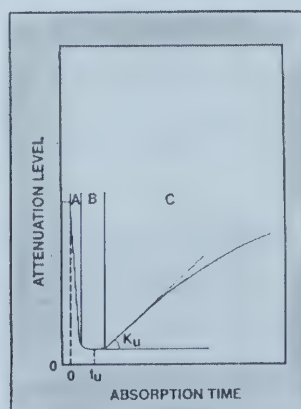
Pan et al (1988a) later developed a new apparatus for ultrasonic measurement in which the sample was mounted horizontally and bombarded with an ultrasonic beam. A schematic diagram for the apparatus used is shown in Figure 2.6. Test liquid was pumped into the space below the sample until it just touched the paper surface. The receiver unit was mounted on top of the generator unit and was always filled with water. A pair of 2 MHz piezoelectric oscillators was used as generator and receiver. The test sample size used was 4cm x 4 cm and was attached to the outer bottom of the receiver unit using a double-sided adhesive tape. The instrument based on this principle and known as the Ultrasonic Wettability tester (UWT) is currently being marketed by Shin Ei Co., Japan and is available in North America through Kaltec Scientific Inc. This was the first commercial ultrasonic instrument for characterising the dynamics of liquid penetration into paper.

Figure 2.6: Schematic Diagram of the apparatus for the ultrasonic measurement of liquid penetration into paper (Pan, 1988)



Tests were conducted using water and papers with varying degrees of sizing. The results obtained were in the form of a plot of the attenuation (dB) against the penetration time. The authors found similarities between the absorption profiles for unsized papers in the short time regime and the profiles for sized papers in the long time regime. This gave an indication of an attenuation factor involved in slowing down of the penetration kinetics due to the sizing. To define the wetting properties, a master curve as shown in Figure 2.7 was used to represent the attenuation-time profiles obtained and certain parameters were defined.

Figure 2.7: Master Curve of the time dependence of acoustic attenuation (Pan, 1988)



The curve consisted of three regimes. 'A' was attributed to the instrument response, 'B' represented transient interactions between the paper surface and the liquid and 'C' represented the penetration into the bulk pores of the paper. The parameters defined were ' t_u ' which is the time at which the minimum value of attenuation is observed and ' K_u ' which is the maximum rate of increase in attenuation, determined at the point of inflection. The authors correlated these parameters with parameters from the Bristow test (K_a - the absorption coefficient and t_w - the wetting time). It was found that ' t_u ' correlated somewhat linearly with ' t_w '. The plot of ' K_u ' against ' K_a ' showed two regimes of different slopes but an overall positive correlation was observed.

In a further study Pan et al (1988b) again found a good linear correlation (very close to 1:1) between ' t_u ' and ' t_w '. The ratio however was different from the previous study which gave a ratio of $t_u/t_w = 1.83$. They concluded that a single value of the ratio could not be assumed for various types of paper. Effects of the two-sidedness of the samples were also studied. They observed that the felt side showed longer wetting times than the wire side, especially at higher levels of sizing agent. This was attributed to the fact that the felt side is usually richer in fine fractions and hence relatively less porous. (It may be noted, however that due to both physical and chemical differences on the 'felt' and 'wire' sides of commercial papers, differences may arise in the actual concentrations of sizing on each side.) As done previously ' K_u ' and ' K_a ' were also correlated. The plot of ' K_u ' vs ' K_a ' showed a nearly horizontal line in the high sizing range and a steep line in the slack sizing range. In comparison to ' K_a ', ' K_u ' was found to be more sensitive to the changes in the surface hydrophobicity in the very slack sizing range.

The ultrasonic method was further developed in Germany at the Institute for Graphic Technology (IGT) from 1988 onwards. The instruments which were developed from the research project at IGT, are currently available from two different companies, Emco GmbH and Emtec Electronic GmbH. The current model available from Emco is the DPM-30 (Dynamic Penetration Measurement)

and from Emtec is the PDA (Penetration Dynamics Analyser). Both instruments are similar in construction and have similar capabilities. Unlike the UWT, the sample is plunged vertically into the beam of an ultrasonic signal of fixed frequency and the change in attenuation during penetration is recorded. Much of the work towards the design and development of this instrument in its present form was done by Gabriel (1999). The working and features of the Emco DPM-30 have been described in detail by Beltz (2000) and for the PDA by Grüner (2002). The principle and features of ultrasonic dynamic penetration measurement instruments for paper in general have also been discussed by Amodei (1997). A detailed description of the principle of operation of the Emco DPM -30, including the output parameters from the instrument is given in Chapter 3. Most of the literature available currently on the use of the ultrasonic method reports use of the above Emco or Emtec instruments. These seem to be more widely used in comparison to the UWT instrument.

Investigations by Beltz (1998) showed that the results from the Emco DPM correlated with the degree of pulp freeness and the degree of sizing of different paper samples tested. In order to validate the test method, Emco GmbH compared the test results to the more conventional Cobb test. Transmission values ' $Tr \%$ ' after 60 seconds were compared to the Cobb-60 test. Also the value of the parameter ' $1/t_B$ ' was compared to the Cobb-60 test. The results were found to correlate with the Cobb-60 test and also showed greater sensitivity to the degree of sizing than the Cobb test. Since the penetration dynamics also depends upon the nature of the surface of the sample (roughness), the results were also compared with the Bekk Smoothness test. The smoothness of the surface of a paper sheet was varied by using different levels of calendering. The results from the Emco DPM were found to correlate with the Bekk smoothness index.

Pan et al (1996) reported use of the UWT to characterise the liquid absorption of ink jet paper. The authors used a horizontal contact Ultrasonic Wettability Tester (UWT-2) and observed a positive correlation between the ink drying rate and the wetting time i.e. the longer the wetting time, the slower the ink drying rate. The wetting times determined by the UWT correlated better with the ink drying rate as compared to wetting times obtained from the Bristow test. They also concluded that the slope of the ultrasonic measurement curve could be treated as an indicator of the liquid absorption rate.

Studies were also conducted by Mailly (1997) to characterise the dynamic phenomena between fluids and coated paperboards. The main interest was to correlate the gloss of varnished coated paperboards with the physical and chemical properties of the paperboard. In this particular work the author used two methods for studying the absorption characteristics of the different paperboards viz. the Bristow test and the Emco ultrasonic dynamic penetration measurement instrument. The operating conditions used for the Emco instrument were: Test liquid - water or oil, Frequency - 2 MHz, Sample dia. - 10 mm, Fall height - 70mm, Time for complete immersion of sample - 40 msec, Testing time - 30 sec. The author noted the Emco output parameters ' S ', ' t_B ' and ' $L\%$ ' to be significant in this study. Parameter ' S ', the steepest rise of the curve was interpreted as a measure of the penetration velocity and ' t_B ' and ' L ' were thought to be indications of the surface characteristics of the samples tested. The author found that the Emco absorption coefficient ' S ' correlated with the coefficient ' K_a ' from the Bristow wheel test and that the parameter ' $L\%$ ' correlated more with the internal and superficial porosity rather than the roughness.

A comparison of results from the Emco ultrasonic method with the Fibro 1100 Dynamic Absorption Tester was made by Phillips (1999). Tests were done on various newsprint samples with water and flexographic inks to understand the penetration and drying of ink into newsprint. The author points out that though the Fibro Dynamic Absorption Testing method can be used to study both penetration

and spreading of the probe liquids, the disadvantage of the method is that the ink is not applied under pressure, thus limiting its applicability in impact printing processes. The ultrasonic method has the advantage that the liquid is applied under slight pressure, but the contact line spreading of the liquid cannot be followed. An Emco DPM 27 instrument was used for the ultrasonic method. The author assumed that the parameters ' S ' (maximum negative gradient or maximum absorption rate) and the time taken to reach this point, ' t_S ' were the important characteristics of the measurement curve. No correlation was found between the specific parameters obtained from the Emco test method and the Fibro DAT method, but each method predicted a slower rate of penetration with flexo ink as compared to water. So the Emco method was concluded to remain mainly qualitative.

Bayer et al (1996) used the Emco DPM 27 in a study to evaluate the effect of paper basis weight, pulp beating degree, filler content and sizing agents on the rate of water penetration. The test sheets were conditioned for 24 hrs at $(23 \pm 1^\circ \text{C})$ and $50 \pm 2\%$ relative humidity). The ultrasonic measurement was done for a time period of 600 sec. It was found that variation of the basis weight from 80 to 200 grams/m^2 did not significantly affect the penetration behaviour (differences were small and within tolerance limits). Sheets formed from pulps with beating degree varied for 14°SR to 61°SR showed that with increase in beating degree, the resistance to penetration increased in the first 4 seconds. Sheets with sizing varied from 0% to 4% AKD (Alkyl Ketene Dimer) were also tested. The results showed that the penetration rate slowed down with increase in sizing, and the parameter ' t_B ' correlated with the sizing content. It was also found that increase in filler (Alphatex) from 0 to 5 % did not have much effect on the penetration rate. However, the rate was greatly decreased with filler content of 7%, presumably because of significance in pore filling. The effect of the same content of different fillers on the penetration rate was also studied. They also found that the penetration process is sensitive to the two-sidedness of paper and the surface roughness. The ultrasonic method was able to detect these phenomena. The

ultrasonic signal transmission value after 60 sec was found to correlate with results from the Cobb test (Tappi 1990).

Bayer et al (2000) investigated the effects of filler on the dynamics of penetration. Based on tests done on various newsprint grades and offset printing paper graded, they found that the penetration is strongly influenced by the filler and sizing content in comparison with the primary fibrous material. Mussalo (1997) studied the use of the ultrasonic method using an Emtec -PDA instrument. The results indicate that the effect of moisture, density, porosity, surface treatment, filler content and kappa number of the pulp can be detected by the method.

Sjögren (1998) has done a detailed evaluation of the Emtec-PDA instrument. This report gives a good overview of the working principles of the Emtec – PDA, which is similar to the Emco – DPM 30. Several paper samples with different filler content, internal and surface sizing were tested using the ultrasonic method. Print quality analysis was also done for the different paper grades. It was found that increased sizing (high ' t_{max} ' and ' $t_{inflexion}$ ' values and low Cobb values) caused increased colour bleeding. However, other parameters from ink jet print quality tests did not correlate with results from the penetration dynamics. Of relevance to the ultrasonic test method, the author has made some investigations, the results of which are summarised below.

- The effect of the force of fixing the sample was studied. It was found that the penetration dynamics were slower in a paper which had been subjected to a 50N compression force in a Prüfbau printability tester. This was attributed to the decrease in the surface porosity of the paper.
- The effect of paper mounting orientation was also studied. It was found that the test method is independent of whether the paper 'machine direction' or the 'cross direction' is parallel to the axis of sample immersion.
- To ensure performance of the instrument in a similar manner with time, the potential of using Millipore® filters as a method of calibration was explored. It

was found that the results with the Millipore filters were not reproducible and hence a Scandinavian coated art paper, Apco II/II was used as a reference standard. The results with this paper were very reproducible in the $\pm 90\%$ confidence interval.

- Effects of conditioning of the paper samples on the instrument results were also studied. It was found that even for a difference in Relative Humidity of 10%, the results were slightly different. This was expected since the moisture content and the fibre stiffness of the paper samples would be different.
- The parameters ' t_{max} ' and ' $t_{inflexion}$ ' from the instrument were found to have some correlation with the Cobb test results. This correlation was higher than that between the parameter ' $G2$ ' (slope) and the Cobb test.

In a personal correspondence, the author indicated reproducibility studies in which a conditioned paper sample was tested every week for a year. The results indicated that the measurements have satisfactory repeatability. The 95% confidence interval for t_{max} is $+ 2.8\%$ and for $t_{inflexion}$ is $\pm 6.7\%$. The author concluded that ageing of the paper could have some effects on the results.

Dietze (1995) evaluated the use of the Emco DPM 27. Various offset grade papers were tested with penetration from either side. It was found that the instrument gave different dynamics for different sides of the paper grade as expected. Also wetting times were found to be faster for lower surface tension printing oils in comparison with water. Correlation of the Emco results with the Cobb test and Bekk smoothness test were also observed. However, correlation could not be found between the Emco results and the printability of the different papers. Dietze concluded that the interpretation of the results was still at a preliminary stage to predict print quality and in order to use the instrument as a quality control tool and arrive at tolerance ranges, more studies of the effects of the in-homogeneity of the paper, surface treatment etc and their effect of the measurements would have been done.

More recent investigations involving the ultrasonic method have been done by Pekarovicova (2001). The study was aimed at assessing the use of water penetration dynamics to predict flexo-printability of linerboard. The parameters from the ultrasonic method were correlated with the flexo-printability characteristics such as reflection density, gloss, print contrast and dot gain. It was found that the print quality using these characteristics decreased with an increasing value of the parameter 'w' (which primarily characterises the porosity and surface roughness of the paper). The correlation was better when done in a narrower spectrum of samples.

The ultrasonic method has also been extended to use in the evaluation of coatings as reported by Baumeister and Grüner (1999). They used an Emtec PDA coating instrument, which is a modified version of the Emtec PDA developed specifically for the evaluation of coatings. Similar attachments are also available from Emco GmbH.

Most of the studies done so far are quite qualitative and mainly involve comparison of results from the ultrasonic method with other test methods. A good review of the physical processes involved during transmission of ultrasound through a paper sheet during penetration by a liquid has been done by Stor-Pellinen et al (2000). The authors used their own instrumental set-up to study the effects of sizing (in terms of contact angle) and frequency of the ultrasound signal. Wetting liquids used were solutions of 0, 10, 25, 50, 80 and 100% iso-propanol in water. A set of 0.5 to 14 MHz ultrasound transducers of 12.5-mm diameter was used as the source for the ultrasound signal. Four characteristics of the resultant measured curves were recorded: the coefficient of inclination, the coefficient of declination, the time and the amplitude at maximum transmission. At a 5 MHz frequency and wetting from one side, a high linear correlation was obtained between the contact angle and the index of declination. At a 1 MHz frequency and wetting from both sides, a high linear correlation was obtained between the iso-propanol concentration and the index of inclination and between the iso-propanol concentration and the time instant of maximum transmission.

The general shape of the curves for one-side and both-sides wetting was similar. The index of inclination was found to increase with frequency. The technique was further extended to study the effect of high power ultrasound on the wetting of paper (Stor-Pellinen et al, 2000b). It was found that 40 kHz high power ultrasound increased the rate of wetting of the paper. This is mainly due to a faster escape of gases from the surface roughness and the pores, promoting faster pore filling.

Stor-Pellinen et al (1995) also developed a method which used ultrasound to measure surface roughness of paper. The measurement principle is based on the attenuation of ultrasound which occurs when it is reflected from a rough surface. A pulse –echo technique was used with a frequency range of 0.5–4 MHz. The test method appears to be promising and showed some correlation with the Bendtsen and Parker-Printsurf roughness measurement methods. More recent developments on this method have been reported by Stor-Pellinen et al (2001). Another report by Haeggström et al (2000) describes a similar ultrasonic technique that can be used to monitor wetting as well as drying processes in paper.

The latest reported studies by Stor-Pellinen et al (2002) involved the use of a slightly different apparatus in which the sample was wetted with a mist pulse of water or iso-propanol. An ultrasonic burst, frequency ranging from 500 to 900, 600 to 1000 and 1300 to 1700 kHz, was transmitted through the sample at a 10 kHz repetition rate. This allowed the wetting dynamics to be monitored at several different frequencies in a single measurement. The shape of the transmission curves obtained suggested that capillary wetting and diffusion wetting processes could be distinguished.

The main advantages of the ultrasonic method compared with the more conventional methods such as the Bristow test, Hercules sizing test and the Cobb test are that the measurement of the dynamics can be done continuously with a

resolution in the millisecond range. Table 2.1 summarises reported literature involving the use of the ultrasonic method to date.

Table 2.1: Brief Chronological Summary of Literature on the use of the Ultrasonic Method

Year	Authors	Remarks
1985a	Pan, Kuga and Usuda	Studies on the effects of sizing on attenuation of a 2 MHz ultrasonic signal. Correlation of results with the Stockigt sizing test.
1985b	Pan, Kuga and Usuda	Correlation of sizing degree with attenuation of the ultrasonic signal. Studies on effect of thickness and basis weight on attenuation.
1985c	Pan, Kuga and Usuda	Studies on effect of roughness, filler content and sizing degree on attenuation and comparison of results with Stockigt test.
1988a	Pan, Kuga and Usuda	Development of Ultrasonic Wettability Tester (UWT). Evaluation of the effect of sizing degree on penetration dynamics. Development of parameters to define the curves obtained from the instrument and correlation of these with the Bristow test results.
1988b	Pan, Kuga and Usuda	Studies on the correlation among parameters obtained from the UWT and effect of two-sidedness of paper samples.
1995	Dietze	Investigations of correlation of results from an ultrasonic Emco DPM 27, with the Cobb Test and Bekk smoothness test. Observed differences in dynamics of penetration between the two sides of paper samples. Attempt to correlate results from ultrasonic measurements with offset print characteristics of different grades of packaging paper.
1995	Stor-Pellinen et al	Development of an ultrasonic technique to measure the surface roughness of paper. Correlation of results with Bendtsen and Parker-Printsurf roughness measurement methods.
1996	Bayer, Mallon and	Studies on the effects of beating degree, basis weight,

Year	Authors	Remarks
	Blechschiidt	filler type and content on penetration dynamics, using an ultrasonic Emco DPM 27. Correlations between ultrasonic test results and Cobb test and Bekk smoothness test.
1996	Pan and Yang	Investigations on the use of the ultrasonic wettability tester for measurements of liquid absorption into ink jet paper. Correlated ink drying rate and wetting time.
1997	Amodei	Review of basic concepts of wave theory with respect to ultrasonic dynamic penetration instruments. Review of background, principle of operation and time regimes typically obtained.
1997	Blechschiidt and Bayer	Overview of the ultrasonic test method and studies of effects of various paper properties on penetration dynamics.
1997	Mailly	Study of the absorption characteristics of different paperboards. Correlation of Emco DPM 27 parameters with parameters from the Bristow test.
1997	Mussalo	Study of the ultrasonic method using an Emtec PDA instrument. Effects of moisture, density, porosity, different surface treatments, filler content, spruce-pine fibre ration and Kappa number on penetration dynamics were investigated.
1998	Beltz	Discussion on principle of working of the Emco DPM 30 instrument. Addresses the effect of basis weight, sizing agents, filler content and smoothness of different paper grades on the ultrasonic method. Correlation of results (effect of sizing) with the Cobb test.
1998	Sjögren	Evaluation of the Emtec PDA instrument. Studies on effects of sample fixing force, paper orientation, relative humidity and the use of Millipore® filters for calibration. Correlated parameters from ultrasonic test with Cobb test results.
1999	Baumeister and Grüner	Measurements of the dynamics of penetration of coating into base papers. An ultrasonic Emtec PDA coating instrument was used, which has special cell inserts for simulating roll-coating conditions.

Year	Authors	Remarks
1999	Gabriel	Investigations into the use of the ultrasonic method for paper and cardboard samples. Effects of structural changes in the paper (damp strain measurements) on the ultrasonic signal were studied. Effects of frequency using 1 MHz and 2 MHz signals, viscosity, surface tension, porosity , machine direction of paper etc were also studied.
1999	Phillips	Investigations on the penetration of water and flexographic inks into various newsprint grades. Comparison of parameters from the ultrasonic method with the parameters from the Fibro Dynamic Absorption testing method.
1999	Richter	Discussions on the physics behind the principle of the ultrasonic instrument (Emco DPM 30).
2000	Bayer and Alber	Evaluation of the effects of filler and sizing content on the absorption properties of printing and speciality papers using an ultrasonic Emco DPM 30 instrument.
2000	Beltz	Review of theory and applications of the ultrasonic instrument (Emco DPM 30).
2000	Haeggström	Development of an ultrasonic technique to monitor moisture content and drying processes in paper.
2000a	Stor-Pellinen et al	Development of an apparatus for measurement of paper wetting using ultrasound. Review of physical processes involved and effects on ultrasonic transmission. Studies on effects of sizing, contact angle and frequency of ultrasound. Probe liquids used were water and aqueous solutions of methanol.
2000b	Stor-Pellinen et al	Studies on the effect of high power ultrasound on the dynamics of wetting of paper.
2001	Pekarovicova and Pekarovic	Evaluation of water penetration dynamics into liner board, using an ultrasonic Emtec PDA instrument. Correlation of results with print quality of flexo printed linerboard using water-based inks.
2001	Stor-Pellinen et al	Studies on the ultrasonic measurement of the change in roughness of paper during wetting.

Year	Authors	Remarks
2002	Grüner	Discussions on interpretation of dynamics and physical processes occurring based on the nature of the shape of curve obtained from the ultrasonic measurement.
2002	Stor-Pellinen et al	Studies on the effect of thickness or basis weight on the ultrasonic signal. Development of a method to follow the absorption coefficient of paper during wetting. Investigations using water and iso-propanol solutions indicating that capillary wetting and diffusion wetting can be differentiated.

3.0 Ultrasonic Dynamic Liquid Penetration Measurement Method

3.1 Brief Overview of Sound Theory

Sound waves travel in the form of longitudinal waves which can be described by the equation for simple harmonic motion as (Richter, 1999):

$$y = A \sin\left[\omega\left(t - \frac{x}{c}\right)\right] \quad (3.1)$$

where, A = Amplitude

$\omega = 2\pi f$ i.e. the angular frequency, where f is the frequency of the wave

x = distance in the x-direction

c = wave velocity

The audible region of sound for humans lies between around 20 Hz to 20 kHz. Sound waves with frequency above the normal human hearing range are called ultrasonic sound waves. The speed of sound depends on the frequency and wavelength of the wave and is given as

$$c = \lambda f \quad (3.2)$$

where, λ = wavelength

As a wave travels from one medium to another, in order that the frequency remains constant, the wavelength and speed change. The speed of sound in a medium depends primarily on the stiffness or elasticity of the medium and secondarily on the density of the medium.

The speed of sound in solids is given as (Wilson, 1994)

$$c = \sqrt{\frac{Y}{\rho}} \quad (3.3)$$

where, Y = Young's Modulus of Elasticity

ρ = density

The speed of sound in liquids is given as (Wilson, 1994)

$$c = \sqrt{\frac{E}{\rho}} \quad (3.4)$$

where, E = Bulk Modulus of Elasticity

ρ = density

The speed of sound in ideal gases is given as (Bhatia, 1967)

$$c = \sqrt{\frac{C_p / C_v RT}{M}} \quad (3.5)$$

where, C_p/C_v = Ratio of specific heat capacities

R = Gas constant

T = Temperature

M = Molecular weight

The speed of sound waves in solids is thousands of metres/sec (for example ~ 4500 m/s in Iron), in water is around 1500 metres/sec and in air is 340 metres/sec. Other relevant equations given by Richter (1999) are summarized as follows.

The acoustic pressure is given by

$$P = \rho c \omega A \cos[\omega(t - \frac{x}{c})] \quad (3.6)$$

The acoustic impedance is given by

$$Z = \rho c \quad (3.7)$$

The Energy per unit volume (J/m^3)

$$\overline{E} = \frac{1}{2} \rho \omega^2 A^2 \quad (3.8)$$

The sound intensity (W/m^2) is given by

$$I = \overline{E} c \quad (3.9)$$

When an ultrasound wave strikes the interface between two fluids or between a fluid and a solid, the wave is partially reflected and transmitted. The level of reflection

and transmission depends on the incident intensity and the impedance of the media. The ratio of the reflected and incident sound intensity is known as the Intensity Reflection Coefficient (R). The ratio of the transmitted and incident sound intensity is known as the Intensity Transmission Coefficient (T).

$$R = \frac{Z_2 - Z_1}{Z_1 + Z_2} \tag{3.10}$$

where, Z_1 = Impedance of medium 1

Z_2 = Impedance of medium 2

Also,

$$T = 1 - R \tag{3.11}$$

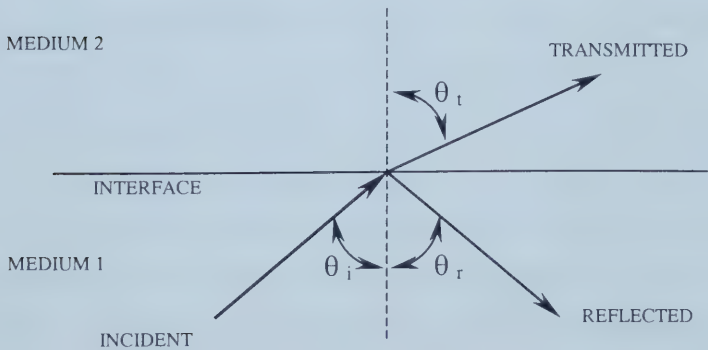
This implies that there will be no reflection if the impedance of the two media is equal. Conversely if there are large differences between the media impedance, there will be almost total reflection i.e. R will be close to one and T will be close to zero.

Figure 3.1 shows the reflection and transmission of a sound wave at the interface of two media. The relationship between the angles of incidence, reflection and refraction (or transmission) is similar to the laws of optics, viz.

$$\theta_i = \theta_r \tag{3.12}$$

and
$$\frac{\sin \theta_i}{\sin \theta_r} = \frac{c_1}{c_2} \tag{3.13}$$

Figure 3.1: Incident, reflected and refracted sound waves



If the boundary dimensions or the roughness of the surface on which a sound wave is incident is comparable to the wavelength of the sound, the sound will be scattered or diffused. A heterogeneous medium means that there are many boundaries within the medium for reflection, refraction and scattering (Amodei, 1997). Such effects of scattering, reflection and absorption cause a decrease in the amplitude (attenuation) and the energy intensity of the sound wave.

The intensity at any point is given by (Richter, 1999)

$$I_x = I_0 \exp(-\alpha x) \quad (3.14)$$

where, α = attenuation coefficient

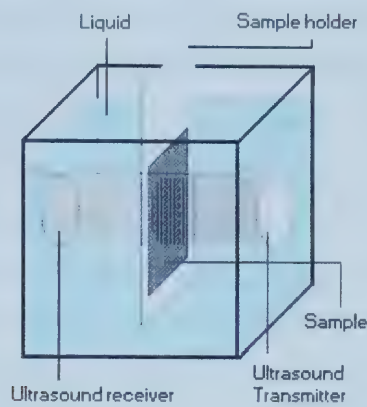
x = path length

The attenuation coefficient has two components attributed to absorption (α_A) and scattering (α_S). Absorption is characterized by energy conversion from one form to another. Scattering causes the decrease in amplitude of the wave. The attenuation of sound waves increases with frequency. For example, for Rayleigh scattering the attenuation is proportional to the fourth power of the frequency. Thus for Rayleigh scattering, the attenuation of a 2 MHz wave would be 16 times more than a 1 MHz wave, if both waves have the same initial amplitude and are passed through the same material.

3.2 Principle of Operation

An ultrasonic signal is generated and passed through a reservoir of the test liquid. The sample to be tested is plunged into the reservoir and into the path of the ultrasonic signal. The amplitude and intensity of the signal change due to absorption and scattering effects as the liquid penetrates into the sample. The principle of operation is depicted in Figure 3.2. This change in intensity is monitored to detect the dynamics of liquid penetration into the porous sample. As previously discussed, the intensity of the ultrasound signal being transmitted through the sample depends on the acoustic properties of the sample as well as the air content of the sample and the various solid-liquid-air interfaces which occur as the liquid penetrates the sample and begins displacing out the air. The output from the instrument is a plot of '*% Transmission*' versus '*time*'.

Figure 3.2: Ultrasonic Method Principle of Operation © Emco GmbH, 2000



3.3 Construction and Working

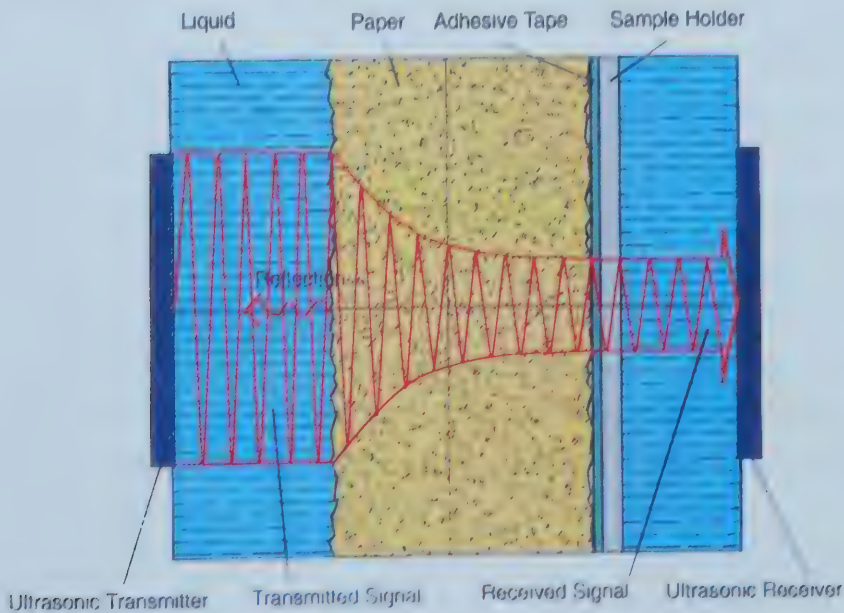
The ultrasonic dynamic penetration instrument used in this study was the Emco DPM-30, the construction of which is shown in Figure 3.3.

Figure 3.3: Construction of Emco-DPM 30



The device consists of a measuring cell in which the ultrasonic transmitter and receiver are fixed. The measuring cell is filled with deionised water. The test liquid is filled in a plastic reservoir, which is inserted into the measuring cell. The sample is affixed to the sample holder using a double-sided adhesive tape. The sample holder is plunged into the test liquid by means of the immersion device. The entire test cycle (immersion of sample, recording of the ultrasound intensity and removal of sample) is controlled by the electronic unit, which is interfaced with a personal computer. During the time when the sample is being lowered but is not yet submerged, the instrument records the unattenuated signal at the receiver end. This signal is the reference level of the 100% signal strength when the signal is unimpeded. After the sample is fully submerged, only a certain proportion of the signal from the emitter is transmitted to the receiver due to reflection, refraction, and absorption processes. Any microstructural change in the material in the path of the signal is detected and the signal strength of the attenuated signal at the receiving end is recorded and plotted versus time. A schematic representation of the attenuation of the signal inside the sample is shown in Figure 3.4.

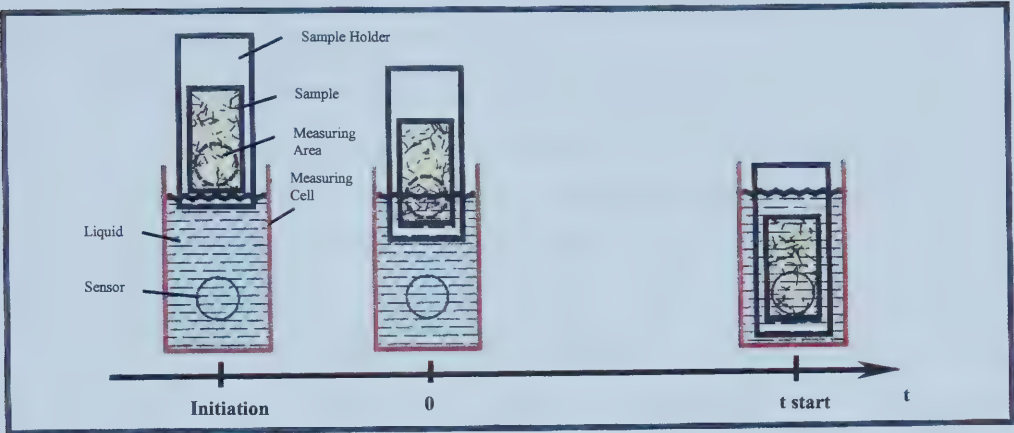
Figure 3.4: Schematic Representation of the attenuation before start of penetration (cross-sectional view) © Emtec GmbH, 2001



The ultrasonic transmitter and receiver are circular in shape. The DPM 30 has two separate concentric transmitters, an inner one of 10-mm diameter and an outer ring of 35-mm diameter. Either or both of the sensors can be used for a measurement. Two liquid fill levels are provided in the sample reservoir. The lower fill level is used if only the 10-mm sensor is used for the measurement. The sensors are made of a piezo-electric ceramic and are located exactly opposite each other. The transmitter is activated by an electronic impulse, which then produces an acoustic signal. The acoustic signal passes through the test liquid and the sample and upon reaching the receiver is converted into an electronic signal. The amplitude is analysed electronically and is stored digitally as a measured value. The frequency of the ultrasonic sensors is fixed during their manufacture. For the examination of paper the manufacturer has found a frequency of 1 to 2 MHz to be suitable and reliable. The frequency of the ultrasound signal for the DPM 30 is set by the manufacturer at 2 MHz and cannot be changed.

The ultrasonic signal at the receiver is stored from the point of complete contact of the test sample and the liquid. The contacting time is automatically determined based on the velocity of immersion and the size of the measured area. During this contacting time the entire measured area gets completely immersed in the test liquid. The speed of immersion can be varied from 10 m/min to 70 m/min. The contact time is determined for each measurement. It starts when the centre of the tested area is immersed into the liquid and stops when the sample holder reaches its final point (the tested area is located completely in the path of the ultrasonic waves at this point). Sample immersion is shown schematically in Figure 3.5. With the maximum immersion speed and the smaller measuring area (10-mm dia.), the contact time is 8 msec and with the larger measuring area the contact time is 31 msec. The complete measurement cycle for analysis and digitalization requires less than 1 millisecond. Hence a very fine resolution on the time axis can be obtained for the penetration dynamics curve. The detailed specifications for the Emco-DPM 30 are given in *Appendix-A*.

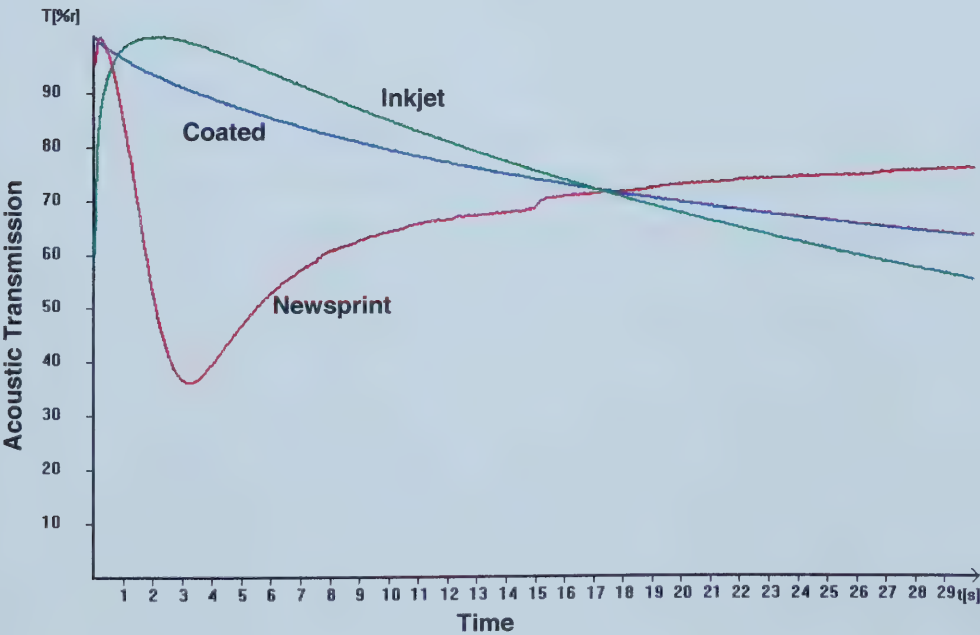
Figure 3.5: Phases of sample immersion © Emtec GmbH, 2001



3.4 Outputs from the Instrument

Typical output curves obtained for three different paper grades are shown in Figure 3.6, below.

Figure 3.6: Typical output curves for some commercial grade paper samples

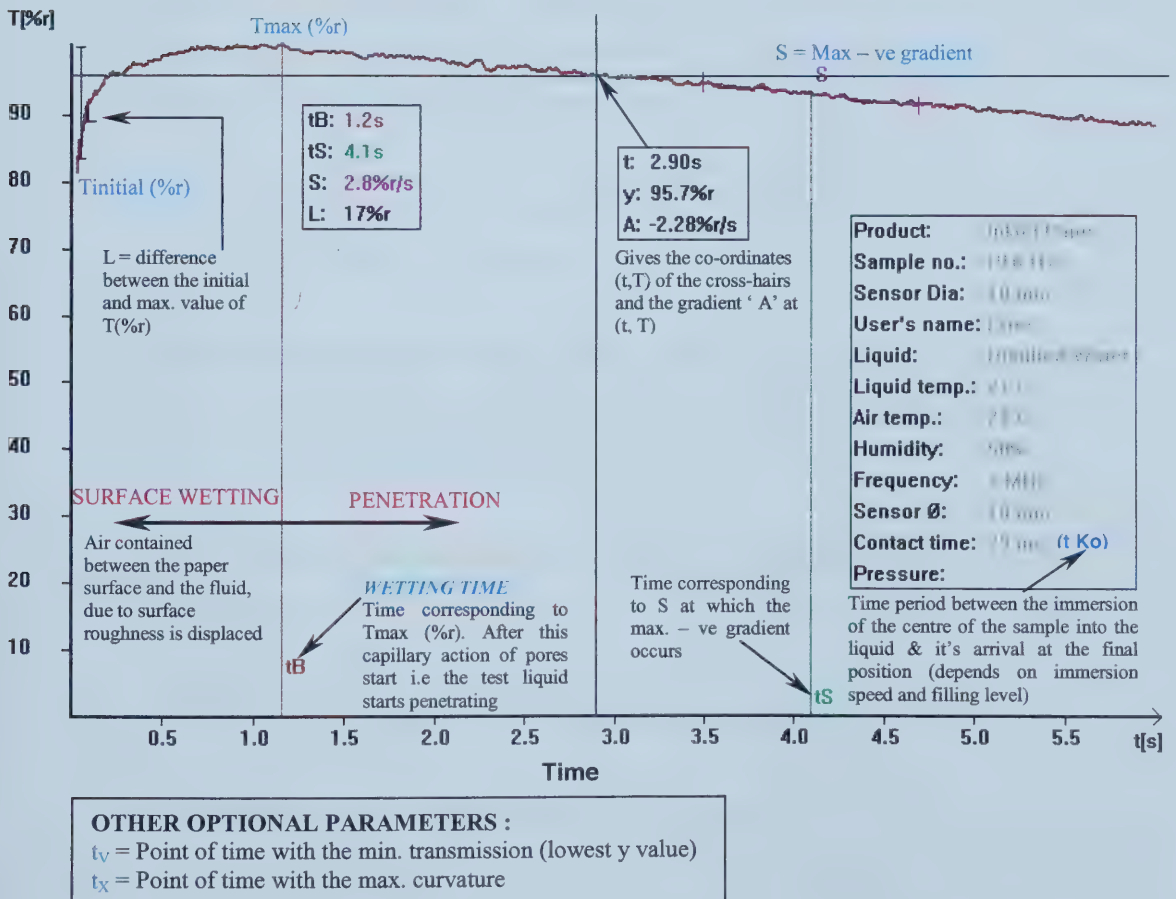


For each curve, the Emco software also calculates several mathematical parameters, which are summarised in Figure 3.7. The output curve typically consists of three regimes

1. **Wetting Regime** - Primarily this involves wetting (with negligible bulk penetration) of the surface of the sample and the displacement of the air from the inter-fibre pore space i.e. the air between the fluid front and the surface of the sample is removed. This displacement of the air from the sample surface causes an increase in the ultrasonic signal. The corresponding time period for this phase is called the 'wetting time' and is dependent on the surface roughness of the paper and its chemical hydrophobicity (i.e. the contact angle between the wetting liquid and the paper surface)
2. **Penetration regime** - After surface wetting occurs, the liquid is drawn into the bulk of the sample due to capillary action. The penetration involves a composite mixture of solid, liquid and air phases. The air from the sample is displaced as the liquid penetrates. In the case of paper and water as the test liquid, this phase may also involve swelling of the paper fibres and destabilization of the material's composition due to breaking of the inter-fibre hydrogen bridge bonding. Fibre components such as cellulose, and hemicellulose have a strong affinity for water molecules. Physically paper fibres have a hollow core (lumen) and micro-porous fibre walls in which the pores can be filled with water. Absorption of water causes the fibres to swell along the length and laterally. However, lateral swelling is around 15-20 times greater than lengthwise swelling. During absorption of water in paper structure, the ratio of swelling in the machine direction, cross direction and z-direction is around 1:2:50. In terms of the current study, this swelling phenomenon is highly pertinent since it influences the material propagation characteristics of an ultrasound wave. Depending on the system (paper grade and liquid penetrant) involved, during the penetration regime, the ultrasound signal may increase or decrease in comparison with dry, air-containing material.

3. **Soaking / Saturation Regime** - Occurs after completion of the penetration phase. No more liquid is absorbed into the sample. In the case of paper, swelling may still occur in this regime. Once the liquid is no longer being absorbed and the sample material is no longer changing due to swelling etc., the signal becomes constant. This step may take several hours or days, depending on the system involved. This regime essentially corresponds to the equilibrium of bulk capillary (inter-fibre) and swelling (intra-fibre) processes.

Figure 3.7: Emco DPM-30 Measured Parameters



The mathematical parameters which are calculated by the Emco software to describe the output curve are related to the above time regimes and are explained by Emco as follows (Figure 3.7)

'L%' is defined as the difference between the maximum transmission value of the output curve and the initial transmission value. This initial increase in signal correlates with the volume of air which is removed from the surface of the sample during the wetting phase.

The duration of this process is defined as ' t_B ' i.e. the time at which the initial maximum transmission value is recorded. ' t_B ' is significantly influenced by the surface activity (wettability) of the paper structure.

'S' is defined as the maximum negative gradient of the curve and the time instant corresponding to this value of slope is called ' t_S '

Other parameters that are possible in the software output but which are not used as often are ' t_V ' which is the time at which the transmission value is lowest and ' t_X ' which is the time at which the curvature is maximum.

A good insight into the different processes occurring that affect the nature of the output curve obtained from the ultrasonic measurement method is given by Stor-Pellinen et al (2000) and are summarized below. The major factors affecting the transmission of the ultrasound signal during a measurement are:

1. Transmission through a rough and porous sheet

When a paper sample is immersed into a liquid, it can be considered as a three-layer system (wetting liquid, air and paper). Since paper is porous the velocity of sound in paper will lie between the velocity in pure cellulose (~2000 m/s) and the velocity in air (340 m/s). The velocity of sound in water is (1480 m/s), but the density of wetted paper is different from water and of pure cellulose.

When the liquid starts penetrating the paper sample, these factors will affect the transmission of the signal through the sample. Considering a case of orthogonal incidence of the ultrasound signal, the acoustic attenuation due to acoustic impedance can be given by

$$A_2 = T_2 A_1 \quad (3.15)$$

$$A_1 = T_1 A_0 \quad (3.16)$$

$$A_2 \times T_1^2 A_0 = (1 - R_1^2) A_0 \quad (3.17)$$

$$\frac{A_2}{A_0} = \left(\frac{2Z_2}{Z_1 + Z_2} \right)^2 \quad Z_2 < Z_1 \quad (3.18)$$

$$\frac{A_2}{A_0} = \left(\frac{2Z_1}{Z_1 + Z_2} \right)^2 \quad Z_2 > Z_1 \quad (3.19)$$

where

T_1 = Transmission coefficient into the sample

T_2 = Transmission coefficient out of the sample

R = Reflection coefficient

A_0 = Amplitude of the incident sound

A_1 = Amplitude of the sound transmitted into the sample

A_2 = Amplitude of the sound transmitted out of the sample

Z_1 = Specific impedance of the wetting agent

Z_2 = Specific impedance of the sample

Another factor influencing the transmission is the surface roughness of the sample, both towards the transmitter end and towards the receiver end. Surface roughness can be defined as the vertical standard deviation of the thickness of the sample per unit area. It may be noted that the surface roughness can increase substantially due to swelling after immersion of the sample into the liquid. The

surface roughness causes backscattering of the incident signal. Its impact on the attenuation of the signal is given by

$$\frac{A_1(\lambda, R_q)}{A_0} = \exp \left[- \left(\frac{\sqrt{8\pi} R_q}{\lambda} \right)^2 \right] \quad (3.20)$$

for one surface and by

$$\frac{A_2(\lambda, R_q)}{A_0} = \exp \left[- \left(\frac{4\pi R_q}{\lambda} \right)^2 \right] \quad (3.21)$$

for both surfaces of the sample, where

λ = wavelength of the incident sound

R_q = surface roughness of the sample

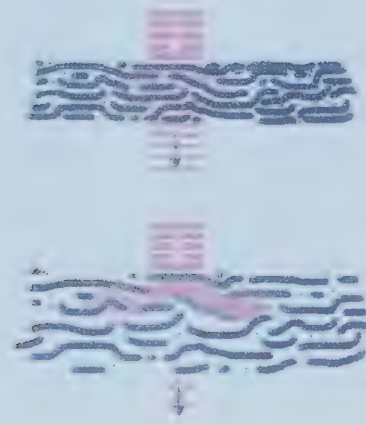
2. Scattering due to air bubbles

The attenuation of sound in a liquid caused by gas bubbles in the liquid mainly result from absorption and scattering effects. After the paper is immersed in the water, the air bubbles from the pores and the roughness volume cause strong scattering of the ultrasonic signal, owing to the differences between the impedance of air and the air displaced by wetting liquid. Depending on the size of the air bubbles relative to the wavelength, the phenomena arising are: diffusion, if $\lambda < D$, stochastic scattering for $\lambda \approx D$ and Rayleigh scattering for $\lambda \gg D$. The attenuation factor is proportional to $D^3 f^4$ for Rayleigh scattering and to Df for stochastic and diffusion scattering. As wetting proceeds and air from the roughness volume and air in the pores of the sample get replaced with water, the transmission signal increases. Further wetting of the fibre walls and fibre lumen causes swelling of the fibres, the effects of which as described below.

3. Effect of stiffness change on transmission

The transmission of the signal in the paper depends upon the structural properties of the paper (mainly the elasticity of the structure). As the liquid penetrates and wets the paper sample, it causes breakage of the fibre bonds and a decrease in the stiffness or loosening of the fibres in the sample as shown schematically in Figure 3.8.

Figure 3.8: Ultrasound transmission in a paper sample during water penetration



This loss of elasticity causes a decrease in the transmission of the ultrasound signal in the sample.

The expression for the absorption coefficient is given by

$$\alpha = \frac{8\pi^2 f^2 \eta}{3\rho c^3} = \frac{8\pi^2 f^2 \eta \sqrt{\rho}}{3K^{1.5}} \quad (3.22)$$

where

f = probing frequency

η = effective viscosity of the system (related to shear modulus of the system)

ρ = effective density of the system

K = effective bulk modulus of the system

The effect of decrease in the stiffness of the paper sample can be seen as a decrease in amplitude of the transmitted sound. The decrease in amplitude is given by

$$A_1 = A_0 e^{-\alpha z} \quad (3.23)$$

$$\frac{A_1}{A_0} = e^{-kK^{-1.5}} \quad (3.24)$$

where

$$k = \frac{8\pi f^2 z \eta \sqrt{\rho_0}}{3}$$

and z = thickness of the sample.

The diffusion of the wetting liquid into the walls of the fibres breaks the interfibre hydrogen bridge bonds. Further, fibre swelling also causes the surface roughness of the paper to increase. This also causes a reduction in the amplitude of the transmitted sound. If the paper is allowed to soak for a considerable amount of time, it will eventually disintegrate into a fibre suspension, in which single fibres are suspended in the wetting liquid. This process will ultimately lead to an increase in transmission.

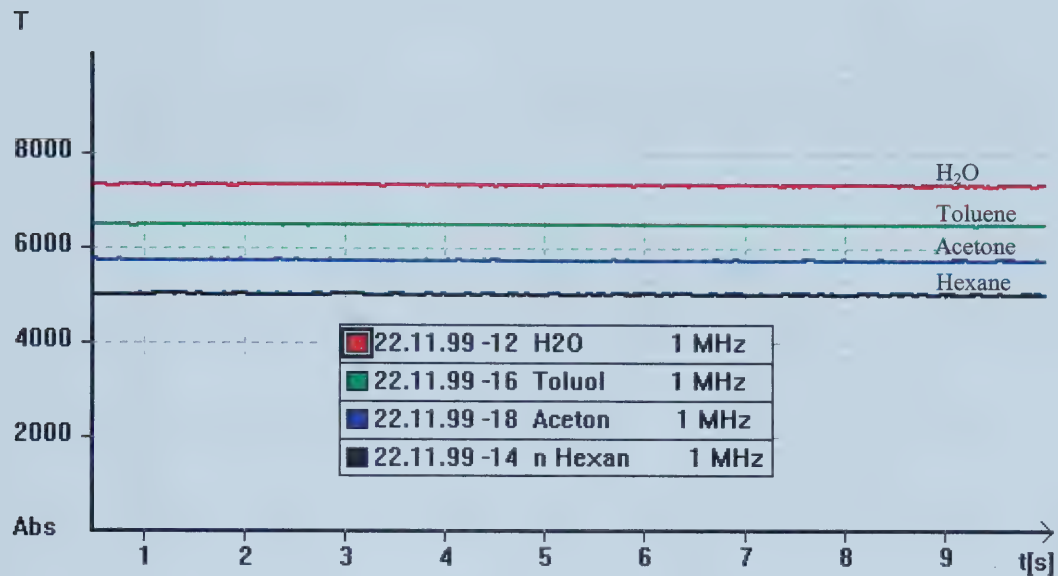
3.5 Other Aspects

- **Standardisation and absolute measurement :**

The ultrasonic wave loses power when it passes through the probe liquid, the sample and the adhesive tape. The power of the transmitter can be changed so that the receiver collects an analysable signal. The power is therefore a measure of the resistance of the medium and material in the beginning and during the measurement of the signal. The Emco-DPM saves all these values during the course of the measurement and can produce an absolute graph for each measurement.

The dampening of the signal is dependent on the materials through which the signal passes. As can be seen in Figure 3.9, water has a lower dampening effect to the ultrasonic signal as compared to less polar organic liquids such as toluene, acetone and hexane.

Figure 3.9: Absolute Graphs - Different Liquids in Measuring Cell Insert, 1 MHz frequency (reproduced from Ultrasound Transmission - Theory and Applications © Emco GmbH 2000)



Also from Figure 3.10, it can be seen that compared with water alone, the sample holder and tape further dampen the signal in the measurement cell. The constant absolute transmission value indicates that there is no change in the liquids or sample.

Figure 3.11 shows the curves obtained with measurements for the same paper grade with different sample holders (polypropylene and teflon lined) and different sensor areas. The dampening effect of the sample holder with teflon coating is lower than that of the polypropylene sample holder. It can be seen that the absolute transmission graphs obtained are similar in shape but do not coincide. This is due to the effect of the different sample holders, measuring cell inserts used and sensor effects.

Figure 3.10: Absolute Graphs - Different Materials in Water, 1 MHz frequency
 (reproduced from Ultrasound Transmission - Theory and Applications © Emco GmbH 2000)

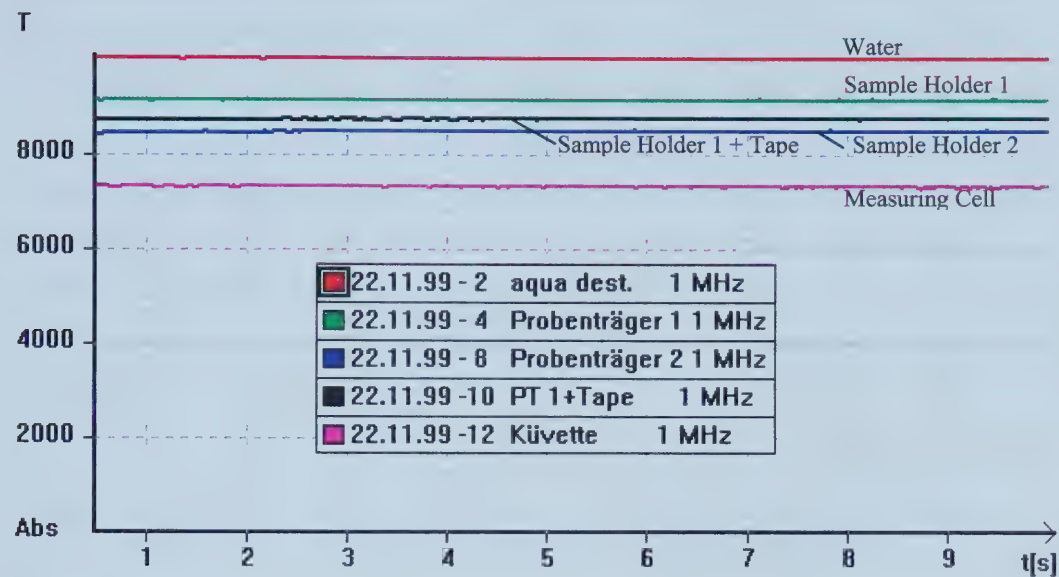
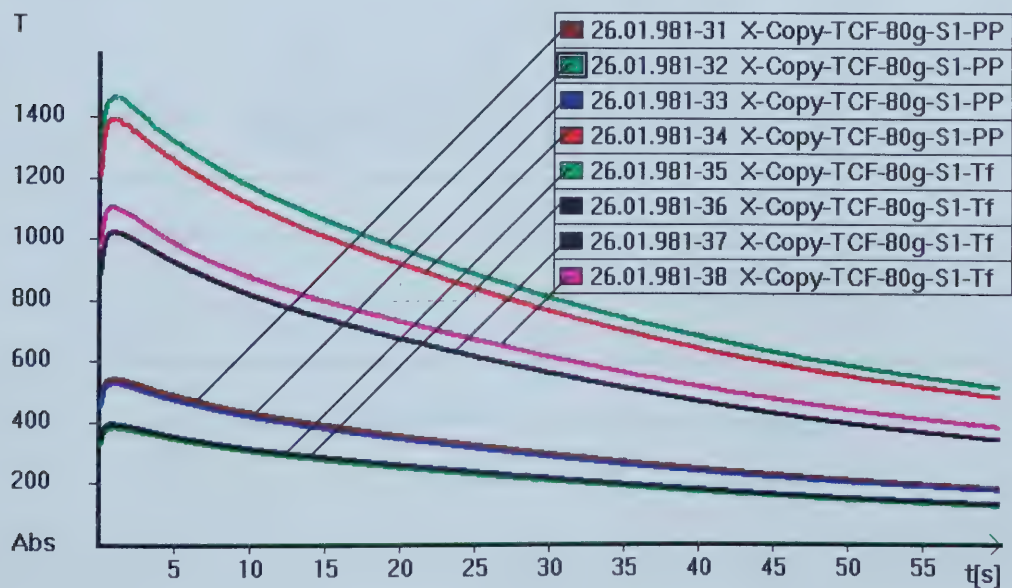


Figure 3.11: Absolute graphs - Same paper grade with different sample holder material and sensor areas, Test liquid - H2O, 2 MHz frequency
 (reproduced from Ultrasound Transmission - Theory and Applications © Emco GmbH 2000)



Standardization is necessary for comparing different dynamic curves. If each curve is normalized on the basis of the maximum absolute value, the different curves for the sample now coincide. Figure 3.12 and Figure 3.13 show the corresponding standardized curves derived from Figure 3.10 and Figure 3.11. Hence, the contributions of the tape, sample holder, dampening effects of the probe liquid etc for different measurements now no longer affect the dynamics. Rather the modified penetration curves are now representative of a constant signal with different T_{abs} values for different materials, but when normalized the constant signal is at the 100 % value. This is especially useful when comparing dynamics of penetration for different paper grades.

Figure 3.12: Standardized graph for Figure 3.10 (reproduced from Ultrasound Transmission - Theory and Applications © Emco GmbH 2000)

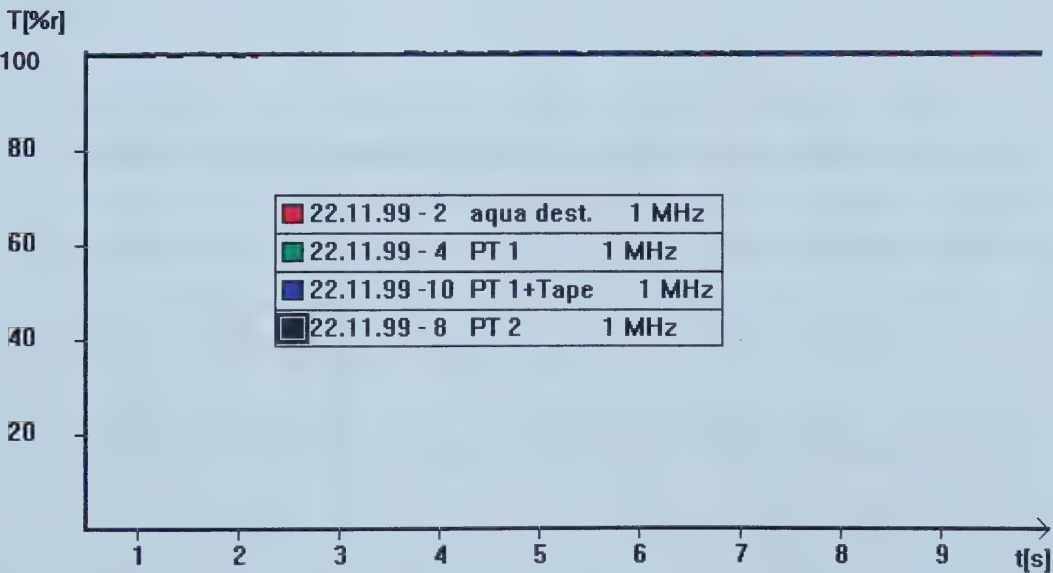
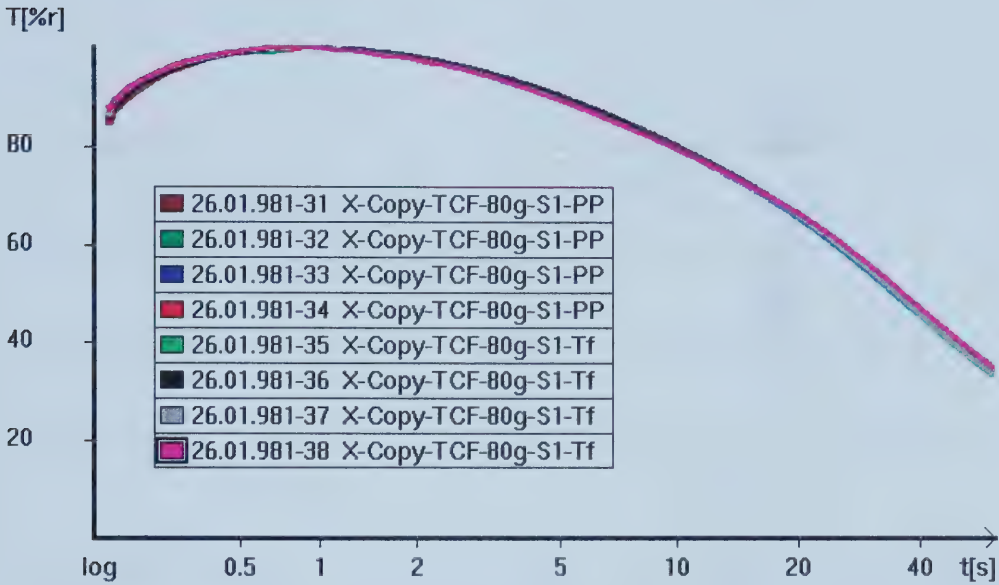


Figure 3.13: Standardized graph for Figure 3.11 - (reproduced from Ultrasound Transmission - Theory and Applications © Emco GmbH 2000)



Standardization also helps overcome the effects of air bubbles trapped between the paper sample and the adhesive tape and the adhesive tape and the sample holder. Air bubbles absorb and reflect the ultrasound totally. The transmitting impedance between the solid/air and liquid/air interface is very high. Thus there are some 'dark spots', as shown schematically in Figure 3.14, in the sample through which no transmission of the ultrasound signal takes place.

At the receiving end, however, the signal received is integrated over the entire measuring area. As shown schematically in Figure 3.15, it can be seen that the air bubbles cause dampening of the ultrasound signal. Since the size and the position of the bubbles do not change during the measurement, the dampening effect remains constant. This influence of the partial coverage of the measuring area by air bubbles can be eliminated by standardizing according to a reference point such as the maximum absolute transmission value. Corresponding standardised curves for measuring areas with and without air bubbles are shown in Figure 3.16.

Figure 3.14: Theoretical measuring area and actual measuring area showing 'dark-spots' caused by air bubbles (reproduced from Ultrasound Transmission - Theory and Applications © Emco GmbH 2000)

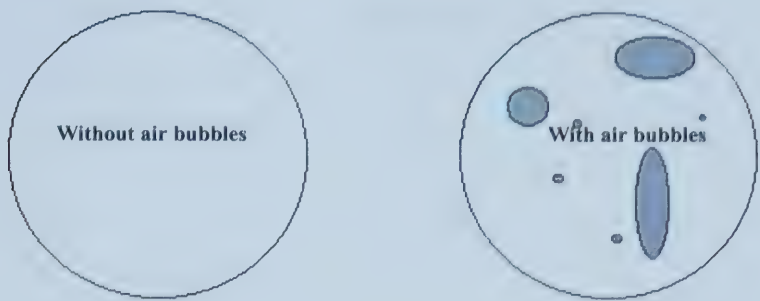
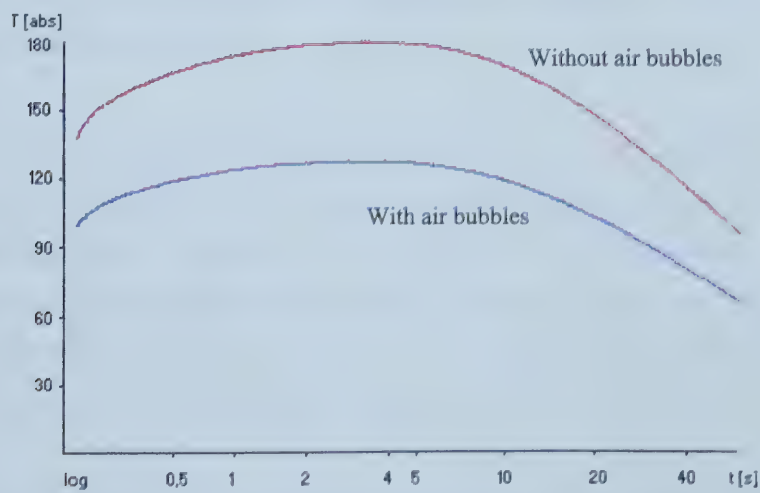
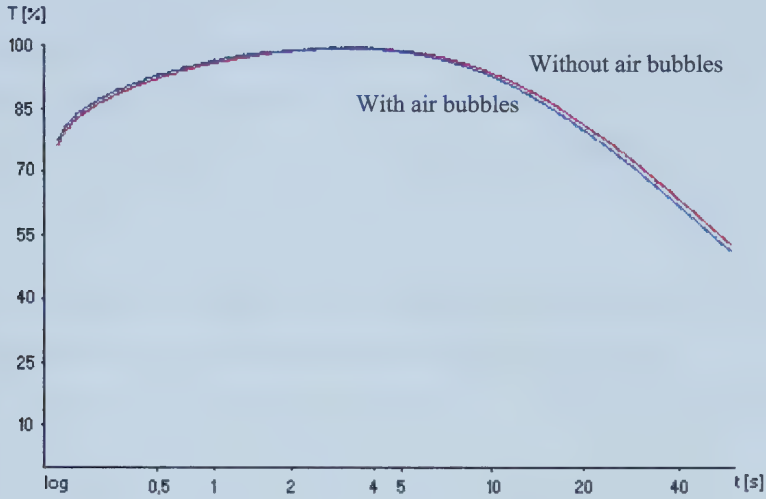


Figure 3.15: Absolute Graph showing effect of air bubbles on the measurement (reproduced from Ultrasound Transmission - Theory and Applications © Emco GmbH 2000)



**Figure 3.16: Standardized Graph (on Maximum) for Figure 3.15 (reproduced from
Ultrasound Transmission - Theory and Applications © Emco GmbH 2000)**



- Measuring area of the instrument was selected by the manufacturer such that the absolute value of transmission at 2 MHz measuring frequency is 10,000 with distilled water in the measuring cell.
- Piezo ceramics are subject to an ageing process as a result of contact with liquids, temperature fluctuations and its use as a sound converter. This has an effect on the ultrasound wave produced. A compensation for each measurement is done automatically during each measurement by the electronics of the DPM 30. The user can check this ageing process aided by an absolute graph in the DPM software and with the electronic measuring cell certificate
- Ultrasound intensity is very sensitive to air content of the sample being tested. The measuring effect is lower with thinner papers with a lower air content as compared to thicker papers. However, no limitations have been specified by the manufacturer on the thickness of the samples or the air content (or porosity). The frequency of the Emco DPM is fixed at 1 MHz or 2 MHz by the manufacturer, depending on the

model. It has been reported to be able to test paper, board, textiles, ceramics, foils and leather, by the manufacturer.

- The instrument also has limitations on the viscosity of the probe liquid. Again no definite value of limiting viscosity is specified by the manufacturer. The manufacturer reports that various liquids such as coating colours, printing inks, glues, varnishes, oils, toluene, starch, latex and resins have been used effectively in the instrument

Summary

- 1) The porous sample is plunged into the path of an ultrasonic signal. Transmission of the ultrasonic signal changes as the liquid penetrates the sample.
- 2) Typical regimes for penetration dynamics for paper are the wetting regime, penetration regime and the saturation regime.
- 3) Parameters generated by the instrument are tB , L , tS and S .
- 4) Sub processes during penetration of polar liquids (e.g. water) into paper and their effect on the ultrasonic signal
 - Displacement of air from the surface roughness volume of paper causes an *increase* in transmission.
 - Displacement of air out of the sample (filling of pores) causes an *increase* in transmission.
 - Wetting of fibre walls results in lower stiffness and elasticity of the fibres and causes a *decrease* in transmission.
 - Swelling of fibres results in breakage of inter-fibre hydrogen bonds and increase in surface roughness and causes a *decrease* in transmission.
 - Scattering of signal due to air bubbles causes a *decrease* in transmission.
- 5) Standardisation of dynamic curves for different systems is necessary for comparison purposes.

4.0 Experimental Work

4.1 Model Pore Structures

Model pore structures were used as a first experimental step in gaining a better understanding of the performance of the Emco DPM. The model pore structures selected were Nuclepore® membranes, Spectra meshes and woven fabrics. The Nuclepore® membranes and Spectra meshes have straight through geometrically well defined pores and can be characterized easily. These were considered as the simplest structures for assessing the ultrasonic method. In comparison to the Nuclepore® membranes and the Spectra meshes, the woven fabrics are not very well defined pore structures. Nevertheless, these pore structures are regular and less complex in comparison to paper and were a good intermediate structure for the purpose of this study.

4.1.1 Nuclepore® Membranes

These membranes have a very precise pore size and narrow pore size distribution and are commonly used in high purity water, food and beverage, pharmaceutical and biological filtration applications. Compared with paper, these are simple pore structures consisting of straight through cylindrical pores which are randomly distributed, as shown for example in Figure 4.1. Commercially available membranes are typically made of polycarbonate or polyester by an ion beam etching process (Kirk and Othmer, 1995). The general characteristics of these membranes per information received from the manufacturer Whatman® (www.whatman.com) are given in Table 4.1. The pore size range available for these membranes from Whatman® is 0.015 microns to 12 microns. For the purpose of the experimental work, membranes of nominal pore sizes 2, 5, 8 and 12 microns were selected. Corresponding specifications for these membranes by the manufacturer are given in Table 4.2. It may be noted that these membranes are two-sided even though they appear to be very smooth on both sides to the naked eye. SEM images of the smooth side or 'glossy side' and of the rough side or 'matte side' are shown in Figure 4.2 and Figure 4.3 respectively. A detail view of the pore on the glossy side is

shown in Figure 4.4 and on the matte side is shown in Figure 4.5. It can be seen that the cross section of the pore is very sharp on the glossy side whereas it is more pitted on the matte side.

The membrane was initially thought to be an 'ideal' model pore structure since it has straight through cylindrical pores. However, further SEM cross-sectional investigations at a later stage revealed that the pores do not have a completely straight through uniform cross-section. Figure 4.6 to Figure 4.9 show that the membrane diameter varies from slightly less than the nominal pore size, on the glossy side, to slightly higher than the nominal pore size on the matte side. For filtration applications, the manufacturer recommends that filtration be done with the glossy side in contact with the service liquid.

Although not exactly 'ideal' structures in terms of having slightly non-uniform cross sectional diameter, these membranes nevertheless were the simplest, most definable and easily available model pore structures for studies on the Emco DPM instrument.

Figure 4.1: Surface View of a 12 micron Nuclepore® Membrane

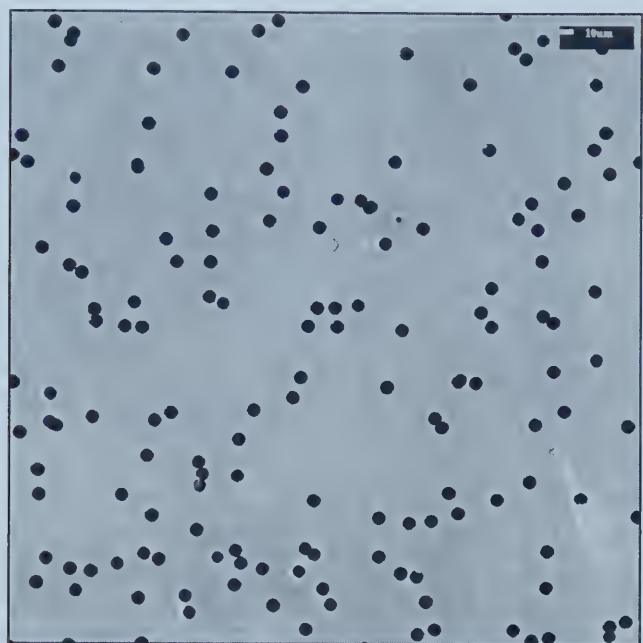


Figure 4.2: Surface View of a 12 micron Nuclepore® Membrane (Glossy-side)

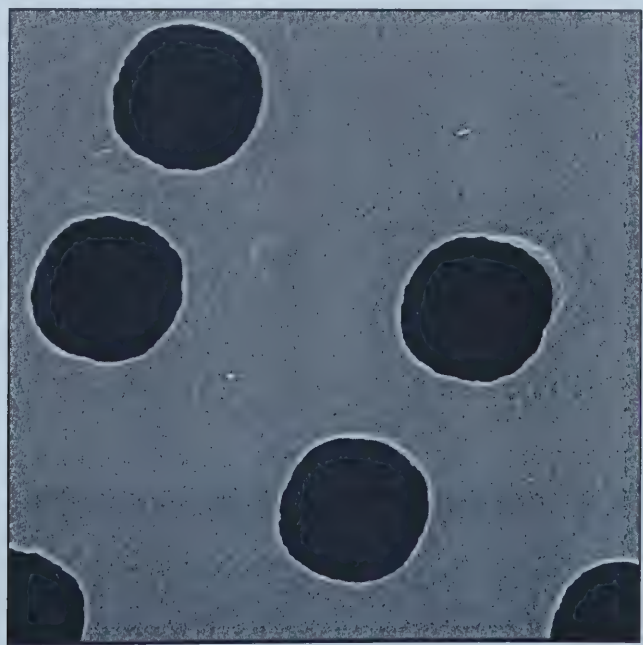


Figure 4.3: Surface View of a 12 micron Nuclepore® Membrane (Matte-side)

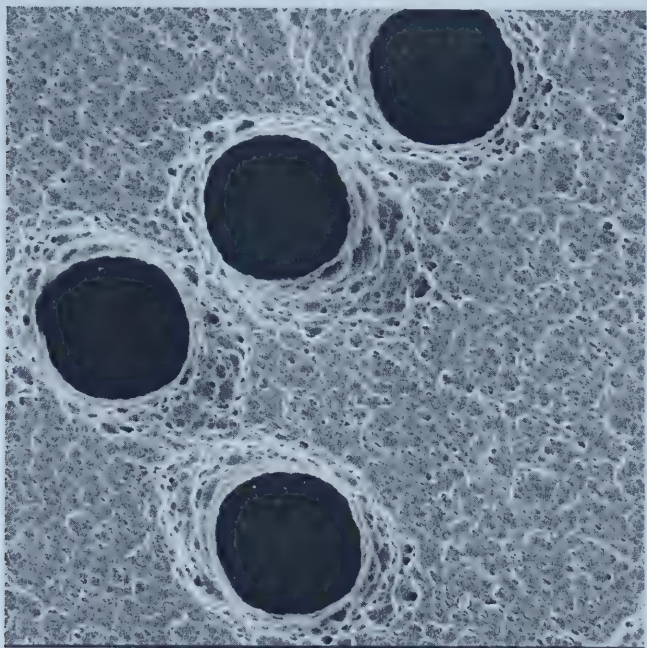


Figure 4.4: Pore detail - 12 micron Nuclepore® membrane (Glossy side)

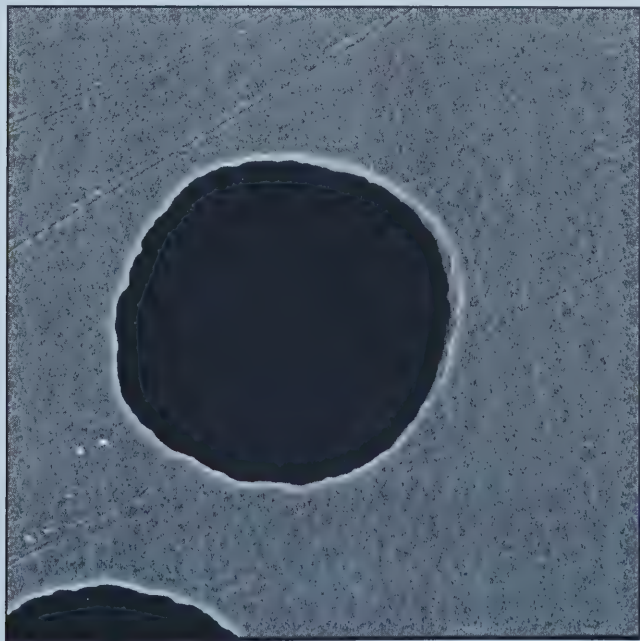


Figure 4.5: Pore detail - 12 micron Nuclepore® membrane (Matte side)

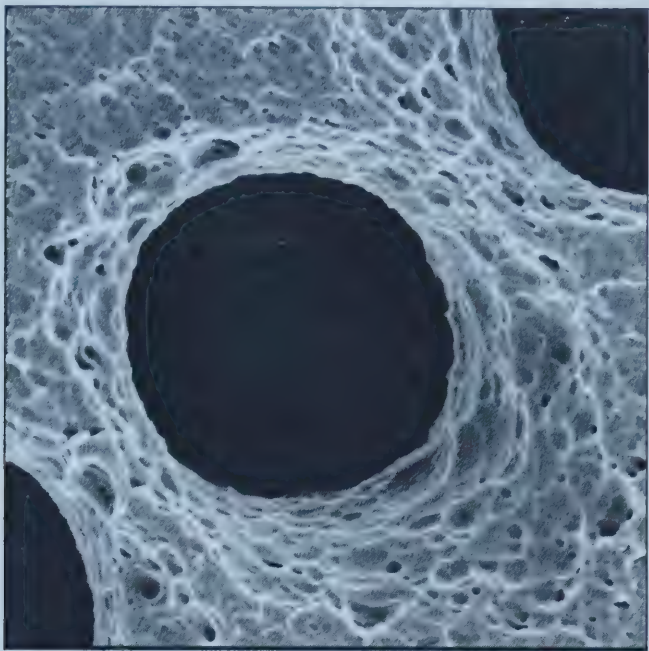


Figure 4.6: Cross Sectional view of a 12 micron Nuclepore® Membrane

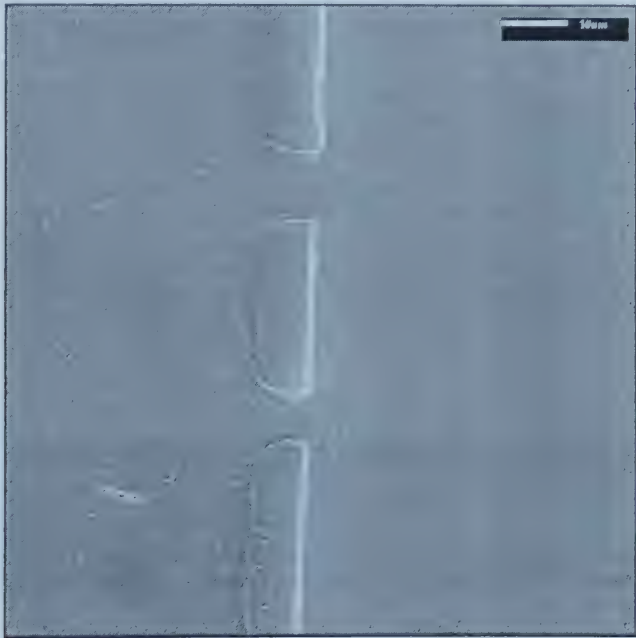


Figure 4.7: Cross Sectional view of an 8 micron Nuclepore® Membrane



Figure 4.8: Cross Sectional view of a 5 micron Nuclepore® Membrane



Figure 4.9: Cross Sectional view of a 2 micron Nuclepore® Membrane

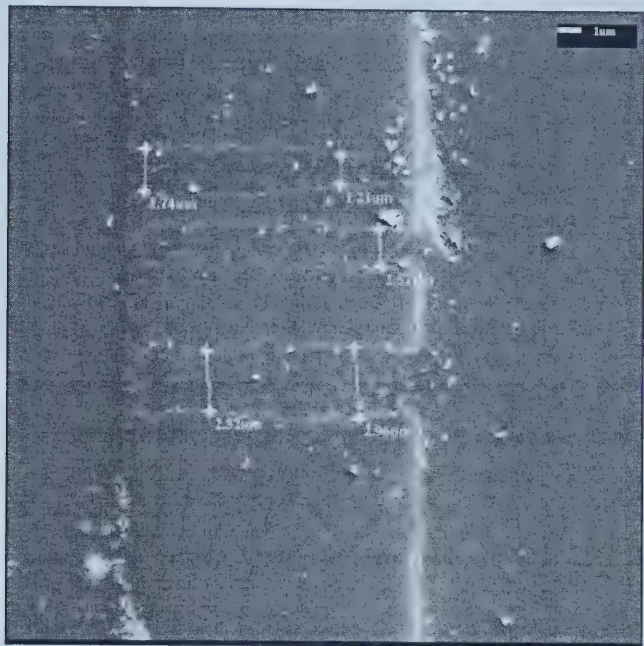


Table 4.1: Nuclepore® Membrane Characteristics © Whatman Inc, 2000

Property		Comments
Material	Polycarbonate	
Thickness (µm)	6-11	
Burst Strength (psig)	>10	1 cm ² unsupported test area
Weight (Tare) (mg/cm ²)	0.6-1	
Specific Gravity Bulk Material (g/cm ³)	1.20	
Heat Sealing Range (°C)	230-275	Difficult to seal
Max Service Temperature (°C)	140	
Flammability	Slow Burn	
Ash Weight (µg /cm ²)	0.92	
Porosity (%)	< 15	
Rated Pore Density (pores/cm ²)	1x10 ⁵ - 6x10 ⁸	Determined by SEM
Rated Pore Size (µm) *	0.015-12.0	Determined by SEM
Surface Texture	Flat and Smooth	
Optical	Translucent	Transparent upon clearing
Refractive Index	1.584 -1.625	
Hydrophilic	Yes	
Hydrophobic	No	
Fibre Releasing	No	
Autoclavable	Yes	121 °C
Water Adsorption (Wt%)	0.24	24 hours in water
Biologic Compatibility	Inert	25 °C
Polymer Structure	Stretched (crystalline)	
Extractables ** (Wt%)	Insignificant	

* Mean pore size is held to a tolerance of +0%/-20% of the Rated Pore Size

** Aqueous extractables are determined by Standard Test Method for Quantity of Water Extractable Matter in Membrane Filters (ASTM D3861-91)

Table 4.2: Nuclepore® Membrane Specifications © Whatman Inc., 2000

Rated Pore Size (µm)	Rated Pore Density ^a (pores/cm ²)	Nominal Weight (mg/cm ²)	Nominal Thickness (µm)	Minimum Water Bubble Point (psi)	Minimum Water Bubble Point (bar)	Typical Flow Rate Water ^b (ml/min/cm ²)	Typical Flow Rate Air ^b (l/min/cm ²)
12.0	1 x 10 ⁵	1.0	8	< 1	< 0.07	3000	85 ^c
8.0	1 x 10 ⁵	1.0	7	2	0.14	2000	40 ^c
5.0	4 x 10 ⁵	1.0	10	2	0.14	2000	55 ^c
2.0	2 x 10 ⁶	1.0	10	8	0.55	350	22

^a Reference only

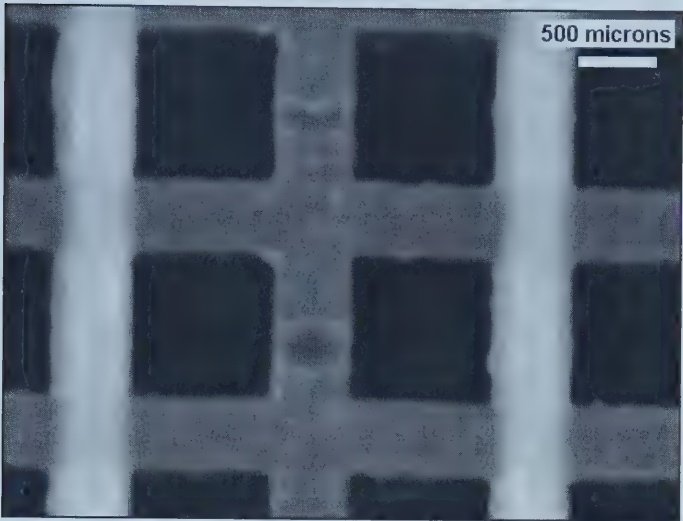
^b Typical initial flow rate using water or air at 10 psi (0.7 bar)

^c 5 psi (0.35 bar)

4.1.2 Voith Spectra Meshes

These pore structure samples were provided by Voith Fabrics (www.voith.com), a manufacturer of papermaking press and dryer fabrics. The sample meshes selected are made of a polyurethane resin and are used as support layers for press felts used in paper machines. These are regular array macropore structures with straight through rectangular or square pores. Pore sizes and thickness of the meshes are of the order of hundreds of microns. Three different types of Spectra meshes were available for testing on the Emco DPM viz. Spectra Q, Spectra T and Spectra F. Optical microscope images of both sides of the different meshes are shown in Figure 4.10 to Figure 4.12. The pores are not clean cut and have some irregularities on one side in the case of Spectra Q. Also the pores are not fully quadrilateral as can be seen in the images for Spectra T and Spectra F. From visual examination of the samples, it appeared that the Spectra F mesh is fabricated from a different grade of polyurethane resin as compared to Spectra Q and Spectra T, which appeared to be similar.

Figure 4.10: (a) Surface View of Voith Spectra Q - Side1



(b) Surface View of Voith Spectra Q - Side 2

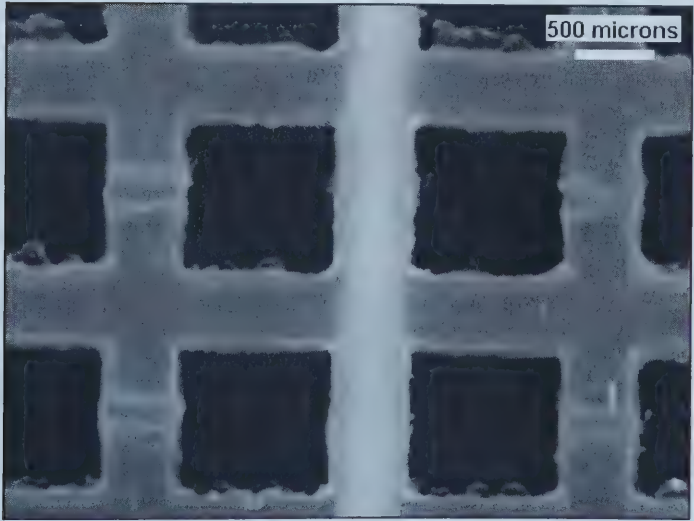
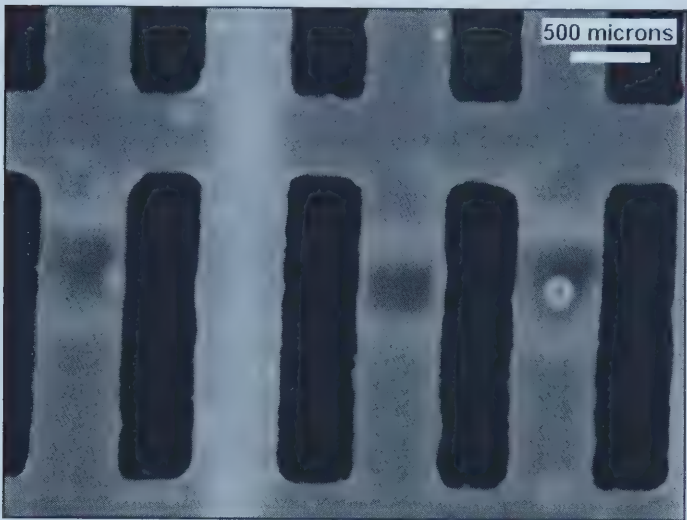


Figure 4.11: (a) Surface View of Voith Spectra T - Side1



(b) Surface View of Voith Spectra T - Side2

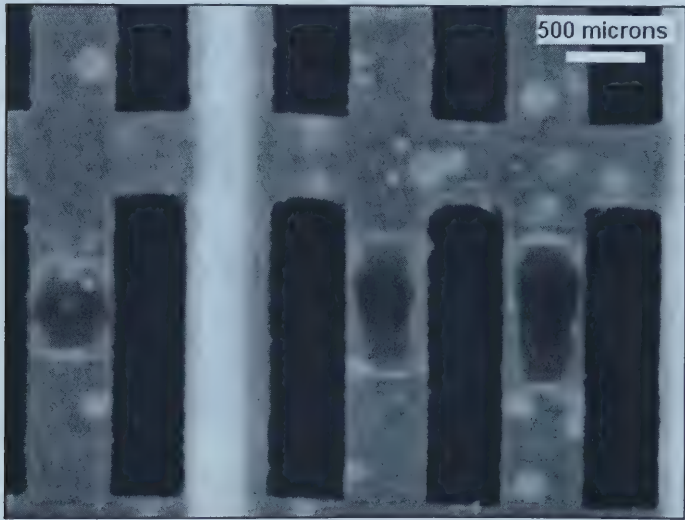
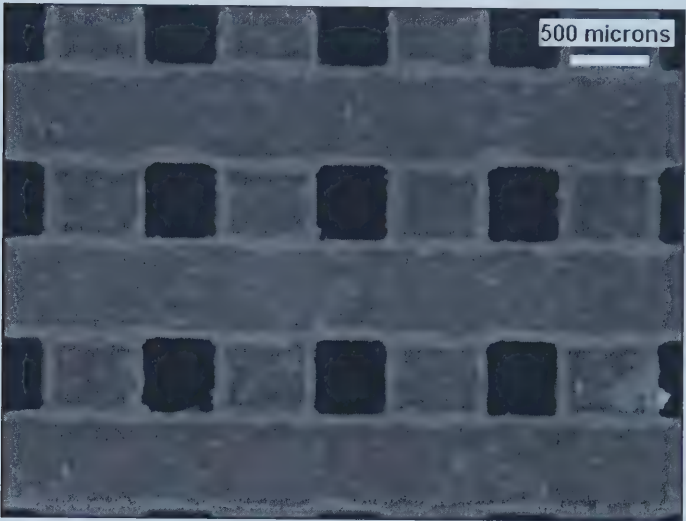
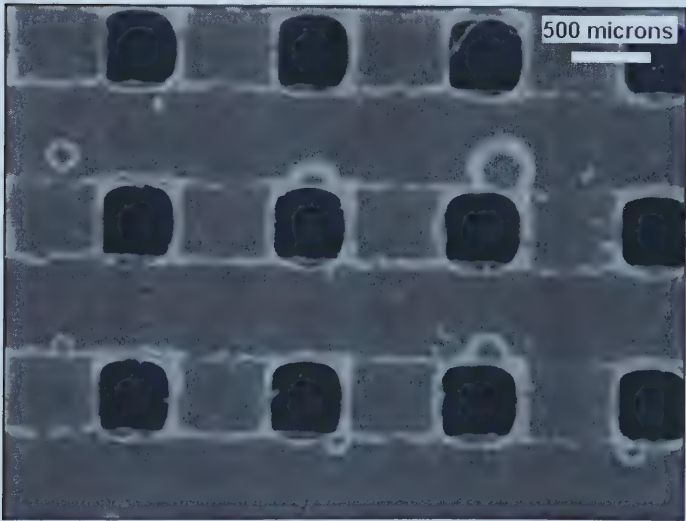


Figure 4.12: (a) Surface View of Voith Spectra F - Side1



(b) Surface View of Voith Spectra F - Side2



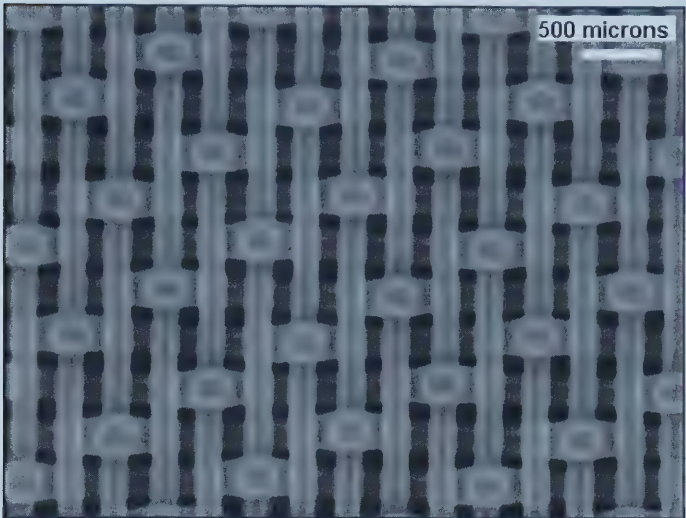
4.1.3 Voith Woven Paper Machine Fabrics

These pore structures were also provided by Voith Fabrics Inc. These structures are woven from polyester terphthalate filament yarn and are used in the forming section of modern paper machines. Their weaves may be single, double or triple layered depending on the grade of paper being manufactured. The set of model pore structures selected are a little more complex than simple straight through pore structures due to the weave pattern. However their pore structures are simple and more definable in comparison with the more complex random network of typical paper structures. Pore sizes and thickness of these fabrics are still of the order of hundreds of microns. Seven different varieties of paper machine fabrics were evaluated.

These are listed below along with a description of the weave type, paper manufacture application and corresponding optical micrograph reference.

- a) Voith 1 - Fine mesh single layer fabric suitable for tissue grades (Figure 4.13)
- b) Voith 2 - Coarse mesh single layer fabric suitable for liner, medium and board grades (Figure 4.14)
- c) Voith 3 - Coarse mesh double layer fabric suitable for liner, medium and board grades (Figure 4.15)
- d) Voith 4 - Medium mesh double layer fabric suitable for news and fine grades (Figure 4.16)
- e) Voith 5 - Fine mesh double layer fabric suitable for tissue grades (Figure 4.17)
- f) Voith 6 - Fine mesh triple layer fabric suitable for tissue grades (Figure 4.18)
- g) Voith 7 - Coarse mesh triple layer - suitable for liner, medium and board grades (Figure 4.19)

Figure 4.13: (a) Surface View of Voith 1 Fabric - Side 1



(b) Surface View of Voith 1 Fabric - Side 2

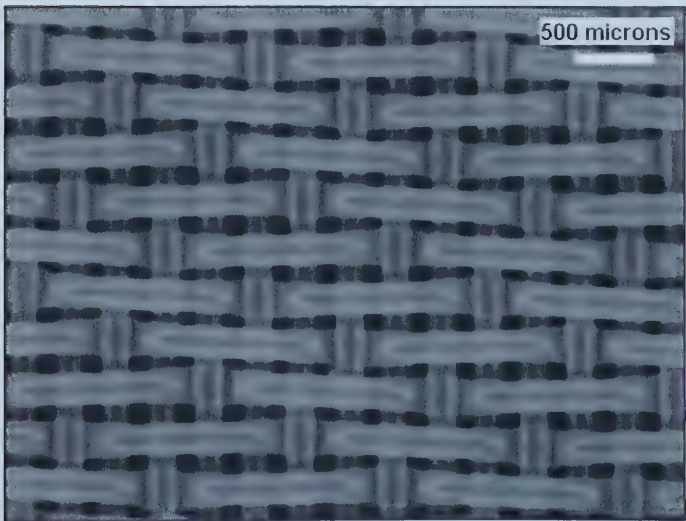
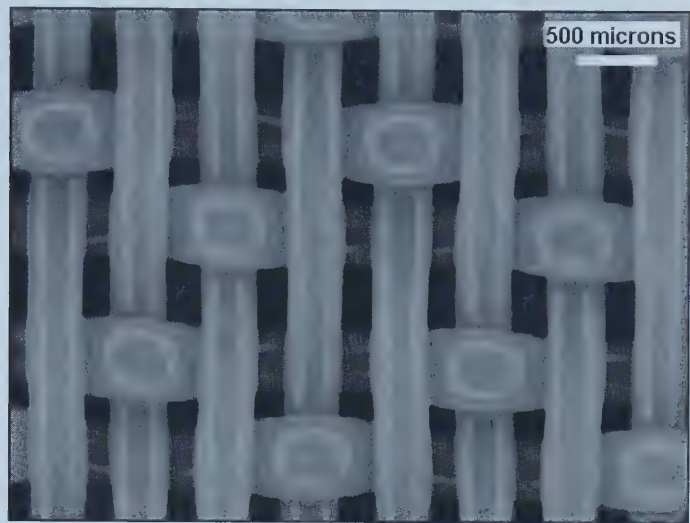


Figure 4.14: (a) Surface View of Voith 2 Fabric - Side 1



(b) Surface View of Voith 2 Fabric - Side 2

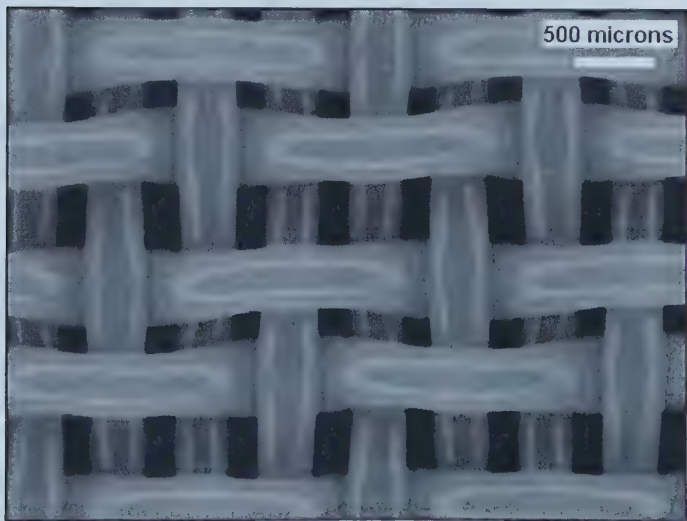
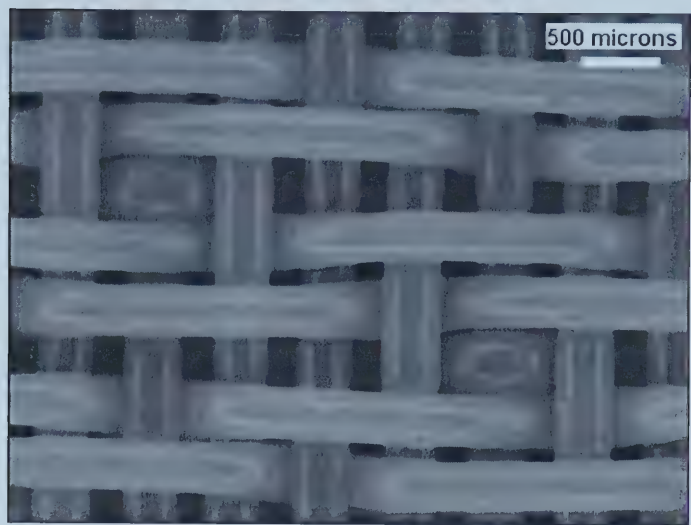


Figure 4.15: (a) Surface View of Voith 3 Fabric - Side 1



(b) Surface View of Voith 3 Fabric - Side 2

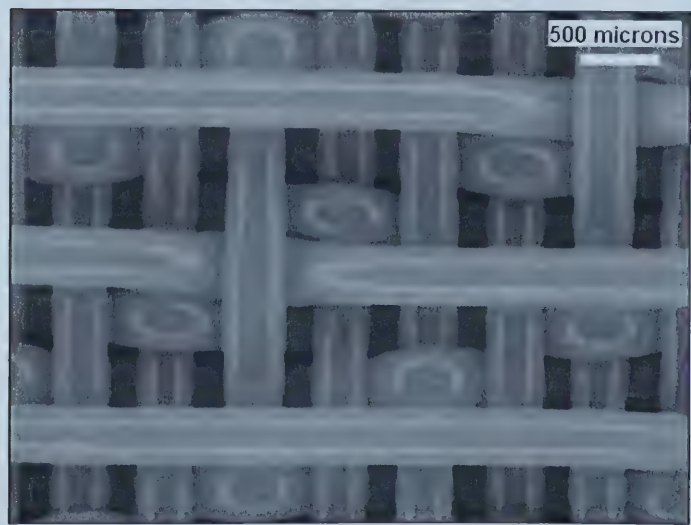
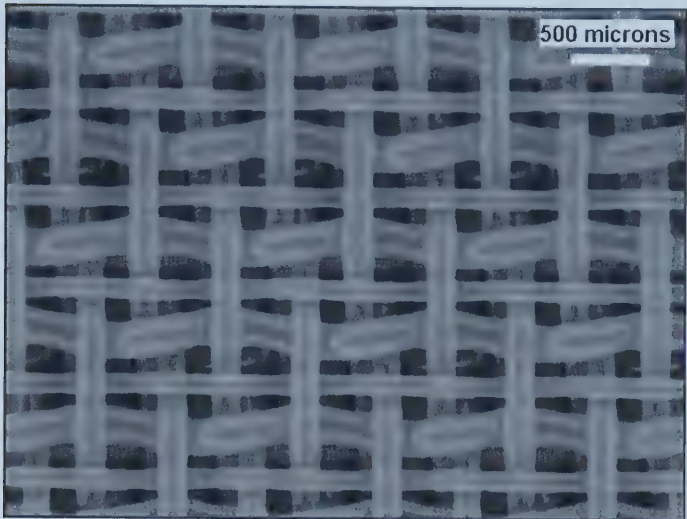


Figure 4.16: (a) Surface View of Voith 4 Fabric - Side 1



(b) Surface View of Voith 4 Fabric - Side 2

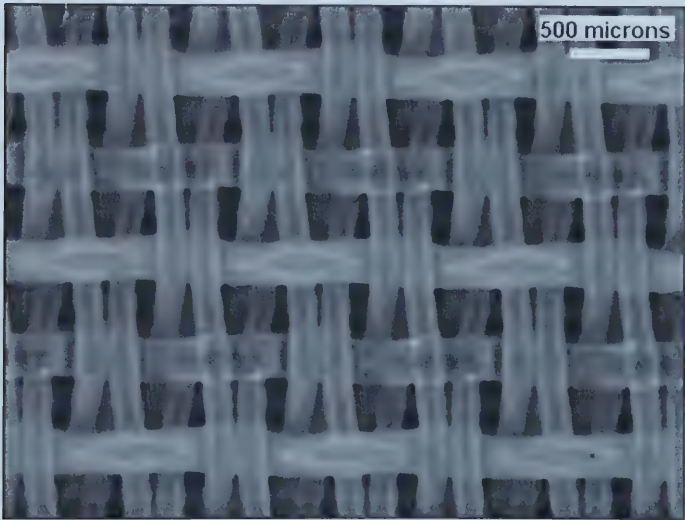
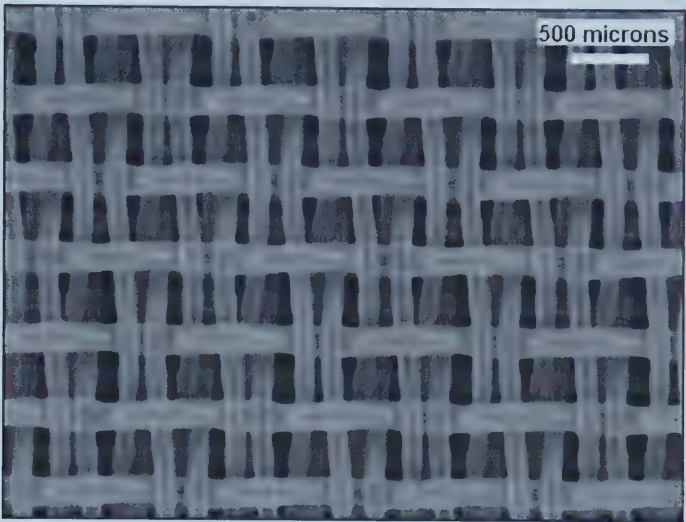


Figure 4.17: (a) Surface View of Voith 5 Fabric - Side 1



(b) Surface View of Voith 5 Fabric - Side 2

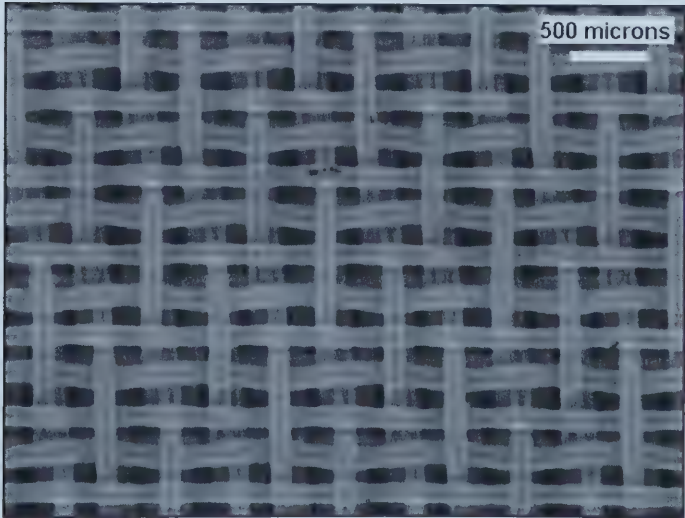
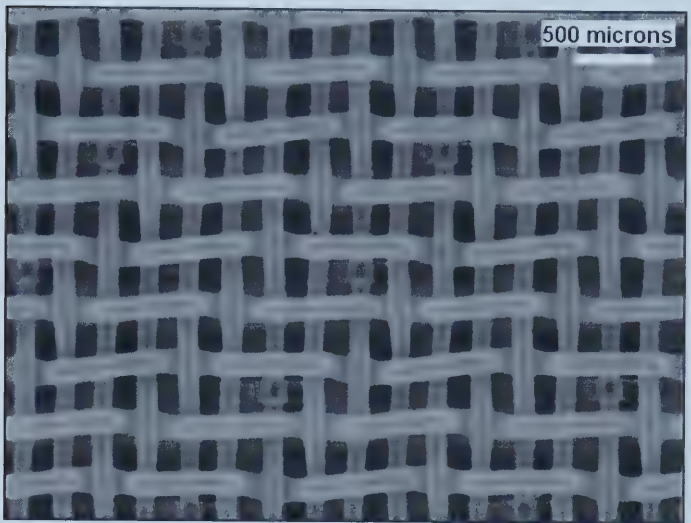


Figure 4.18: (a) Surface View of Voith 6 Fabric - Side 1



(b) Surface View of Voith 6 Fabric - Side 2

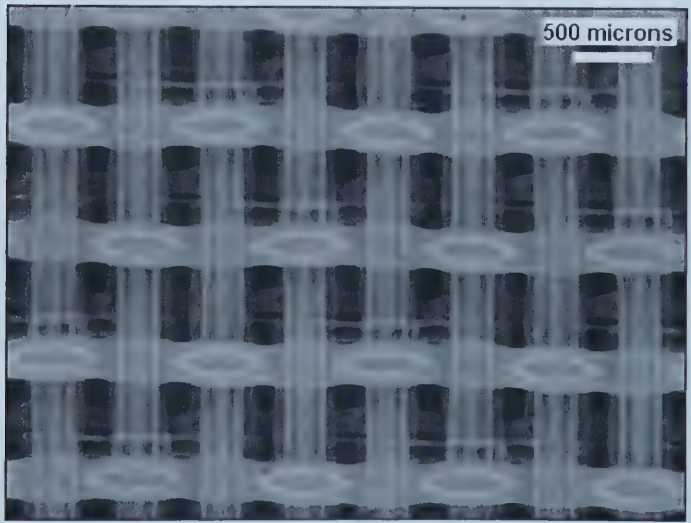
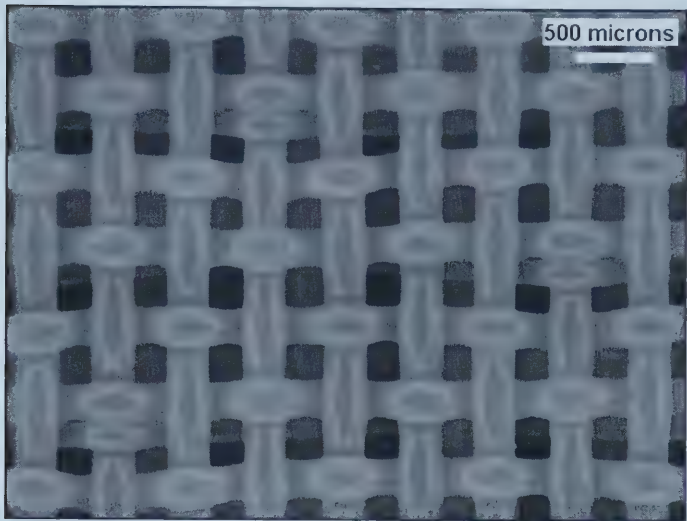
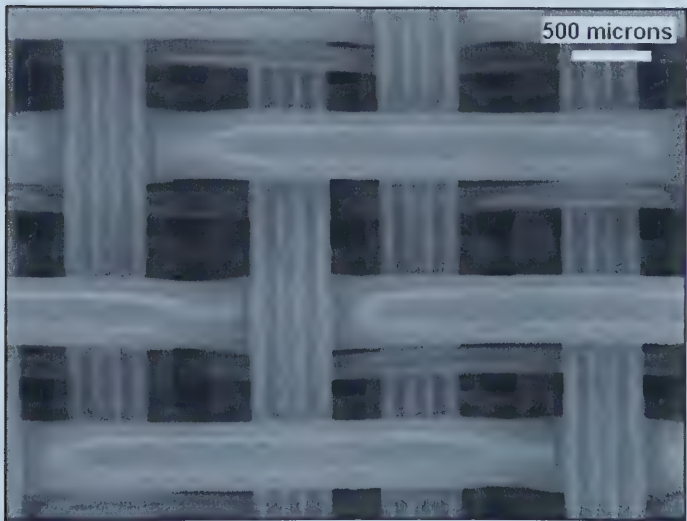


Figure 4.19: (a) Surface View of Voith 7 Fabric - Side 1



(b) Surface View of Voith 7 Fabric - Side 2



4.1.4 Micro-Etch® Screens

These metal screens are manufactured by Buckbee-Mears Inc. (www.buckbeemears.com) by a photochemical etching process. They feature higher tolerance hole sizes and greater dimension stability than woven wire screens, and because they are photochemically etched, the metal is not mechanically perforated, resulting in greater material integrity and a cleaner burr-free perforation. The material of construction is SS316. A surface view of a typical micro-etch screen is shown in Figure 4.20. The pores do not have a uniform straight through cross section as in the case of the polycarbonate membranes. The pores are tapered either from one side through the sample or from both sides towards the centre. The nature of the photochemical etching process does not allow for manufacture of straight through cylindrical pores. The different meshes chosen for this study included hole size range from 120 to 200 microns, porosity range from approx. 10 to 40% and thickness from approx. 125 to 200 microns. Manufacturer’s specifications for the samples chosen are given in Table 4.3.

Figure 4.20: Surface view of Micro-Etch® screen © Buckbee-Mears Inc

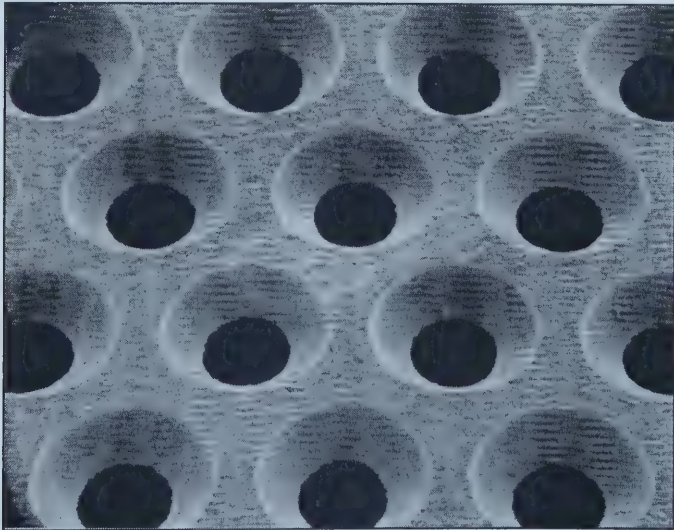


Table 4.3: Micro-etch® screen characteristics

Material Type	Part Number	Thickness (mm)	Hole Size	Hole Profile *	Pitch (mm)	Orientation	Open Area at normal hole size
SS 316	8-6-2	0.203	0.229	B	0.394	90°	26%
SS 316	6-4-4	0.152	0.178	B	0.254	90°	38%
SS 316	6-6-0	0.152	0.152	A	0.394	90°	11%
SS 316	5-3-8	0.127	0.152	B	0.254	90°	28%
SS 316	5-1-4	0.127	0.152	A	0.284	60°	27%

* - Hole Profile Code A: Coned Hole / B: Etched equally from both sides (50/50)

4.1.5 Micro-Mesh® Precision Sieves

These sieves are also manufactured by Buckbee-Mears Inc., by an electroforming process which result in 'smooth', flat surface, non-woven mesh structures as can be seen in Figure 4.21. These sieves are available in either nickel or copper. For the purpose of the study with the Emco DPM, samples chosen had a hole size range of 7 to 140 microns, porosity range of 36-78% and thickness ranging from 5 to 30 microns. Manufacturer's specifications for the samples chosen are given in Table 4.4.

Figure 4.21: Surface view of Micro-mesh® precision sieve © Buckbee-Mears Inc.

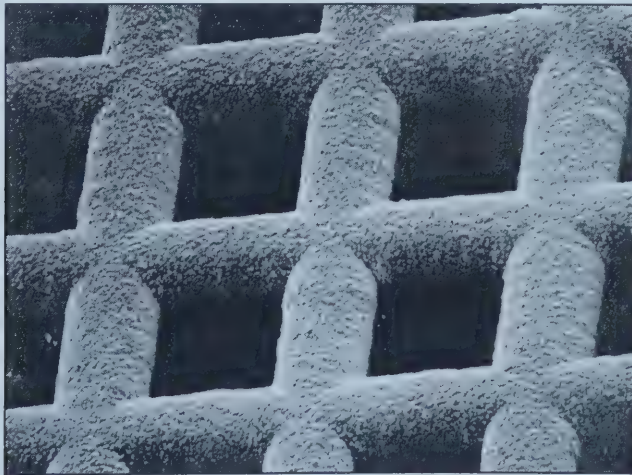


Table 4.4: Micro-mesh® precision sieve characteristics

Lines / cm	Max Size (cm)	Space (mm)	Wire (mm)	Maximum Transmission *	Nickel Part Number	Copper Part Number
787	15.2 x 15.2	0.007	0.005	36.0%	MN - 47	MC - 47
196	27.9 x 27.9	0.039	0.011	59.0%	MN - 41	MC - 41
78	15.2 x 15.2	0.112	0.014	78.0%	MN - 32	MC - 32
59	27.9 x 27.9	0.144	0.024	73.0%	MN - 28	MC - 28

* Transmissions are based on 0.005 mm thickness.

4.2 Commercial Printing Paper Grades and Glass-fibre paper

Commonly used commercial printing paper grades were also identified for tests in this study. They are listed below along with an identification of the manufacturer, application and the corresponding SEM micrograph reference

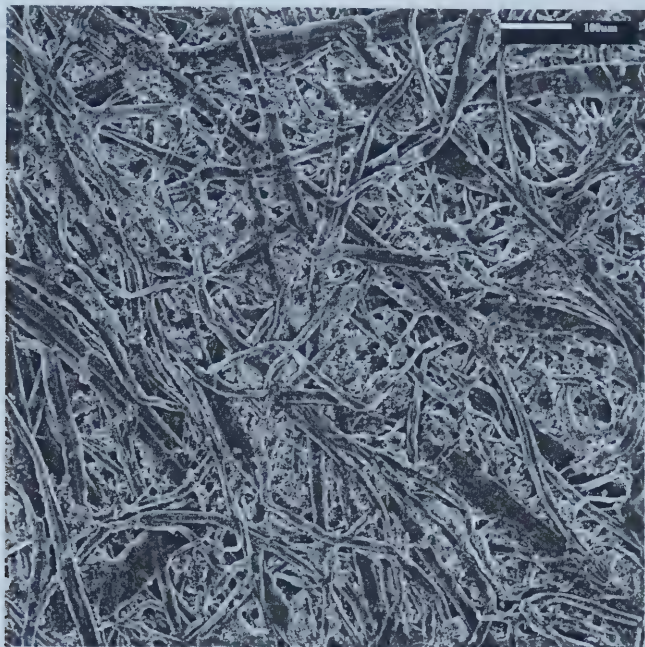
1. Weyerhaeuser First Choice (WFC) 'plain' ink jet grade
2. Hammermill (H) xerographic color printer grade
3. Champion 'plain' ink jet (CIJ) grade
4. Alberta Newsprint Company - Offset newsprint grade (ANC-Off)
5. Alberta Newsprint Company - Rotogravure newsprint grade (ANC-Roto)

In addition to the above commercial paper grades, non-swelling glass fibre paper structures were also identified for testing as part of this study. The grades selected were Whatman® glass microfibre series filter papers and a hydrophobic paper, and are listed below along with the corresponding SEM micrograph reference.

1. Grade GF/A (1.6 μm)
2. Grade GF/B (1.0 μm)
3. Grade GF/F (0.7 μm)
4. Grade 1PS - Phase separating paper, cellulose, silicone impregnated.

The above grades are the currently available equivalent grades to those used by Haynes (1977) in previous studies on kinetics of capillary imbibition. The first three differ in fibre diameter, packing density and particle retention size, while the last grade is a hydrophobic filter.

Figure 4.22: Commercial Weyerhaeuser First Choice (WFC) 'plain' ink jet grade



(Above view magnified x10 times)

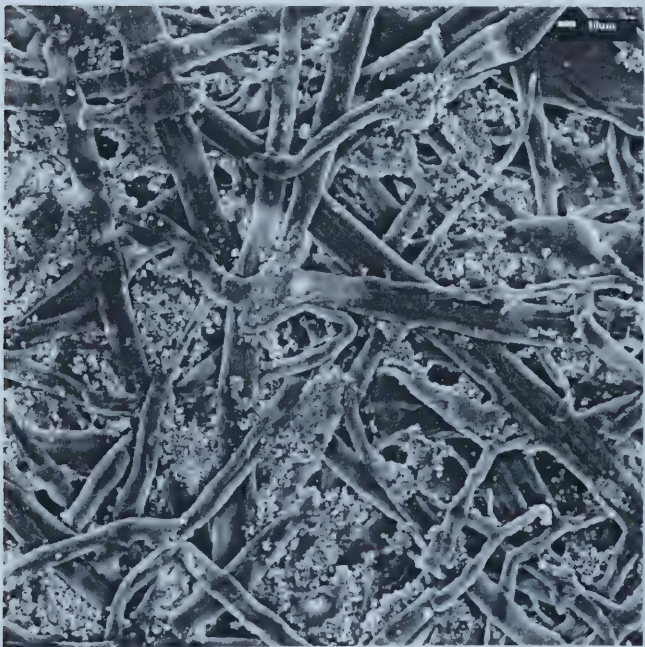


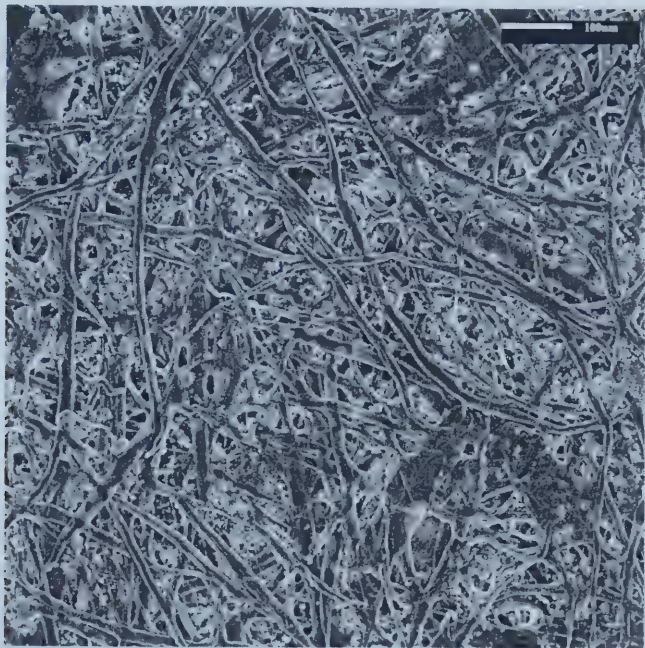
Figure 4.23: Commercial Hammermill (H) xerographic color printer grade



(Above view magnified x10 times)



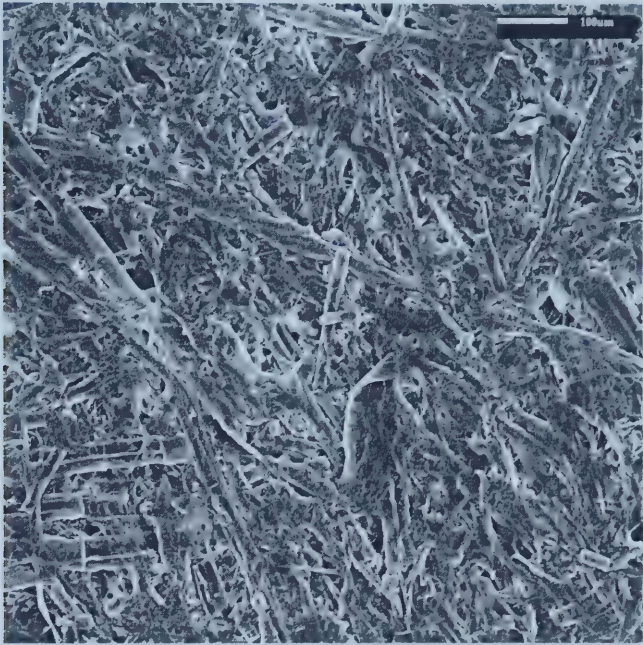
Figure 4.24: Commercial Champion 'plain' ink jet (CIJ) grade



(Above view magnified x10 times)



Figure 4.25: Commercial Alberta Newsprint Company - Offset newsprint grade (ANC-Off)



(Above view magnified x10 times)

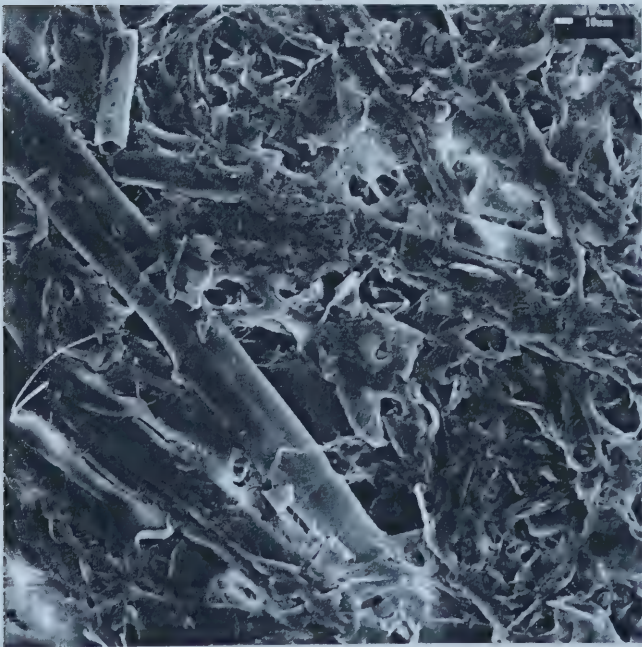
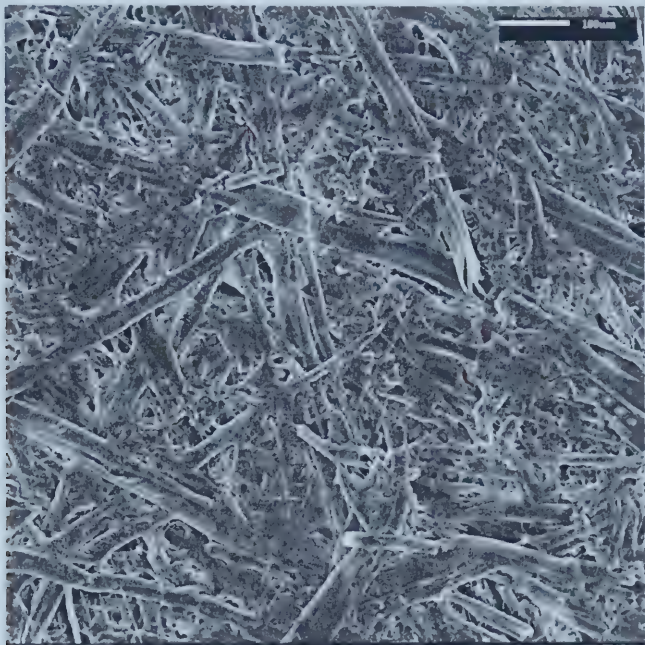


Figure 4.26: Commercial Alberta Newsprint Company - Rotogravure newsprint grade (ANC-Roto)



(Above view magnified x10 times)

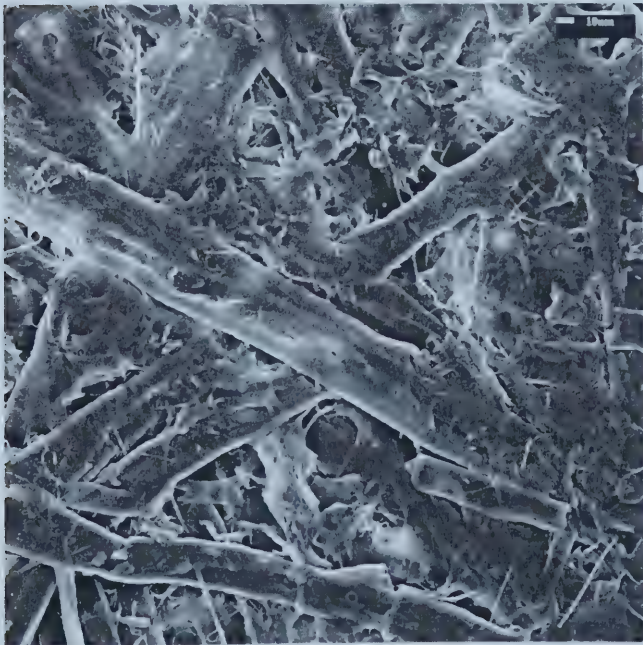
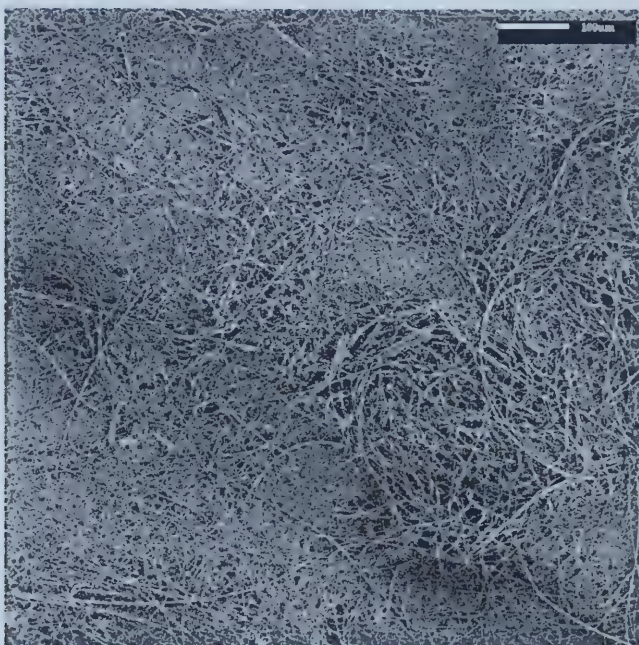


Figure 4.27: Whatman® Glass Fibre Filter Paper Grade- GF/A



(Above view magnified x10 times)

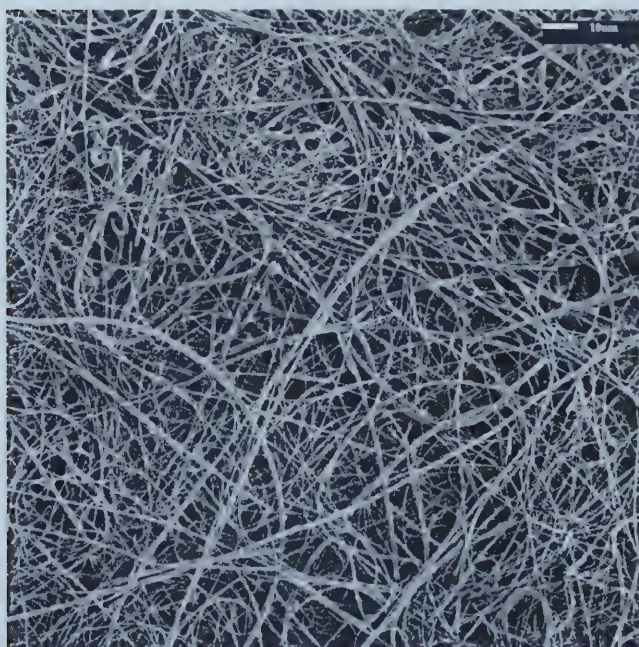
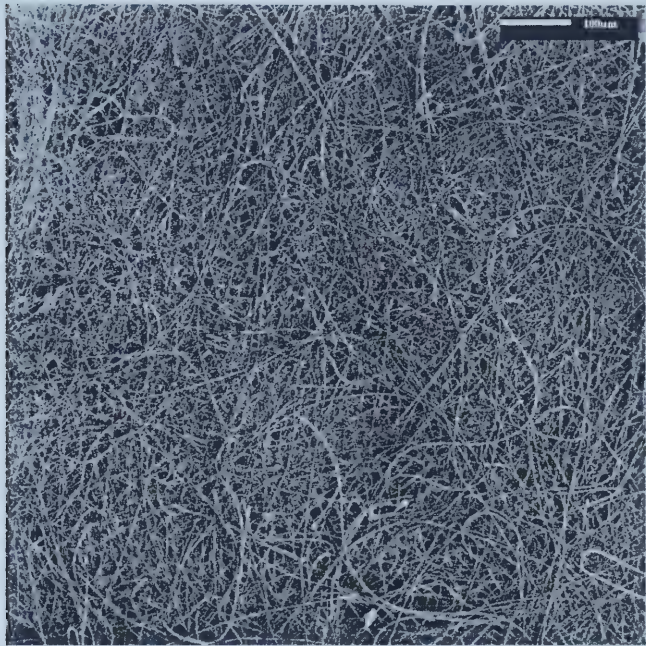


Figure 4.28: Whatman® Glass Fibre Filter Paper Grade - GF/B



(Above view magnified x10 times)

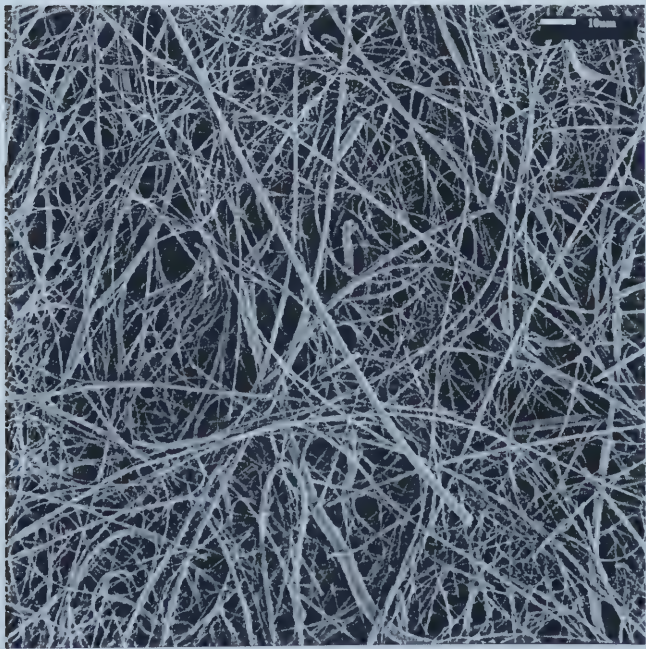
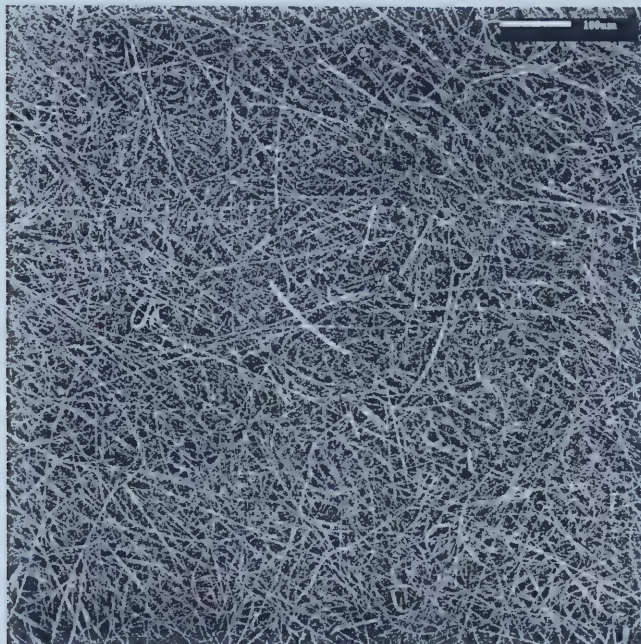


Figure 4.29: Whatman® Glass Fibre Filter Paper Grade - GF/F



(Above view magnified x10 times)

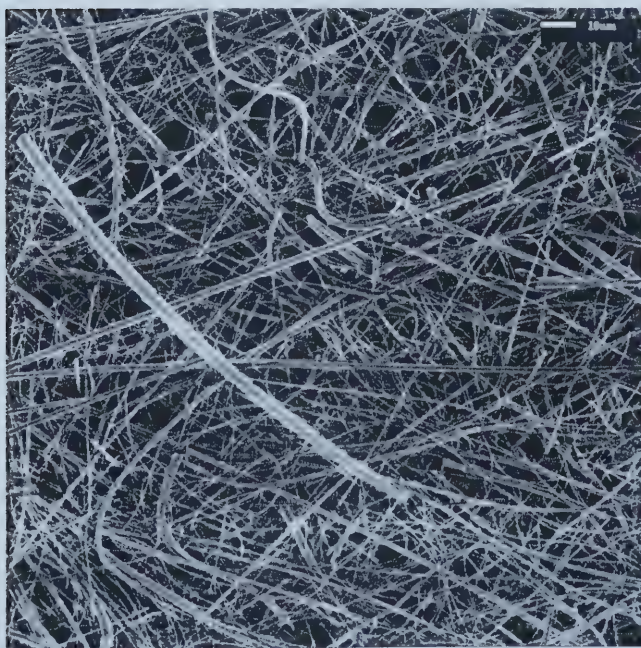
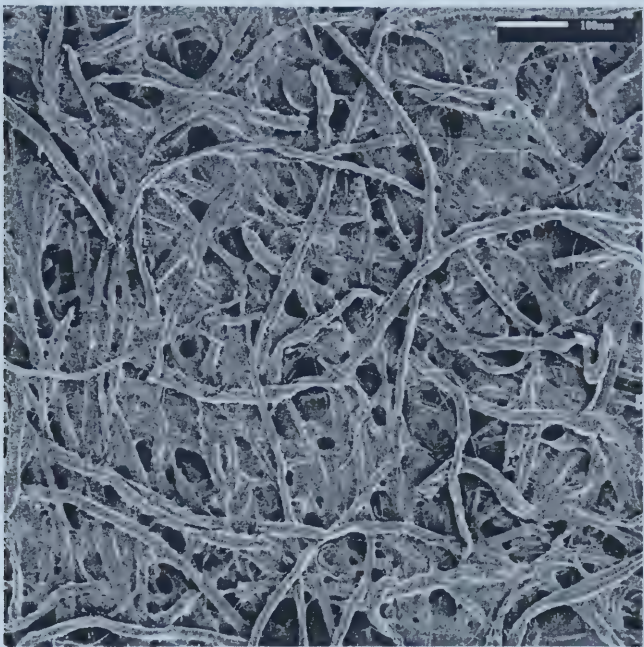
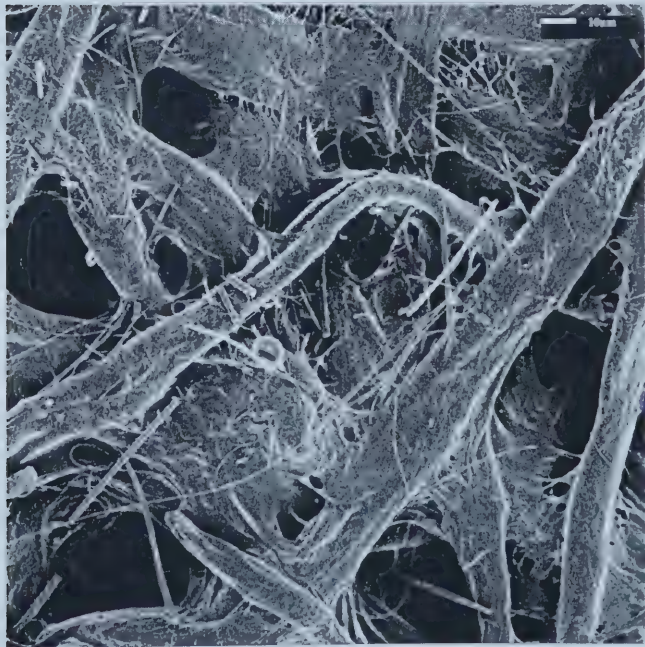


Figure 4.30: Whatman® Phase Separation Filter Paper Grade - 1PS



(Above view magnified x10 times)



4.3 Pore Structure Characterization

The following sections describe the various methods used for characterization of the different model pore structures and commercial paper samples. Permeability of the model pore structures was measured using a variable head permeameter. The paper grades were characterized in terms of pore size distribution, mean flow pore diameter and permeability using a capillary flow porometer. Thickness measurements for all samples were done using an automatic thickness tester. Image analysis was used for measuring the porosity of the model pore structures. Contact angle measurements were done for the model pore structures to describe the wettability for the different probe liquids used. A summary of the results obtained from all the characterization methods used in this study is given in Table 4.17 for the model pore structures and in Table 4.18 for the commercial paper grades.

4.3.1 Permeability Measurements using a Variable Head Permeameter

Darcy (1856) experimentally established that the volumetric rate of flow, Q , through a sand bed was directly proportional to the pressure difference, ΔP across the bed. Darcy's law is valid in the creeping flow regime ($Re < 1$) and can be expressed in a form

$$\frac{Q}{A} = \frac{K}{\mu} \frac{\Delta P}{L} \quad (4.1)$$

where, K , is defined as the permeability of the porous medium.

Permeability can be explained as the ease with which a fluid flows through a porous medium. It depends not only on the porosity of the medium, but also on the tortuosity of the pores. Hence it does not necessarily have a direct correlation with porosity. Two porous media with the same porosity could have largely different permeability values. In the above form of Darcy's law, it can be seen that, K , is dependent only on the nature of the porous medium. Permeability can thus be used as a means of characterizing a porous medium. Permeability is an

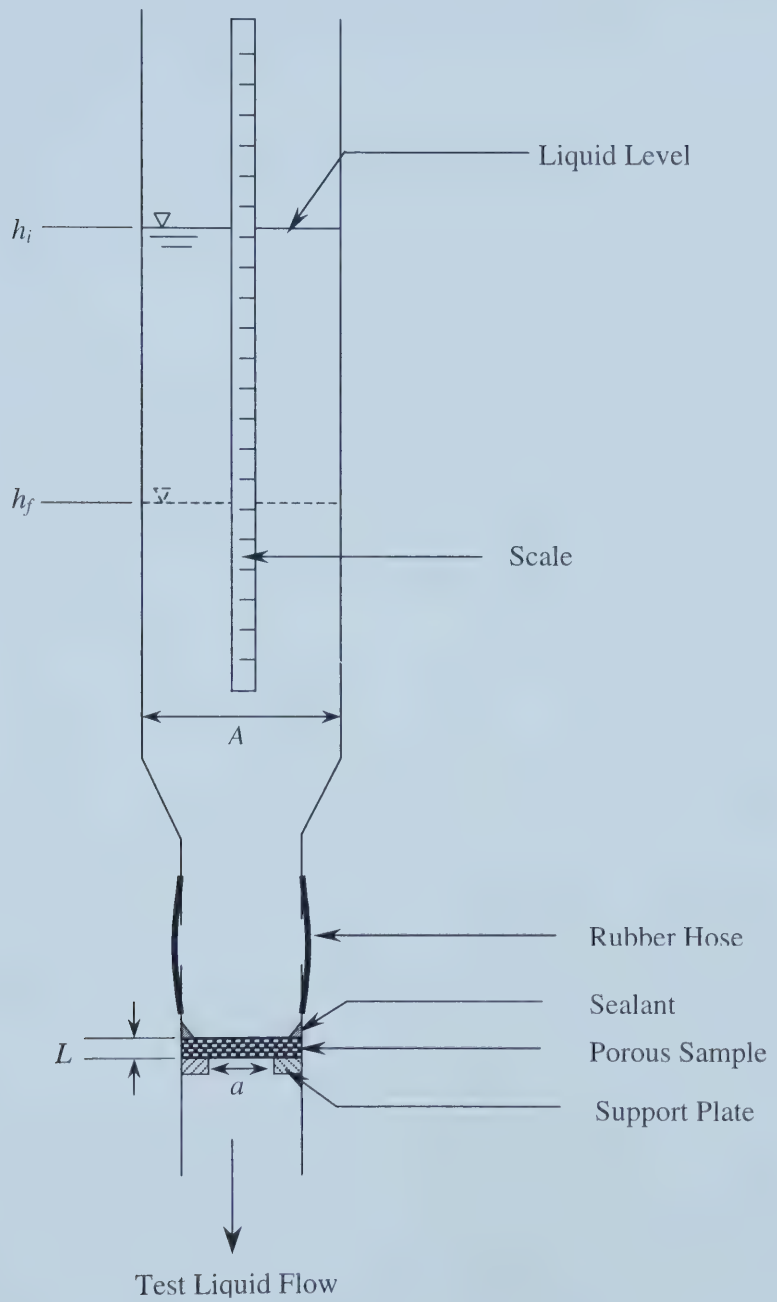
anisotropic property that is dependent on the direction of fluid flow. It is independent of the properties of the fluid flowing through the medium. The permeability of the various model pore structures which were characterized with the ultrasonic method, were determined using the set-up and method described below.

Experimental Set-up

A variable head permeameter type apparatus was used for the determination of permeability. A diagram of the apparatus used is shown in Figure 4.31.

A 1m long glass column of 3.295 cm inside diameter was connected with a rubber hose to another glass fitting in which the porous sample was mounted. A circular metallic ring of inside diameter 1.038 cm (effective flow diameter of the porous sample) was fixed to the inner walls of the lower glass fitting using a sealant. This was used as the support ring for the porous sample. The sealant used formed a metal to glass bond and prevented any leakage along the periphery of the ring. The sealant used was a high temperature silicone gasket maker (Permatex® Ultra Copper supplied by Loctite Canada Inc.). A scale was fixed along the length of the glass column as shown in Figure 4.31 to measure the level of the liquid at any time. The diameters were measured with a Vernier Caliper gauge. An average of three separate measurements are reported and used for further calculations.

Figure 4.31: Variable Head Permeameter



Theory

As shown in Figure 4.31, the different parameters described are:

h_i = initial head of liquid above sample

h_f = final head of liquid above sample

A = cross sectional area of the glass column based on internal diameter

a = flow area for the porous sample

L = thickness of the porous sample

In this system, the head of liquid above the sample and the volumetric flow rate through the sample vary with time. Pressure on the downstream side of the porous sample is atmospheric and on the upstream side is determined by the head of liquid available which drives the liquid through the sample. If at any time, t , the liquid head available is, h , and the volume of liquid in the column is, V , then it follows from Darcy's law that

$$\frac{dV}{dt} = \frac{K}{\mu} \frac{a(h\rho g)}{L} \quad (4.2)$$

Now $V = Ah$ (4.3)

The volume in the column decreases as the head decreases. Therefore differentiating equation (4.3) gives

$$dV = -Adh \quad (4.4)$$

Substitution in equation (4.2) gives

$$-A \frac{dh}{dt} = \frac{K}{\mu} \frac{a(h\rho g)}{L} \quad (4.5)$$

$$-\frac{dh}{h} = \frac{K}{\mu} \frac{a}{A} \frac{\rho g}{L} dt \quad (4.6)$$

Integrating gives

$$-\int_{h_i}^{h_f} \frac{dh}{h} = \frac{K}{\mu} \frac{a}{A} \frac{\rho g}{L} \int_0^t dt \quad (4.7)$$

$$-[\ln h]_{h_i}^{h_f} = \frac{K}{\mu} \frac{a}{A} \frac{\rho g}{L} t \quad (4.8)$$

$$\ln \frac{h_i}{h_f} = \frac{K}{\mu} \frac{a}{A} \frac{\rho g}{L} t \quad (4.9)$$

Rearranging gives

$$K = \frac{a}{A} \frac{\mu L}{\rho g t} \ln \frac{h_i}{h_f} \quad (4.10)$$

The above equation can be used to calculate the permeability from experimental data. A plot of ' $\ln(h_i/h_f)$ ' against ' t ', should give a straight line from whose slope the value of, K , can be calculated.

Experimental Procedure

The circular porous samples evaluated were mounted on the support ring. Sealant was also applied along the junction of the glass walls of the column and the porous sample to prevent any leakage of the test liquid. A rubber stopper was used to plug the outlet of the permeameter and the column was completely filled with the test liquid. A funnel was used to pour the test liquid very slowly down the wall of the glass tube, to prevent air bubbles from forming and being entrapped in the test liquid. After filling, the column was allowed to stand for ~10 minutes. The rubber stopper was then quickly removed from the outlet. The liquid level was allowed to drop a distance of ~ 10 cm from the top of the column. The stopwatch was started and the time for a drop in level for a certain distance (typically ~ 10 cm for most samples) was noted. Before each test run the temperature of the test liquid was noted, in order that the appropriate value of density and viscosity be used in the calculations for permeability. Experimental methods specific to the type of pore structure being tested are further elaborated below.

Nuclepore® Membranes

Initially the membranes were tested with distilled water. It was found that the membranes clogged very easily. Water from a Millipore® Q water purification system was used for the experiments. In the Millipore® Q system, water essentially flows through a Prefilter Cartridge (CP20 012 04), a Super C Carbon Cartridge (CDFC 012 04), two Ion Exchange Cartridges (CDMB 012 04) and finally through a Twin 90 Filter unit (PMEG 090 02). Water from the Millipore Q® unit was further filtered on a 0.22-micron Millipore® filter, under vacuum, before each run to ensure that the water is completely free of any fine particulate matter which could cause plugging of the Nuclepore® membrane pores during the permeability tests. Fresh samples and freshly filtered water were used for each test. The column openings were covered with aluminum foil between runs to reduce any dust contamination from the air.

Voith Spectra Meshes and Voith Fabrics

These samples are more porous than the Nuclepore® membranes. Drainage with water was extremely fast. To slow down the flow through the sample and ensure that the fluid flow was in the Darcy flow regime (Reynolds number < 1), it was necessary to use a test liquid of higher viscosity. For this purpose a 25% by weight polyethylene glycol (PEG) 35000 aqueous solution was prepared and used for the Voith samples. Approximately 2 litres of this solution was prepared using a mixing tank with a helical ribbon impeller. During the dissolution process of the PEG powder in the water, numerous small bubbles were entrained in the liquid. The solution was therefore allowed to stand for a day to allow the air bubbles to escape.

The viscosity of this solution was approx. 0.5 Pa-s. Special precaution was taken while filling the column with the PEG 35000 solution, since the liquid has a very high viscosity, and small air bubbles easily become entrained and take a very long time to escape out of the column. Therefore the liquid was poured very slowly and carefully down the walls of the column. In the case of the Voith samples, the same sample was tested three times with the PEG 35000 solution.

The viscosity of the 25% PEG 35000 solution in the required temperature range at which the permeability experiments were carried out, was determined using a Canon-Fenske Viscometer. The data obtained is given in *Appendix B*. For water viscosity data from literature was used (CRC Handbook, 1988-89)

Results

The results obtained for the Nuclepore®, Voith-Spectra and Voith woven fabrics are summarized in Table 4.5 to Table 4.7 respectively. Three separate runs were performed for each pore structure. The three data sets were used in the plot of $\ln (h_i/h_f)$ versus t . The 95% confidence intervals were calculated for the linear regression coefficient, which gave the slope of the line used for calculating the permeability of the sample. The raw experimental data, the plots showing height versus time information and the plots used for calculating the permeability values are given in *Appendix C*.

Table 4.5: Permeability Calculations - Nuclepore® Membranes

Size (micron)	Pore dia ^a (micron)	Thickness ^b (micron)	Porosity ^c (%)	Viscosity (cP)	Density (g/cm ³)	Slope	Permeability k _{expt} (m ²)
2	1.51	9.25	4.37	0.9111	0.997	0.00059	5.12E-15 ± 0.5%
5	4.20	11.13	5.37	0.9219	0.997	0.00377	3.98E-14 ± 0.6%
8	6.90	8.25	3.80	0.9437	0.997	0.00640	5.14E-14 ± 0.7%
12	10.76	8.50	5.50	0.9437	0.997	0.03537	2.92E-13 ± 0.6%

^a From SEM measurements

^b From Automatic Micrometer measurements (See Table 4.11)

^c From Image analysis system (See Table 4.12)

Table 4.6: Permeability Calculations - Voith Spectra Meshes

Type	Pore size (micron) ^a		Thickness ^b (micron)	Porosity ^c (%)	Viscosity (cP)	Density (g/cm ³)	Slope	Permeability k _{expt} (m ²)
	a	b						
T	429	1929	990.5	34.25	539.86	1.05	0.01400	7.32E-09 ± 0.6%
Q	893	893	809.5	39.05	524.69	1.05	0.02060	8.56E-09 ± 0.1%
F	446	446	777.5	13.05	539.86	1.05	0.00338	1.39E-09 ± 0.5%

^a From Optical Micrograph measurements

^b From Automatic Micrometer measurements (See Table 4.11)

^c From Image analysis system (See Table 4.13)

Table 4.7: Permeability Calculations - Voith Woven Fabrics

Voith Fabrics	Thickness ^b (micron)	Porosity ^c (%)	Viscosity (cP)	Density (g/cm ³)	Slope	Permeability k _{expt} (m ²)
1	442.0	45.6	524.69	1.05	0.001637	3.71E-10 ± 0.1%
2	846.5	44.2	524.69	1.05	0.003480	1.51E-09 ± 0.2%
3	1159.0	39.8	532.71	1.05	0.003379	2.04E-09 ± 0.2%
4	773.0	41.0	524.69	1.05	0.002661	1.06E-09 ± 0.8%
5	552.5	36.6	539.86	1.05	0.001841	5.37E-10 ± 0.1%
6	716.5	32.8	539.86	1.05	0.002778	1.05E-09 ± 0.2%
7	1260.5	37.7	528.53	1.05	0.003283	2.14E-09 ± 0.1%

^b From Automatic Micrometer measurements (See Table 4.11)

^c Estimated from basis weight and density of fabric material (See Table 4.14)

4.3.2 Capillary Flow Porometry

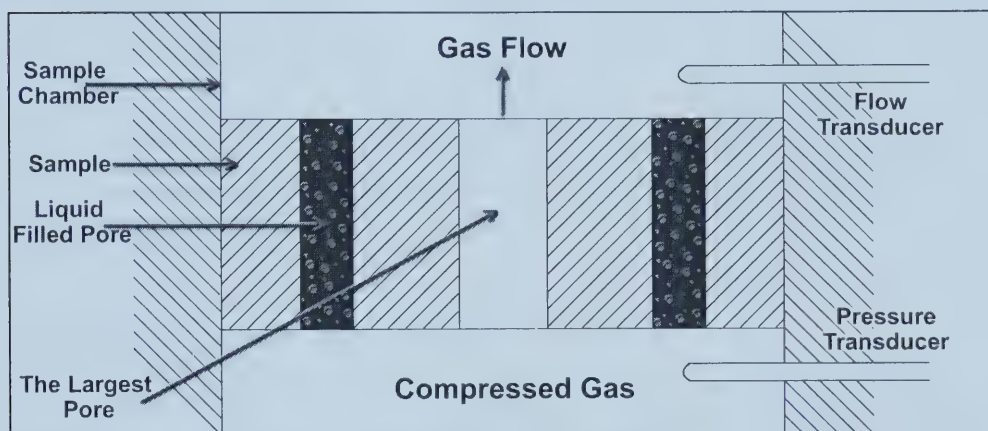
The variable head permeameter described previously was not suitable for permeability measurements with paper samples. The liquid head in the glass column was insufficient for driving any flow through paper samples. Over the years various experimental set-ups have been developed for measuring permeability in paper and other fibrous materials such as textiles. Miller et al (1977,1991,1992) for example developed an apparatus for measuring the in-plane permeability of textile fabrics. Studies on both in-plane and transverse permeability were done by Peterson (1970). Studies on permeability of paper were also done by Lindsay (1990). More recent studies on in-plane permeability were done by Vomhoff (2000). Schwartz (1998) used a commercially available capillary flow porometer (supplied by Porous Materials Inc., www.pmiapp.com) for studies involving flow characteristics and pore size distributions of paper in the transverse or z-direction and the in-plane or x-y direction. For the purpose of this study a Capillary Flow Porometer (Porous Materials Inc., Model AF 18) was used for measuring the flow characteristics of the paper samples. The specifications of the particular model used for the tests are given in *Appendix D*.

Principle of Operation

The test sample is first wet with an inert, low vapour pressure silicon liquid which has a very low surface tension of 16 dynes/cm. A fully wetted sample is placed in the sample chamber and the chamber is sealed. Air is then allowed to flow into the chamber behind the sample (Figure 4.32). The generated flow versus pressure data are stored and displayed in real time producing a 'wet-curve'. The pressure at which the capillary action of the fluid within the pore is overcome (largest pore) is the bubble point. After determination of the bubble point, the pressure is increased and the gas flow is measured until all pores are empty of liquid. The sample is then considered dry and the wet curve becomes linear at this stage. The pressure is then incrementally decreased in steps and the

flow versus pressure data is recorded to produce a 'dry-curve'. The flow - pressure data for the wet sample (wet-curve) and for the dry sample (dry curve) is then used to calculate a number of parameters such as the largest pore size, pore size distribution, gas permeability, envelope surface area and mean flow pore size diameter.

Figure 4.32- Flow Porometry Operation Principle (Gupta K., 2002 © Porous Materials Inc.)

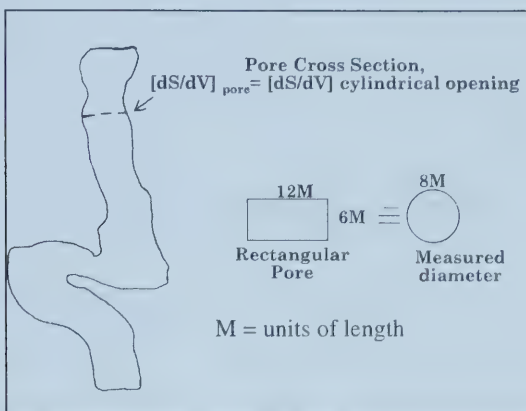


A good overview of the principles of capillary flow porometry and derivations of the equations used to calculate the pore sizes from thermodynamic principles is given by Jena (2002).

Definition of pore diameter:

For systems having cylindrical pores, the pore size is defined by the diameter of the pore. However, in systems which have irregular cross sections, most experimental methods including porosimetry and gas adsorption methods use the following definition for the pore diameter at a given location as shown in Figure 4.33.

Figure 4.33: Pore Size (Gupta K., 2002 © Porous Materials Inc.)

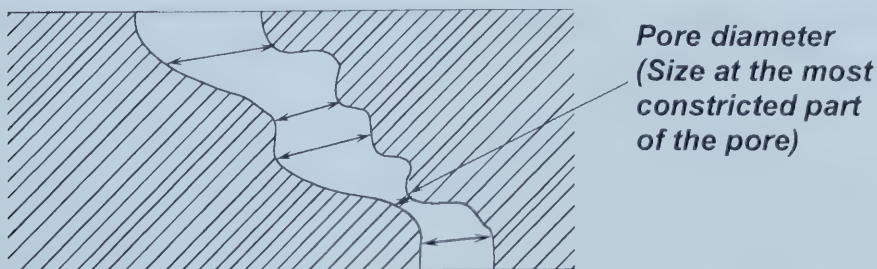


Thus the pore size is defined as the diameter of a cylinder having a surface to volume ratio equal to the measured surface-volume ratio of the pore of irregular cross section.

Measured pore size by flow porometry:

It may be noted that porometry determines the pore diameter at the most constricted part of the pore. The pressure of the gas required to displace the liquid from the pore and overcome its capillary pressure is highest at the most constricted part of the pore as show in Figure 4.34. Only when this pressure is reached is the gas able to displace the liquid completely and permit flow through the pore.

Figure 4.34: Measured Pore Diameter in Porometry (Jena A., 2002a © Porous Materials Inc.)



The pore diameter at a given pressure is calculated from equation (4.11) (Jena A., 2002)

$$D = \frac{4\gamma_{l/g}}{P} \quad (4.11)$$

Measurable Pore Characteristics: (Jena A., 2002)

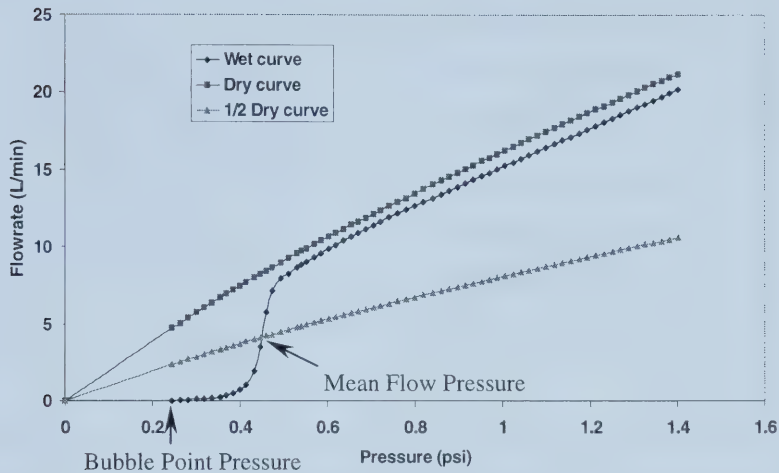
Largest Pore Diameter (Bubble Point Pore Diameter):

The pressure required to empty the largest pore and to initiate the gas flow through the sample is called the 'bubble point pressure'. The corresponding pore diameter at this pressure is called the 'bubble point diameter'. At this pressure the first air bubbles appear in the liquid displaced from the sample. It may be noted that the bubble point diameter of all the pores is the largest of the most constricted pore diameter. A wet-curve obtained from a typical test and the corresponding definition of the bubble point pressure is shown in Figure 4.35.

Mean Flow Pore Diameter:

Typical wet and dry curves are shown in Figure 4.35. From the data of the dry curve, half of the measured flow rate is calculated and plotted against the differential pressure. This is called the 'half-dry' curve. The pressure at which the half-dry curve and the wet curve intersect is called the 'mean flow pressure'. At this pressure the flow rate through the wet sample is half of that through the dry sample. The corresponding diameter at the mean flow pressure is called the mean flow pore diameter. The mean flow pore diameter signifies that half of the flow through a dry sample is through pores with a diameter greater than the mean flow pore diameter and the other half is through pores having a diameter smaller than the mean flow pore diameter.

**Figure 4.35- Bubble Point Pressure and Mean Flow Pressure (Jena A., 2002a
© Porous Materials Inc.)**



Pore Distribution

The pore size distribution is calculated from the wet and dry curves and pressure data. If at pressure P_j , the corresponding flow rate on the wet curve is $F_{w,j}$ and the flow rate on the dry curve is $F_{d,j}$, then;

Percentage flow through wet sample at pressure $P_j = (F_{w,j}/F_{d,j}) \times 100$

Percentage flow through wet sample at pressure $P_{j+1} = (F_{w,j+1}/F_{d,j+1}) \times 100$

Percentage flow through pores of diameter between D_j and $D_{j+1} =$

$$[(F_{w,j+1}/F_{d,j+1}) \times 100] - [(F_{w,j}/F_{d,j}) \times 100]$$

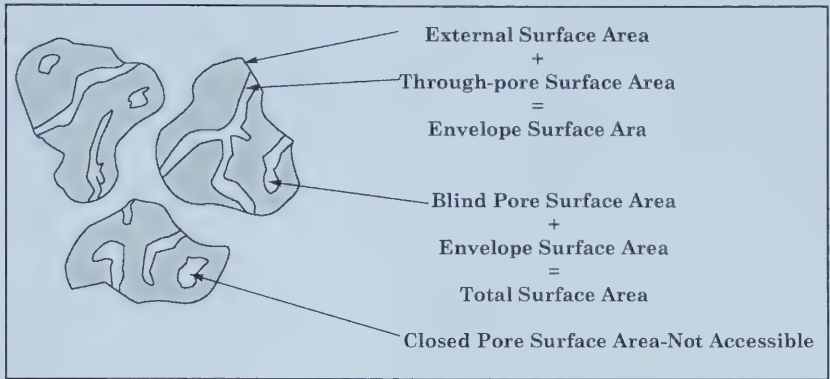
Gas Permeability

The flow rate versus differential pressure data from the dry curve is used to calculate the gas permeability using Darcy's law

Envelope Surface Area

The envelope surface area is defined as the total surface area of the porous system excluding the surface area of the 'blind' or 'dead-end' pores as shown in Figure 4.36.

Figure 4.36: Envelope Surface Area and Total Surface Area (Gupta K., 2002 © Porous Materials Inc.)



The envelope surface area has a retarding effect on the flow rate of the fluid, and therefore affects the flow rate of the fluid through the porous material.

Other measurable characteristics from flow porometry are flow rate distribution, fractional pore number distribution, liquid permeability, Gurley permeability and Frazier permeability.

Features of Capillary Flow Porometry:

Unlike mercury porosimetry and gas adsorption techniques which also account for the blind pores, capillary flow porometry measures characteristics only of the pores which are available for flow of a fluid through the porous sample. A good comparison of the common characterization techniques is given by Venkatraman(2002) and is reproduced in Table 4.8. This table gives an idea of the capabilities and limitations of capillary flow porometry. Capillary flow porometry is useful for characterizing porous materials in which transport or flow characteristics are important e.g. evaluation of filters, paper surfaces for coating or printing etc.

Table 4.8: Comparison of Characterization Techniques (Venkatraman S., 2002 © Porous Materials Inc.)

Characteristic	Capillary Flow Porometer	BET Sorptometer	Mercury Porosimeter
Pore size	Size at most constricted part of the pore	Each pore measured as several pores	Each pore measured as several pores
Pore diameter	Diameter of cylinder whose surface/volume ratio (dS/dV) is same as that of the pore		
Pore diameter range	Cylindrical Pore 0.013 to 500 μm	Cylindrical Pore 0.00035 to 0.2 μm	Cylindrical Pore 0.0035 to 500 μm
Largest Pore Size	Can be measured	Cannot be measured	Cannot be measured
Pore Volume	Cannot be measured	Can be measured	Can be measured
Pore size distribution	Based on flow	Based on volume	Based on volume
Surface Area	Through-pores only	Through-pores and blind pores	Through-pores and blind pores
Permeability	Can be measured	Cannot be measured	Cannot be measured
Adsorption, desorption & chemisorption	No	Yes	No
Density	No	Yes	Yes
Test Pressure	Up to 500 psig	Below atmospheric pressure	Up to 60,000 psig pressure
Test Temperature	Room temperature	-195°C	Room Temperature

Experimental Work

Nuclepore® Membranes

The first set of tests was done on the Nuclepore® Membranes. As discussed previously, these membranes have a simple pore structure and were used to assess the performance of the capillary flow porometer, since accurate data on the sample pore sizes was verified using SEM image analysis. Nuclepore® 2, 5, 8 micron membranes were evaluated. The diameter of the test sample was 4 cm and the wetting liquid used was Galwick® which has a surface tension of 16 mN/m. Three individual samples of each membrane size were tested and the data averager feature in the software was used to derive the average results. Results obtained are shown in Table 4.9, Figure 4.37 and Figure 4.38. The pore size distribution is narrow as expected and the results appear to be quite reasonable. The permeability values obtained were also comparable to results from the variable head permeameter. For all samples, including paper and Voith fabric samples, a wet-up / dry-down run was carried out for each test.

Commercial Paper Samples

Weyerhaeuser First Choice, Champion Ink Jet, Hammermill Xerographic Colour and Alberta Newsprint Company - Rotogravure commercial grades were used as the selected test papers. The sample diameter was 4 cm and wetting liquid used was Galwick®. Three individual samples of each paper grade were tested to give the average results. Tests were done with flow through the felt side as well as flow through the wire side, for the wet curves. Results obtained are given in Table 4.9, Figure 4.39 and Figure 4.41. Slight differences were observed in the results with flow through on the felt side from flow through on wire side. In the case of the Weyerhaeuser First Choice paper, a 2.5 cm diameter sample was used for the tests.

Voith Woven Fabrics

A 4 cm diameter sample was found to be too large and porous for testing. Under such conditions the pressure drop across the sample was very low and comparable to the pressure drop in the connected fittings and tubing of the air supply lines and the test

chamber, without the sample. The software indicated a warning for such conditions. The size of the sample was therefore decreased to 2 cm, 1 cm and 0.5 cm respectively. Results were finally obtained with the 0.5 cm sample. A low wetting liquid, water, was used here, since the order of magnitude of the pore sizes is very large (hundreds of microns). Three individual samples of each fabric were tested to give the average results. Results obtained are shown in Table 4.9, Figure 4.40 and Figure 4.42.

It may be noted that the instrument software calculates the air permeability for flow and pressure increments over the entire pressure range of the test and reports the average value as the Darcy permeability constant. From the pressure versus flow curves, it can be seen that the curve is linear only at very low pressure i.e. in the Darcy regime. Permeability values were therefore corrected and were based on this regime of the pressure-flow curve (The flow data was used for differential pressures up to 1 psi for the paper sample, 0.03 psi for the Nuclepore® membranes and 0.005 psi for the Voith fabric samples).

A detailed error analysis for the performance of the capillary flow porometer is reported by Dixon (2002). Surface tension and wetting (contact angles) are important parameters governing the outputs from the capillary flow porometer. It may be noted that surface tension of the silicone oil, Galwick®, used in this study was not measured separately. Supplier data of 16 m-N/m was used for estimation of the pore size distribution. Complete wetting of the samples was also assumed. The evaporation effects of wetting liquid, operator, machine and number of runs were evaluated for stainless steel filters and filter paper by Dixon (2002). The error using silicone oils as the wetting agent and filter paper as the test sample is estimated to be < 5%.

In this study, for the commercial paper grades, the % error in the value of the mean flow pore diameter was calculated from the results from three separate runs and using a fresh paper sample for each run. The results are given in Table 4.10. The error in the mean flow pore diameter varied from $\pm 1.2\%$ to $\pm 6.3\%$.

Table 4.9: Summary of Results - Capillary Flow Porometry

Sample	D _{min} microns	D _{mean flow} microns	D _{bubble pt} microns	D _{max PSD} microns	Perm Coeff Darcy (m ²)
Paper Grades					
Alberta Newsprint Co -Roto*	0.16	1.37	9.41	0.16	0.0067 (6.61E-15)
Alberta Newsprint Co -Roto-Rev **	0.18	1.49	8.77	0.20	0.0067 (6.61E-15)
Champion Ink Jet*	0.42	2.48	14.73	0.47	0.0233 (2.30E-14)
Champion Ink Jet- Rev **	0.26	2.54	14.93	0.32	0.0305 (3.01E-14)
Hammermill Color*	0.24	1.48	8.80	0.25	0.0159 (1.57E-14)
Hammermill Color-Rev **	0.21	1.36	11.59	0.22	0.0172 (1.69E-14)
Weyerhaeuser First Choice*	0.38	1.71	12.24	0.38	0.0250 (2.47E-14)
Weyerhaeuser First Choice-Rev **	0.24	1.52	11.31	0.43	0.0294 (2.90E-14)
Voith Fabrics					
Voith 1	165.24	255.28	392.80	249.31	600.83 (5.93E-10)
Voith 2	60.45	493.15	668.90	504.99	1085.06 (1.07E-9)
Voith 3	245.99	373.21	486.96	336.26	1056.14 (1.04E-9)
Voith 4	27.36	431.96	645.64	391.20	2340.88 (2.31E-9)
Voith 5	41.74	307.79	317.24	299.03	463.98 (4.58E-10)
Voith 6	64.49	296.03	473.99	271.84	1098.56 (1.08E-9)
Voith 7	80.67	544.76	1845.63	537.80	2398.03 (2.37E-9)
Nuclepore® Membranes					
Nuclepore® 2 micron	1.80	1.87	3.40	1.90	0.011 (1.09E-14)
Nuclepore® 5 micron	4.93	5.24	5.51	5.19	0.036 (3.55E-14)
Nuclepore® 8 micron	7.86	7.97	8.86	7.89	0.045 (4.45E-14)

* Air flow on wire-side of paper sample
** Air flow on felt-side of paper sample

D_{min} = Smallest detected pore diameter
D_{mean flow} = Mean flow pore diameter
D_{bubble pt} = Bubble point pore diameter
D_{max PSD} = Diameter at maximum pore size distribution
1 Darcy = 9.87 x 10⁻¹³ m²

Figure 4.37: Pore Size Distributions for Nuclepore® Membranes

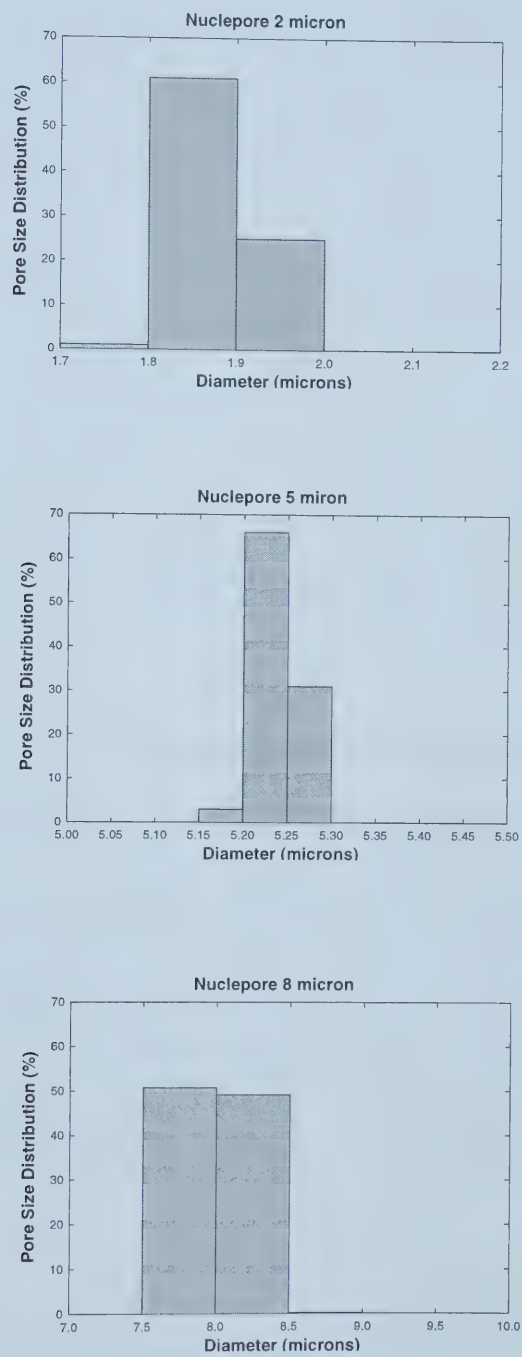


Figure 4.38: Nuclepore® Membranes - Differential Pressure vs Air flow rate

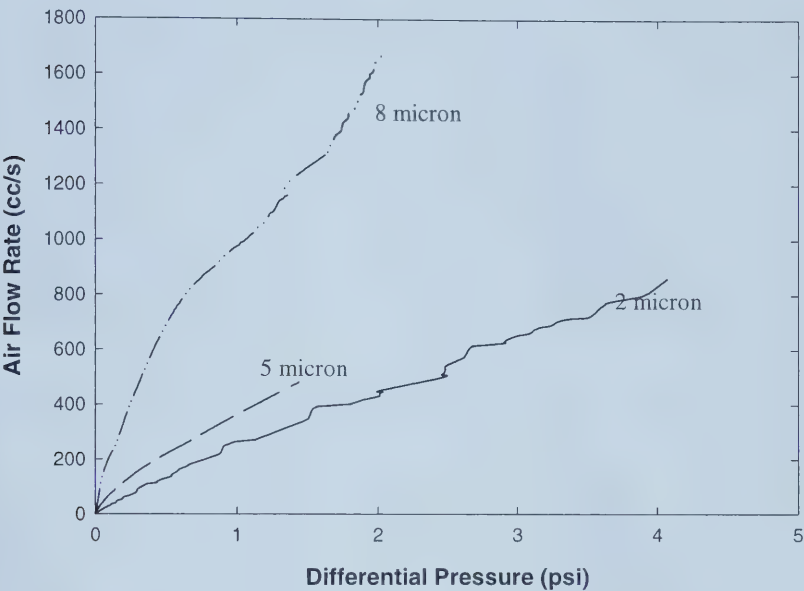


Table 4.10: PMI - Capillary flow porometry tests with commercial paper grades

Sample	Run 1	Run 2	Run 3	Mean	Std Dev	Std Error	% Error
ANC - Roto	1.3989	1.367	1.3536	1.37	0.023	+ 0.027	+ 1.96
ANC - Roto - Rev	1.4628	1.5847	1.4314	1.49	0.081	+ 0.094	+ 6.26
CIJ	2.4339	2.4214	2.48	2.44	0.031	+ 0.036	+ 1.49
CIJ - Rev	2.4224	2.4684	2.5408	2.48	0.060	+ 0.069	+ 2.78
H	1.578	1.4689	1.4885	1.51	0.058	+ 0.067	+ 4.44
H - Rev	1.3921	1.3754	1.3641	1.38	0.014	+ 0.016	+ 1.18
WFC	1.7589	1.7892	1.7139	1.75	0.038	+ 0.044	+ 2.49
WFC - Rev	1.5328	1.4886	1.5317	1.52	0.025	+ 0.029	+ 1.92

Figure 4.39: Pore Size Distributions for Commercial Paper Grades

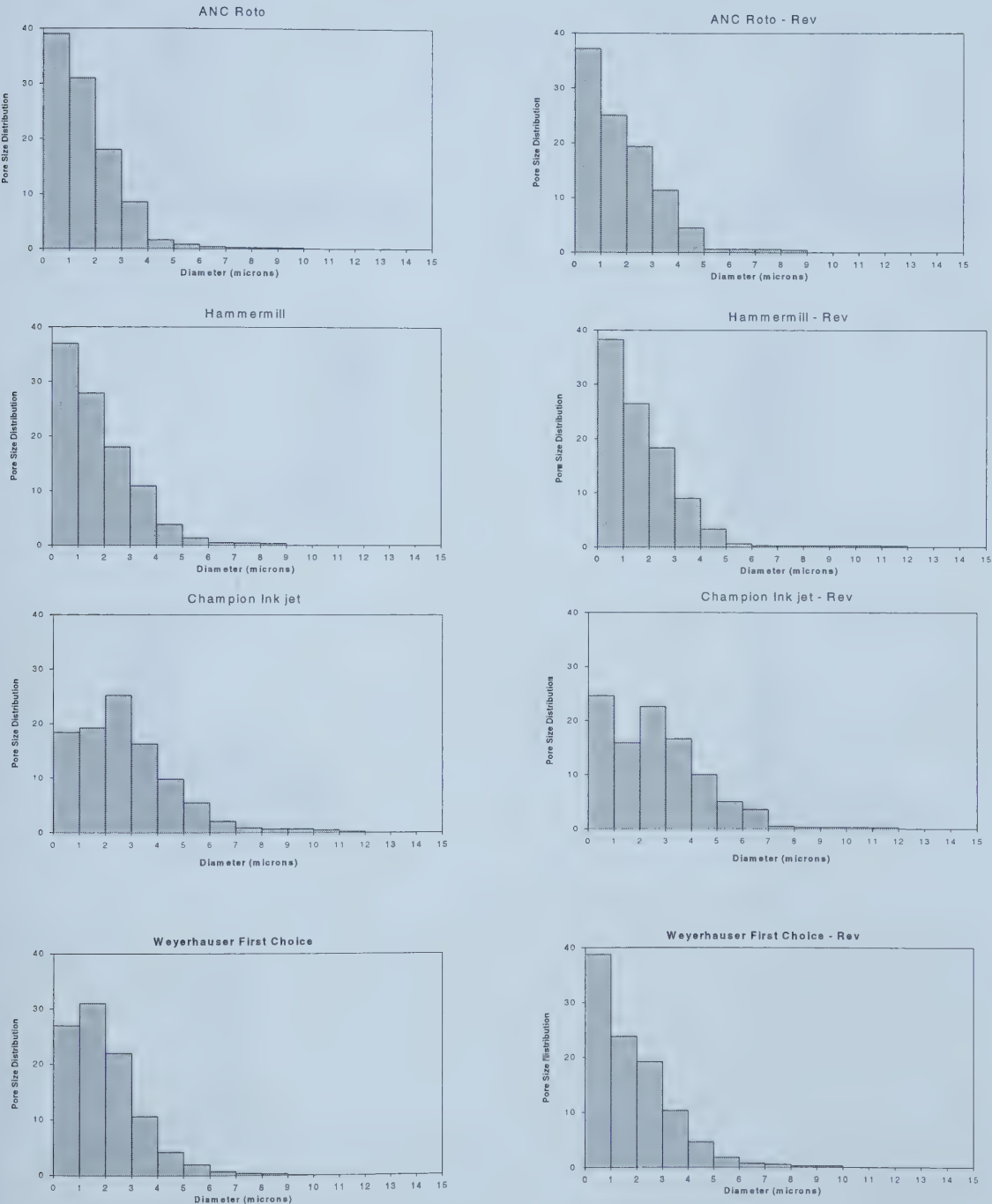


Figure 4.40: Pore Size Distributions for Voith Fabrics

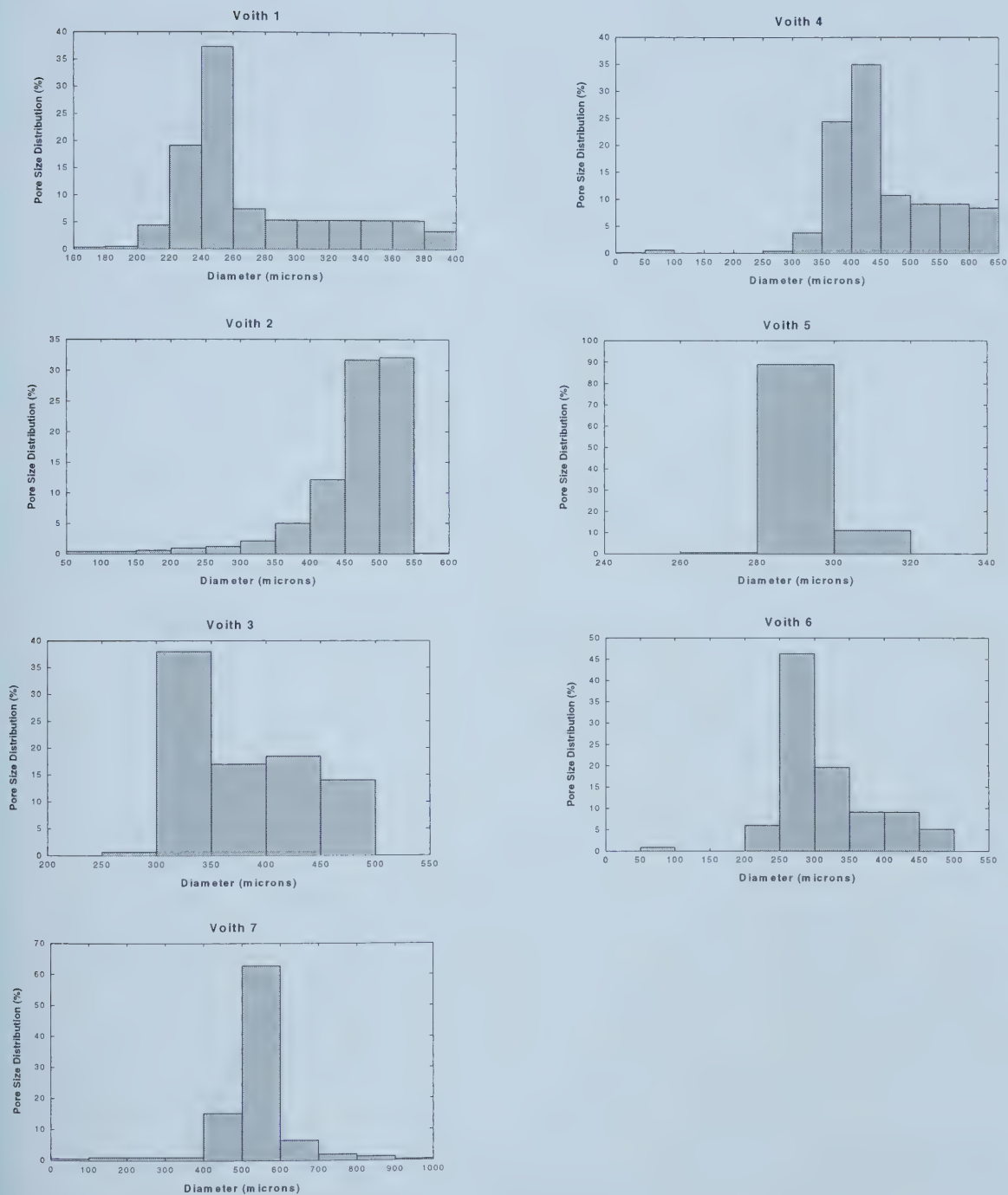


Figure 4.41: Commercial Paper Grades - Differential Pressure vs Air flow rate

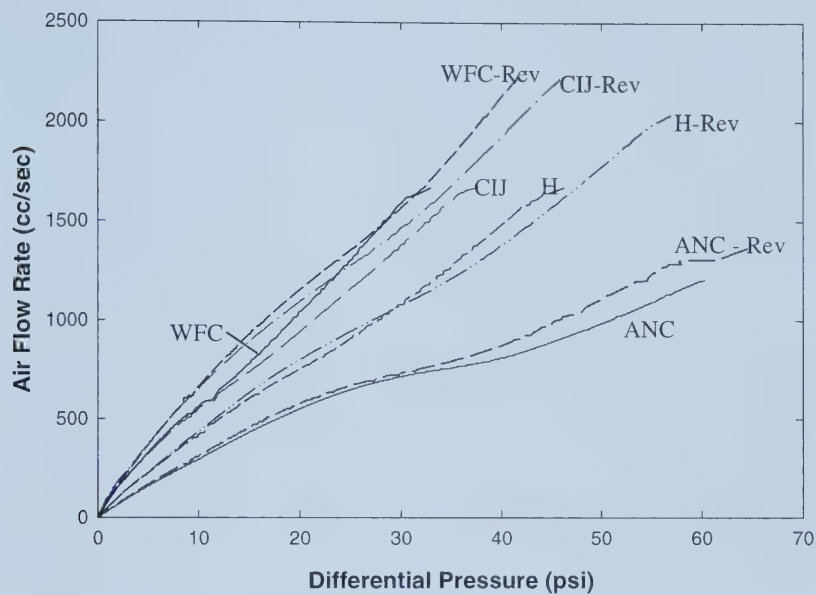
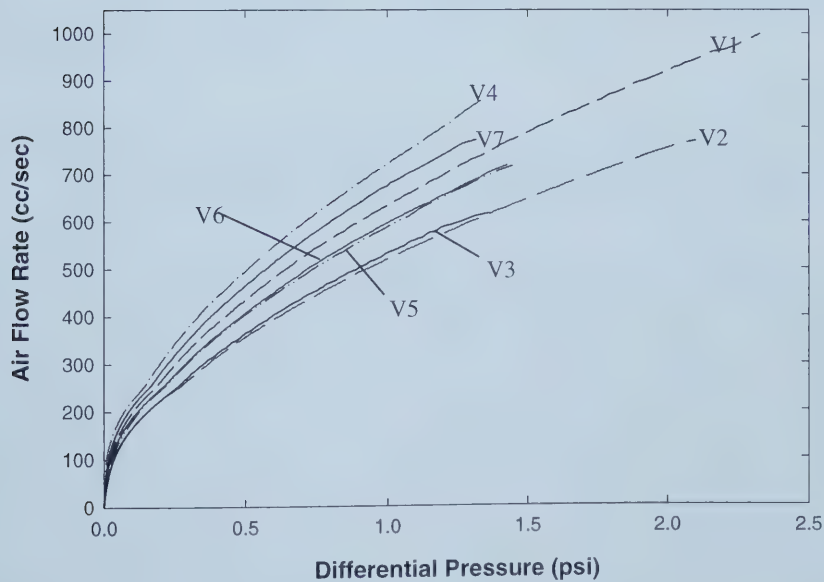


Figure 4.42: Voith Fabrics - Differential Pressure vs Air flow rate



4.3.3 Thickness measurements

Calculation of the permeability from the data obtained from the variable head permeameter and capillary flow porometer required data on the thickness of the different materials. Thickness measurements were evaluated using an automatic 89-100 Thickness Tester (Thwing Albert Instrument Company). This type of instrument is typically used for measuring the thickness or caliper of paper sheets. This instrument allows a number of measurements to be done continuously under a constant pressure. The instrument reports individual test results as well as the average value, high value, low value and the standard deviation. Standard errors based on 95% confidence were also calculated and have been reported as a percentage of the mean. For the various porous samples including commercial paper and glass fibre paper, ten individual measurements were performed in different regions of the test sample. In the case of the Nuclepore® membranes, four sandwiched sheets were tested simultaneously and the results obtained were divided by four to arrive at the individual thickness values for a single sheet. The results obtained are summarized in Table 4.11. The thickness values obtained for the Nuclepore® membranes were comparable to the nominal thickness values specified by the vendor.

Table 4.11: Thickness Measurements of various porous samples based on automatic caliper instrument (Thwing Albert 89-100 Thickness Tester)

Commercial Paper Samples - Thickness Measurements (microns)					
Sample	Avg.	High	Low	Std. Dev.	% Error
Weyerhaeuser First Choice	110.5	111.5	109.5	0.5	± 0.29
Champion Ink jet	98.0	100.0	96.0	1.5	± 0.97
Hammermill Color	120.0	122.0	119.0	1.0	± 0.53
Alberta Newsprint - Offset grade	81.0	82.5	80.0	1.0	± 0.78
Alberta Newsprint - Rotogravure grade	77.0	79.0	74.0	1.5	± 1.23

Table is continued on next page...

Glass Fibre Filter Paper - Thickness Measurements (microns)					
Sample	Mean	High	Low	Std. Dev.	% Error
GF/F	425.5	434.0	415.5	5.5	± 0.82
GF/B	655.5	671.5	647.0	9.0	± 0.87
GF/A	261.5	271.5	249.5	6.5	± 1.57
1PS	179.5	184.0	177.0	2.0	± 0.70
Voith Fabrics - Thickness Measurements (microns)					
Sample	Mean	High	Low	Std. Dev.	% Error
Voith 1	442.0	442.5	441.0	0.5	± 0.07
Voith 2	846.5	848.5	845.0	1.0	± 0.07
Voith 3	1159.0	1165.5	1156.0	3.0	± 0.16
Voith 4	773.0	775.0	771.5	1.0	± 0.08
Voith 5	552.5	554.0	552.0	0.5	± 0.06
Voith 6	716.5	718.0	715.0	1.0	± 0.09
Voith 7	1260.5	1271.0	1251.0	6.5	± 0.33
Voith Spectra Meshes - Thickness Measurements (microns)					
Sample	Mean	High	Low	Std. Dev.	% Error
Spectra T	990.5	1015.5	973.0	13.5	± 0.86
Spectra Q	809.5	813.0	805.5	2.5	± 0.20
Spectra F	777.5	800.5	752.0	12.5	± 1.02
Nuclepore® Membranes - Thickness Measurements (microns)					
Sample	Mean	High	Low	Std. Dev.	% Error
Nuclepore® 2 micron	9.25	9.63	9.0	0.25	± 1.71
Nuclepore® 5 micron	11.13	11.63	10.13	0.37	± 2.10
Nuclepore® 8 micron	8.25	9.0	7.75	0.5	± 3.83
Nuclepore® 12 micron	8.5	9.0	8.25	0.25	± 1.86

4.3.4 Porosity measurements

Nuclepore® Membranes

The Nuclepore® membranes essentially have straight through cylindrical pores. These pores are randomly distributed and further some of the pores overlap resulting in a "figure 8" shaped pore. In order to obtain a fairly accurate value for the porosity of the membranes, three SEM images of each membrane type were taken. The percentage area occupied by the pores was then determined for each image using a KDY Xpert Image analysis system (Nashua, NH). The results obtained are given in Table 4.12. For the purpose of this study, the average porosity value was used.

Voith Spectra Meshes

These are regular pore structure with pore sizes in the order of hundreds of microns. Images of each side were taken on the KDY system and the percentage area occupied by the pores was determined for each side using the KDY Xpert Image analysis system. The results obtained are shown in Table 4.13. The average porosity value was used for the purpose of calculations.

Voith Woven Fabric Structures

Since these are single, double or triple layered woven fabrics, the exact shape of the pores is difficult to define in comparison with the Nuclepore® membranes and the Voith Spectra Meshes. The porosity of the sample was estimated using a method which is typically used for paper. The basis weight, gsm (grams per square meters) of the sample was found by weighing a sample of known area. The gsm was then divided by the thickness to obtain the bulk density of the sample. The bulk density and actual density of the fabric material (PET) was used to obtain the porosity. The density of the PET material used for making the fabrics was 1.38 g/cm^3 (Value informed by manufacturer Synstrand, the monofilament division of Voith). The results are summarized in Table 4.14.

Table 4.12: Porosity - Nuclepore® Membranes

Nuclepore ®	Porosity (%)			Mean	Std Dev	% Error
2	4.6	4.4	4.1	4.37	0.32	± 8.33
5	5.4	5.7	5.0	5.37	0.37	± 7.97
8	3.2	4.6	3.6	3.80	0.47	± 14.25
12	5.4	5.6	5.5	5.50	0.07	± 1.48

Table 4.13: Porosity - Voith Spectra Structures

Spectra	Porosity (%)		Mean	Std Dev	% Error
Q	38.9	39.2	39.05	0.21	± 0.8
T	36.1	32.4	34.25	2.62	± 10.8
F	11.5	14.6	13.05	2.20	± 23.8

Table 4.14: Porosity - Voith Woven Fabrics

Voith	Sample size mm	Area mm ²	Weight g			Mean g/m ²	Thk. microns	Porosity %	% Error
1	59 x 77	4543	1.2638	1.2640	1.2639	278.2	442.0	45.6	± 0.08
2	60 x 76	4560	2.3546	2.3547	2.3546	516.4	846.5	43.5	± 0.08
3	58 x 75	4350	2.7671	2.7671	2.7671	636.1	1159.0	40.8	± 0.16
4	58 x 74.5	4321	1.8900	1.8900	1.8900	437.4	773.0	40.3	± 0.08
5	58 x 75	4350	1.2150	1.2152	1.2151	279.3	552.5	35.8	± 0.07
6	58 x 75	4350	1.4109	1.4109	1.4109	324.3	716.5	32.7	± 0.09
7	56 x 75	4350	2.8270	2.8270	2.8270	649.9	1260.5	37.6	± 0.33

4.3.5 Contact angle measurements

Experimental work

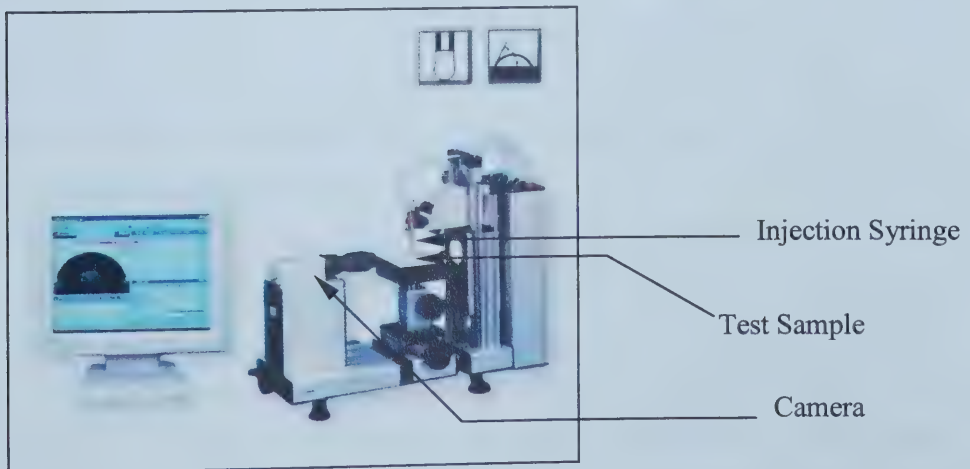
Contact angle measurements were used to characterize the wettability of the different systems involved in the Emco testing work. The test liquids of varying surface tension selected for experiments with the ultrasonic method were aqueous methanol solutions, properties of which are summarized in Table 4.15.

Table 4.15: Properties of aq. methanol solutions at 20 °C (CRC Handbook, 1988-89)

% Wt.	ρ (kg/m ³)	μ (mPa-s)	γ (mN/m)
0	998.2	1.002	72.75
6	988.0	1.195	62.26
20	966.6	1.605	47.00
40	934.7	1.837	34.51
70	871.5	1.367	26.17
100	791.7	0.586	22.65

Contact angles were measured on an Axisymmetric Drop Shape Analysis System supplied by Krüss GmbH (www.kruss.de), Model DSA 10 MK2 (See Figure 4.43).

Figure 4.43: Drop Shape Analysis System (Krüss GmbH - DSA 10 MK2)



This analysis system captures an image of the drop on the substrate and digitally a curve is fitted approximating the shape of the drop. The system reports both the left and right-hand side contact angle, the mean contact angle, the drop volume, base diameter and height of the drop. The time taken to ensure that the fitted curve matched the drop shape profile well was around 15-30 seconds. It was assumed that within this time the contact line had reached its equilibrium position. A minimum of three separate measurements was completed for each system. The average value was used in the analysis to characterize the wettability of the substrate with a particular liquid. It may be noted that for each measurement the drop was deposited (via a micro-syringe) on an area different from the previous measurement. Fresh substrate samples were used for measurements with other test liquids. The raw data obtained for all the measurements from the instrument software is reported in *Appendix E*.

Nuclepore® Membranes :

The Nuclepore® membranes, which were used as model pore structures, are made of PC (polycarbonate). The hydrophilic Nuclepore® membranes are essentially polycarbonate membranes with a hydrophilic surface coating of PVP (polyvinylpyrrolidone). A smooth non-porous polycarbonate film obtained from the manufacturer (Whatman filters) was used as the substrate for contact angle measurements with different probe liquids on PC. In order to measure the contact angles of the different probe liquids on PVP, the PC film was dip-coated with PVP in the laboratory and the contact angle measurements were conducted on these coated films. These coatings were prepared from 10 gms of a PVP-60 solution (55% wt. water) dissolved in 200 gms of water magnetically stirred, for 30 minutes. The PC membrane was then immersed in this solution, removed and allowed to drip dry.

The results obtained with the commercially uncoated PC membrane are shown in Figure 4.44. In the measurements with 100% methanol it was observed that the methanol wetted the surface very rapidly (i.e. very low contact angle) making it difficult to digitally capture the image for accurate measurement. Results obtained with PVP coated PC are shown in Figure 4.45. It was observed that the drop spread very rapidly on contact with the PVP, since PVP is very hydrophilic. Contact angles were measured after the drop was

no longer spreading. In the case of measurements with 70% and 100% methanol, the spreading was extremely rapid, due to the lower surface tension. This made it impossible to capture a suitable image for measurement. The contact angle would probably be less than 5 degrees in these cases.

Contact angle measurements were also evaluated with the different probe liquids on the porous Nuclepore® Membranes. The results obtained are shown in Figure 4.46 to Figure 4.49 respectively. In the case of the Nuclepore® 2 micron membrane with 70% and 100% methanol, it was observed that the drops spread very rapidly forming a thin film, again making it impossible to capture a suitable image for contact angle measurement.

Voith Spectra® Meshes:

A flat smooth, non-porous sample was not available for this model pore structure from the manufacturer. Contact angle measurements were done using the porous substrate. These structures are very porous and have large pores in the order of hundreds of microns. Owing to this, it was difficult to get a spherical drop on these structures. The shape of the drops obtained for most of the readings were elongated or 'sausage' shaped. Large drops were used for the measurements. For all the Spectra mesh structures, in the case of measurements with 100% methanol, the drops sank into the substrate immediately making it impossible to capture an image. For tests with 70% methanol and Spectra T, the drops also sank in immediately. Only very large elongated drops could be obtained after flooding of the sample. Results obtained are shown in Figure 4.50 to Figure 4.52.

Voith Woven Fabrics :

Here again non-porous samples of the different fabrics were not available from the manufacturer. Contact angle measurements with porous fabric samples were attempted. A drop of water when contacted with the sample sank in almost immediately

into the sample and spread laterally, making it impossible to capture any image for contact angle measurements.

Summary of Results

The mean values of the contact angles obtained for different pore structures with different liquids are given in Table 4.16.

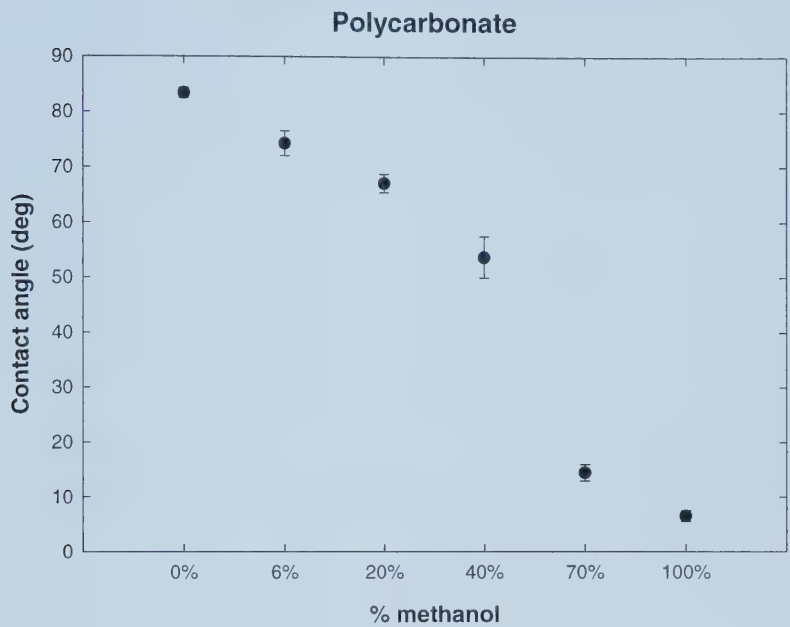
Table 4.16: Mean Contact Angle Values

Sample	Test Liquid					
	Water	6%	20%	40%	70%	100%
PC	83.4 ± 0.9%	74.3 ± 2.4%	67.1 ± 2.1%	53.8 ± 5.4%	53.8 ± 8.1%	6.6 ± 8%
PVP	11.8 ± 3%	10.5 ± 6%	9.9 ± 3%	8.7 ± 8%	< 5	< 5
Nuc 2	68.2 ± 4.2%	57.3 ± 2.5%	39.7 ± 2.8%	38.1 ± 8.4%	< 5	< 5
Nuc 5	72.0 ± 2.1%	60.3 ± 8.2%	41.4 ± 3.2%	44.0 ± 6.8%	13.9 ± 7.4%	6.9 ± 65%
Nuc 8	67.5 ± 19%	60.3 ± 4.8%	60.3 ± 20%	48.1 ± 19%	7.13 ± 1.6%	9.2 ± 6.5%
Nuc 12	67.3 ± 2.6%	63.5 ± 3.1%	54.6 ± 4.7%	40 ± 6.4%	8.6 ± 11%	7.6 ± 6.7%
Spectra F	83.5 ± 5.4%	79.9 ± 2.3%	74.1 ± 3.8%	61 ± 12.4%	66.9 ± 6.9%	9.3 ± 12%
Spectra Q	97.3 ± 3%	99.7 ± 2.8%	78.5 ± 3%	70.9 ± 7.2%	71.2 ± 11%	< 5
Spectra T	89.8 ± 3%	90.2 ± 2.6%	88.4 ± 2.9%	70.4 ± 12%	75.9 ± 28%	< 5

Note:

Initial contact angle measurements with water were done using a manual goniometer manufactured by Rami Hart Inc. The raw data obtained from these measurements are given in *Appendix E*. The results were quite comparable to those obtained with the drop shape analysis system.

Figure 4.44: Contact Angle Measurements - Smooth non-porous polycarbonate Membrane



Note - 95% confidence intervals were used for plotting all error bars

Figure 4.45: Contact Angle Measurements - Polyvinylpyrrolidone coating on solid polycarbonate membrane

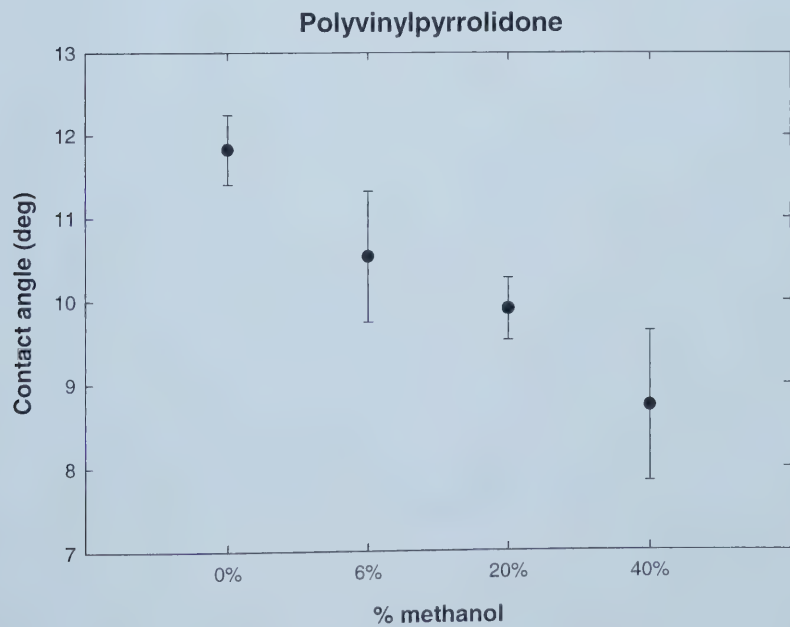


Figure 4.46: Contact Angle Measurements - Nuclepore® 2 micron membrane

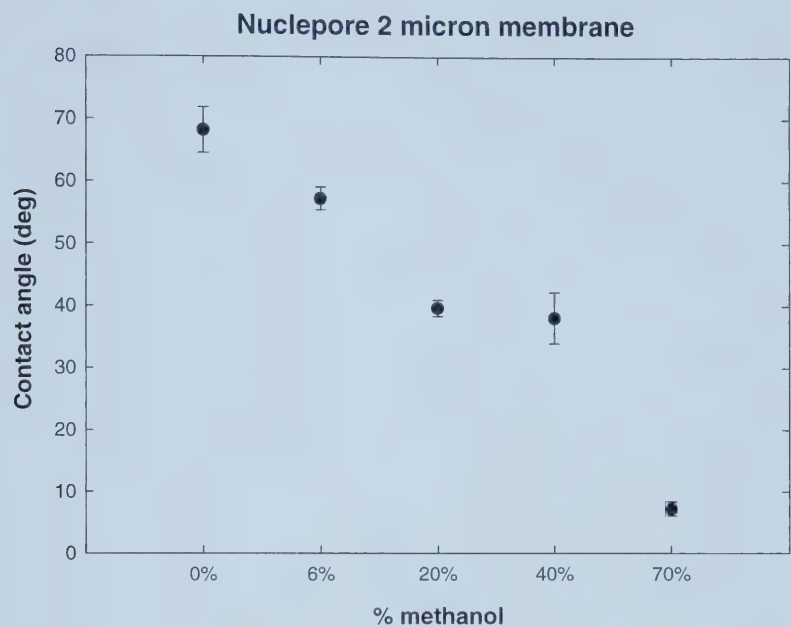


Figure 4.47: Contact Angle Measurements - Nuclepore® 5 micron membrane

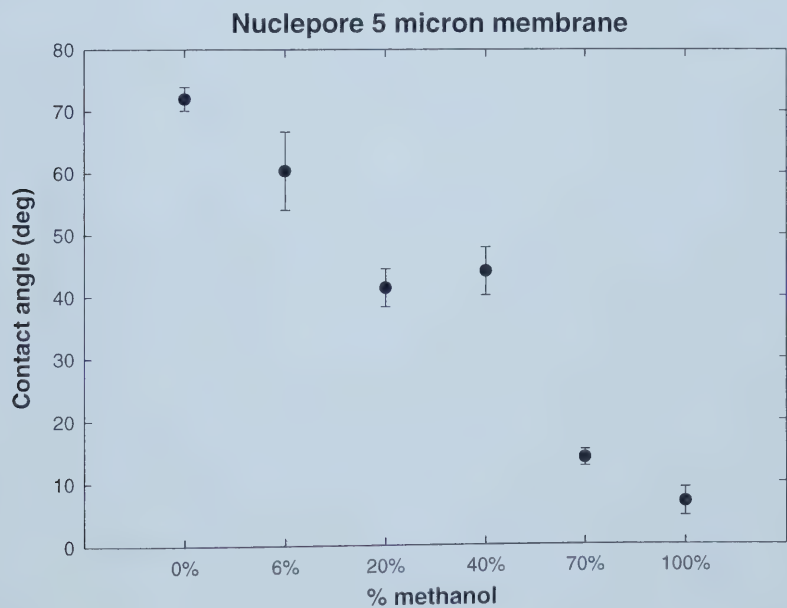


Figure 4.48: Contact Angle Measurements - Nuclepore® 8 micron membrane

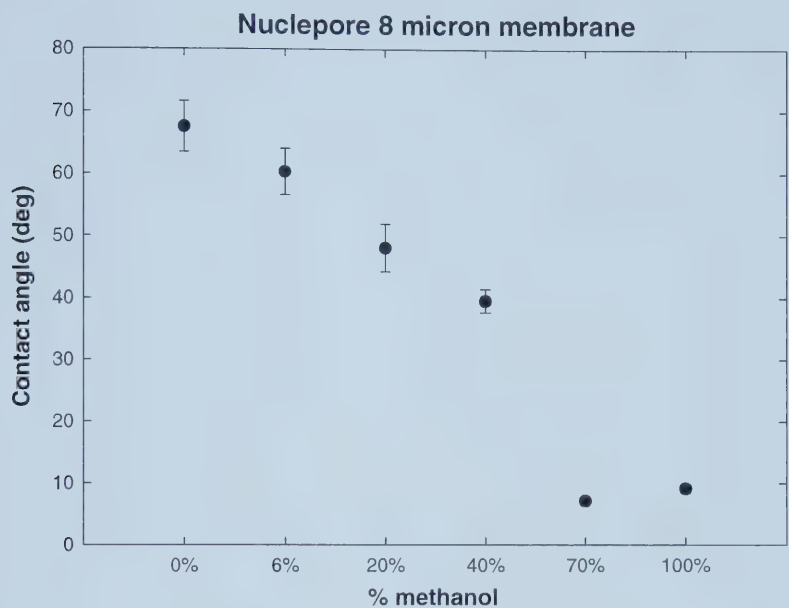


Figure 4.49: Contact Angle Measurements - Nuclepore® 12micron membrane

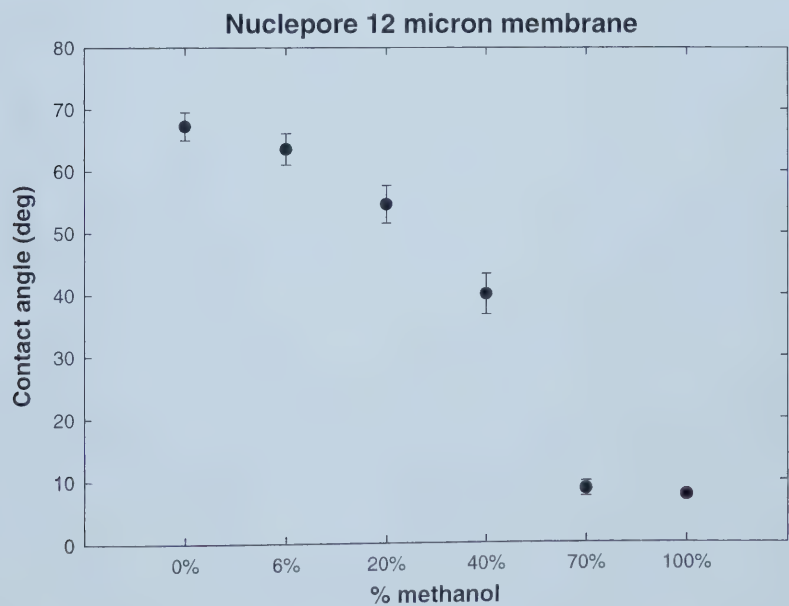


Figure 4.50: Contact Angle Measurements - Voith Spectra F Mesh

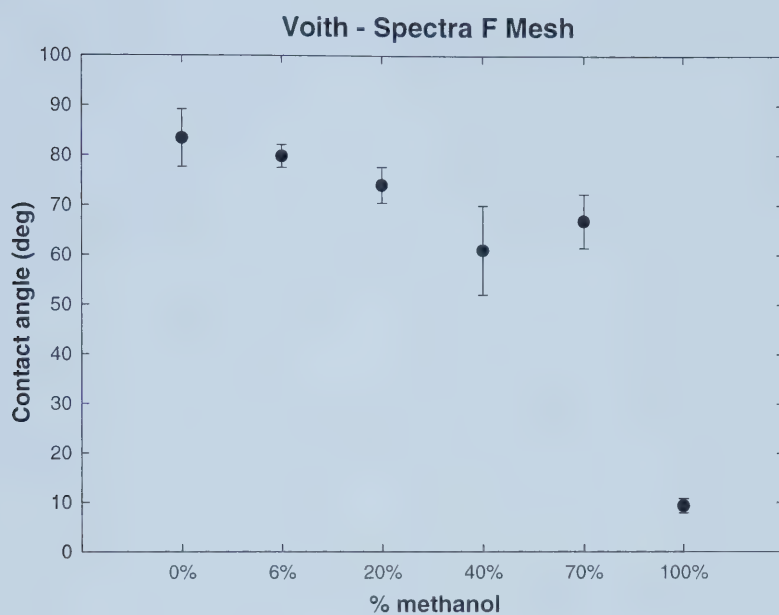


Figure 4.51: Contact Angle Measurements - Voith - Spectra Q Mesh

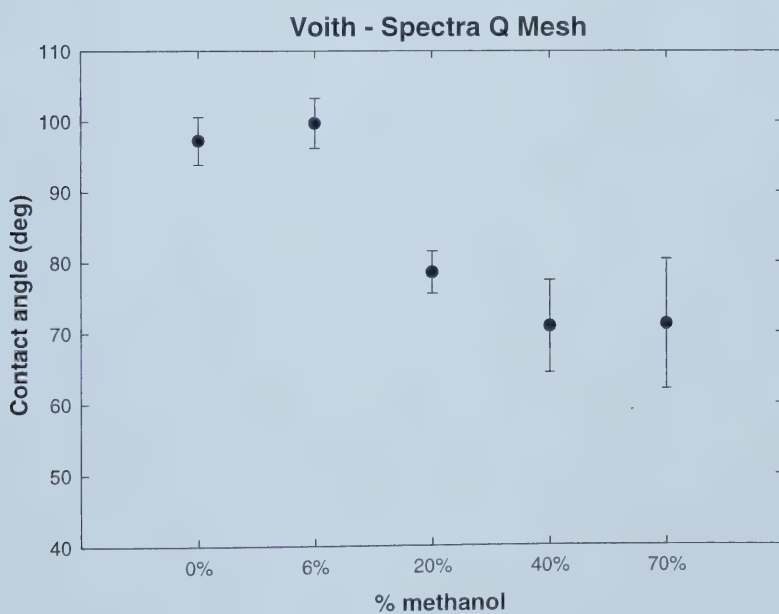


Figure 4.52: Contact Angle Measurements - Voith - Spectra T Mesh

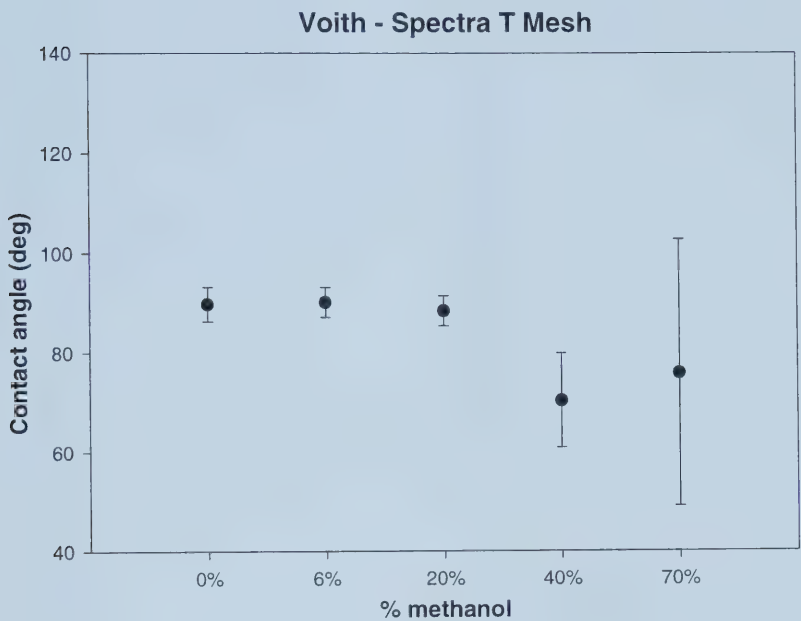


Table 4.17: Summary of Characterization - Model Pore Structures

Sample	Pore Size (micron)	Thickness ³⁾ (micron)	Porosity (%)	Permeability (m ³)	D _{nom} (micron)	D _{total flow} (micron)	D _{total at} (micron)	D _{mean res} (micron)	Contact Angle (degrees)					
									Water	6% methanol	20% methanol	40% methanol	70% methanol	100% methanol
Nuclepore Membranes	2 micron	1.51 ¹⁾	4.4 ³⁾	5.12E-15 ⁵⁾ 1.09E-14 ⁶⁾	1.80	1.87	3.40	1.90	68.18 ⁷⁾ 64.26 ⁸⁾	57.27 ⁷⁾ 52.33 ⁸⁾	39.69 ⁷⁾ 31.74 ⁸⁾	38.12 ⁷⁾ 29.73 ⁸⁾	< 5 ⁷⁾	< 5 ⁷⁾
	5 micron	4.2 ¹⁾	5.4 ³⁾	3.98E-14 ⁵⁾ 3.55E-14 ⁶⁾	4.93	5.24	5.51	5.19	72.00 ⁷⁾ 67.46 ⁸⁾	60.32 ⁷⁾ 54.55 ⁸⁾	41.38 ⁷⁾ 31.82 ⁸⁾	44.00 ⁷⁾ 35.22 ⁸⁾	13.90 ⁷⁾	6.85 ⁷⁾
	8 micron	6.9 ¹⁾	3.8 ³⁾	5.14E-14 ⁵⁾ 4.45E-14 ⁶⁾	7.86	7.97	8.86	7.89	67.53 ⁷⁾ 64.09 ⁸⁾	60.30 ⁷⁾ 56.32 ⁸⁾	60.30 ⁷⁾ 56.32 ⁸⁾	48.09 ⁷⁾ 42.79 ⁸⁾	7.13 ⁷⁾	9.16 ⁷⁾
	12 micron	10.76 ¹⁾	5.5 ³⁾	2.92 E-13 ⁵⁾	-	-	-	-	67.25 ⁷⁾ 62.13 ⁸⁾	63.52 ⁷⁾ 57.99 ⁸⁾	54.55 ⁷⁾ 47.78 ⁸⁾	40.02 ⁷⁾ 29.70 ⁸⁾	8.63 ⁷⁾	7.63 ⁷⁾
Non porous PC	-	-	-	-	-	-	-	-	83.40	74.32	67.13	53.77	14.47	6.55
PVP coated PC	-	-	-	-	-	-	-	-	11.83	10.53	9.90	8.73	< 5	< 5
Volith Spectra Meshes	T	429 x 1929 ³⁾	34.3 ³⁾	7.32E-09 ⁵⁾	-	-	-	-	89.75 ⁷⁾ 58.16 ⁸⁾	90.18 ⁷⁾ 58.93 ⁸⁾	88.44 ⁷⁾ 55.78 ⁸⁾	70.40 ⁷⁾	75.88 ⁷⁾ 26.89 ⁸⁾	< 5 ⁷⁾
	Q	893 x 893 ³⁾	39.0 ³⁾	8.56E-09 ⁵⁾	-	-	-	-	97.25 ⁷⁾ 64.38 ⁸⁾	99.72 ⁷⁾ 68.74 ⁸⁾	78.52 ⁷⁾ 15.05 ⁸⁾	70.85 ⁷⁾	71.16 ⁷⁾	< 5 ⁷⁾
	F	446 x 446 ³⁾	13.1 ³⁾	1.39E-09 ⁵⁾	-	-	-	-	83.45 ⁷⁾ 73.66 ⁸⁾	79.85 ⁷⁾ 69.34 ⁸⁾	74.05 ⁷⁾ 62.22 ⁸⁾	60.98 ⁷⁾ 44.92 ⁸⁾	66.86 ⁷⁾ 52.99 ⁸⁾	9.33 ⁷⁾
Volith Woven Fabrics	1	-	45.6 ⁴⁾	3.71E-10 ⁵⁾ 5.93E-10 ⁶⁾	165.24	255.28	392.80	249.31	-	-	-	-	-	-
	2	-	44.2 ⁴⁾	1.51E-09 ⁵⁾ 1.07E-09 ⁶⁾	60.46	493.15	688.90	504.99	-	-	-	-	-	-
	3	-	39.8 ⁴⁾	2.04E-09 ⁵⁾ 1.04E-09 ⁶⁾	245.99	373.21	486.96	336.26	-	-	-	-	-	-
	4	-	41.0 ⁴⁾	1.06E-09 ⁵⁾ 2.31E-09 ⁶⁾	27.36	431.96	645.64	391.20	-	-	-	-	-	-
	5	-	36.6 ⁴⁾	5.37E-10 ⁵⁾ 4.58E-10 ⁶⁾	41.74	307.79	317.24	299.03	-	-	-	-	-	-
	6	-	32.8 ⁴⁾	1.05E-09 ⁵⁾ 2.07E-09 ⁶⁾	64.49	296.03	473.99	271.84	-	-	-	-	-	-
	7	-	37.7 ⁴⁾	2.14E-09 ⁵⁾ 2.37E-09 ⁶⁾	80.67	544.76	1845.63	537.80	-	-	-	-	-	-

Notes

- 1) From SEM measurements
- 2) From Automatic Caliper Instrument measurements
- 3) From Image Analysis
- 4) Estimated from density, thickness and weight/area of sample
- 5) Calculated from Variable Head Permeameter data
- 6) From Capillary Flow Porometry
- 7) Apparent Contact Angle value on composite structure (Hydrophilic membranes with PVP coating)
- 8) True contact angle value calculated using Cassie-Baxter(1944) Equation

Table 4.18: Summary of Characterization - Commercial Paper Grades

Sample	Thickness ¹⁾ (micron)	Basis ²⁾ Wt. (g/m ²)	Bulk ²⁾ Density (g/cm ³)	Filler ²⁾ (%)	Bendtsen ²⁾ Porosity (mL/min)	Permeability ³⁾ (m2)	D _{min} (microns)	D _{mean flow} (microns)	D _{bubble pt} (microns)	D _{max PSD} (microns)
WFC	110.5	85.6	0.78	15.5	621	2.47E-14	0.38	1.71	12.24	0.38
CUJ	98.0	75.3	0.75	9.7	908	2.30E-14	0.42	2.48	14.73	0.47
H	120.0	99.4	0.88	22.7	345	1.57E-14	0.24	1.48	8.80	0.25
ANC - Roto	77.0	48.0	0.58	0.7	293	6.61E-15	0.16	1.37	9.41	0.16

Notes

- 1) From Automatic Caliper Instrument measurements
- 2) Data from Alberta Research Council
- 3) From Capillary Flow Porometry

4.4 Dynamics of Liquid Penetration using Emco DPM -30

Test Procedure

The following procedure steps were common for all the model pore structures, glass fibre and commercial paper samples that were tested.

- After start-up of the electronic unit, a warm-up time of 10 minutes was allowed (as recommended by the manufacturer) and a couple of 'dummy' runs with only the sample holder were done before testing of samples.
- All model pore structures (Nuclepore® membranes, Voith Spectra meshes and Voith Fabrics) were pre soaked overnight in pure methanol, rinsed in fresh methanol solution and then allowed to dry completely before testing. The purpose of this was to remove any residual chemicals from the manufacturing process, such as lubricating oils etc.
- For tests with aqueous methanol solutions, a master batch of each concentration of aqueous methanol was prepared. Fresh probe liquid was used for each test run.
- Samples were affixed to the sample holder using the double-sided tape provided by the manufacturer. During application of the roller for fixing the sample, the sample was covered with a protective paper to ensure that dust from the roller did not contaminate the sample.
- It was observed that during the initial tests with aqueous methanol solutions, plunging of the samples resulted in release of fine air bubbles that were introduced during preparation of the solution. This initial rise of air bubbles into the path of the ultrasonic signal greatly affected the signal transmission. In order to eliminate this effect, the empty sample holder was plunged several times into the test liquid until all the bubbles were 'knocked-out' of the solution and a constant transmission was obtained.
- For all the tests both the 10mm and 35 mm sensors were used for measurement of the ultrasonic transmission, except for the Nuclepore® 5 micron sample. For the Nuclepore® 5 micron membrane, sample sizes available were only 50 mm x 20 mm, hence testing was done using only the smaller 10mm sensor for this case.

- A minimum of three separate measurements were done for each combination of probe liquid and porous sample. These results are given in *Appendix F*. Results reported here are the average of the curves obtained from the different runs. The average curve is generated by the Emco DPM software. The standard deviation and percentage standard errors on the mean were also calculated from the data from the individual curves. The results are reported in Table 4.22(a) to (d).
- Fresh test samples were used for each run for tests with the Nuclepore® membranes, glass fibre paper and commercial paper samples. For Spectra Meshes and Voith woven fabrics, the same sample was tested each time. After each run, the sample was allowed to dry completely in the mounted position, without removing it from the adhesive tape.

A summary of the test procedures for different samples is given in Table 4.19. Relevant details and observations for each class of pore structures are given in the respective sections below.

Table 4.19: Test Procedure Summary

	Step	Nuclepore® Membranes	Spectra Meshes	Voith Fabrics	Commercial paper & Glass fibre paper
1.	Presoaking in methanol	Yes	Yes	Yes	No
2.	Conditioning in constant temperature and humidity room	No	No	No	Yes
3.	Probe liquids				
	Distilled water	Yes	Yes	Yes	Yes
	6% aq. methanol	Yes	Yes	No	No
	20% aq. methanol	Yes	Yes	No	No
	40% aq. methanol	Yes	Yes	No	No
	70% aq. methanol	Yes	Yes	No	No
	100% methanol	Yes	Yes	No	No
	Polydimethylsiloxane	No	No	No	Yes
4.	Sensors used 10mm & 35mm	Yes, except for 5-micron Membrane	Yes	Yes	Yes
5.	Penetration from one side	Yes	Yes	Yes	Yes

	Step	Nuclepore® Membranes	Spectra Meshes	Voith Fabrics	Commercial paper & Glass fibre paper
6.	Penetration from both sides	No	Yes, with distilled water only	Yes, with distilled water only	No

Nuclepore® Membranes

These membranes have a thickness of the order of approx. 10 microns. Membranes of higher thickness are not available commercially. Handling of these membranes is quite difficult, because they are very thin. Testing of samples was initially done with penetration of the probe liquid from both sides. Immersion of the samples at the maximum immersion speed resulted in some experimental problems such as slight dislocation of the sample due to its flimsy nature. It was also difficult to keep the sample taut and retain this tautness after immersion. It may be noted that Emco mentions that the instrument is sensitive to the thickness (and hence the air content of the sample). In view of this the tests were carried out with penetration of the probe liquid from one side. It was ensured that the entry of the liquid during the test was through the 'glossy side' of the membrane. Care was taken while mounting the test sample to avoid formation of any 'wrinkles' while sticking the sample to the tape. Since the pore size of the membranes is very small, care was taken to avoid contamination of the samples as far as possible. The membranes were handled with broad tipped forceps to avoid any contamination.

Initially the membranes were tested "as-is" without any pretreatment with methanol. As an example, the results obtained for the 2 micron membrane are shown in Figure 4.53. The manufacturer's catalogue indicated that the membranes are inert to methanol. A confirmation on this was also obtained from the manufacturer. The sets of experiments were repeated after pre-treating the membranes with methanol. The results obtained from this set of experiments for the 2 micron membrane are shown in

Figure 4.54. It can be seen that there are differences in the results obtained after pretreatment with methanol. Further investigation and inquiries to the manufacturer's

R&D department revealed that the polycarbonate membranes actually had a coating of PVP (polyvinylpyrrolidone) which is used to make the surface of the membrane hydrophilic. PVP is soluble in methanol, however, it is difficult in this case to predict how much had been removed and hence the results obtained so far were uncertain.

PVP-free membranes were obtained from the manufacturer and the experimental sets were repeated after pretreatment of the membranes in methanol. The average results of three different runs using both sensors for each membrane with different probe liquids are shown in Figure 4.55 to Figure 4.58. The same results for a particular probe liquid with different membranes are shown in Figure 4.59 to Figure 4.64. These results were considered as the final results for Nuclepore® membranes with the different probe liquids and were used for further analysis.

Figure 4.53: Nuclepore® 2 micron - 'Untreated' PC membrane with different probe liquids

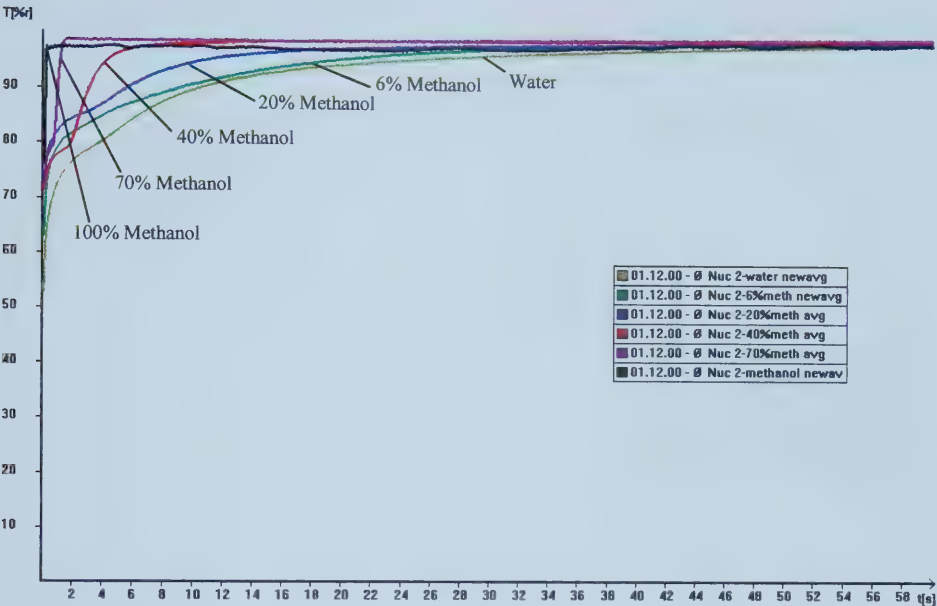


Figure 4.54: Nuclepore® 2 micron - 'Methanol Treated' PC membrane with different probe liquids

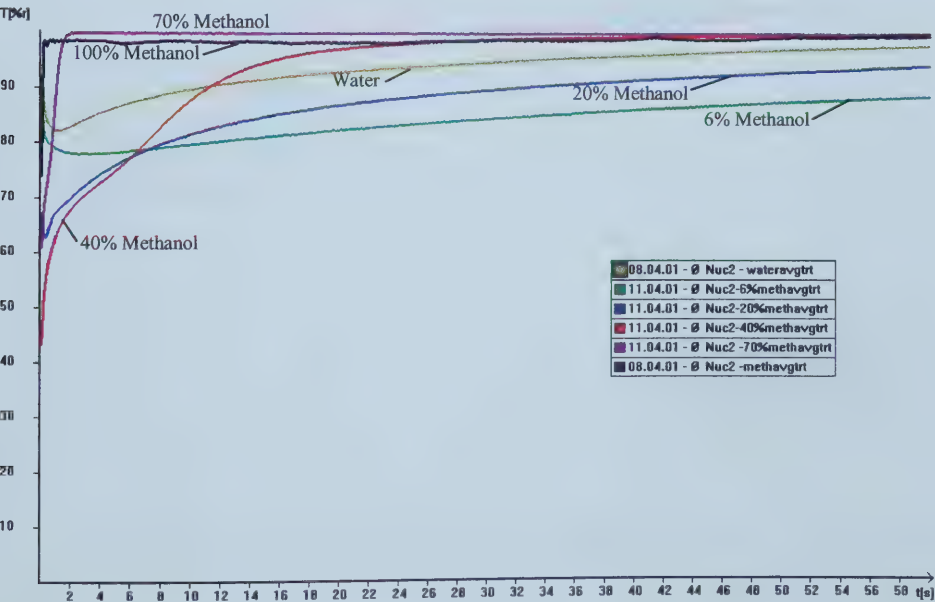
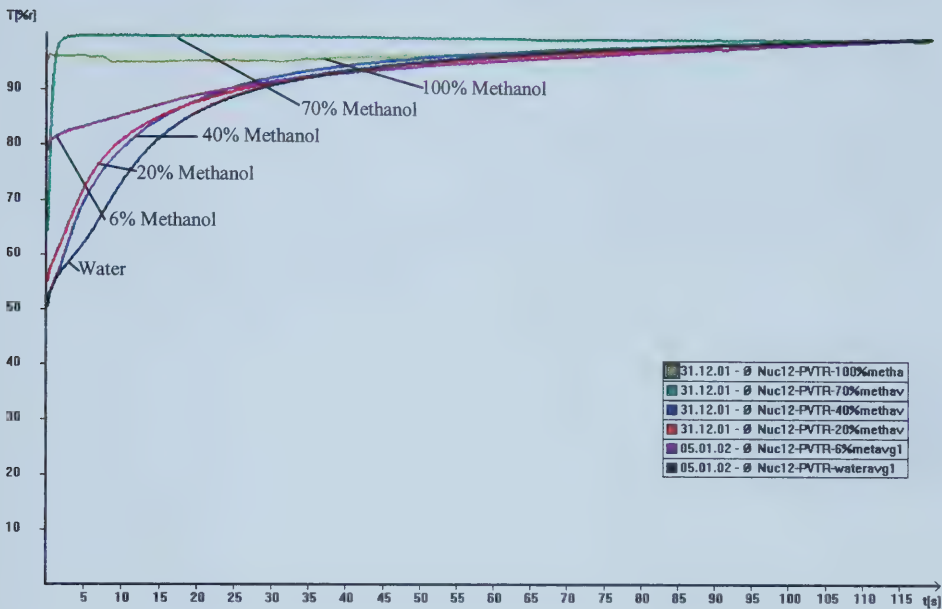
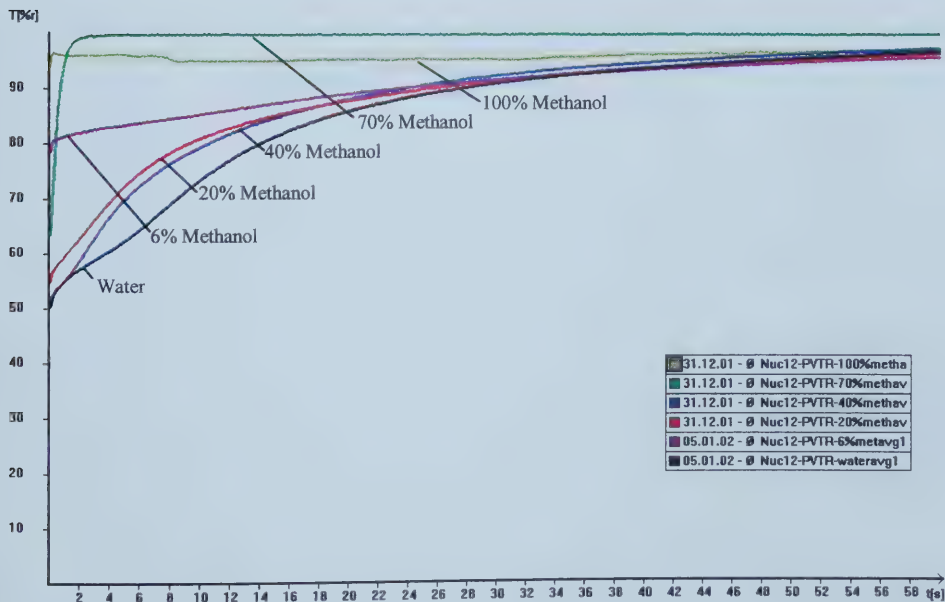


Figure 4.55: (a) Nuclepore® 12 micron - different probe liquids (long time regime)



(b) Nuclepore® 12 micron - different probe liquids (intermediate time regime)



(c) Nuclepore® 12 micron - different probe liquids (short time regime)

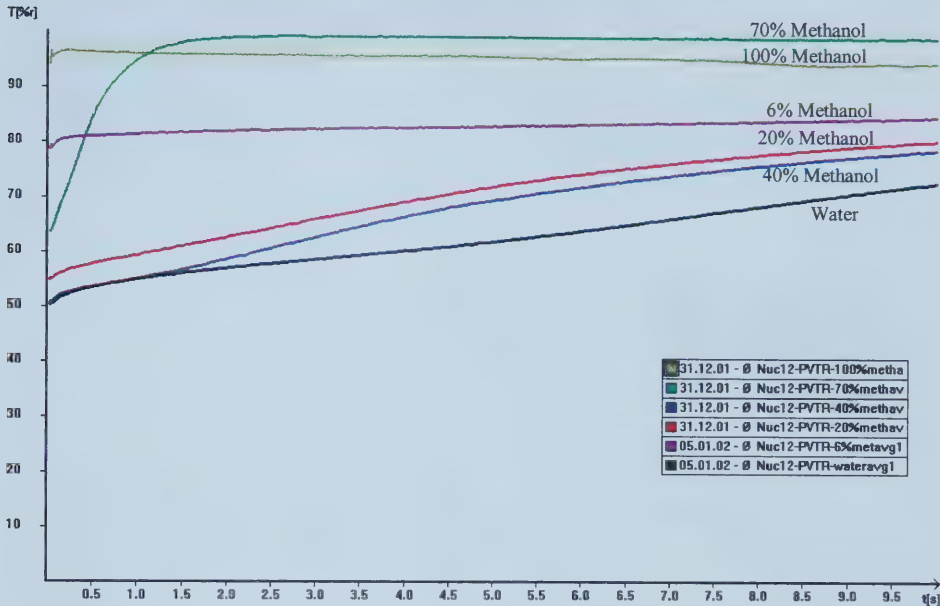
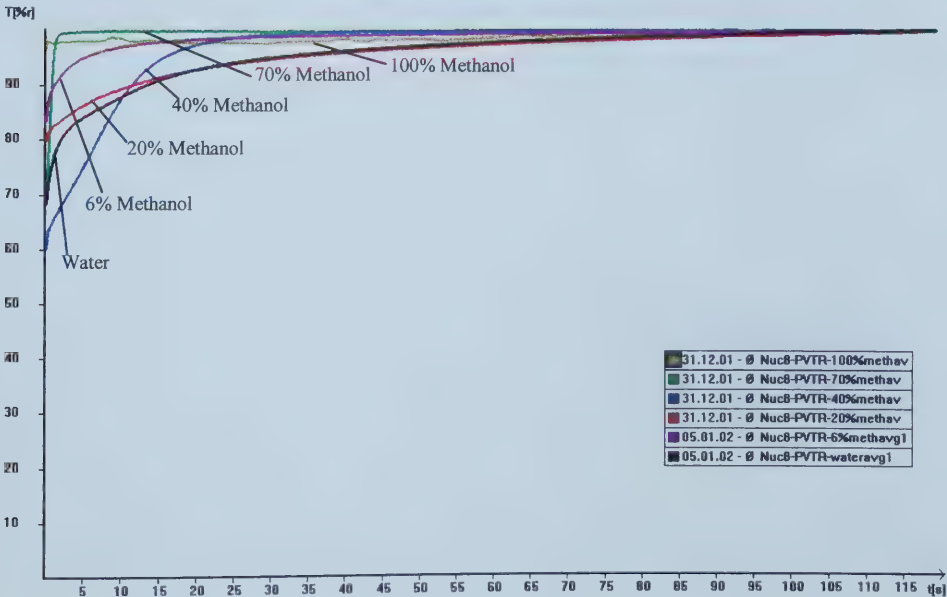
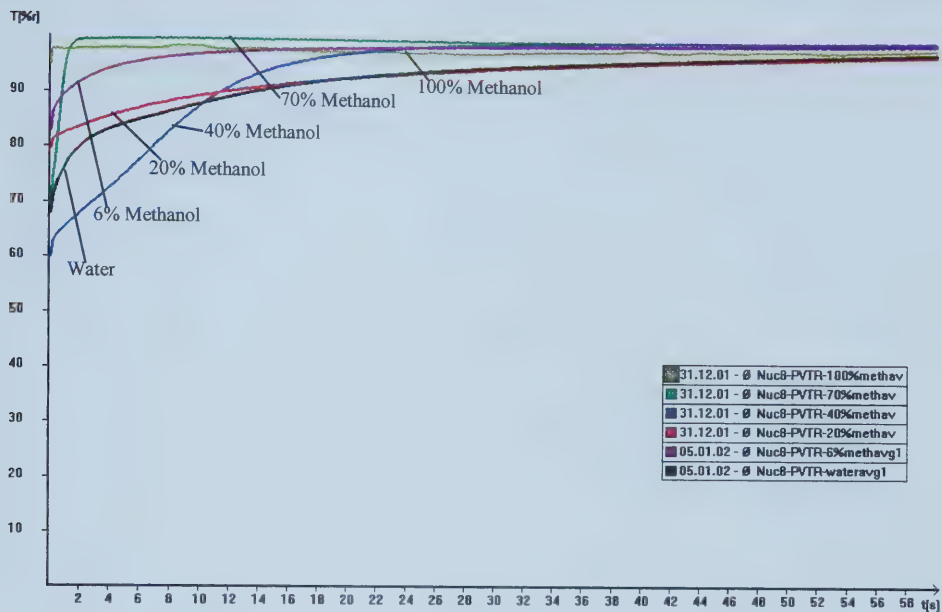


Figure 4.56: (a) Nuclepore® 8 micron - different probe liquids (long time regime)



(b) Nuclepore® 8 micron - different probe liquids (intermediate time regime)



(c) Nuclepore® 8 micron - different probe liquids (short time regime)

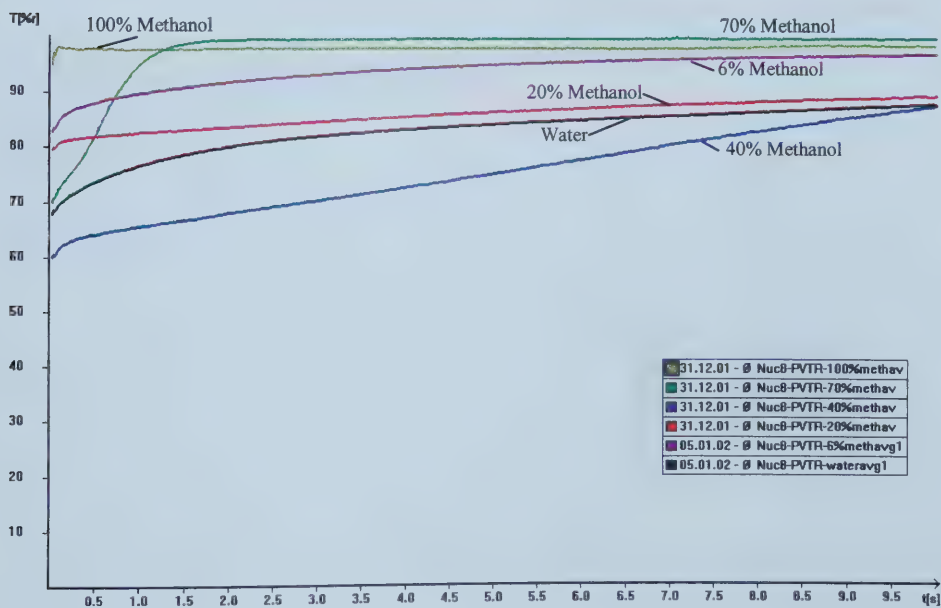
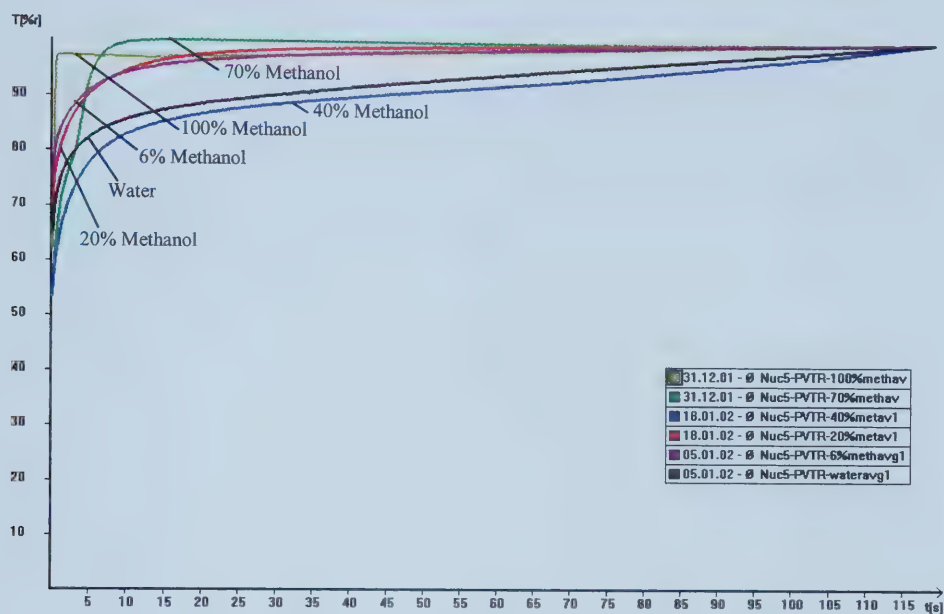
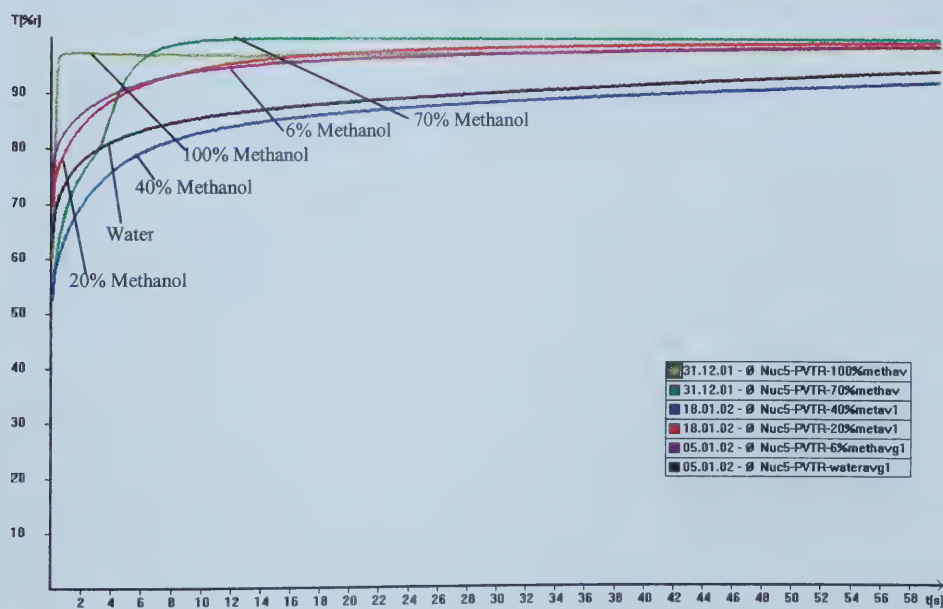


Figure 4.57: (a) Nuclepore® 5 micron - different probe liquids (long time regime)



(b) Nuclepore® 5 micron - different probe liquids (intermediate time regime)



(c) Nuclepore® 5 micron - different probe liquids (short time regime)

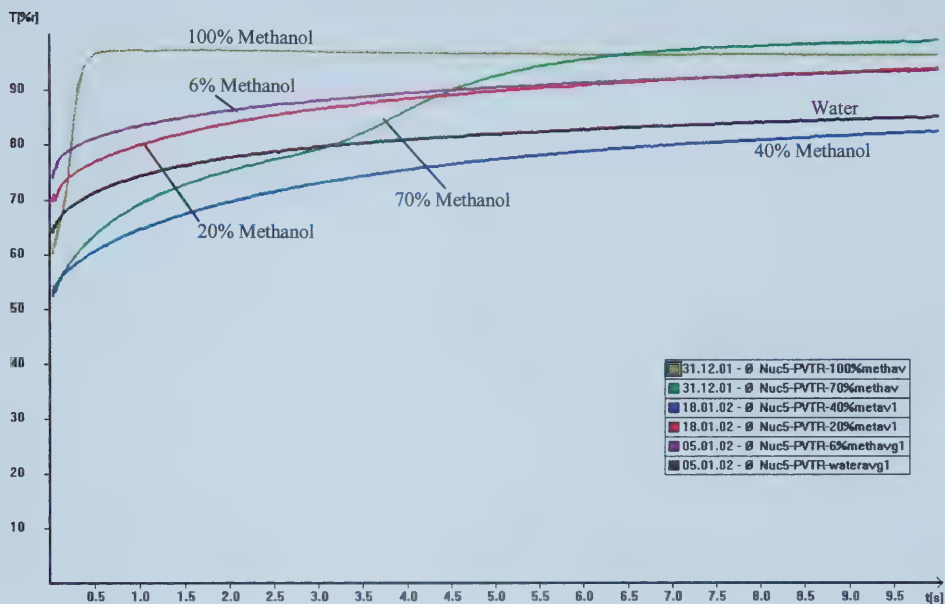
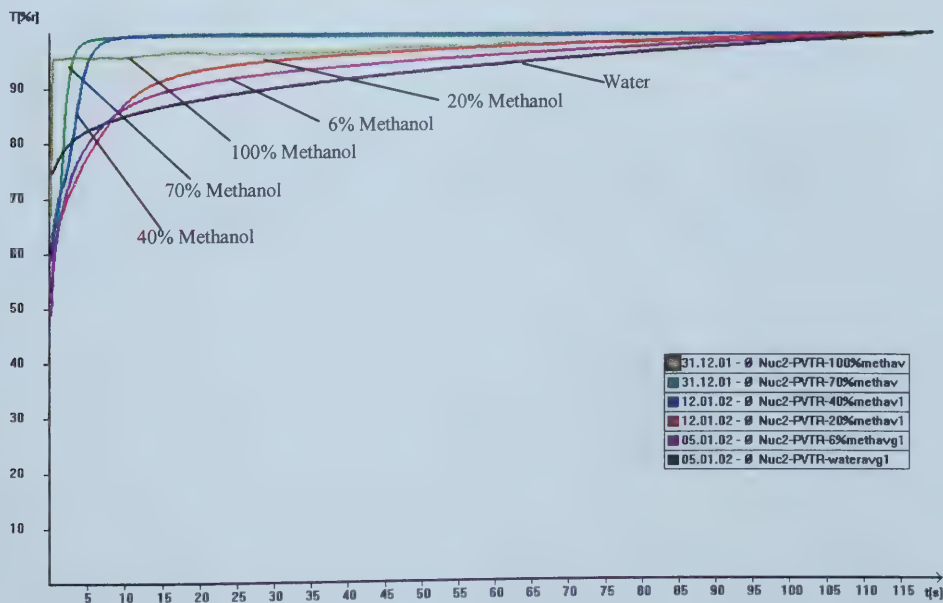
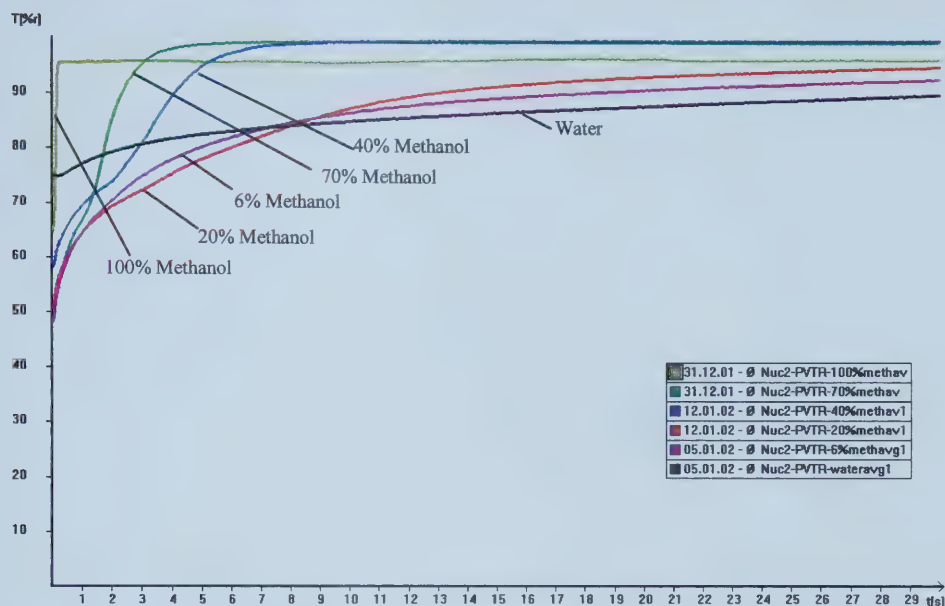


Figure 4.58: (a) Nuclepore® 2 micron - different probe liquids (long time regime)



(b) Nuclepore® 2 micron - different probe liquids (intermediate time regime)



(c) Nuclepore® 2 micron - different probe liquids (short time regime)

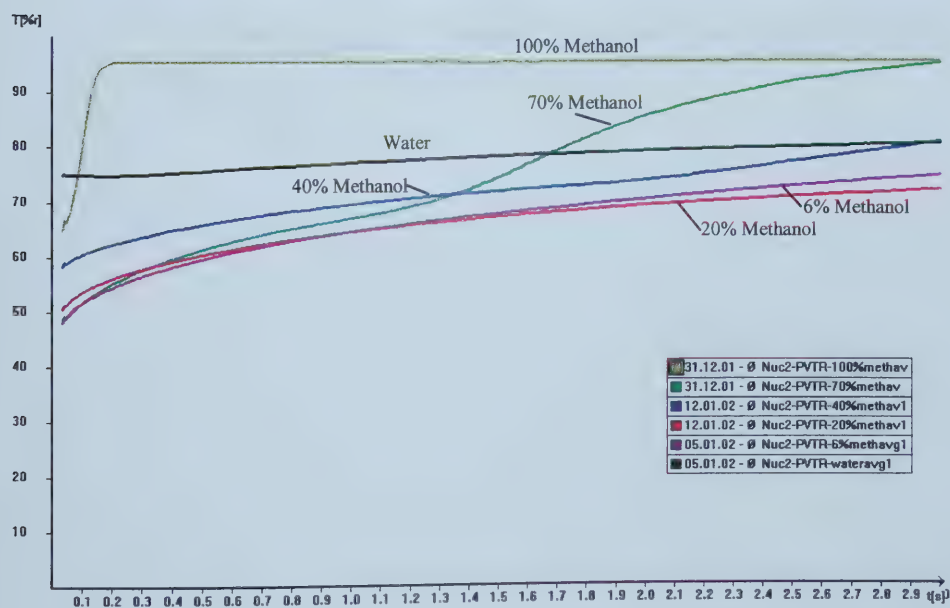


Figure 4.59: Different Nuclepore® Membranes - Distilled Water

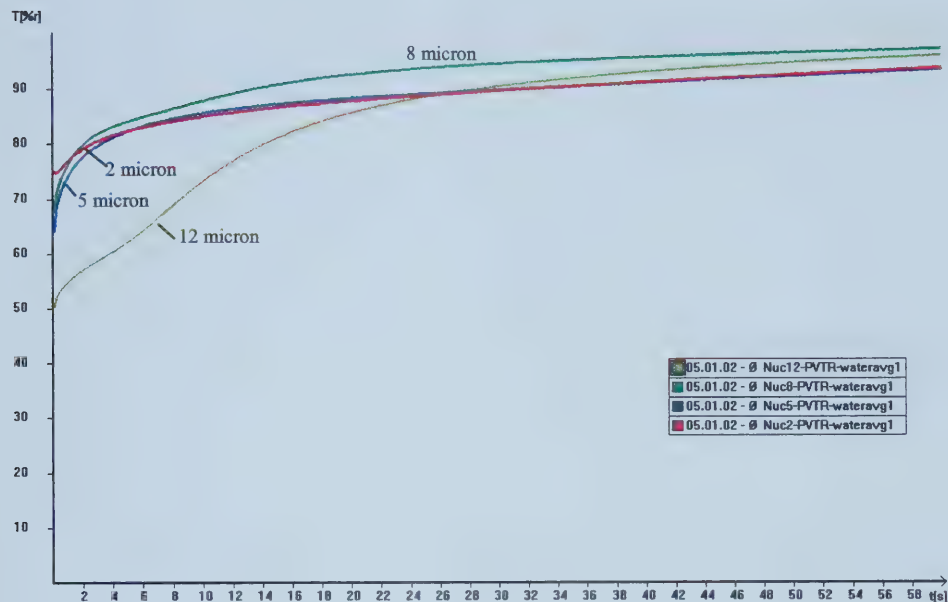


Figure 4.60: Different Nuclepore® Membranes - 6% Methanol

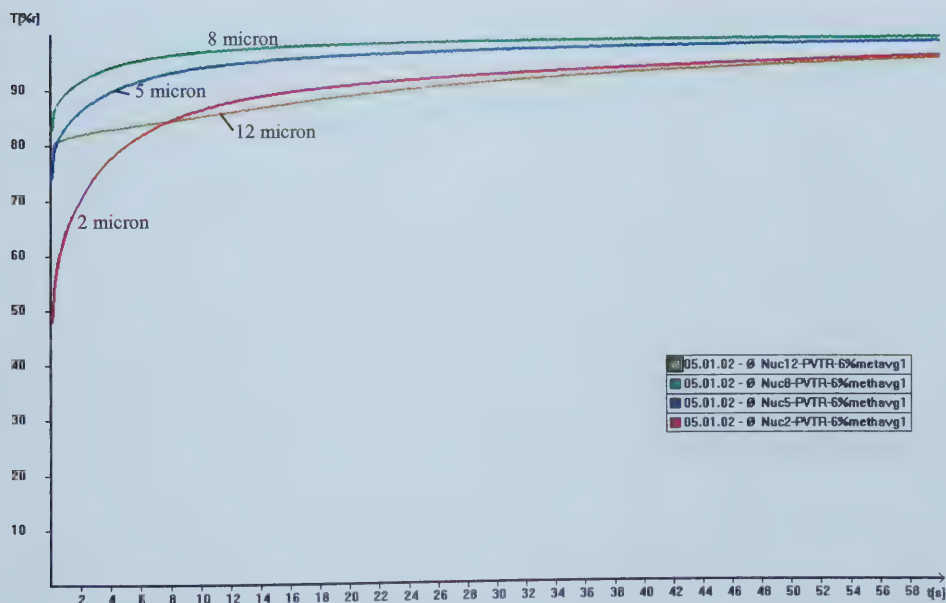


Figure 4.61: Different Nuclepore® Membranes - 20% Methanol

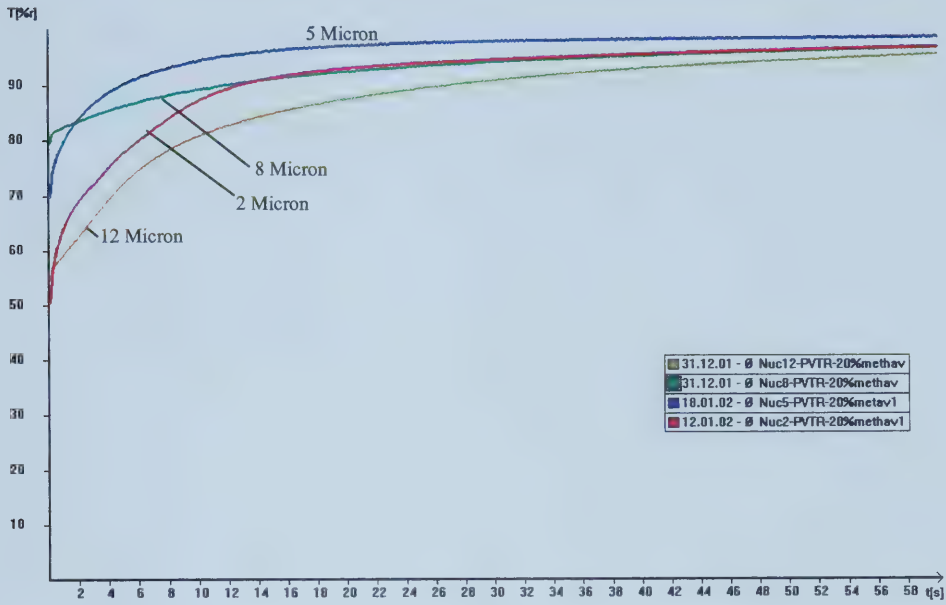


Figure 4.62: Different Nuclepore® Membranes - 40% Methanol

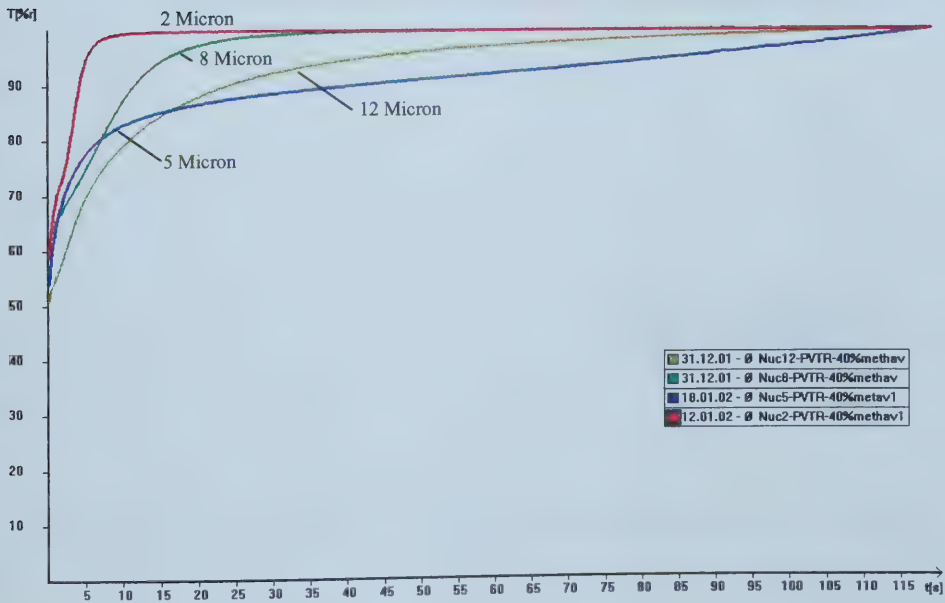


Figure 4.63: Different Nuclepore® Membranes - 70% Methanol

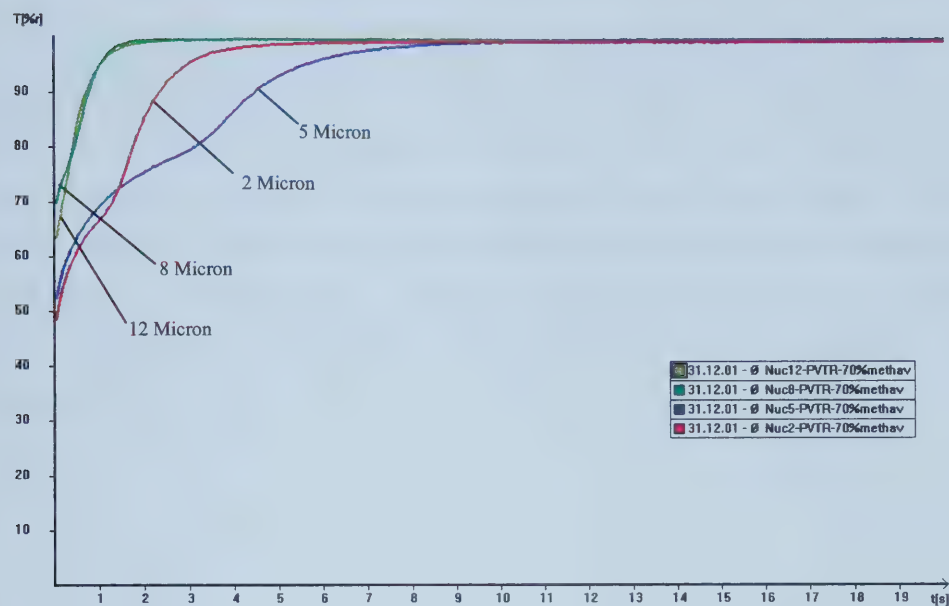
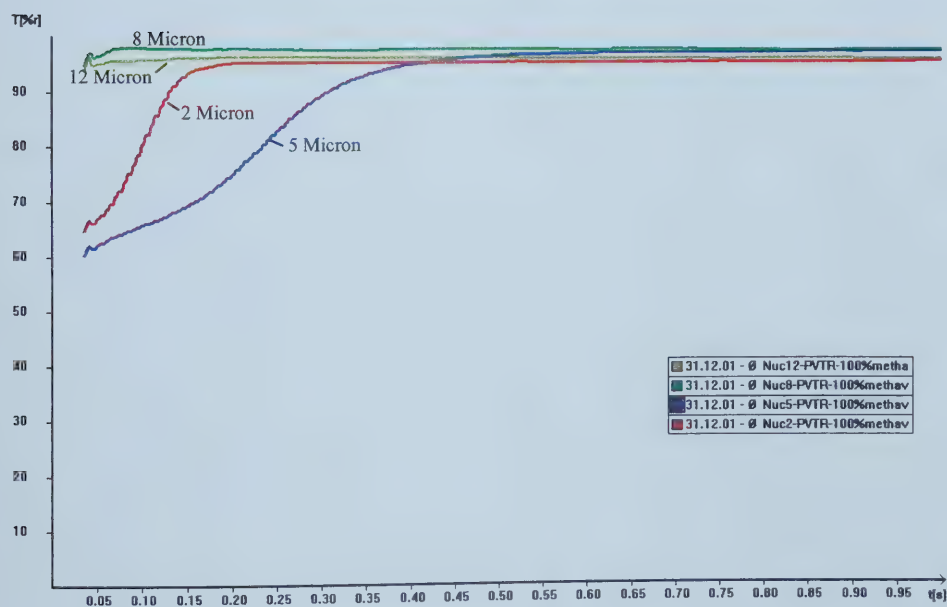


Figure 4.64: Different Nuclepore® Membranes - 100% Methanol



Voith Spectra Meshes

All tests were done with the penetration of the probe liquid from 'side 1' of the sample. The probe liquids used were distilled water and 6%, 20%, 40%, 70% wt aqueous methanol solutions and pure methanol. The results obtained for each Spectra mesh with the different probe liquids are shown in Figure 4.65, Figure 4.66 and Figure 4.67. Figure 4.68 to Figure 4.73 show the same results of the dynamics obtained for a particular probe liquid with the different meshes. The samples were also tested with liquid penetration from both sides using distilled water as the probe liquid. The results obtained are shown in Figure 4.74.

Figure 4.65: Spectra F - Different Probe Liquids

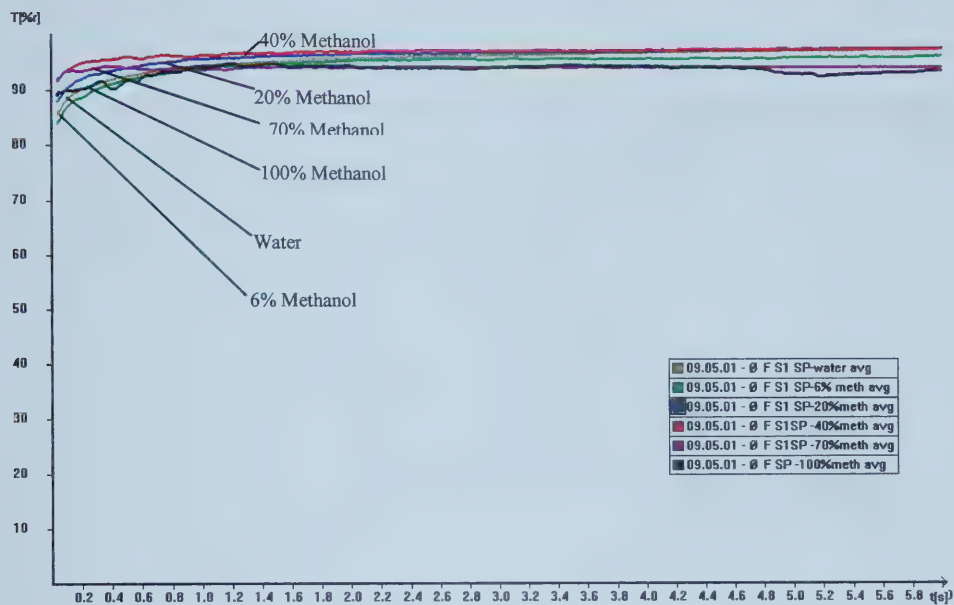
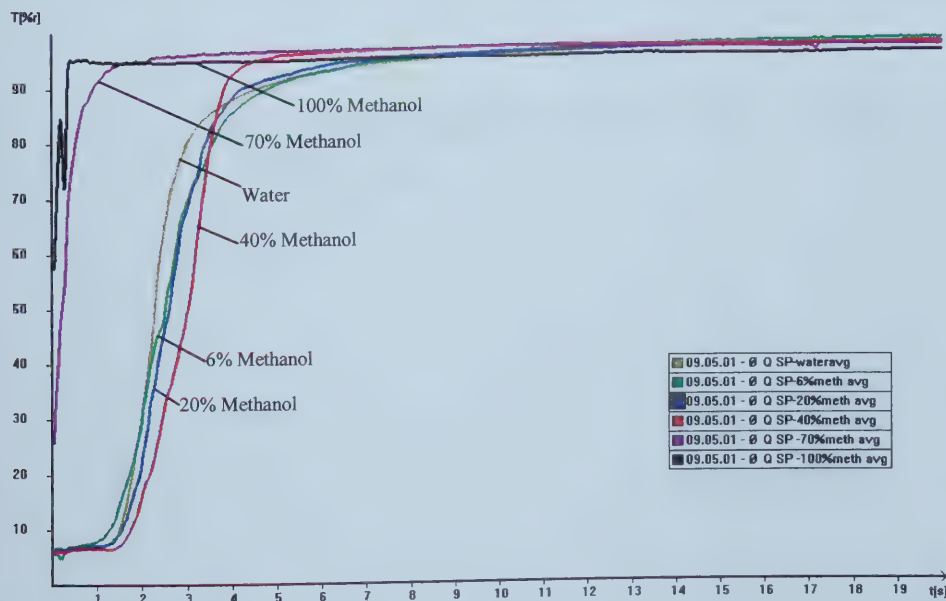


Figure 4.66: (a) Spectra Q - Different Probe Liquids (Long Time Regime)



(b) Spectra Q - Different Probe Liquids (Short Time Regime)

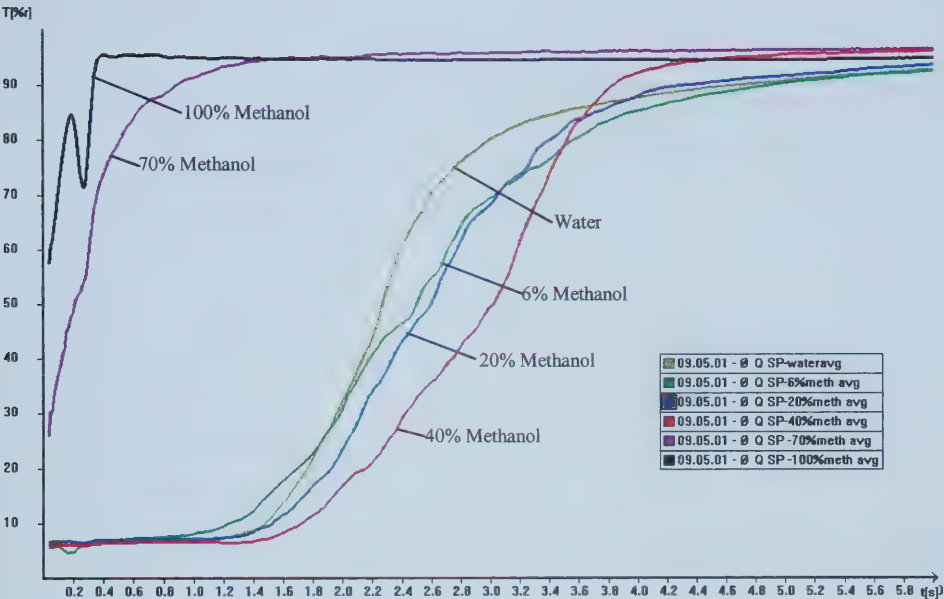
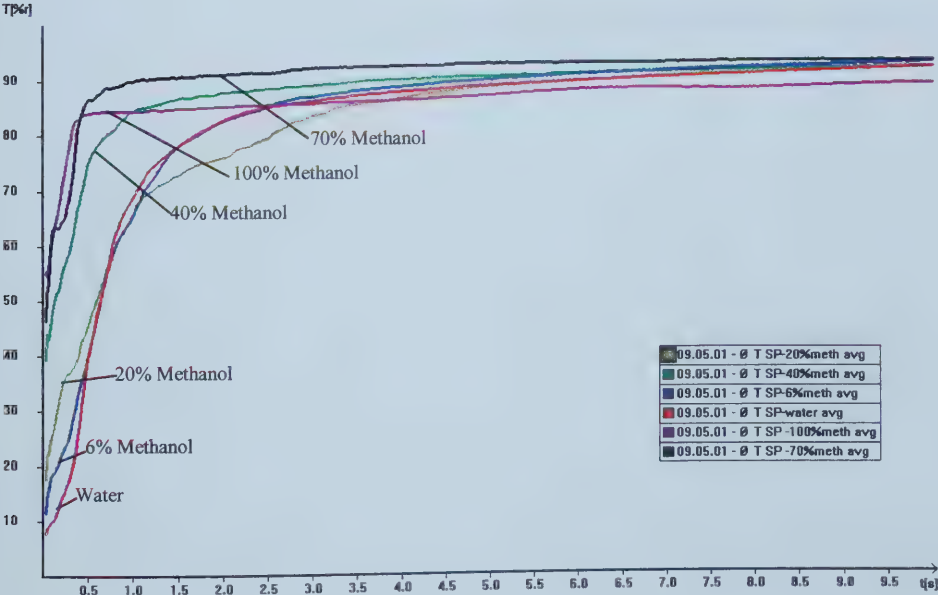


Figure 4.67: (a) Spectra T - Different Probe Liquids (Long Time Regime)



(b) Spectra T - Different Probe Liquids (Short Time Regime)

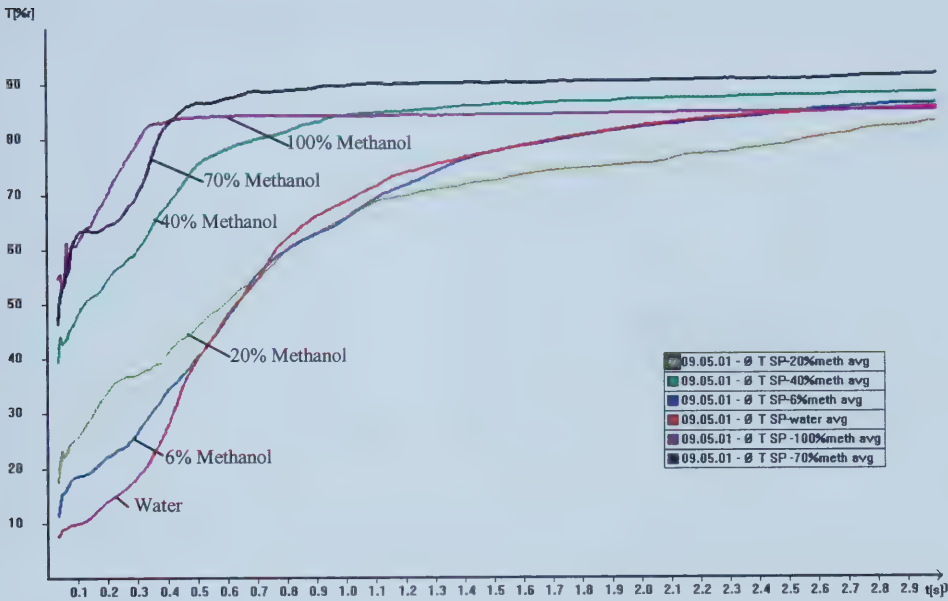


Figure 4.68: Different Spectra Meshes - Distilled Water

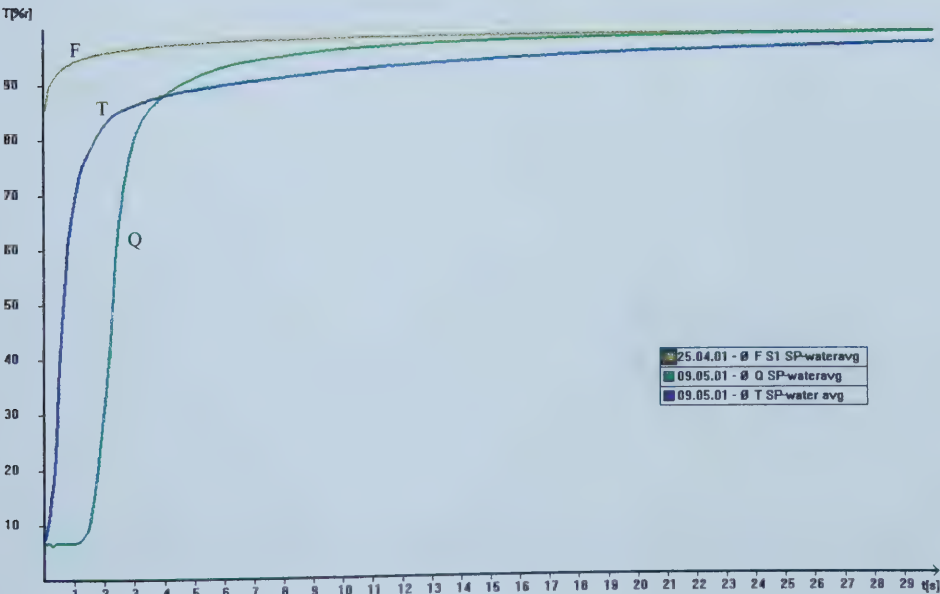


Figure 4.69: Different Spectra Meshes - 6% methanol solution

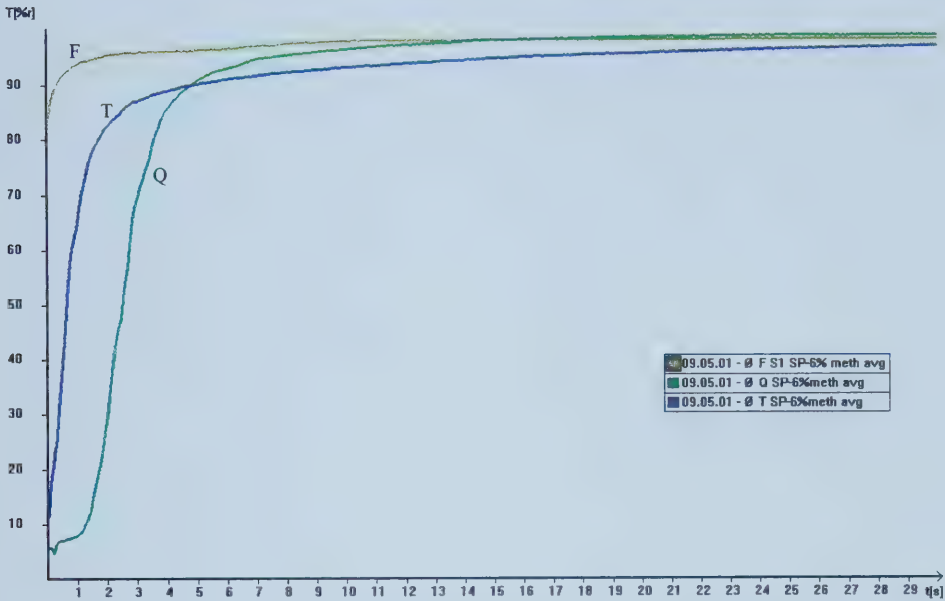


Figure 4.70: Different Spectra Meshes - 20% methanol solution

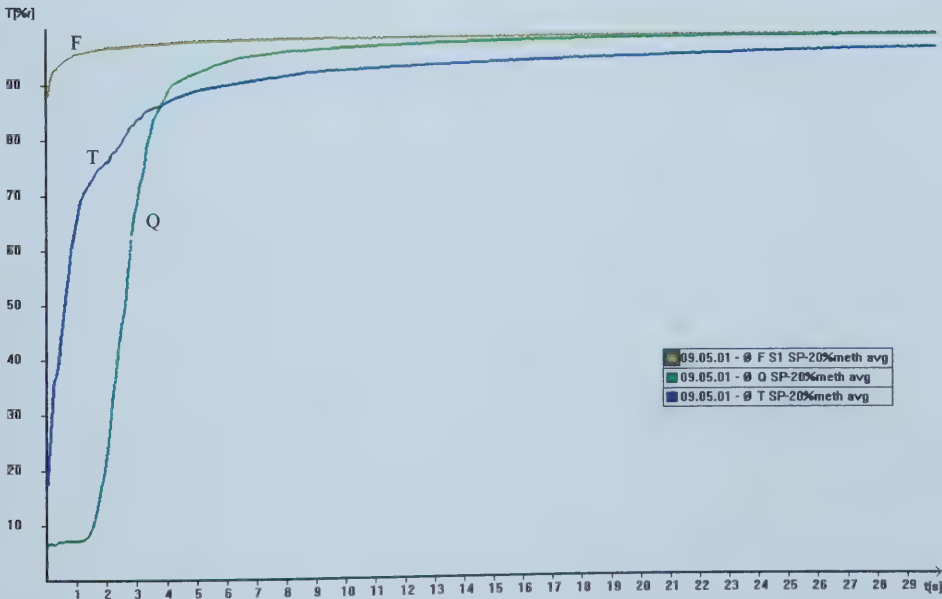


Figure 4.71: Different Spectra Meshes - 40% methanol solution

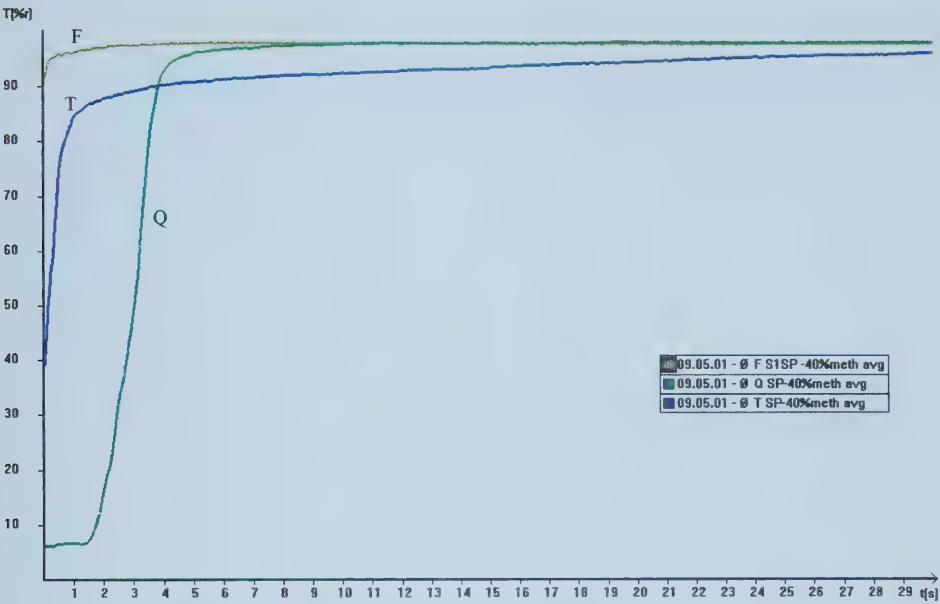


Figure 4.72: Different Spectra Meshes - 70% methanol solution

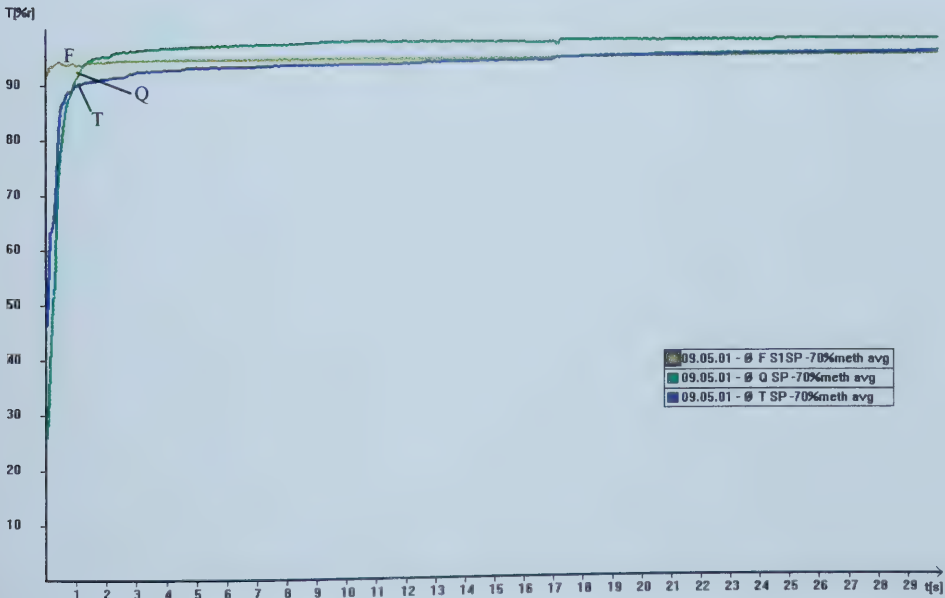


Figure 4.73: Different Spectra Meshes - 100% methanol solution

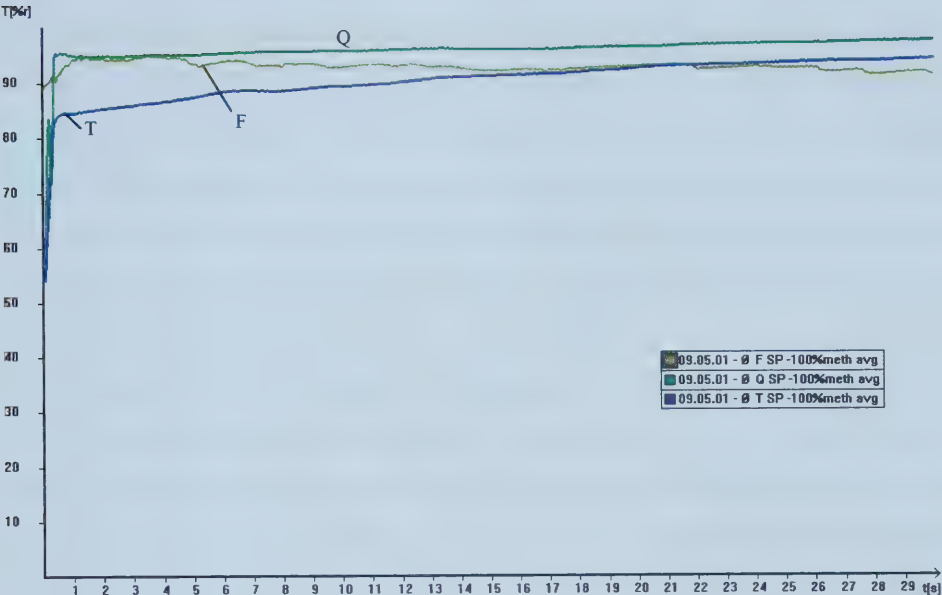
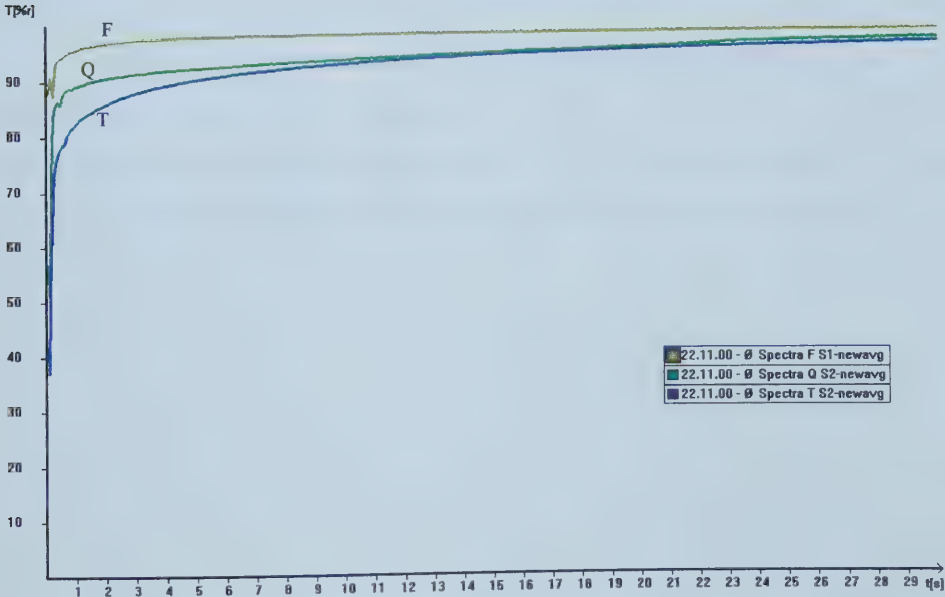


Figure 4.74: Different Spectra Meshes - Distilled water (penetration from both sides of sample)

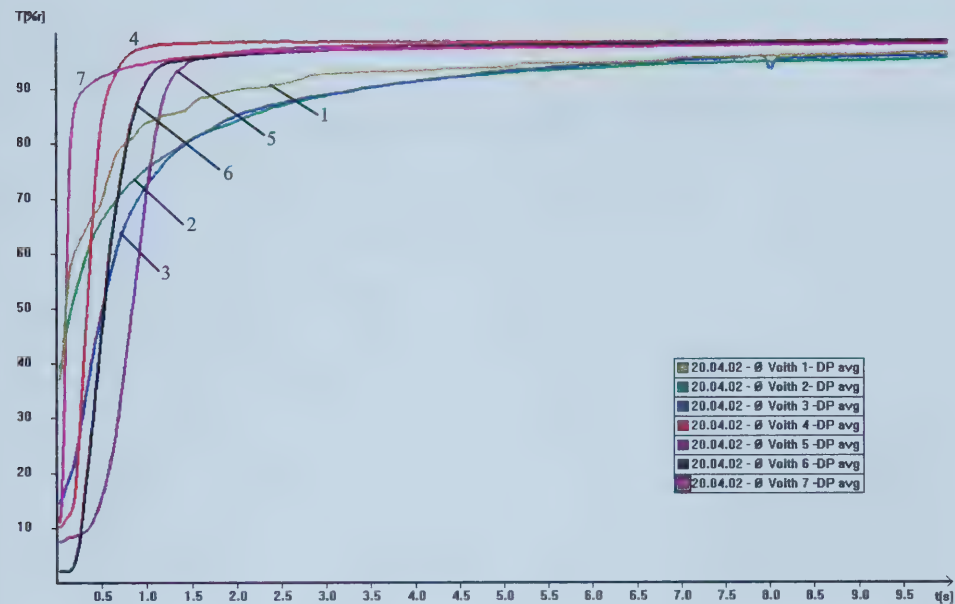


Voith Fabrics

The test liquid used for this set of model pore structures was distilled water. The Voith fabric samples are 'two-sided' depending on the number of weave layers, and do not have a smooth surface for mounting on the double sided adhesive tape. In view of this, the tests were initially done with penetration of the probe liquid from both sides. The average curves obtained for the seven different fabric samples with penetration of water from both sides are shown in Figure 4.75 (a) and (b). Tests were also tried with methanol as the probe liquid. However, it was observed that the sample was wetted and penetrated too rapidly for the instrument to detect any dynamics.

The samples were also tested with penetration of liquid from one side. The average curves obtained are shown in Figure 4.76 (a) and (b). For this set of runs, the same sample was remounted each time on the double-sided adhesive tape after allowing the sample to dry completely in between runs. It may be noted that sample remounting is an important issue for this set of results. Since the surface of the sample is not smooth and only the 'knuckles' of the fibres are in contact with the tape, conceivably each remounting of the sample could result in a different air layer formation between the sample and the tape. The force with which the roller is applied to the sample during mounting is also important in order to ensure that the sample 'sticks' well to the tape surface. For samples which are double or triple layer weave structures and essentially 'two-sided', both sides were tested separately with penetration of liquid from one side. The differences in penetration dynamics for the samples (Voith 2, 3 & 7) which were tested on both sides separately for liquid penetration, from one side only can be seen in Figure 4.77.

Figure 4.75: (a) Voith Woven Fabrics - Penetration with water from both sides
(Long time regime)



(b) Voith Woven Fabrics - Penetration with water from both sides
(Short time regime)

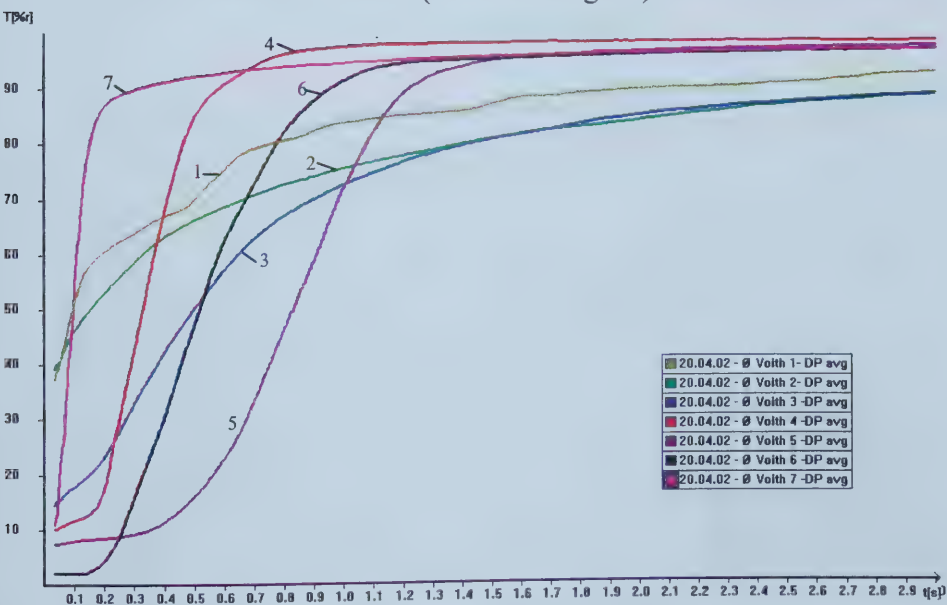
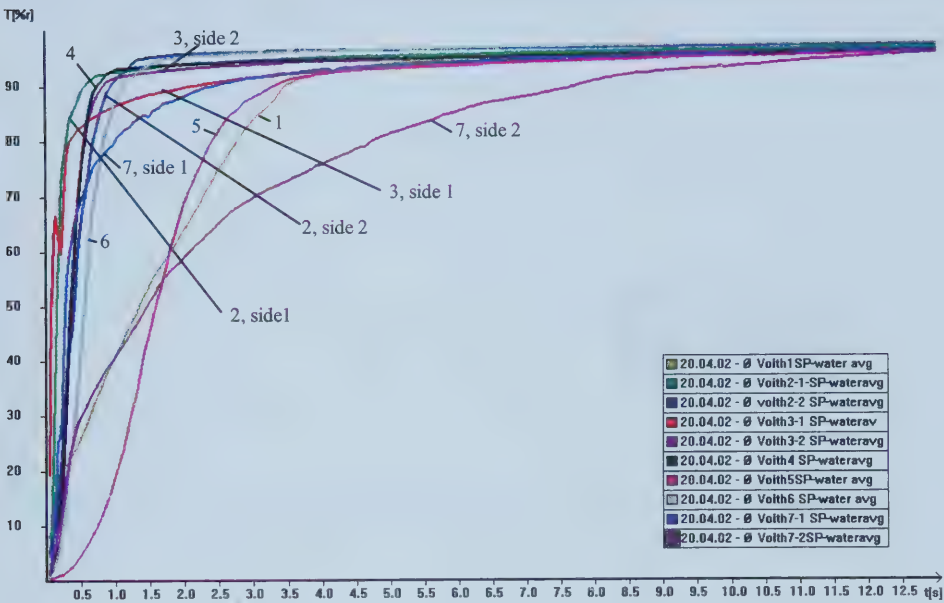


Figure 4.76: (a) Voith Woven Fabrics - Penetration with water from one side
(Long time regime)



(b) Voith Woven Fabrics - Penetration with water from one side
(Short time regime)

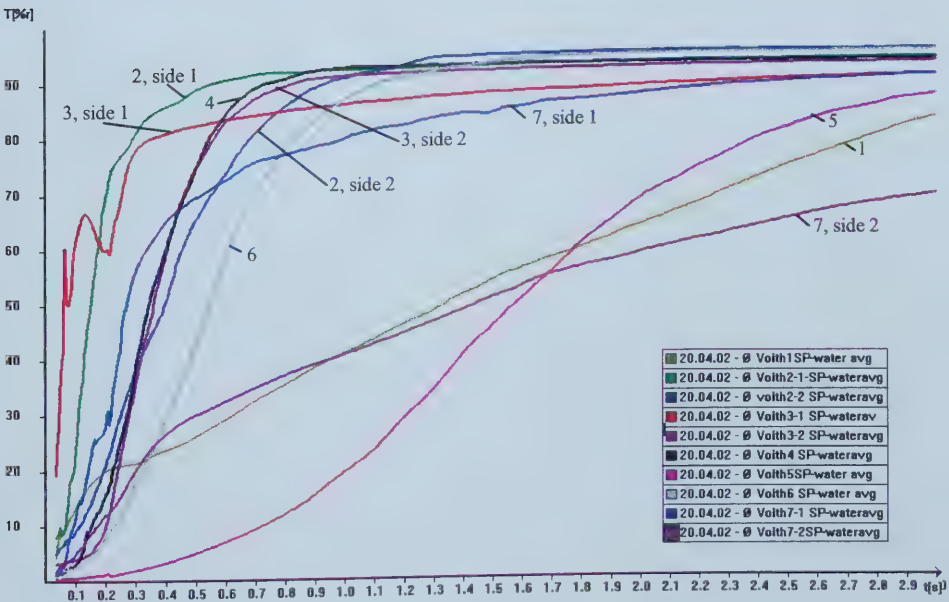
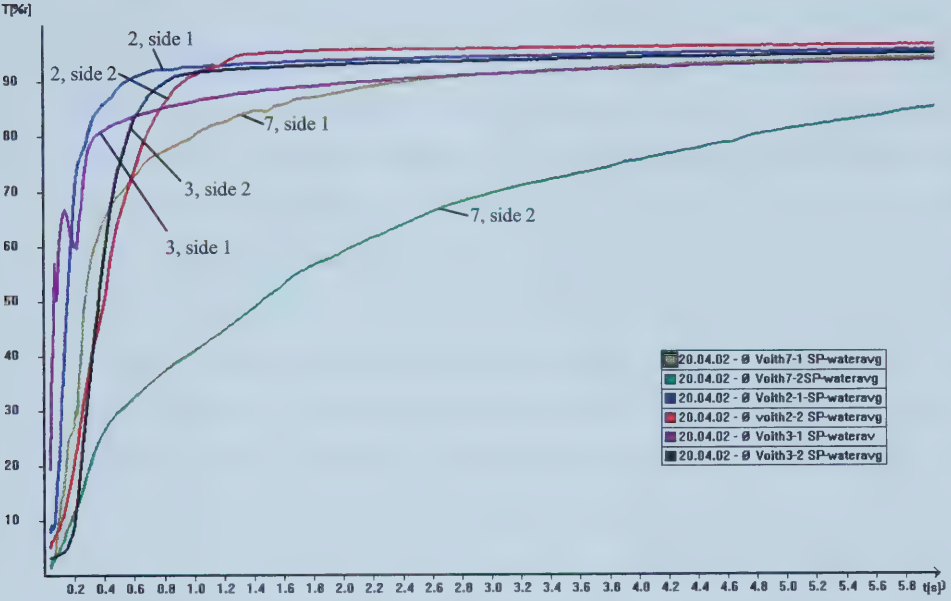


Figure 4.77: Voith Woven Fabrics - Penetration with water from one side
(Comparison of Side 1 with Side 2)



Micro-etch® Screens

Initially screen sample 6-4-4 was tested with penetration of liquid from both sides as well as from one side. The test liquid used was distilled water. The average results obtained from the runs with 6-4-4 are shown in Figure 4.78. The dynamics obtained were very fast. The curve obtained was very flat except in the initial 50 msec time regime where some dynamics can be noticed. The SS316 material of the screens had a high contact angle with water. This could be easily seen if a small drop of water was placed on the surface of the sample. The drop did not spread and wet the surface of the sample. Similar results were obtained with another sample 8-6-2 as can also be seen in Figure 4.78. The results obtained with the two samples and with a 6% wt. methanol solution in water are shown in Figure 4.79. The response of the instrument to liquid penetration in these metal screen samples was not clear. The very quick response obtained was probably because the transmission of ultrasound in metals is very high. The results were sent to Emco GmbH for their comments and to find out their experience with testing of metal porous samples. However, no response has been obtained from Emco to date.

Micro-mesh® Precision Sieves

Sample 150 lpi (59 lines/cm) was tested with water with penetration from one side. The results obtained are shown in Figure 4.80.

Figure 4.78: Micro-Etch® screen samples 6-4-4 and 8-6-2 - Results with penetration of water from one side and both sides

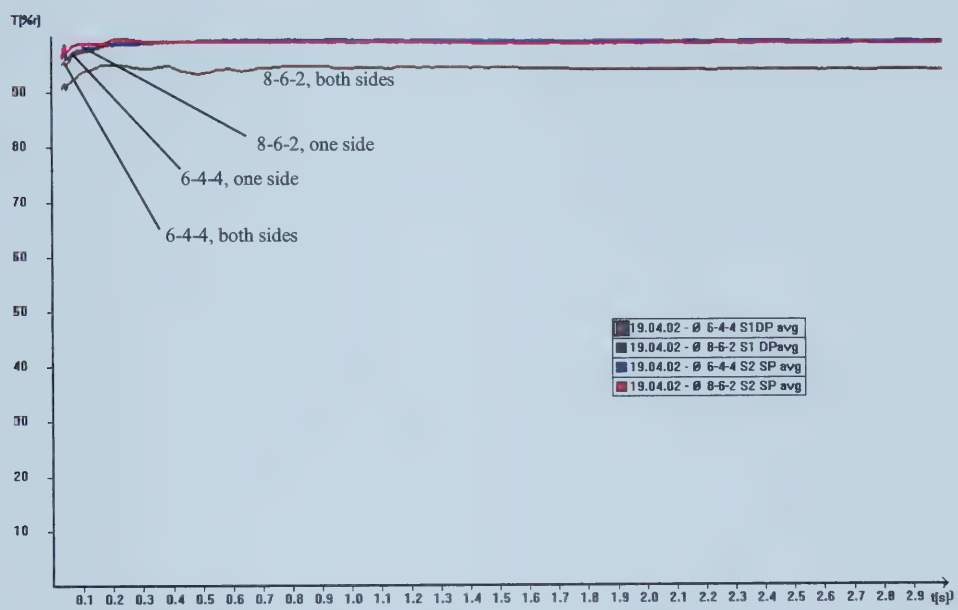


Figure 4.79: Micro-Etch® screen samples 6-4-4 and 8-6-2 - Results with penetration of 6%wt methanol solution from one side

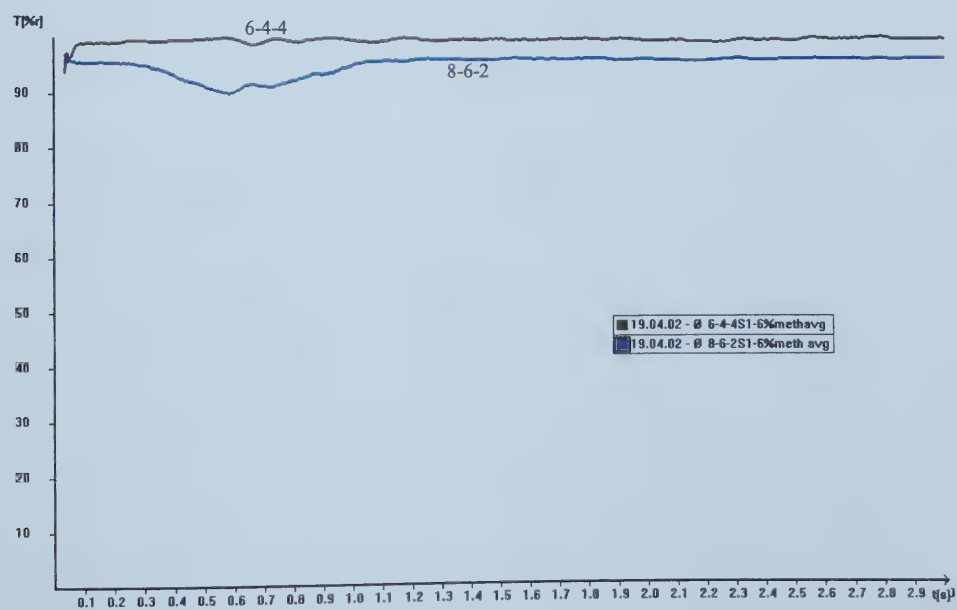
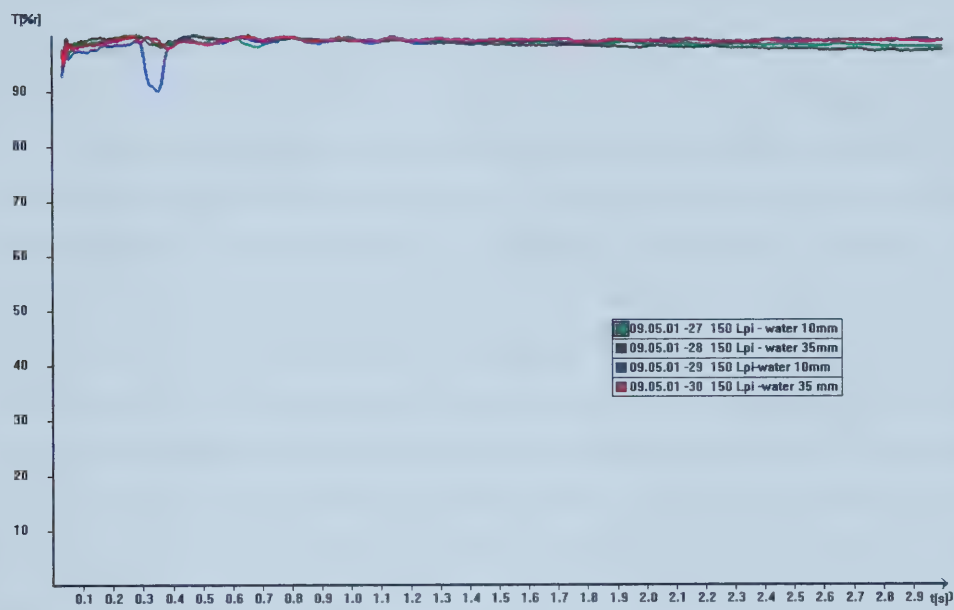


Figure 4.80: Micro-mesh® sieve sample 150 lpi - Results with penetration of water from one side



Commercial grade paper and glass-fibre paper

It has been observed in other reported tests using the Emco, that papers belonging to a similar grade give similar absorption profiles. For example, tests with various ink jet paper samples with different degrees of sizing will give similar shaped output curves with faster or slower penetration dynamics. However, tests with different grades of paper usually give very different absorption profiles. These profiles often show several different transition regions. As discussed earlier, the ultrasound transmission signal at the receiver is affected not only by the penetration of the test liquid into the paper structure, but also by the swelling and bonding of the cellulose fibres. In order to gain a better understanding of the absorption profiles given by the instrument, tests were conducted using different paper grades with swelling and non-swelling test liquids. The test liquids used were deionised water and an inert, non-swelling, low viscosity polydimethylsiloxane (PDMS) fluid (Dow Corning 200® fluid 1cSt). As an alternative, non-swelling glass fibre structures were also used for these tests.

The paper samples were conditioned in a constant temperature and humidity room (25°C and 50% RH) for a week. For all paper grades tests with liquid penetration from one side were done with the test liquid entering on the 'smooth' or 'felt' side of the paper.

The following were observed during the tests for particular grades of paper:

Hammermill / Champion - Numerous tiny bubbles were observed sitting on the surface of the test sample.

ANC - Offset and ANC - Rotogravure - Initial rapid degassing of the sample observed, bubbles escaped out from the sides and the surface. Tiny bubbles were observed on the surface of the sample

GF/A and GF/B - These are very soft and delicate glass fibre papers. Samples easily compressed under pressure from the sample-mounting roller. The surface of the sample puffed (pockets were formed) due to air escaping from its surface during the test process

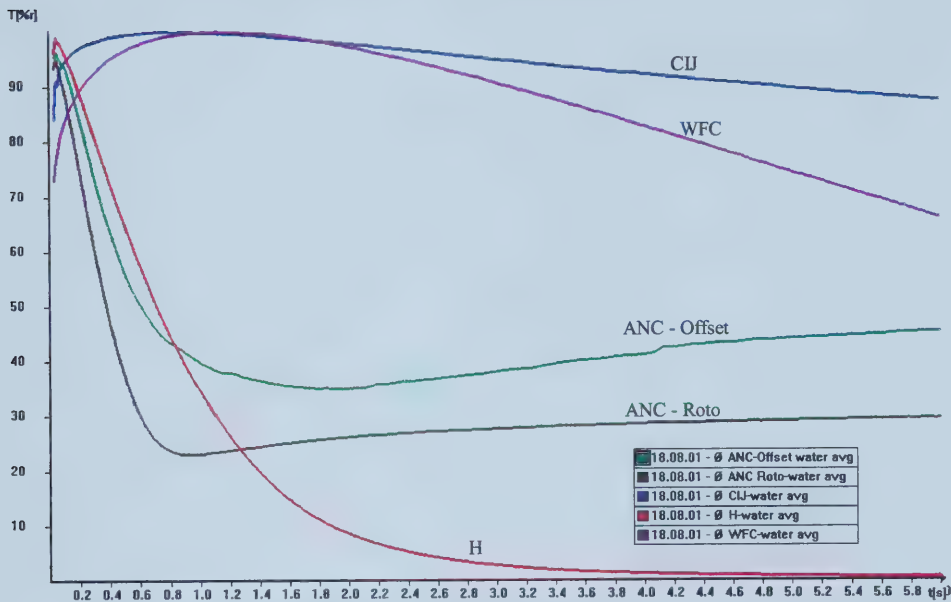
GF/F - Initial rapid degassing of the sample was observed. Air was seen escaping out from the sides of the sample.

1PS - Initially an attempt was made to measure penetration dynamics with test liquid penetration only from one side. However, after the sample was plunged into the test liquid it separated from the adhesive tape. Therefore, for this particular sample, testing was done with penetration of the test liquid from both sides.

The absorption profiles obtained from the tests on the different paper grades with water are shown in Figure 4.81, and with the non-swelling polydimethylsiloxane fluid are shown in Figure 4.82. The profiles obtained were very reproducible.

The absorption profiles obtained from the test on the different glass fibre papers with water are shown in Figure 4.83. The tests with filter grades GF/A and GF/B were not very reproducible, probably due to the fact that the samples were soft and compressible with the sample mounting roller pressure. However, the trend in all the results was similar. It can be seen that the GF/A, GF/B and GF/F grades gave profiles in which the transmission increases continuously as the water penetrated the samples. Results with the 1PS grade were quite different and showed two different regimes in which the signal initially increased to a maximum and then decreased again till it became constant. The 1PS glass filter grade has a hydrophobic surface treatment. The exact nature of the surface treatment is not known, but undoubtedly this would have been the main reason governing the absorption profile obtained. Corresponding absorption profiles with polydimethylsiloxane fluid are shown in Figure 4.84.

Figure 4.81: (a) Penetration Dynamics - Different Paper Grades with Water
(Short Time Regime)



(b) Penetration Dynamics - Different Paper Grades with Water
(Long Time Regime)

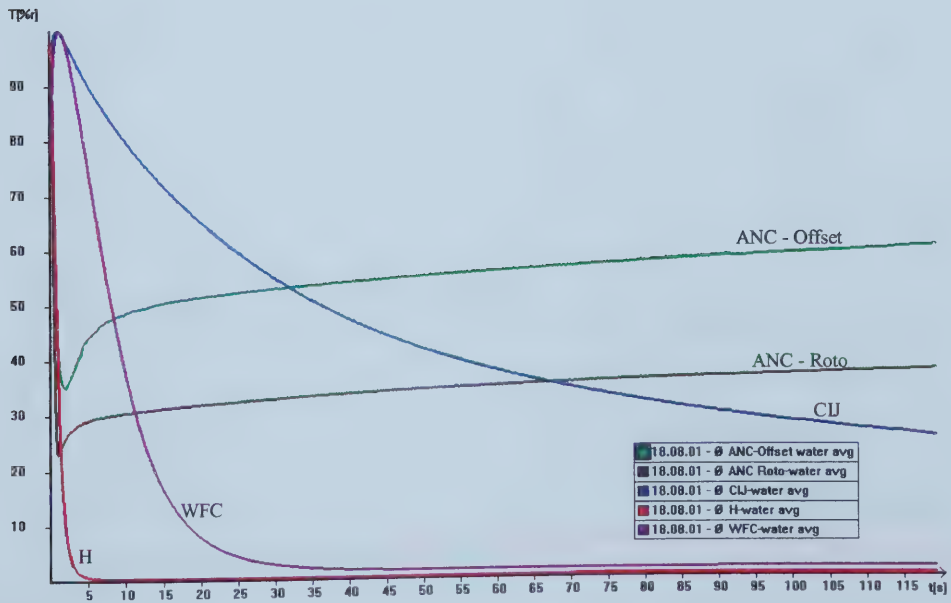


Figure 4.82: Penetration Dynamics - Different Paper Grades with Polydimethylsiloxane (Dow Corning 200 ® Fluid)

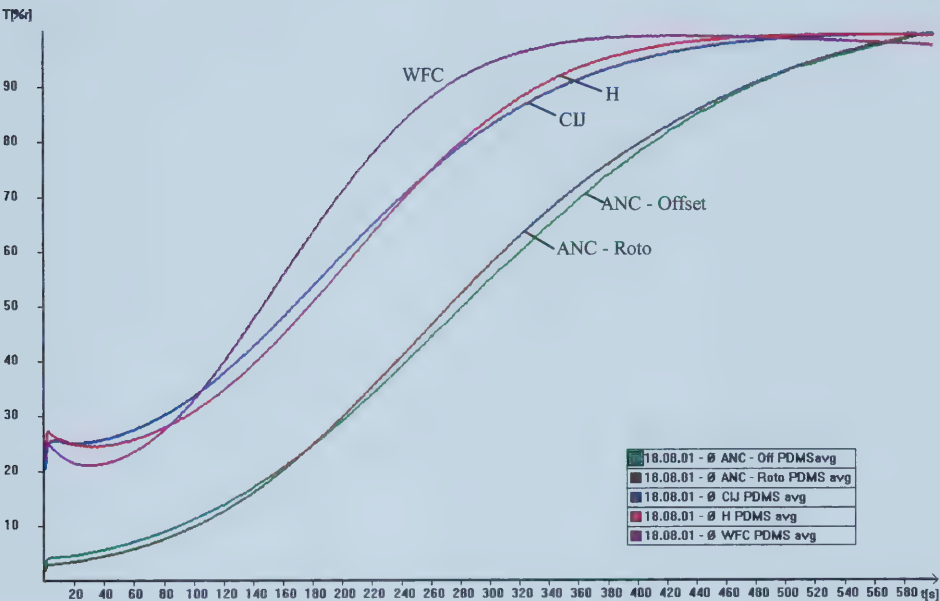
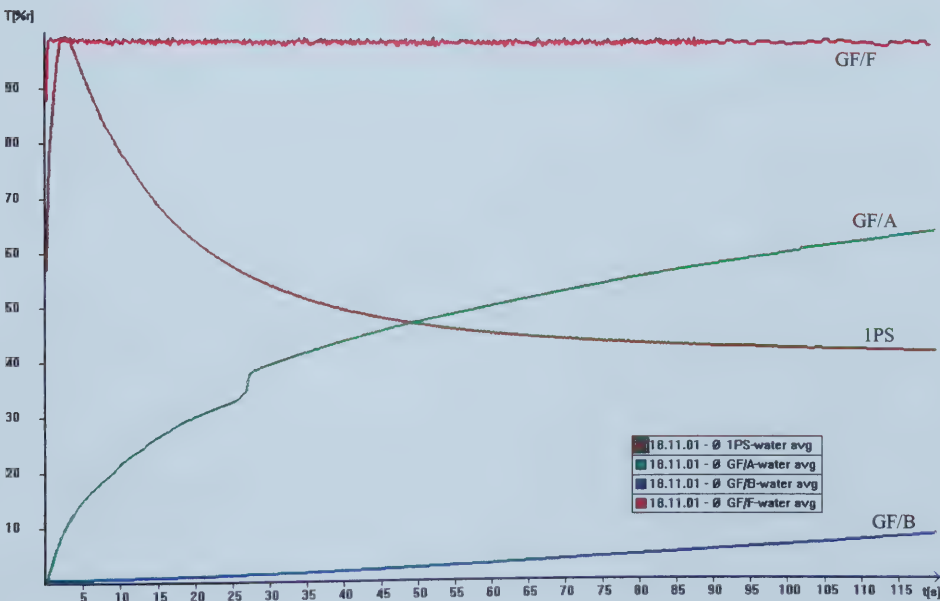


Figure 4.83: (a) Penetration Dynamics - Glass Fibre Paper with Water



(b) - Penetration Dynamics - Glass Fibre Paper With Water

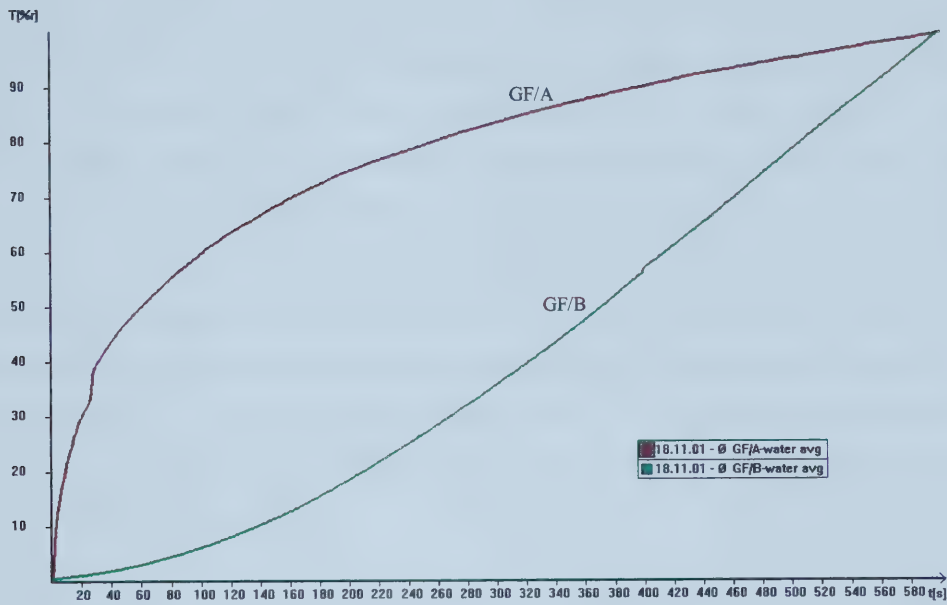
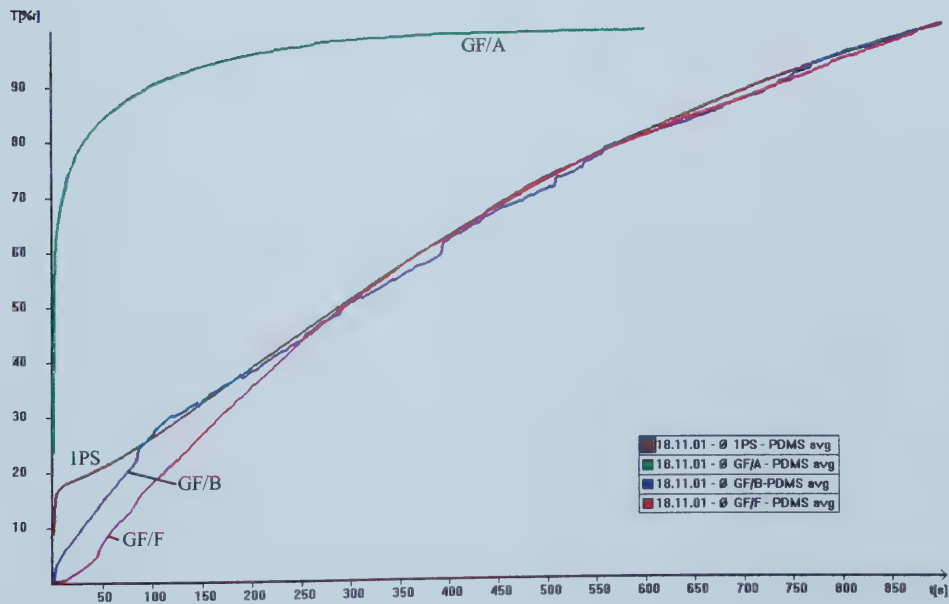


Figure 4.84: Penetration Dynamics - Glass Fibre Paper with Polydimethylsiloxane (Dow Corning 200 ® Fluid)



Emco Output Parameters

The parameters generated by the Emco software to describe the curves obtained with the model pore structures are shown in Table 4.20. It can be seen that the ' t_B ' values generated are nearly the same, irrespective of the system. Furthermore, ' t_S ' values generated were almost close to the ' t_B ' values or near the end of the curve. ' $\%S$ ' values generated were close to zero. For the case of the model pore structure systems, ' t_S ' and ' $\%S$ ' were considered to be irrelevant and ' t_B ' and ' $L\%$ ' were considered to be more important for the penetration dynamics measurements. ' t_B ' values were corrected in order to make this parameter more meaningful and to be able to distinguish the value of this parameter among the different systems. The time at which the transmission reached 95% was used as the ' t_B ' value for the model pore systems. The results with the corrected ' t_B ' values for the different model pore structures are shown in Table 4.21. These values were used for further analysis work.

Table 4.20: Summary - Emco Software generated output parameters for average curves

Nucleopore Pretreated	Water				6% methanol				20%methanol				40% methanol				70% methanol				100% methanol			
	L	tB	S	tS	L	tB	S	tS	L	tB	S	tS	L	tB	S	tS	L	tB	S	tS	L	tB	S	tS
2	24	103	-	-	51	103	-	-	49	103	0.02	116	41	42	0.05	49	51	103	-	103	33	103	0.02	115
5	44	103	-	-	30	103	0.02	114	34	103	-	-	25	103	0.05	114	47	19.2	0.02	93	39	103	0.1	110
8	32	103	-	115	17	103	0.02	111	20	103	-	-	40	102	0.1	110	30	103	0.07	105	3.4	103	0.07	104
12	49	103	0.07	109	20	103	0.12	110	44	103	0.1	105	49	103	0.07	109	36	103	0.07	103	4.4	103	0.15	117

Spectra	Water (1 side)				6% methanol				20%methanol				40% methanol				70% methanol				100% methanol			
	L	tB	S	tS	L	tB	S	tS	L	tB	S	tS	L	tB	S	tS	L	tB	S	tS	L	tB	S	tS
T	92	103	0.05	104	87	103	0.02	103	80	103	0.02	106	58	103	0.02	105	51	103	0.02	118	44	103	0.05	105
Q	93	103	0.02	103	94	32	0.05	104	93	103	0.02	104	93	103	0.02	108	72	103	0.05	104	42	103	0.07	115
F	14	103	-	104	15	70	0.05	116	12	103	0.05	114	8	103	0.02	110	7	103	-	104	5	3.5	1.12	4.7

Voith	Water (1 side)				Water (2 sides)			
	L	tB	S	tS	L	tB	S	tS
1	94	103	0.02	117	60	103	0.02	104
2-1	92	103	0.05	108	59	103	0.05	104
2-2	95	103	0.02	106				
3-1	76	103	0.10	111	84	88	0.02	93
3-2	97	103	0.05	118				
4	98	103	0.07	103	89	28	0.06	90
5	99	103	0.02	115	92	103	0.05	104
6	99	103	0.05	106	98	103	0.07	112
7-1	99	103	0.05	108	81	84	0.02	92
7-2	98	103	0.07	110				

Paper Grades	Water				PDMS			
	L	tB	S	tS	L	tB	S	tS
WFC	24	1.1	8.7	4.7	74	427	0.07	466
CIJ	9	0.8	2.8	2.9	78	580	0.07	597
H	-1	0.04	87	0.23	68	554	0.05	585
ANC-Roto	-0.7	0.04	162	0.19	97	584	0.05	598

Table 4.21: Summary - Emco output parameters for average curves (corrected)

Nuclepore Pretreated	Water				6% methanol				20%methanol				40% methanol				70% methanol				100% methanol			
	L	tB	S	tS	L	tB	S	tS	L	tB	S	tS	L	tB	S	tS	L	tB	S	tS	L	tB	S	tS
2	25	65.9	-	-	51	48.4	-	-	49	29.2	0.02	116	41	5.1	0.05	49	51	3.0	-	103	34	0.2	0.02	115
5	35	69.5	-	-	25	13.2	0.02	114	29	11.2	-	-	46	86.0	0.05	114	46	5.6	0.02	93	38	0.4	0.1	110
8	32	31.1	-	115	17	5.3	0.02	111	20	33.0	-	-	40	15.8	0.1	110	29	1.0	0.07	105	3	<0.04	0.07	104
12	50	48.7	0.07	109	21	54.2	0.12	110	45	50.5	0.1	105	49	42.7	0.07	109	36	1.0	0.07	103	4	0.04	0.15	117

Spectra	Water (1 side)				6% methanol				20%methanol				40% methanol				70% methanol				100% methanol			
	L	tB	S	tS	L	tB	S	tS	L	tB	S	tS	L	tB	S	tS	L	tB	S	tS	L	tB	S	tS
T	92	17.3	0.05	104	86	14.0	0.02	103	78	20.7	0.02	106	56	20.9	0.02	105	49	18.0	0.02	118	45	30.8	0.05	105
Q	93	7.9	0.02	103	94	7.0	0.05	104	94	6.6	0.02	104	94	4.5	0.02	108	71	1.8	0.05	104	42	0.5	0.07	115
F	14	1.5	-	104	15	1.1	0.05	116	12	0.8	0.05	114	8	0.3	0.02	110	8	20.6	-	104	6	0.04	1.12	5

Voith	Water (1 side)				Water (2 sides)			
	L	tB	S	tS	L	tB	S	tS
1	93	5.6	0.02	117	61	5.3	0.02	104
2-1	92	3.4	0.05	108	60	7.4	0.05	104
2-2	95	1.4	0.02	106				
3-1	73	7.4	0.10	111	85	6.2	0.02	93
3-2	97	4.8	0.05	118				
4	99	4.4	0.07	103	90	0.7	0.06	90
5	99.5	8.0	0.02	115	93	1.5	0.05	104
6	99	1.8	0.05	106	98	1.4	0.07	112
7-1	99	6.4	0.05	108	87	1.2	0.02	92
7-2	98	11.0	0.07	110				

Paper	Water				PDMS			
	L	tB	S	tS	L	tB	S	tS
Grades								
WFC	22	1.12	8.7	4.7	74	419	0.07	466
CIJ	8	0.76	2.8	2.9	77	580	0.07	597
H	0.0	0.04	87	0.23	68	541	0.05	585
ANC-Roto	0.0	0.04	162	0.19	98	599	0.05	598

Note: Here t_B values are based on time values corresponding to 95% Transmission

Table 4.22: Summary of error calculations for Emco average results

(a) Nuclepore® Membranes

Test liquid - 100% methanol

Time (sec)	12 μm (%Tr)	8 μm (%Tr)	5 μm (%Tr)	2 μm (%Tr)
0.04	93.5 \pm 2.7%	93.4 \pm 2.2%	59.6 \pm 0.6%	64.1 \pm 2%
0.24	95.9 \pm 1.5%	97.5 \pm 0.8%	80.2 \pm 0.9%	95.1 \pm 1.7%
0.32	95.8 \pm 1.4%	97.3 \pm 0.8%	90.4 \pm 0.5%	95.2 \pm 1.7%
0.44	95.8 \pm 1.3%	97.5 \pm 0.6%	95.5 \pm 0.6%	95.2 \pm 1.7%
Max Error	2.7%	2.2%	1.6%	2.3%

Test liquid - 70% methanol

Time (sec)	12 μm (%Tr)	8 μm (%Tr)	5 μm (%Tr)	2 μm (%Tr)
0.4	79.9 \pm 3.5%	78.7 \pm 3.3%	62.0 \pm 5.0%	59.3 \pm 0.8%
1.0	94.6 \pm 1.5%	94.7 \pm 3.1%	69.1 \pm 4.0%	66.8 \pm 0.5%
2.0	98.6 \pm 0.5%	99.0 \pm 0.6%	75.3 \pm 2.7%	85.2 \pm 1.9%
3.0	99.0 \pm 0.4%	99.2 \pm 0.3%	79.3 \pm 2.6%	95.1 \pm 1.3%
5.0	99.4 \pm 0.2%	99.4 \pm 0.2%	92.8 \pm 2.4%	98.5 \pm 0.6%
Max Error	3.5%	5%	5.2%	2.1%

Test liquid - 40% methanol

Time (sec)	12 μm (%Tr)	8 μm (%Tr)	5 μm (%Tr)	2 μm (%Tr)
1	54.9 \pm 4.0%	65.3 \pm 2.3%	67.9 \pm 4.8%	69.2 \pm 0.8%
3	62.7 \pm 7.3%	69.9 \pm 3.1%	74.2 \pm 3.4%	80.7 \pm 0.8%
5	69.7 \pm 7.5%	74.8 \pm 2.9%	77.8 \pm 3.0%	94.5 \pm 0.9%
10	79.0 \pm 5.1%	87.2 \pm 2.4%	82.7 \pm 1.9%	99.2 \pm 0.3%
15	84.4 \pm 3.8%	94.2 \pm 1.8%	85.4 \pm 1.2%	99.5 \pm 0.3%
20	87.8 \pm 2.8%	97.1 \pm 1.3%	87.1 \pm 0.6%	99.6 \pm 0.2%
40	94.4 \pm 1.3%	99.4 \pm 0.3%	90.1 \pm 1.2%	99.7 \pm 0.1%
60	96.9 \pm 0.5%	99.7 \pm 0.2%	91.7 \pm 2.2%	99.7 \pm 0.1%
80	98.2 \pm 0.35	99.8 \pm 0.1%	93.5 \pm 1.8%	99.9 \pm 0.1%
Max Error	7.8%	3.1%	7.1%	1.7%

Test liquid - 20% methanol

Time (sec)	12 μm (%Tr)	8 μm (%Tr)	5 μm (%Tr)	2 μm (%Tr)
1	59.3 \pm 4.3%	82.3 \pm 4.4%	80.2 \pm 2.5%	64.3 \pm 0.9%
5	72.1 \pm 3.4%	86.1 \pm 2.6%	90.3 \pm 1.1%	77.7 \pm 1.2%
10	80.7 \pm 2.7%	89.1 \pm 1.9%	94.6 \pm 0.7%	87.1 \pm 0.9%
20	87.6 \pm 2.0%	92.6 \pm 1.3%	97.5 \pm 0.5%	93.2 \pm 0.8%
30	91.2 \pm 1.6%	94.5 \pm 0.1%	98.3 \pm 0.2%	95.0 \pm 0.8%
50	94.9 \pm 1.1%	96.6 \pm 0.5%	98.9 \pm 0.1%	96.8 \pm 0.6%

Time (sec)	12 μm (%Tr)	8 μm (%Tr)	5 μm (%Tr)	2 μm (%Tr)
Max Error	4.9%	4.6%	4.9%	1.5%

Test liquid - 6% methanol

Time (sec)	12 μm (%Tr)	8 μm (%Tr)	5 μm (%Tr)	2 μm (%Tr)
1	84.8 \pm 5.6%	89.4 \pm 0.9%	83.9 \pm 2.6%	64.4 \pm 4.0%
5	86.6 \pm 4.6%	94.7 \pm 0.4%	91.3 \pm 1.4%	79.9 \pm 2.1%
10	88.1 \pm 3.7%	96.8 \pm 0.5%	94.4 \pm 2.8%	86.3 \pm 1.5%
20	90.9 \pm 2.2%	98.1 \pm 0.4%	96.4 \pm 2.4%	90.7 \pm 1.1%
30	92.7 \pm 1.4%	98.6 \pm 0.4%	97.2 \pm 1.8%	92.7 \pm 1.0%
50	95.1 \pm 0.7%	99.1 \pm 0.3%	98.1 \pm 1.2%	95.0 \pm 0.8%
Max Error	6.1%	1.3%	6.3%	6.5%

Test liquid - Water

Time (sec)	12 μm (%Tr)	8 μm (%Tr)	5 μm (%Tr)	2 μm (%Tr)
2	56.7 \pm 2.3%	79.7 \pm 0.9%	75.1 \pm 6.7%	78.9 \pm 6.8%
10	72.2 \pm 4.4%	87.5 \pm 1.2%	83.7 \pm 4.1%	84.8 \pm 5.0%
20	84.6 \pm 2.7%	92.6 \pm 1.0%	87.0 \pm 2.9%	87.7 \pm 4.0%
40	92.7 \pm 1.4%	96.0 \pm 0.8%	90.6 \pm 1.9%	91.4 \pm 2.4%
60	96.0 \pm 0.9%	97.6 \pm 0.6%	93.3 \pm 1.4%	94.2 \pm 1.6%
Max Error	4.4%	1.4%	7.2%	9.5%

(b) Spectra Meshes

Test liquid - 100% methanol

Time (sec)	Q (%Tr)	T (%Tr)	F (%Tr)
0.04	56.3 \pm 8.3%	52.1 \pm 27.5%	-
0.12	74.2 \pm 4.8%	62.5 \pm 8.1%	-
0.32	84.0 \pm 2.3%	80.1 \pm 1.8%	-
0.52	94.5 \pm 1.5%	83.5 \pm 1.9%	-
Max Error	8%	27%	-

Test liquid - 70% methanol

Time (sec)	Q (%Tr)	T (%Tr)	F (%Tr)
0.52	80.2 \pm 9.3%	86.4 \pm 1.4%	93.7 \pm 0.3%
1	91.1 \pm 4.5%	89.7 \pm 1.6%	93.3 \pm 0.6%
2	94.8 \pm 2.4%	90.8 \pm 1.5%	94.0 \pm 1.1%
Max Error	32%	9%	2.3%

Test liquid - 40% methanol

Time (sec)	Q (%Tr)	T (%Tr)	F (%Tr)
1	6.7 \pm 22.0%	84.3 \pm 1.7%	95.9 \pm 0.2%
3	7.0 \pm 11.5%	88.9 \pm 1.3%	96.9 \pm 0.5%
5	95.9 \pm 0.7%	90.5 \pm 1.2%	97.5 \pm 0.3%
Max Error	57%	22%	1.3%

Test liquid - 20% methanol

Time (sec)	Q (%Tr)	T (%Tr)	F (%Tr)
1	7.2 \pm 18.2%	65.7 \pm 19.3%	95.4 \pm 0.3%
2	23.7 \pm 42.3%	75.9 \pm 15.8%	96.4 \pm 0.3%
4	88.2 \pm 7%	86.6 \pm 3.1%	97.2 \pm 0.3%
6	94.1 \pm 2.6%	89.7 \pm 1.3%	97.8 \pm 0.3%
Max Error	44%	26%	0.8%

Test liquid - 6% methanol

Time (sec)	Q (%Tr)	T (%Tr)	F (%Tr)
1	8.2 \pm 50.7%	65.6 \pm 13.5%	93.7 \pm 1.9%
2	31.2 \pm 55.3%	82.4 \pm 0.8%	95.2 \pm 1.4%
4	85.5 \pm 6.3%	88.7 \pm 0.3%	95.7 \pm 1.1%
8	95.3 \pm 1.8%	92.2 \pm 1.1%	97.4 \pm 1.0%
10	96.4 \pm 1.4%	93.1 \pm 1.0%	97.9 \pm 1.1%
Max Error	65%	71%	3%

Test liquid - Water

Time (sec)	Q (%Tr)	T (%Tr)	F (%Tr)
1	7.0 \pm 20.3%	68.8 \pm 11.4%	94.1 \pm 1.7%
2	32.4 \pm 30.8%	82.7 \pm 3.2%	95.7 \pm 1.4%
5	91.1 \pm 1.9%	88.9 \pm 1.1%	97.4 \pm 0.9%
10	96.2 \pm 0.7%	92.3 \pm 0.9%	98.2 \pm 0.7%
Max Error	48%	58%	2%

(c) Voith Fabrics

Test liquid - Water (liquid penetration from both sides)

Time (sec)	V1 (%Tr)	V2 (%Tr)	V3 (%Tr)	V4 (%Tr)	V5 (%Tr)	V6 (%Tr)	V7 (%Tr)
0.2	60.3 \pm 26%	52.6 \pm 29%	22.9 \pm 21%	17.2 \pm 34%	8.6 \pm 3%	4.3 \pm 14%	86.3 \pm 5%
0.4	66.6 \pm 23%	62.9 \pm 28%	41.7 \pm 19%	41.7 \pm 19%	10.3 \pm 17%	29.8 \pm 9%	91.0 \pm 1%
0.8	80.4 \pm 9%	72.4 \pm 22%	66.6 \pm 9%	66.8 \pm 31%	45.7 \pm 47%	81.5 \pm 10%	93.7 \pm 0.3%
1	83.6 \pm 7%	75.3 \pm 20%	72.3 \pm 7%	72.3 \pm 7%	71.7 \pm 19%	91.1 \pm 3%	94.4 \pm 0.4 %

Time (sec)	V1 (%Tr)	V2 (%Tr)	V3 (%Tr)	V4 (%Tr)	V5 (%Tr)	V6 (%Tr)	V7 (%Tr)
2	89.6 \pm 4%	84.0 \pm 13%	84.8 \pm 3%	84.8 \pm 3%	96.5 \pm 1%	95.9 \pm 2%	96.2 \pm 1%
3	92.6 \pm 2%	88.6 \pm 9%	88.7 \pm 2%	88.7 \pm 2%	97.5 \pm 1%	96.9% \pm 1.5	97.0 \pm 1%
Max Error	27%	29%	21%	62.1%	59%	44%	32%

(d) Commercial Paper Grades

Test liquid - Water

Time (sec)	WFC (%Tr)	CIJ (%Tr)	H (%Tr)	ANC - R (%Tr)
tB(sec)	1.17 \pm 8.5%	0.98 \pm 21.9%	0.04 \pm 9.8%	0.03 \pm 1.3%

Test liquid - PDMS

Time (sec)	WFC (%Tr)	CIJ (%Tr)	H (%Tr)	ANC - R (%Tr)
100	33.0 \pm 2.3%	33.6 \pm 5.2%	31.0 \pm 7.2%	9.9 \pm 7.4%
200	71.0 \pm 5.1%	59.4 \pm 5.0%	57.1 \pm 2.9%	29.6 \pm 3.8%
300	94.5 \pm 2.8%	83.0 \pm 3.3%	84.4 \pm 1.1%	57.4 \pm 1.6%
400	99.4 \pm 0.5%	95.0 \pm 1.6%	96.9 \pm 0.9%	79.4 \pm 1.1%
500	99.8 \pm 0.1%	99.0 \pm 0.5%	99.6 \pm 0.3%	92.9 \pm 0.5%
600	99.9 \pm 0.04%	99.9 \pm 0.03%	99.9 \pm 0.1%	99.9 \pm 0.06%
Max error	7.9%	7.9%	8.8%	22%

5.0 Analysis and Discussion

5.1 Model Pore Structures

5.1.1 Theoretical Calculations using Lucas-Washburn Equation

The Lucas-Washburn equation is defined by equation (2.5) in its most commonly used form and by equation (2.6) in terms of porosity and permeability. The Nuclepore® membranes were the only model pore structures for which the complete set of required parameters in the Lucas-Washburn equation could be measured. Hence, it was possible to theoretically calculate the dynamics of penetration of the various probe liquids for these structures. In the case of the Spectra meshes, accurate contact angle data could not be obtained because of their porous structure and unavailability of non-porous samples. Nevertheless, for the purpose of comparison of the relative dynamics, theoretical calculations were done for a scenario of a particular probe liquid penetrating the different pore structures. These calculations assume that the contact angle for a particular probe liquid is the same for the different Spectra Mesh samples, since they are made of the same material. The contact angle was assumed to be zero for the purpose of these calculations.

Nuclepore Membranes:

Dynamics of liquid penetration were calculated for the different Nuclepore membranes using both the afore mentioned forms of the Lucas-Washburn equation. Actual measured values of pore diameter, permeability, thickness and porosity were used in the calculations. The trends obtained for different probe liquids were similar for all the membranes of a particular pore size. Trends obtained with both forms of the Lucas-Washburn equation were similar with small differences in the actual dynamics. The theoretically calculated absorption curves using both forms of the Lucas-Washburn equation, for the Nuclepore 12 micron membrane with different probe liquids, are shown in Figure 5.1 and Figure 5.2 respectively.

Figure 5.1: Dynamics of penetration in Nuclepore® 12 micron based on Lucas-Washburn equation (calculated using Equation 2.5 based on measured values of r and θ and literature values of γ and μ)

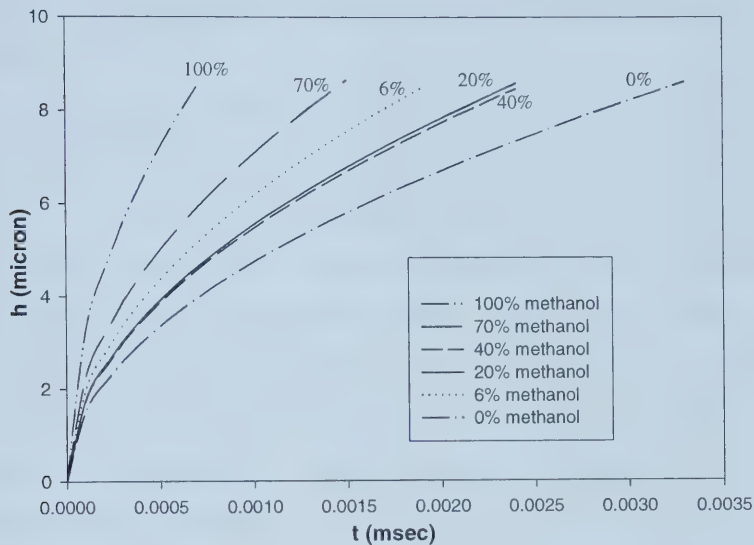
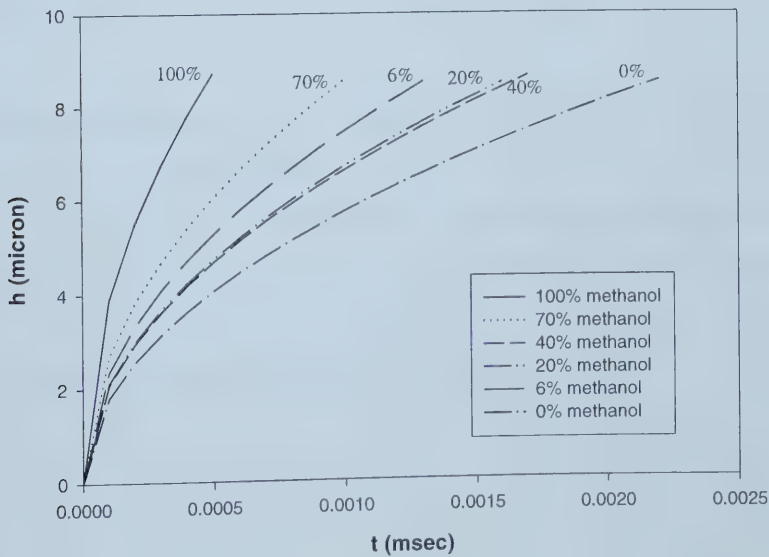


Figure 5.2: Dynamics of penetration in Nuclepore® 12 micron based on Lucas-Washburn equation (calculated using Equation 2.6 based on measured values of ε , K and θ and literature values of γ and μ)



It should be noted that the above plots are based on the assumption that the dynamic contact angle remains constant and corresponds to the value of the equilibrium contact angle of the different probe liquids on the solid polycarbonate surface. Also resistance effects of the air escaping out of the capillaries have been neglected.

From the above theoretically calculated plots, it can be seen that the dynamics of the 40% methanol solution and 20% methanol solution are very close. This is mainly due to the physical properties of the methanol solutions. Even though the surface tension and contact angle of the 40% methanol solution are lower than for the 20% methanol solution, it has a higher viscosity. The ratio ($\gamma \cos \theta / \mu$) (i.e. driving force/resisting force) of both the solutions are nearly equal and hence liquid penetration dynamics obtained are very close. From the theoretically calculated plots, liquid penetration dynamics for the Nuclepore membranes can be summarized as:

For a particular membrane:

Dynamics of 100% > 70% > 6% > 20% > 40% > 0% methanol

For a particular probe liquid:

Dynamics of 12 micron > 8 micron > 5 micron > 2 micron (this trend is consistent with the permeability of the different Nuclepore membranes)

Spectra Meshes:

The hydraulic radius was used as the equivalent pore radius for the quadrilateral shaped pores of the Spectra Meshes. It may be noted that sample F' has been included in this calculation, even though it is made of a different polyurethane resin than Q and T. Hence, the true comparison of the trends is between pore structures Q and T. The curves obtained from both forms of the Lucas-Washburn equation for water are shown in Figure 5.3 and Figure 5.4 respectively.

Figure 5.3: Dynamics of penetration of water in Spectra Meshes based on Lucas-Washburn equation (calculations based on measured values of r , θ assumed as zero and literature values of γ and μ)

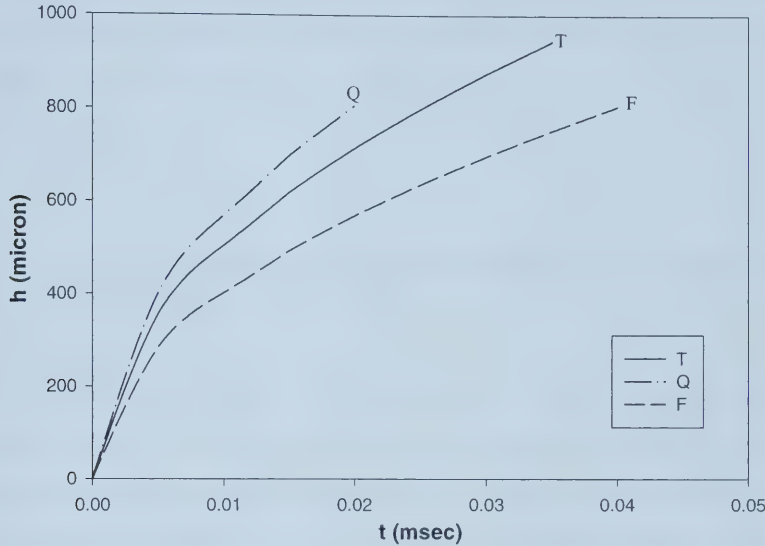
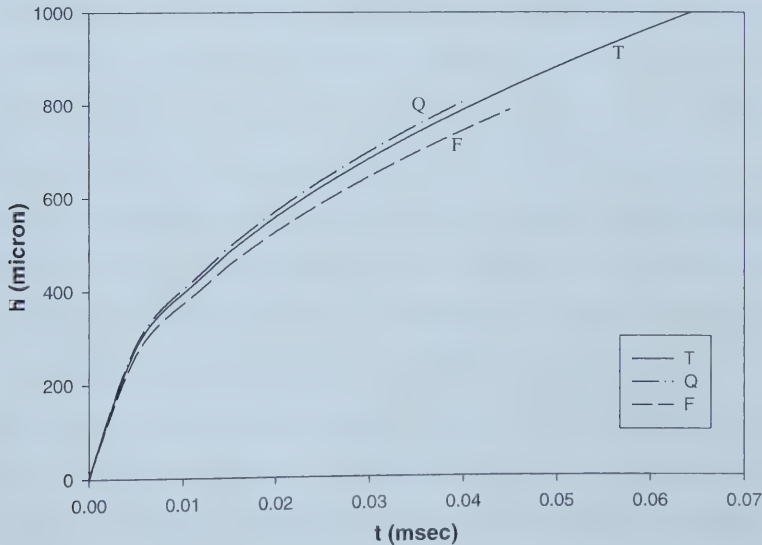


Figure 5.4: Dynamics of penetration of water in Spectra Meshes based on Lucas-Washburn equation (calculations based on measured values of ε , K , θ assumed as zero and literature values of γ and μ)



It can be seen that the trends obtained are similar even though there are differences in the actual dynamics calculated with the different forms of the Lucas-Washburn equation. The trends obtained from the theoretical calculations for a particular probe liquid i.e. dynamics of $Q > T > F$ are consistent with the measured porosity and permeability data.

5.1.2 Comparison of theoretical trends with results from the ultrasonic method for model pore structures

The results obtained from tests on model pore structures using the Emco DPM show similar shapes of curves. The curves obtained for any system increase gradually from an initial %Tr (no penetration) value to a final value of 100% Tr (complete penetration). This indicates an increase in ultrasound transmission, as the liquid penetrates and displaces the air out of the sample, until complete penetration is achieved and the ultrasonic signal becomes constant at the max 100% Tr value.

Nuclepore membranes:

Comparison of the above theoretically calculated trends with the curves from the Emco DPM (Figures 4.55 to 4.58) showed that penetration dynamics in terms of %Tr matched the theoretically predicted trends for only the 12 micron membrane (Figure 4.55b and 4.55c). The dynamics obtained with 100% methanol were very rapid and possibly indicate limitations of the instrument to detect dynamics for such systems i.e. of very low porosity and low surface tension (faster wetting). In the case of the Nuclepore® 8-micron membrane, the 40% methanol solution showed slower penetration dynamics in the initial time regime of up to 10 seconds (Figure 4.56b). After this time, the dynamics increased and matched the theoretical trends from the Lucas-Washburn equation. However, in this case, the 20% methanol solution absorption profile obtained was closer to the absorption profile of water than the 40% methanol solution. Penetration dynamics obtained for the Nuclepore® 5 micron membrane (Figure 4.57b) showed that the absorption profiles

for the 6% and 20% methanol solutions were quite close and the profile for the 40% methanol solution was the slowest and quite close to the profile for water. For the Nuclepore® 2-micron membrane (Figure 4.58b), absorption profiles for the 40% and 20% methanol solutions were faster than those obtained with 6% methanol and water.

The 20% and 40% methanol solution curves seemed to cause anomalies in the trends for the Nuclepore® 8 micron, 5 micron and 2 micron structures. If these systems were omitted from the analysis then the Emco results would give the following trend in liquid penetration dynamics of 100% > 70% > 6% > 0% methanol for all the membrane samples, thereby matching the theoretical trends for the high and low surface tension ranges. It may be noted that the viscosity of methanol solutions increase in the 20% to 40% concentration range, before decreasing again for > 40% concentration. Furthermore, it should also be noted that the Nuclepore® membranes are a difficult pore structure to work with due to the low porosity and small pore size and thickness. These membranes are susceptible to plugging, which could potentially impact test results significantly, especially for the smaller pore size membranes.

Comparison of the curves obtained from the Emco with a fixed probe liquid but different membranes (Figure 4.59 to Figure 4.64) did not show any consistent trends. The trends obtained in the penetration dynamics are summarised below.

Water: N8>N12>N2~N5

6% methanol: N8>N5>N2>N12

20% methanol: N5>N2>N8>N12

40% methanol: N2>N8>N12>N5

70% methanol: N12~N8>N2>N5

100% methanol: N12~N8>N2>N5

Spectra Meshes:

For the Spectra F structure, the penetration dynamics with all the probe liquids was very fast and the curves obtained were very close (Figure 4.65), thus making it

difficult to practically differentiate the absorption profiles for the systems involving this pore structure. In the case of the Spectra Q structure (Figure 4.66), penetration dynamics with 100% and 70% methanol were very fast. The curves obtained with 40%, 20%, 6% and 0% methanol started at almost the same %Tr initial value and were quite close. Also some sort of 'wetting delay' can be observed, during which the transmission value is constant for some time. In the case of the Spectra T samples, the curves obtained seem to vary with the concentration of the methanol solution in a time regime up to 80 msec (Figure 4.67b). After this the 6% methanol curve 'slowed down' in comparison to the 20% methanol and water curves.

The ultrasonic method indicated that for the different probe liquids used the penetration dynamics were $F > Q > T$ (Figure 4.69 to Figure 4.74). Here F appears to be in contradiction with the theoretical trend. However, as mentioned earlier, F is chemically slightly different to sample Q and T and possibly has greater wetting characteristics. The trend in penetration dynamics, Q faster than in T, for all the probe liquids, is consistent with the theoretically calculated trends from the Lucas-Washburn equation.

5.1.3 Comparison of parameters obtained from the ultrasonic method with measured characteristics of the model pore structures

Nuclepore Membranes:

The parameters obtained from the ultrasonic method were compared to other measured characteristics. Combinations of these parameters based on their effect as described by the Lucas-Washburn equation were also compared. Figure 5.5 shows a comparison of the tB values with the L% values obtained from the different tests. No correlation can be seen between tB and L%. Trends for a particular membrane and different probe liquid are also not consistent. Figure 5.6 and Figure 5.7 show plots of different measured properties such as porosity, permeability and combinations of these. The (thickness x porosity) value is representative of the pore volume of the sample. Correspondingly tB and L% values obtained from the instrument have been replotted in Figure 5.8 for different probe liquids. These

figures indicate some correlation between L% and Porosity for the results with the 40% methanol and 0% methanol solutions. For water, tB also shows some correlation with (thickness x porosity). The parameters were also compared with a 'penetration coefficient' defined as $k\gamma\cos\theta/(\epsilon\mu)$ as shown in Figure 5.9. Trends in this case were also inconsistent.

Figure 5.5: Comparison of Emco parameters 'tB' and 'L%' for Nuclepore® Membranes

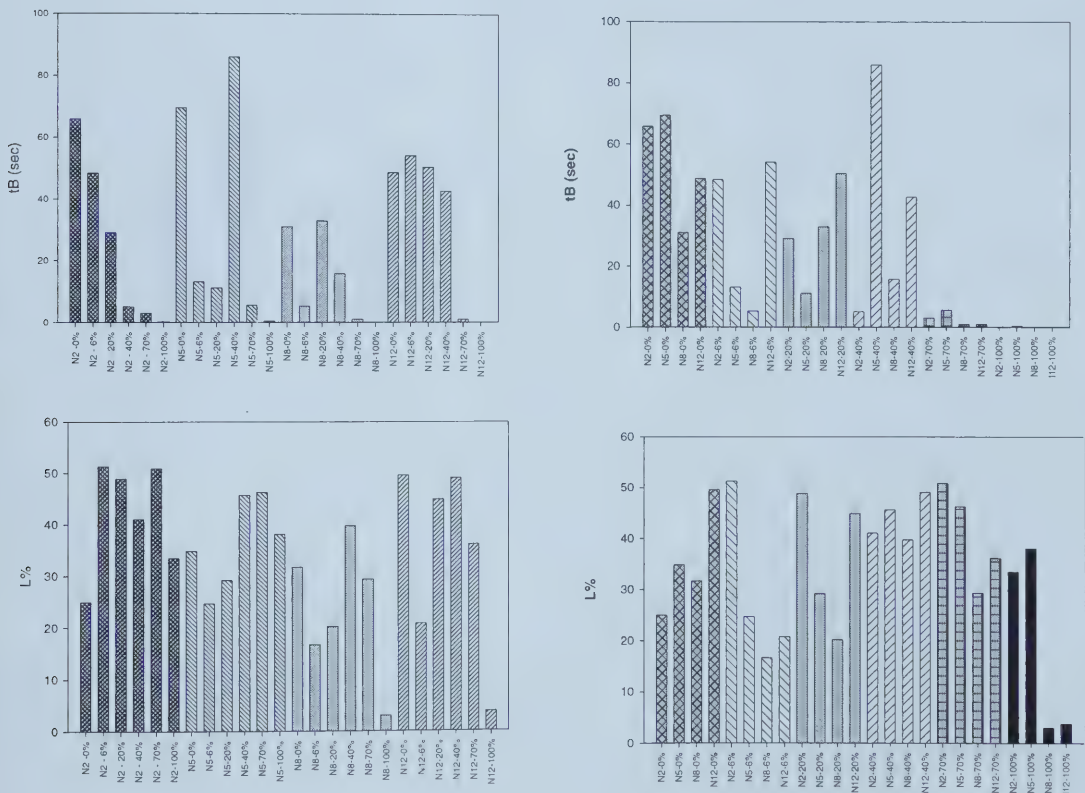


Figure 5.6: Nuclepore® Membranes - Porosity and Permeability

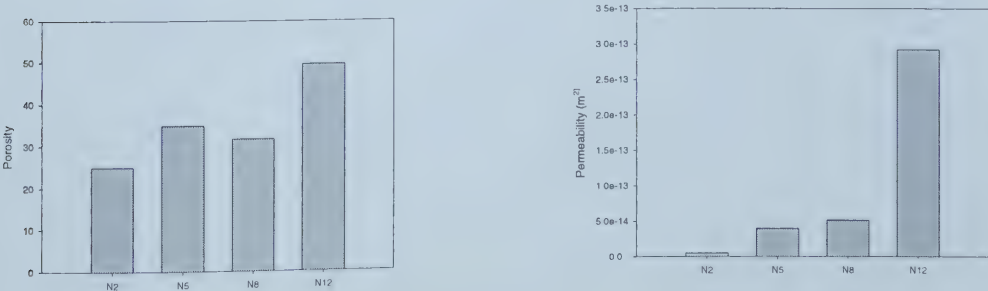


Figure 5.7: Nuclepore® Membranes - Derived Characteristics (k/ϵ , $k/\epsilon r$, $thk. \times \epsilon$)

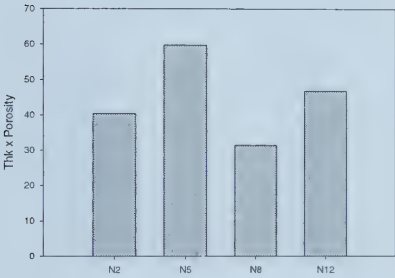
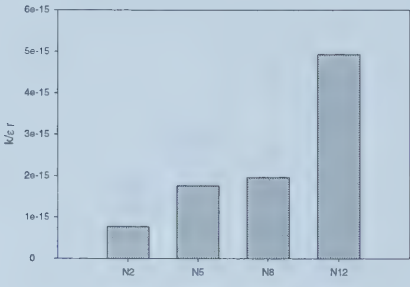
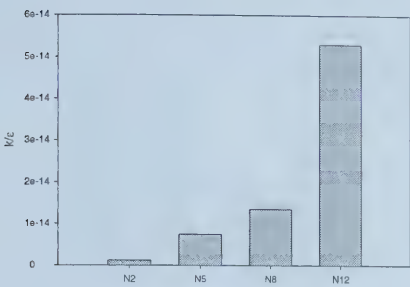


Figure 5.8: Nuclepore® Membranes - Emco parameters 'tB' and '%L' for different probe liquids



Nuclepore® Membranes - Emco parameters 'tB' and '%L' for different probe liquids (continued)

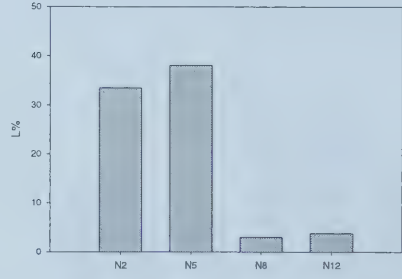
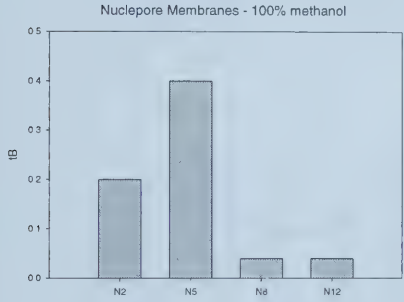
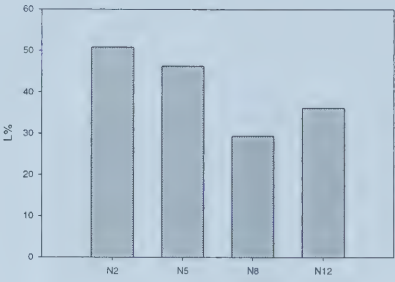
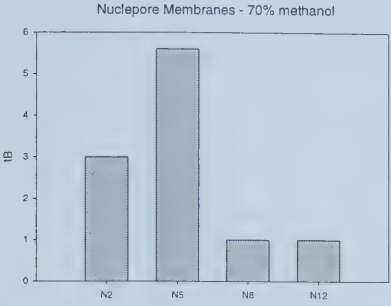
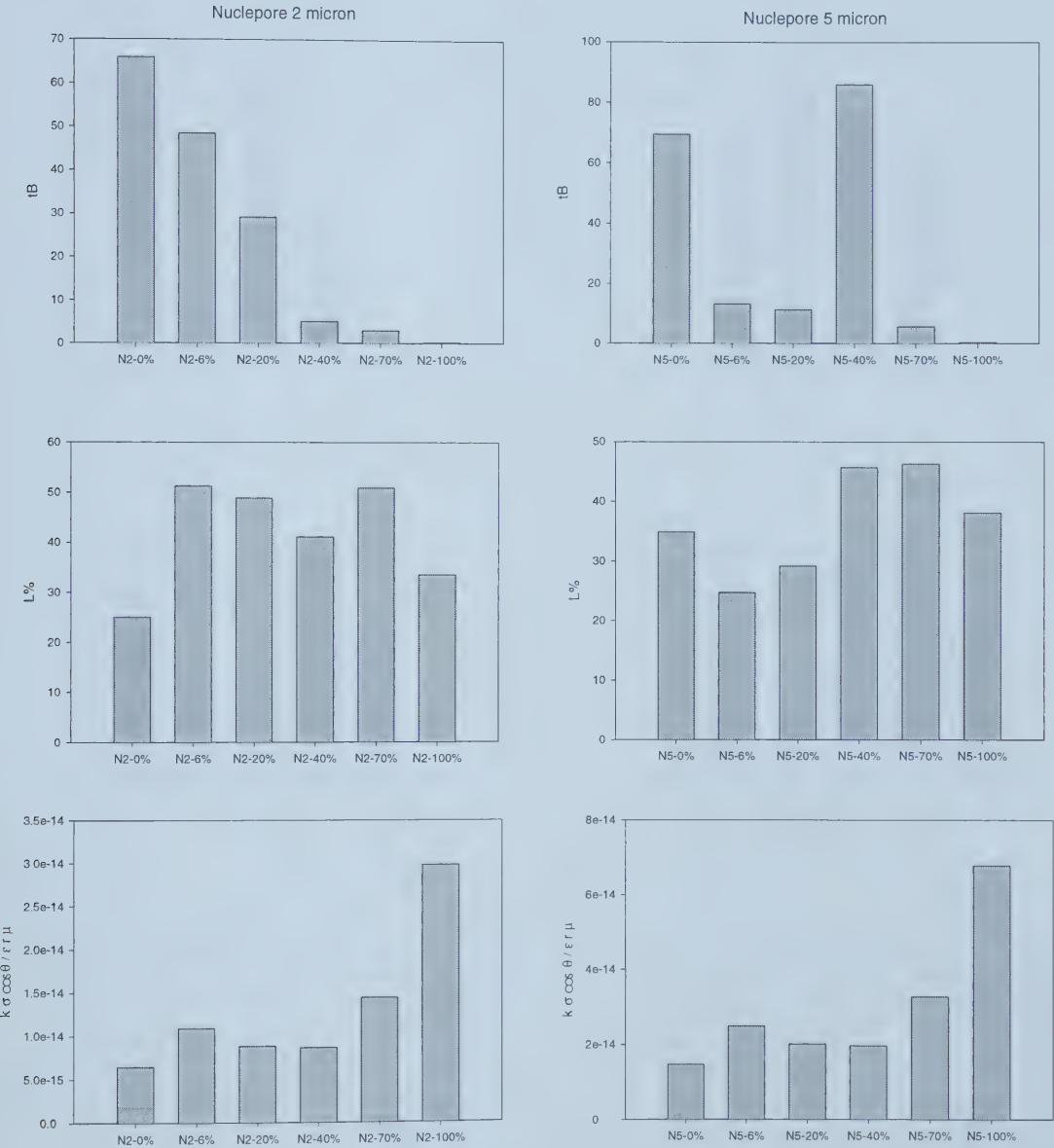
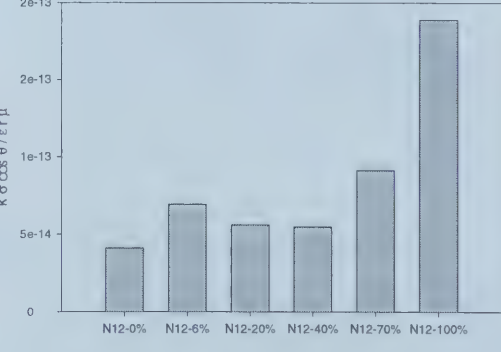
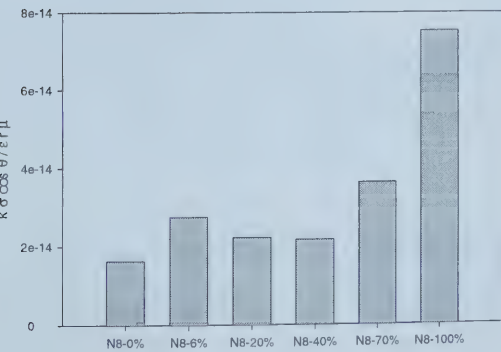
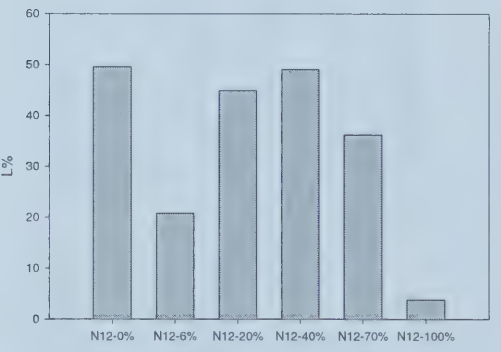
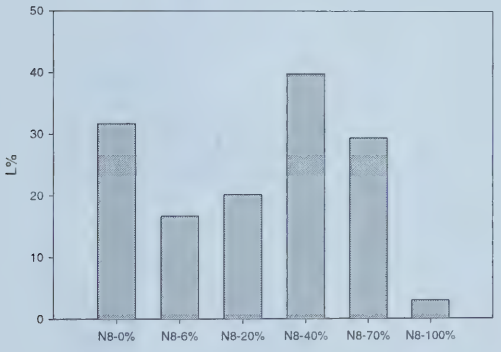
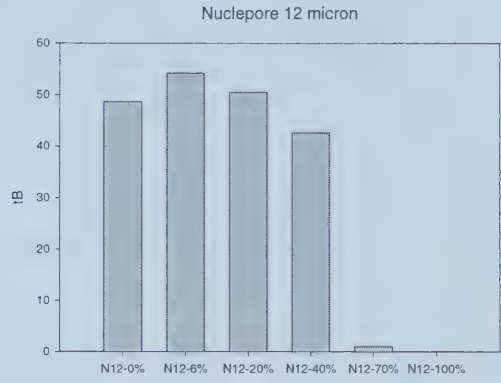
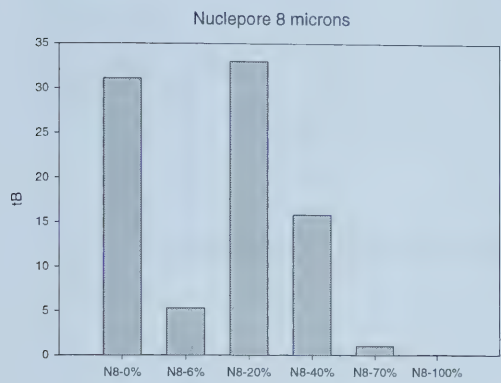


Figure 5.9: Nuclepore® Membranes - Comparison of Emco parameters with penetration coefficient



Nuclepore® Membranes - Comparison of Emco parameters with penetration coefficient (continued)



Spectra Meshes:

Figure 5.10 shows a comparison of the Emco parameters 'tB' and 'L%'. It can be seen that the Emco parameter 'L%' decreased with increase in concentration (or wettability) of the methanol solution. Also 'tB' for Spectra Q and F decreased with the increase in concentration of the methanol solution, thus indicating a lower 'tB' value for faster penetration dynamics.

Figure 5.10: Comparison of Emco parameters 'tB' and 'L%' for Spectra Meshes

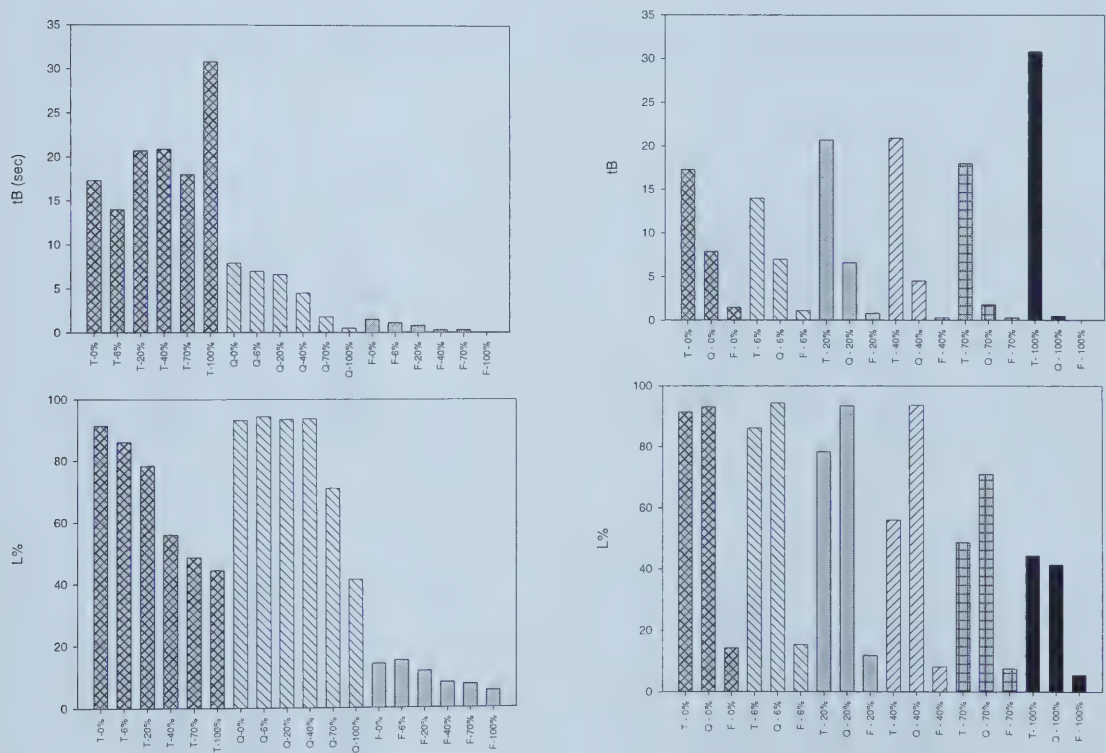


Figure 5.11 and Figure 5.12 show plots of different measured properties such as porosity, permeability and combinations of these.

Figure 5.11: Spectra Meshes - Porosity and Permeability

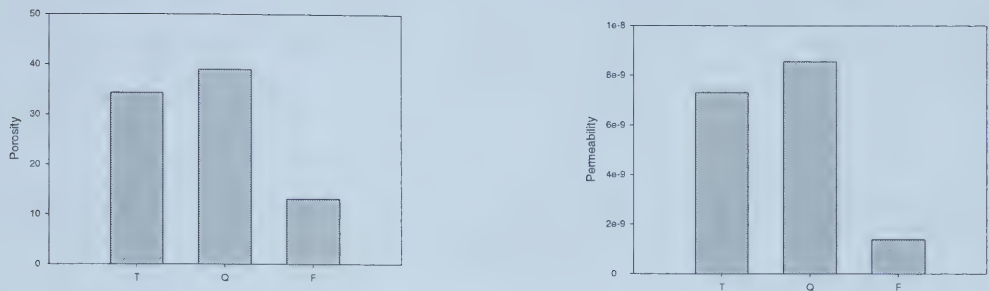
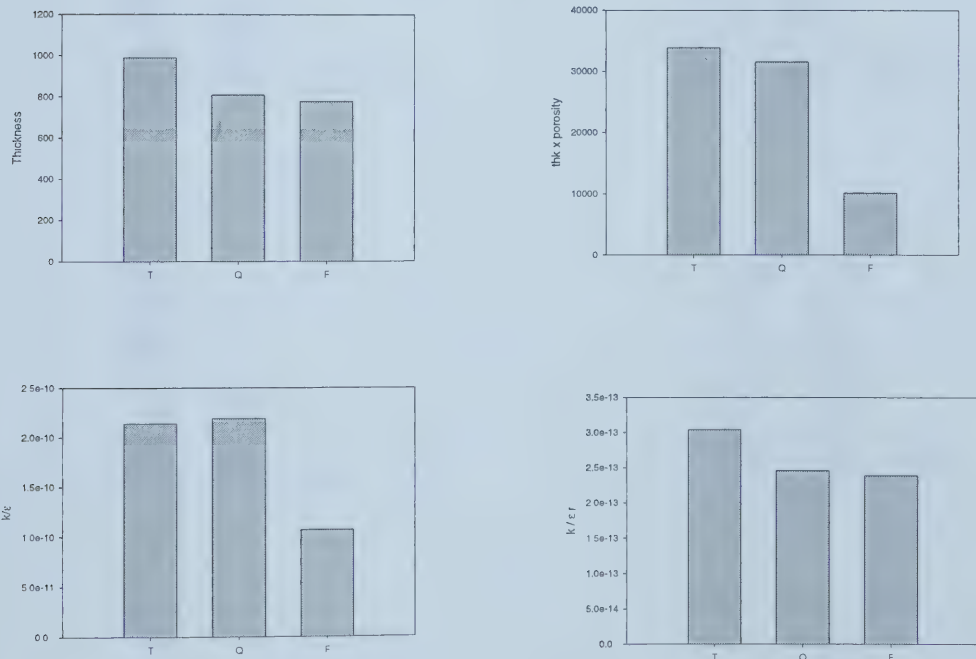


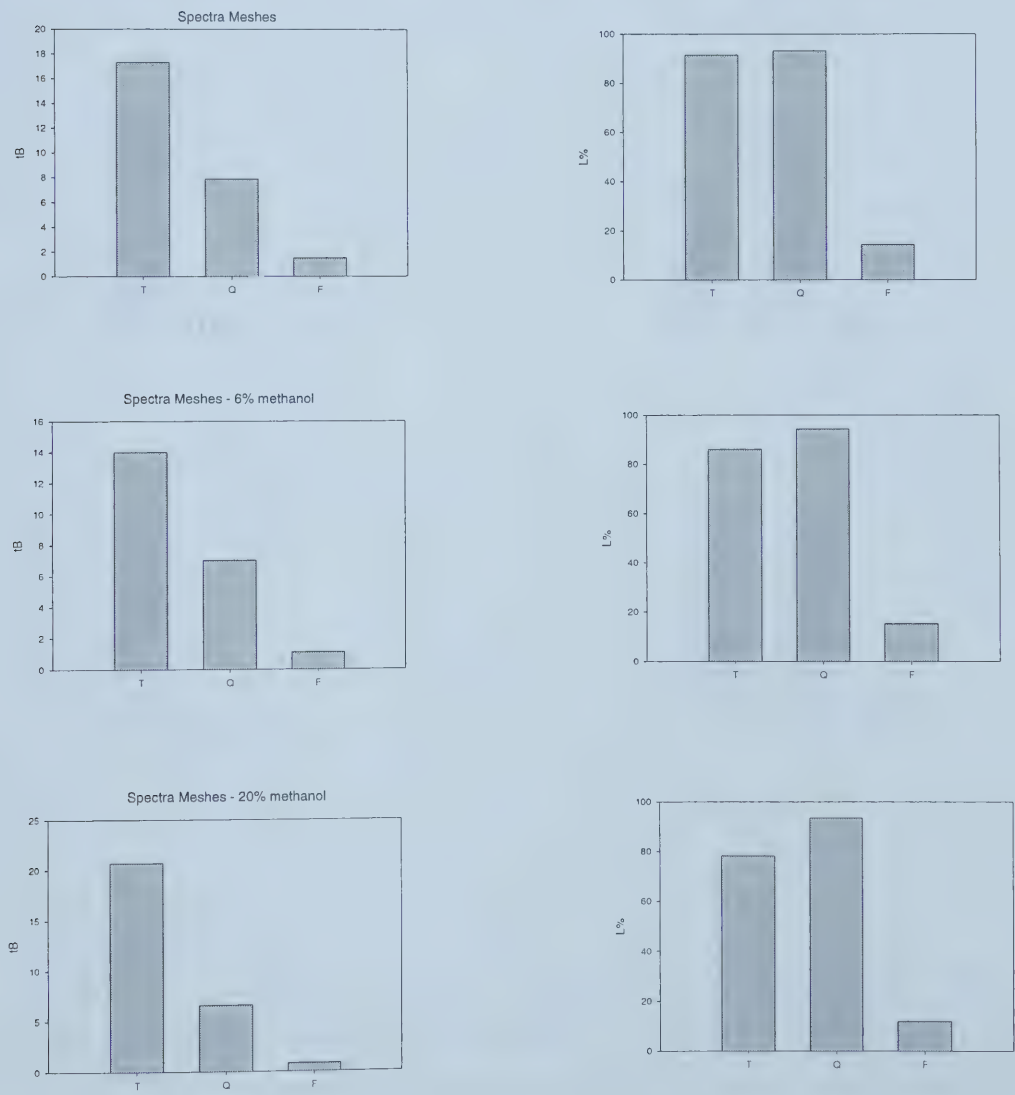
Figure 5.12: Spectra Meshes - Derived Characteristics (k/ϵ , $k/\epsilon r$, $thk. \times \epsilon$)



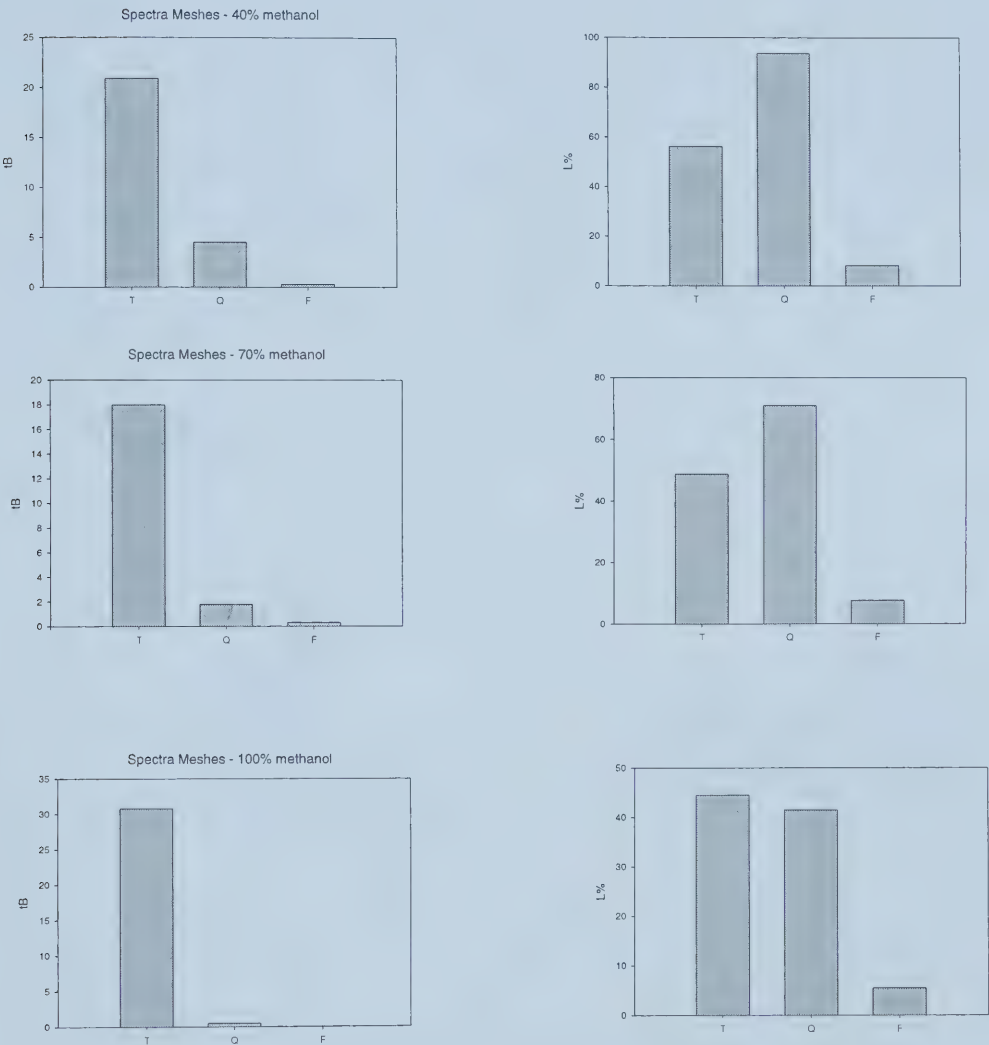
Trends for a particular mesh and different probe liquids are shown in Figure 5.13. For a particular probe liquid and different Spectra Meshes, the trends obtained for tB and $L\%$ are consistent i.e. $T > Q > F$ for tB , and $Q > T > F$ for $L\%$. $L\%$ trends

showed similarity with the porosity and permeability trends i.e. a higher value of $L\%$ for higher porosity. Furthermore, trends obtained for parameter tB were similar to trends for $(thk \times \epsilon)$ and $(k/\epsilon r)$. In comparison to the Nuclepore® membranes, the Spectra Meshes showed very consistent trends among the different systems involved.

Figure 5.13: Spectra Meshes - Emco parameters 'tB' and '%L' for different probe liquids



Spectra Meshes - Emco parameters 'tB' and '%L' for different probe liquids (continued)



Voith Fabrics

For tests done with water with penetration from both sides of the sample (Figure 4.75), the trends in the penetration dynamics are $V7 > V4 > V6 > V5 > V1 > V3 \sim V2$. The Emco parameters obtained are shown in Figure 5.14. Other measured

characteristics are shown in Figure 5.15. The ultrasound method gave lower values of 'tB' for the fabrics with higher permeability (e.g. V4, V6, V7) and higher values of 'tB' for the fabrics with lower permeability (e.g. V1, V2, V3). No clear correlations were observed between the Emco parameters and any of the other measured characteristics. Unlike the case of the Spectra meshes, the L% parameter seemed to show a negative correlation with the porosity of the sample i.e. lower value of L% at higher porosity (Figure 5.14 and 5.15). Porosity of the Voith fabrics was estimated by a somewhat crude method using the weight of the sample and the thickness in order to obtain "ballpark" values. Accurate porosity measurements would be necessary for a better comparison with the Emco parameters.

Figure 5.14: Emco parameters 'tB' and 'L%' for Voith Fabrics

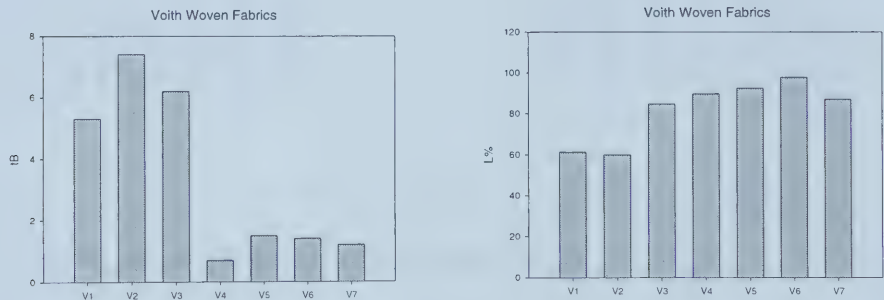
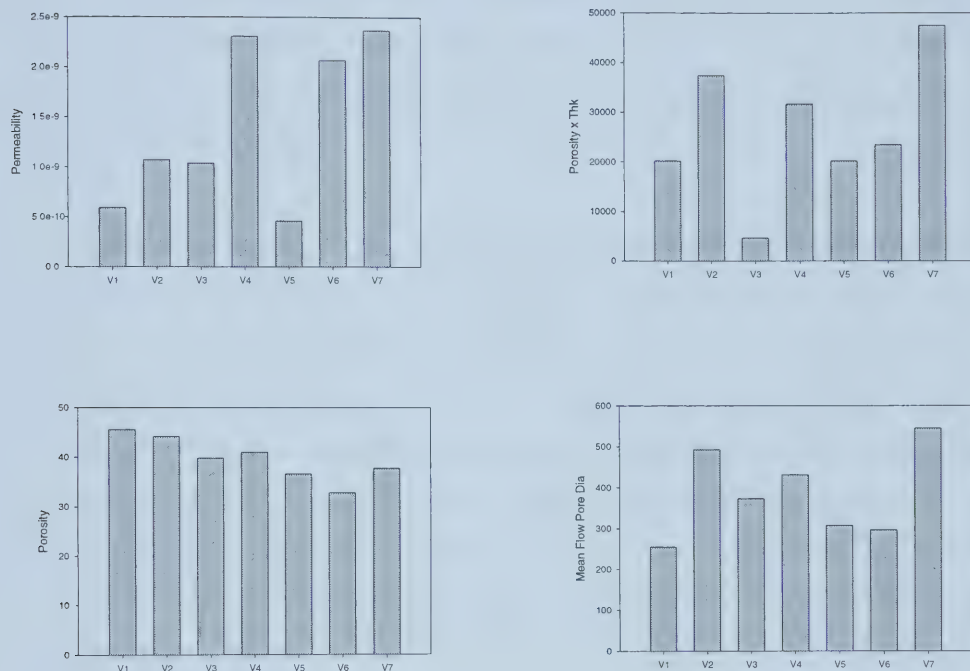


Figure 5.15: Voith Fabrics - Other characteristics



5.2 Commercial Paper Grades and Glass Fibre Paper

In the case of the tests of paper with water i.e. a system involving swelling of the fibres, different absorption profiles are obtained for the different paper grades (Figure 4.81). The absorption profiles show different regimes in which the transmission signal increases or decreases. In contrast, the shapes of the absorption profiles obtained in the tests with the non-swelling liquid are similar (Figure 4.82). For all the test samples the curves begin at some low initial transmission value and then increase as air is displaced from the sample. These results are quite similar to those obtained with the model pore structures. For the case of the tests with non-swelling glass fibre paper and water, similar curves, which increase from a low to a high transmission value, are also obtained.

This indicates that the nature of the absorption profile obtained depends to a large extent on the degree of swelling phenomena occurring. The Emco is sensitive not only to the dynamics of penetration, but also with polar liquids to the swelling dynamics occurring. Hence comparative testing of paper using a non swelling solvent could be a valuable means of delineating the potential changes in pore structure caused by swelling.

Emco results from the tests with non-swelling polydimethylsiloxane (PDMS) were compared with the other measured characteristics of paper. From Figure 4.82, it can be seen that the trends for the penetration dynamics are $WFC > CIJ \sim H > ANC-Roto$. The dynamics for CIJ and H grades were quite close. The Emco parameters from the tests with PDMS are shown in Figure 5.16. Here it can be seen that similar trends for 'tB' and 'L%' were obtained with the different paper samples. The tests with water are shown in Figure 5.17. In this case also, trends for 'tB' and 'L%' were similar for the tested paper samples. Other measured characteristics are shown in Figure 5.18.

Figure 5.16: Emco Parameters for Commercial Paper Grades - Tests with PDMS

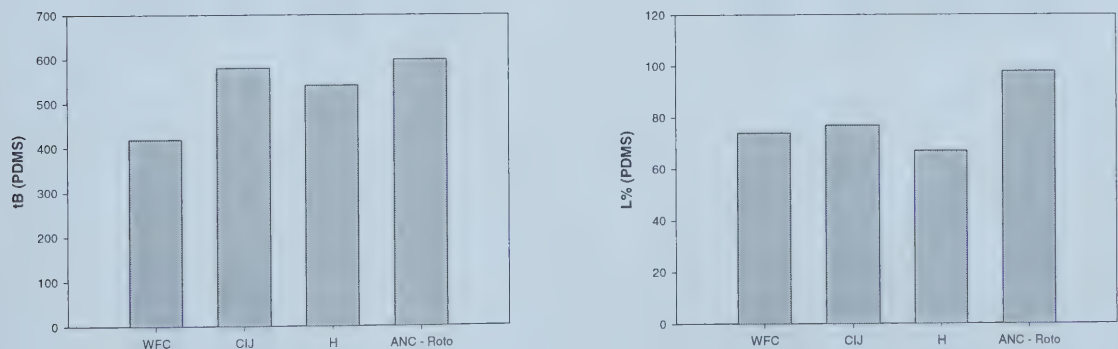


Figure 5.17: Emco Parameters for Commercial Paper Grades - Tests with Water

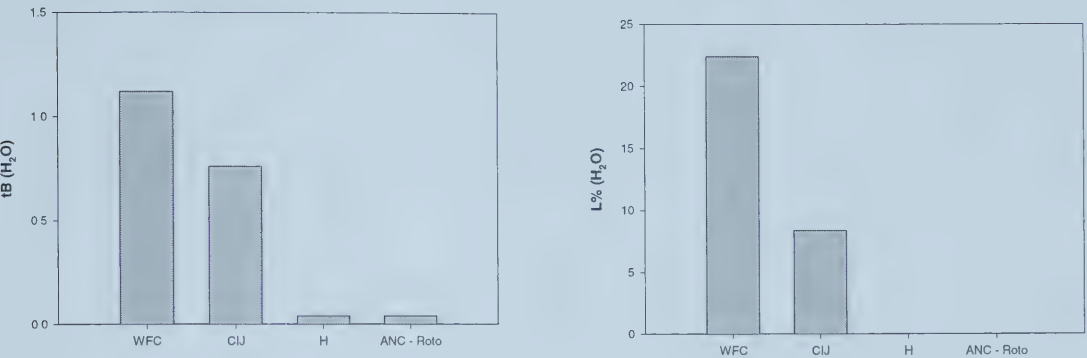
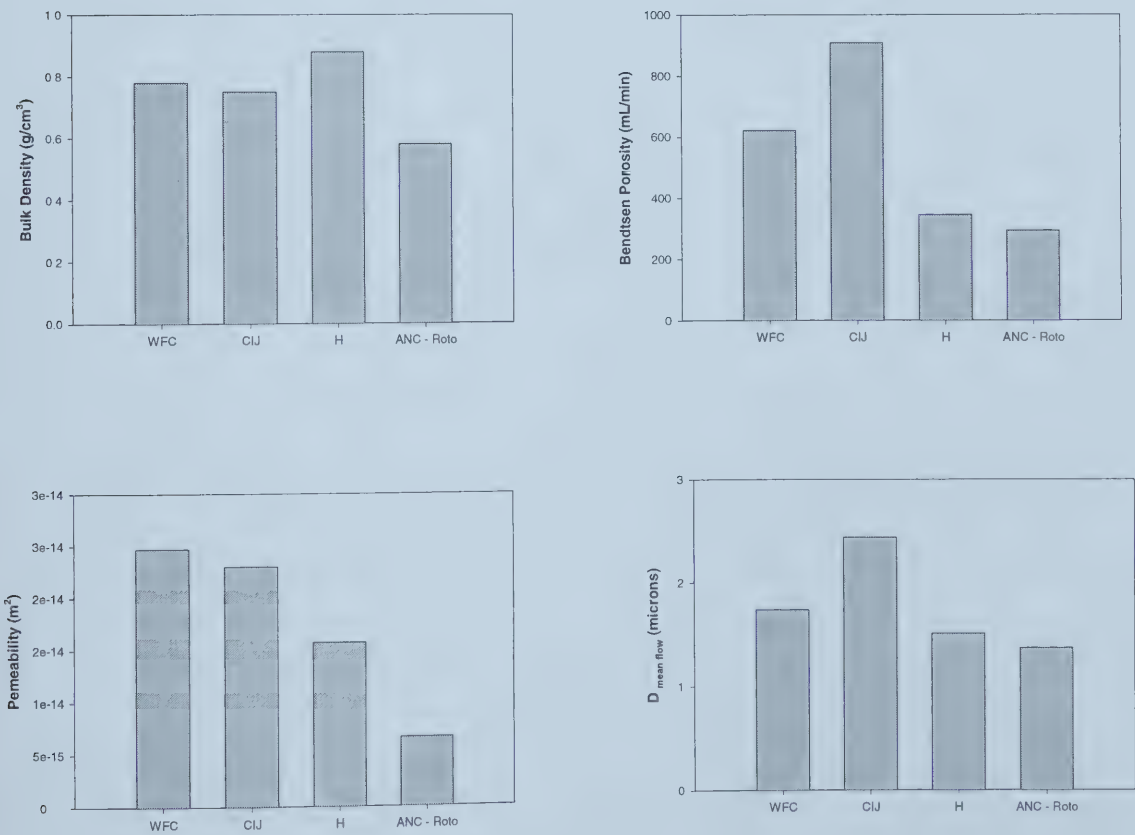


Figure 5.18: Other Measured Characteristics of Commercial Paper grades



Also the tB and L% values with the tests with PDMS showed similar trends as the permeability for the different paper grades i.e. lower tB and L% values for higher permeability samples.

6.0 Conclusions and Future Work

6.1 Conclusions

The comparison of the results from the ultrasonic method with theoretical calculations and other measured characteristics are summarized below.

Nuclepore® Membranes:

Absorption profiles obtained with the different probe liquids and the 12 micron membrane showed similar trends as predicted by the Lucas-Washburn equation. In contrast, the 8 micron, 5 micron and 2 micron membranes showed some anomalies with respect to the theoretical trends. Overall the ultrasonic method seemed to differentiate consistently between the higher and lower surface tension probe liquids. However, further comparison of the curves obtained for the different micron size membranes with a particular probe liquid did not give consistent results. Anomalies in the trends could potentially be due to limitations of the instrument for the systems involved i.e. very low porosity samples with small pore diameters. Further, even though precautions were taken to minimise contamination effects, these membranes are susceptible to plugging and ideally the experiments would have had to be performed in a 'clean room' with very pure water in order to avoid any particulate contamination.

Spectra Meshes:

Theoretical trends could not be calculated for a particular pore structure with different probe liquids due to the lack of appropriately measured contact angle data on a non-porous sample. However curves obtained from tests on different Spectra mesh samples, with a particular probe liquid, gave similar trends i.e. trends obtained for Emco parameters $L\%$ and tB were similar. The dynamics obtained with different probe liquids for a particular pore structure appeared to vary with the concentration of the methanol solutions. Further the $L\%$ values appeared to depend on the porosity of the Spectra T and Q structures i.e. a lower

porosity gave a lower L% value of lower initial attenuation of the ultrasonic signal. However in contrast, the L% value was higher for lower pore volume (thk. x porosity) as seen in Figure 5.11 and 5.13. The L% parameter represents the attenuation of the ultrasonic signal before the onset of wetting and penetration and therefore is expected to be representative of the initial condition (or dry state) of the porous sample. Since the attenuation of the ultrasonic signal is significantly dependent on the air content of the sample, L% would depend not only on the pore volume, but also on the roughness of the surface of the sample. Roughness measurements would therefore be useful for further confirming this effect.

For the tests with a particular probe liquid and different Spectra meshes 'tB' showed dependence on the pore volume (thickness x porosity) i.e. a lower 'tB' value was obtained for lower pore volume (Figure 5.12 and 5.13). This could be attributed to the penetrating liquid having to displace a lower air volume out of the sample for the ultrasonic transmission to reach 95%. For the tests with different probe liquids and the Spectra Q and T structures, it can be seen that Spectra Q which has a higher permeability gave lower 'tB' values or faster penetration dynamics with all the probe liquids (Figure 5.13).

Voith woven fabrics:

The curves obtained with penetration of water from both sides showed trends which matched the measured permeability values of the different fabrics. The higher permeability samples such as V7, V6 and V4 showed quicker dynamics (lower tB values) as compared to the lower permeability samples such as V1, V2 and V3 which showed slower dynamics (higher tB values).

Commercial paper grades:

Different absorption profiles or shapes of curves were obtained in tests with water. However, similar shaped profiles were obtained when the swelling effects were eliminated by using of a non-swelling probe liquid. The Emco parameters tB and L% showed similar trends for the paper grades WFC, CIJ, ANC -R and H (Figure 5.16 and 5.17). For the paper samples, the bulk density of

the samples could be considered as characteristic of the pore volume or air content of the samples. From Figure 5.16 and Figure 5.18, it appears that the initial attenuation of the ultrasonic signal as indicated by 'L%' shows dependence on the bulk density i.e. lower bulk density (e.g. ANC) gave a higher value of 'L%'. Also 'tB' values from tests with PDMS showed some dependence on the mean flow pore diameter i.e., with the exception of CIJ, samples such as H and ANC, with a lower mean flow pore diameter showed higher 'tB' values indicating slower penetration dynamics (Figure 5.16 and 5.18). 'tB' from tests with PDMS and water also showed dependence on the permeability of the paper samples i.e. lower 'tB' value for higher permeability samples (Figure 5.16 and 5.18). Comparison of the ultrasonic absorption profiles from tests with PDMS (Figure 4.82) show that penetration dynamics is most rapid in WFC and slowest in ANC, with CIJ and H intermediate to these. Similar trends can also be seen in the airflow - pressure drop plots for these paper samples (Figure 4.39).

The above results show some interesting trends for some of the liquid-pore structure systems investigated. It appears that the parameter 'tB' could be dependent on the pore volume, permeability, penetration coefficient and potentially the mean flow pore diameter in the case of paper. The parameter 'L%' could be dependent on the porosity and pore volume. However, surface roughness would also impact the Emco parameters and the contribution of this needs to be further investigated.

The findings in this study are limited to some extent due to the characteristics of the model pore structures used and hence the results so far cannot be confidently generalised to any system without further investigations. The Nuclepore® membranes and the Spectra Meshes are somewhat extreme in terms of thickness, porosity and pore sizes when compared to typical ranges for paper. The Nuclepore® membranes have very low porosity (< 6 %), thickness and small pore size whereas the Spectra meshes have large macroscopic pores and high porosity and thickness. The theoretical calculations with the Lucas-Washburn equation were limited due to unavailability of smooth non-porous

samples for contact angle measurements. Experimental determination of porosity and surface roughness for all the samples involved would have also been useful in the assessment of the ultrasonic method absorption profiles.

The ultrasonic method output is dependent on a number of different processes, which occur when a liquid penetrates a more complex pore structure such as paper. Inherent in the absorption profiles obtained are other effects such as surface properties, elastic properties and swelling effects, all of which may respond at different times. The ultrasonic method does however have advantages over other liquid absorption test methods in terms of the time resolution possible and the ease and time required to do a test.

Interpretation of the y-axis or %Transmission as it relates to prediction of performance of the paper is still an issue with this measurement technique. Grüner (2002) attempted to describe the nature of different shapes of absorption curves and processes occurring during measurement in terms of the properties of the paper. He describes general profiles and different time regimes which would be obtained during tests with sized paper with water, unsized paper with water, low and high calendered paper with water and uncoated paper with low and high viscous oils. Based on all the reported studies using this method and results obtained in this study, it appears that the ultrasonic method at this juncture can at best be used as a qualitative or semi-qualitative tool. Due to the complexity of the paper structure and the various processes occurring during liquid penetration into paper, quantification of the results, especially accurate interpretation of the y-axis is difficult.

Also, unlike the model pore structures which are somewhat more 'ideal' to characterise, characterisation of the paper structure itself is quite complicated. SEM images help to some extent in getting an idea of the surface and cross sectional pore structures of a paper sample. Based on the experiments done in this study, the PMI capillary flow porometer appears to be a useful method for characterising the flow properties of paper. Use of this instrument along with the

Emco has the potential to help in better understanding the flow and liquid penetration properties of the paper structure.

Emco GmbH have recently indicated that they have developed a new electronic unit, which will report the output in terms of the 'decibel (dBA) level' on the y-axis. However, whether this will aid in interpretation of the absorption profiles obtained in any way is yet to be seen. Some of the samples which were used in this study were sent to Emco GmbH for tests using the new dBA method. No feedback has been obtained from Emco to date. It would however, be interesting to compare the absorption profiles obtained in this study with the profiles from the new method.

Despite the complexities involved, the ultrasonic method is useful as a comparative tool in evaluating effects of sizing, filler, swelling and other factors affecting dynamics of penetration and can be used for comparing different grades of paper for similar end use. In terms of designing new paper basesheet structures, papermakers would always need a 'point of reference' or historical data of outputs from the ultrasonic method on 'proven' grades of papers to compare the absorption profiles and predict performance depending upon end use.

6.2 Future Work

Evaluation of model pore structures with an intermediate range of porosity and pore sizes may help in further confirmation of some of the conclusions made in this study and better comparison with theoretical models. Ideal model pore structures would be similar to the Nuclepore® membranes, but of greater thickness, higher porosity and available in different pore sizes. Contact angle, porosity and surface roughness measurements for all the pore structures would complete the data set of required parameters for a more complete assessment of the ultrasonic method.

An intermediate step towards trying to better understand the outputs obtained from the Emco would be to decouple the swelling phenomena from a pure capillary flow through porous media phenomena. Emco GmbH have also recently

developed an ultrasonic method for measuring the dynamics of swelling or expansion of paper when contacted with a liquid such as water. Measurements of swelling using swelling and non swelling probe liquids would help in understanding the contributions of swelling dynamics which are inherent in the outputs from the Emco.

Print quality is the ultimate test for measuring the performance of printing paper grades. A systematic and thorough investigation for various grades of paper comparing ultrasonic tests with print quality analysis would help in evaluating whether the prediction of print quality of paper from simple tests with the ultrasonic method would be possible. This would be a valuable tool for papermakers in assessing new basesheet designs. The PMI capillary flow porometer could also be used in tandem with the ultrasonic method (Oliver et al 2002) for measuring permeability and pore size distribution and characterizing the paper sheets in the in-plane and the through-plane direction. Results from this method can also be included as part of the investigation towards interpretation of the ultrasonic absorption profiles and prediction of print quality of paper.

Evaluation of edge penetration effects in tests on paper using the ultrasound method would also be useful. After the sample is plunged into the test liquid, penetration will take place not only through the surface of the sample (z-direction), but also through the edges of the sample (x-y direction). Inclusion of additional tests on the paper samples, by taping the edges of the samples to eliminate edge penetration effects would enable an ultrasonic measurement with penetration only in the through plane direction.

References

1. "The Future of Paper.....from cyberspace to fibrespace", www.cppa.org/english/info/future.htm
2. Adams K.L., Rebenfeld L., "In-plane flow of fluids in fabrics: Structure / Flow Characterization", Textile Research Journal, Vol. 57, No.11, Nov 1987.
3. Adams, K.L., Miller B., Rebenfeld L., "Forced in-plane flow of an epoxy resin in fibrous network", Polymer Engineering and Science, Vol. 26 No 20, Nov 1986.
4. Allem Rafik, Zou Xuelun, Uesaka Tetsu, " Relationship between Coating Uniformity and Basestock Structures. Part 1: Lightweight Coated Papers", Pita Coating Conference, 27-37 (2001).
5. Amodei O., " The study of liquid penetration properties of paper through the use of ultrasound", Process & Product Quality Conference & Trade Fair, 1997 pp 59-65
6. Aspler J., "Interactions of ink and water with the paper surface in printing", Nordic Pulp and Paper Research Journal No 1, 68-74, 1993
7. Baumeister M., Grüner G., "Einsatz eines innovativen Meßverfahrens bei der Entwicklung neuartiger Streichfarbenadditive (*Use of an innovative laboratory measuring method in the development of new forms of coating additives*)", Wochenblatt für Papierfabrikation, 16 pp 1023-1031 (1999)
8. Bayer R., Alber W., " Bewertung des Füllstoffeinsatzes bei der Papiererzeugung durch Penetrationsmessungen nach der Ultraschallmethode (*Evaluation of the filler application during the paper production by penetration measurements according to the ultrasonic method*)" PTS Report No. AiF 11491B (2000) (<http://www.pts-papertech.de>)
9. Bayer R., Mallon U. & Blechschmidt J., "Penetrationsverhalten von Papieren - Meßmöglichkeiten gestern und heute (*Penetration of Paper- Past and Present Measurement*)", DasPapier, 9/1996 pp. 494-500
10. Beltz R., "An innovative method for studying the composition of paper and other materials, liquids and the dynamics of their interaction", PTS Report, Emco GmbH Technical Literature (1998).

11. Beltz R., "Ultrasound Transmission - An innovative method for studying the composition of paper and other materials, liquids and the dynamics of their interaction", Theory and Applications, Emco GmbH (2000).
12. Bhatia A.B., "Ultrasonic Absorption", pp 14, Monographs on the Physics and Chemistry of materials, Oxford at the Clarendon Press, 1967.
13. Blechschmidt J., Bayer R., " Measurement of penetration dynamics as an innovative method for the complex characterisation of papers", Project Report - Papiertechnische Stiftung Institut für Zellstoff und Papier Heidenau (PTS), Germany (1997)
14. Borhan A., Rungta K, "An experimental study of the radial penetration of liquids in thin porous substrates", J. Colloid Interface Sci., 158, 403-411 (1993)
15. Bousfeld D.W., Pellerin P., "Modelling of short time penetration into complex porous structures",
16. Brasquet C., LeCloirec P., "Pressure drop through textile fabrics - experimental data modelling using classical models and neural networks", Chemical Engineering Science 55 (2000) 2767-2778.
17. Bristow J. A., "The Paper Surface in Relation to the Network", Paper Structure and Properties - International Fiber Sciences and Technology Series / 8, pp 169-182, Marcel Dekker Inc. 1986
18. Bristow J. A., "The Pore Structure and the Sorption of Liquids", Paper Structure and Properties - International Fiber Sciences and Technology Series / 8, pp 183-201, Marcel Dekker Inc. 1986
19. Bristow J.A, " The absorption of water by sized papers", Svensk Papperstidning No 2 pp 33-39 Jan (1968)
20. Bristow J.A., " Liquid Absorption into paper during short time intervals", ", Svensk Papperstidning No 19 pp 623-629 Oct 1967.
21. Brodeur P. H., "Out-of-plane ultrasonic testing of paper materials using fluid filled rubber wheels", Tappi Journal, 77, No.3, 213-218 (1994).
22. Brodeur P.H., Gerhardstein J.P., " Overview of Applications of Ultrasonics in the Pulp and Paper Industry", Proceedings of IEEE International Ultrasonics Symposium, Sendai, Japan, October 1998.

23. Cassie A.B., Baxter S., "Wettability of Porous Surfaces", Trans. Farad. Soc. 40, 546-551 (1944).
24. Chatterjee P. K., "The Sonic velocity response during the absorption of water in paper", Svensk Papperstidning **74**, No. 17, 503-508 (1971).
25. Clark D., "Globalization, changing markets and the challenge to paper coating technology", Tappi Coating Conference, Toronto, May 3, 1999
26. Craver J. K., Taylor D. L., " Sonic velocity response of wet strength paper", Pulp and Paper Magazine of Canada, T-331 - T-336, July 1966
27. CRC Handbook of Chemistry and Physics, 69th edition, 1988-89, CRC Press Inc., Boca Raton, Florida, pp. F-40, F-34, D-238
28. Darcy H., "Les Fontaines Publiques de la Ville de Dijon", Dalmont, Paris (1856)
29. Dietze Jörg, "Vergleichende Penetrationsuntersuchungen an Druckpapieren unterschiedlicher Provenienz mit Hilfe von Ultraschall (*Comparative penetration investigations of printing papers using ultrasound*) ", Thesis, Technische Hochschule Leipzig (1995)
30. Dixon J.S., "Error Analysis in Capillary Flow Porometry", Porous Materials Inc. Technical Literature, 2002
31. Dullien F.A., "Single Phase Flow through Porous Media and Pore Structure", Chemical Engineering Journal, 10 (1975) 1-34/
32. Eklund D., "Review of Surface Application", pp. 833-869, Oxbridge 1989
33. Emco GmbH, " Dynamic Penetration Measurement - User Manual and Operating Instructions" (1998)
34. Gabriel Gerhard, "Meßtechnische Erfassung der Wechselwirkungen zwischen Flüssigkeiten und Papieren mittels Ultraschall (*Measurements of the interactions between liquids and papers by means of ultrasound*)", Ph.D. Thesis, Technischen Universität Graz (1999)
35. Gane P., "Absorption Properties of Coatings", Pira Coating Conference, Nov 2000.
36. Gane P.C., " Observing Fluid Transport into Porous Coating Structures: Some Novel Findings", Tappi Advanced Coating Fundamentals Symposium, Toronto, 213-236, 1999.

37. Grüner G., " New measuring methods to study the quality of paper and process liquids, their interaction and its influence to converting processes" Emtec Measuring Systems Technical Literature (2002)
38. Gupta K, " Porous Materials and their Structure", Porous Materials Inc. Technical Literature, 2002
39. Haeggström E., Vuohelainen R., Stor-Pellinen J., Mauri Luukkala, Hannu Lätti, " Paper surface make up process observed by ultrasound", Tappi Journal Peer Reviewed Paper, Oct (2000).
40. Hayes R.E., Bertrand F. H., Tanguy P. A., "Modelling of Fluid -Paper Interaction in the Application Nip of a Film Coater", Transport in Porous Media, 1441, 1-18, 1999.
41. Haynes J. M., Everett D.H., Miller R. J., "Kinetics of capillary imbibition by fibrous materials", Fibre-Water Interactions in Paper Making, Vol. 2, pp 519-534 Sep 1977
42. Hoyland R.W., "Swelling during the penetration of aqueous liquids into paper", Fibre-Water Interactions in Paper Making, Vol. 2, pp 557-577 Sep 1977
43. Hoyland R.W., Howard P., Field R. "The Fundamental Properties of Paper Related to its Uses", Tech. Div. BPBIF, pp 464 (1976)
44. Japanese Industrial Standard - Testing Method for Stöckigt Sizing Degree of Paper, JIS P 8122-1976 (Reaffirmed: 1984)
45. Jena A, "Fundamentals of Capillary Flow Porometry", Porous Materials Inc. Technical Literature, 2002a
46. Jena A., "Interpretation of Anomalous Results (Case Studies)", Porous Materials Inc. Technical Literature, 2002b
47. Jena A., Gupta N., "Measuring in layers", Ceramic Industry, Feb 2001
48. Johnson R.W., Amick T. J., Abrams L., Maynard R. B., "Use of Hg-Porosimetry to Characterize Pore Structure and Model End-use Properties of Coated Papers", Tappi Coating/Papermakers Conference, New Orleans (1998)
49. Jykri Stor-Pellinen, Edward Haeggström, Mauri Luukkala, "Measurement of paper wetting processes by ultrasound transmission", Meas. Sci. Technol. 11 pp 406-411 (2000a)

50. Jykri Stor-Pellinen, Edward Haeggström, Mauri Luukkala, "Measurement of the effect of high-power ultrasound on wetting of paper", *Ultrasonics*, 38 pp 953-959 (2000b)
51. Jykri Stor-Pellinen, Edward Haeggström, Timo Karppinen, Mauri Luukkala, "Air coupled ultrasonic transmission measurement through paper during wetting", *Meas. Sci. Technol.* 13 pp 770-774 (2002)
52. Jykri Stor-Pellinen, Edward Haeggström, Timo Karppinen, Mauri Luukkala, "Air coupled ultrasonic transmission measurement of the change in roughness of paper during wetting", *Meas. Sci. Technol.* 12 pp 1336-1341 (2001)
53. Jykri Stor-Pellinen, Mauri Luukkala, "Paper roughness measurement using airborne ultrasound", *Sensors and Actuators – A* 49, 37-40 (1995).
54. Kim-Habermehl L., Roper J. A., DeWildt D., & Jones S., " An overview of the light weight coated papers market", *Tappi Coating Conference Proceedings*, 1999, 1-1 pp 1- 18
55. Kirk-Othmer Encyclopaedia of Chemical Technology -"Membrane Technology" R. W. Baker, John Wiley and Sons Inc., 1995
56. Lindsay, J. D., "The anisotropic permeability of paper", *Tappi J.*, 73 (5), pp 223-229 (1990)
57. Lindström T., " The concept and measurement of fibre swelling", *Paper Structure and Properties - International Fiber Sciences and Technology Series / 8*, pp 75- 97, Marcel Dekker Inc. 1986
58. Lucas, R., "Ueber das Zeitgesetz des kappilaren Aufstiegs von Flüssigkeiten (*On the dynamics of the capillary rise of liquids*)", *Kolloid Zeitschr*, 23, 15 (1918)
59. Lyne M.B., "Wetting and Penetration of Liquids into Paper", *Ninth Annual Summer Institute in Polymer Science and Technology* (1979)
60. Lyne M.B., Aspler J.S., " Wetting and the sorption of water by paper under dynamic conditions", *Tappi J.*, Vol. 65, No 12, Dec 1982
61. Marmur A. J. *Colloid Interface Sci.* 124, 161 (1988)
62. Marmur A. J. *Colloid Interface Sci.* 124, 301 (1988)
63. Marmur A., "Equilibrium and Spreading of Liquids on Solid Surfaces", *Advances in Colloid and Interface Science*, 19 (1983), 75 -102.

64. Marmur A., Cohen R., "Characterization of Porous Media by the Kinetic of Liquid Penetration: The Vertical Capillaries Model", J. Colloid and Interface Sci. 189, 299-304 (1997).
65. Miller B., "The Wetting of Fibres", Surface Characteristics of Fibres & Textiles" Part II, Marcel Dekker (1977)
66. Miller B., Friedman H. L., "Absorption rates for materials under compression", Tappi J. pp 161-164 Dec 1992
67. Miller B., "The penetration of liquids into fiber networks", J. Applied Polymer Science: Applied Polymer Symposium 47, 403-415 (1991).
68. Morrow N.R., " Physics and Thermodynamics of Capillary Action in Porous Media", Ind. Eng. Chem., Vol. 62 No 6, June 1970.
69. Mussalo Eveliina, " Paperin Absorptio-ominaisuuksien mittaaminen ultraäänellä (*Liquid Penetration into paper measured by ultrasound*)", Thesis, Lappeenranta University of Technology, 1997.
70. Oliver J.F., " Wetting and penetration of paper surfaces", ACS Symposium Series No 200, Colloids and Surfaces in Reprographic Technology (1982).
71. Oliver J.F., Agbezuge L., Woodcock K., "A diffusion approach for modelling penetration of aqueous liquids into paper", Colloids and Surfaces A, 89, 213-226 (1994).
72. Oliver J.F., Chen J., Tosto F., Costa P., Silvy J., Proc. COST ACTION E11 Final Workshop Epsoo, Finland, October 2001.
73. Oliver J.F., Jones A.Y., "The inter-relationship between paper structure and print quality in ink jet printing", Mat. Res. Soc. Symp. Proc., Vol. 197, 309-318 (1990)
74. Oliver J.F., D'Souza E., Hayes R.E., "Application of ultrasonic and porometric techniques to measure liquid penetration in digital printing papers", Imaging Science and Technology, NIP 18, Conference Proceedings, International Conference on Digital Printing Technologies, San Diego, Sep 29, 2002, Vol. 8
75. Pan Y., Kuga S., Usuda M., " An ultrasonic technique to study wetting and liquid penetration of paper", Tappi Journal, 71, No. 5, 119-123 (1988a).

76. Pan Y., Kuga S., Usuda M., " Correlation of ultrasonic method and Bristow's test in evaluation of wetting properties of paper ", Sen-I Gakkaishi, 44, No. 6, 271-274 (1988b).
77. Pan Y., Kuga S., Usuda M., " Evaluation of paper sizing measurement by ultrasonic measurement", ISF -85, 20-24, Hakone, Japan, August (1985b)
78. Pan Y., Kuga S., Usuda M., " Measurement of sizing degree of paper by ultrasonic wave", Japan TAPPI/CPPA Pulp and Paper Technology Conference Preprints, Oct 15-17, pp 199-203 (1985c).
79. Pan Y., Kuga S., Usuda M., Kadoya T., " Ultrasound can evaluate paper sizing", Tappi Journal, **68**, No. 9, 98-102 (1985a).
80. Pan Y., Yang S., " Wetting and liquid absorption characteristics of ink jet paper" Recent Progress in Ink Jet Technologies II, Chapter 6, Ink and Media pp 486-490 Originally published in 12th International Congress on Advances in Non-Impact Printing Technology Proceedings (1996) pp 399
81. Pekarovicova A., Pekarovic J., " Water penetration dynamics and flexo printability of liner board", Western Michigan University, Department of Paper and Printing Science and Engineering, Kalamazoo, MI 49008-5060 (2001)
82. Peterson R.M., "Two dimensional flow of incompressible fluids through deformable porous media", Tappi J., Vol. 53, No.1, pp 71-77, Jan 1970
83. Phillips B., " Penetration and spreading of water and flexographic inks into newsprints: Part II comparison of penetration methods", Pira Newsprint Conference, 1999, pp 35-40.
84. Poulin N, Tanguy P.A., "Numerical and Physical Modeling of the Permeability of Paper to CMC and Coating Liquids," Canadian Journal of Chemical Engineering, Vol. 75 (1997)
85. Rasi M., Koponen A., Aaltosalmi U., Timonen J., Kataja M., "Permeability of Paper: Experiments and Numerical Simulations", Tappi International Paper Physics Conference, San Diego (1999).
86. Richter K. P., " Ultrasonic measurements - Physical Background", Emco GmbH Technical Literature (1999).
87. Ruoff A.L., Prince J.C., Giddings J.C., Stewart G.H., Kolloid-Z, 166(2) (1959) 144.

88. Ruoff A.L., Prince J.C., Giddings J.C., Stewart G.H., *Kolloid-Z*, 173(1) (1960) 14.
89. Salminen P. J., " Water transport into paper - the effect on some liquid and paper variables", *Tappi J.*, 195-200, Sep 1988.
90. Schwartz N. R., "Paper Surface Characterization in Relation to the Spreading of Hot Melt Phase Change Inks", M.S. Thesis, University of Massachusetts, Lowell (1998)
91. Scriven L.E., Chen K.S., "Liquid penetration into a deformable porous substrate", *Tappi J.*, 155-161, Jan 1990.
92. Sjögren M., "Paper Wettability Measurements – An evaluation of the Emtec - PDA " Thesis, - Department of Industrial Technology, Mid Sweden University, Örnköldsvik (1998).
93. Tappi Test Method T441 om-90 - Water absorptiveness of sized (non-bibulous) paper and paperboard (Cobb test) (1990)
94. Taylor D. L., Dale R. D., "Water retention of coating colours", *Tappi Journal*, **50**, No.11, 536-541 (1967).
95. Titus M., "Ultrasonic technology - measurements of paper orientation and elastic properties", *Tappi Journal*, **77**, No. 1, 127-130 (1994).
96. Tollenaar D., "Capillarity and wetting in paper structures: Properties of porous systems", *Surfaces and Coatings related to paper and wood*, R.H. Marchessault and C. Skaar (eds), Syracuse University Press, Syracuse, NY 1967, pp. 195-219
97. Tomimasu H., Suzuki K., Ogura T., "The effect of basestock structure on coating weight distribution", *Tappi J.*, 179-187, May 1990
98. V. Mailly, *Revue A.T.I.P.*, Vol. 51, No 03, May/June 1997
99. Venkatraman S., " Selection of Pore Characterization Techniques", *Porous Materials Inc. Technical Literature*, 2002
100. Vomhoff H., "On the in-plane permeability of water saturated fibre webs", *Nordic Pulp and Paper Research Journal*, 15 (3), pp 200-210 (2000).
101. Washburn E.W., " The Dynamics of Capillary Flow", *The Physical Review*, Vol. 27 No. 3, March 1921.
102. Waterhouse J. F., "Ultrasonic testing of paper and paperboard: principles and applications", *Tappi Journal*, **77**, No. 1, 120-126 (1994).

103. Williams G.J, Drummond J.G.," Preparation of large structures for the microscopical study of paper structure ", Journal of Pulp and Paper Science, Vol.26, No.5, May 2000.
104. Wilson J.D., "College Physics", pp 458, 2nd Ed, Prentice Hall, Englewood Cliffs, New Jersey, 1994.

APPENDIX - A

Specifications of the Emco - DPM 30

Electronic Unit:

Ambient Temperature Range	0°C to +50°C
Power Supply	230V AC \pm 10%, 50 Hz 115 V AC \pm 10%, 60 Hz
Dimensions	370 mm x 120mm x 300 mm
Weight	5 kg
Measuring Duration	1 sec to 9999 sec (to be set by the user)

Measuring Cell:

Dimensions	130mm x 180mm x 110mm
Weight	3.5 kg

Volumes of measuring cells and cell inserts

Measuring Cell - Fill level 1	680 ml of test fluid
Measuring Cell - Fill level 2	560 ml of test fluid

Cell insert - Fill level 1	90 ml of test fluid
Cell insert - Fill level 2	55 ml of test fluid

Time for complete contact or immersion of the sample

Cell insert at fill level 1	31 millisec
Cell insert at fill level 2	8 millisec

Measuring Area:

Circular concentric areas of diameter 10 mm and 35mm respectively.

Frequency: Standard 2 MHz

Immersion Appliance:

Dimensions	150mm x 400mm x 255mm
Weight	7 kg

Sample Holders:

For measuring areas of 10 mm and 35 mm and upper or lower filling levels the following types of sample holders were available at ARC.

Type 4 (Figure A.1)	Material - Acrylic glass with Teflon coating - Polypropylene
Type 7 (Figure A.2)	Material - Stainless Steel Open sample holder for bi-directional contact with the test liquid. Samples are fixed to the holder with the help of magnetic strips

Figure A.1: Type 4 Sample Holder

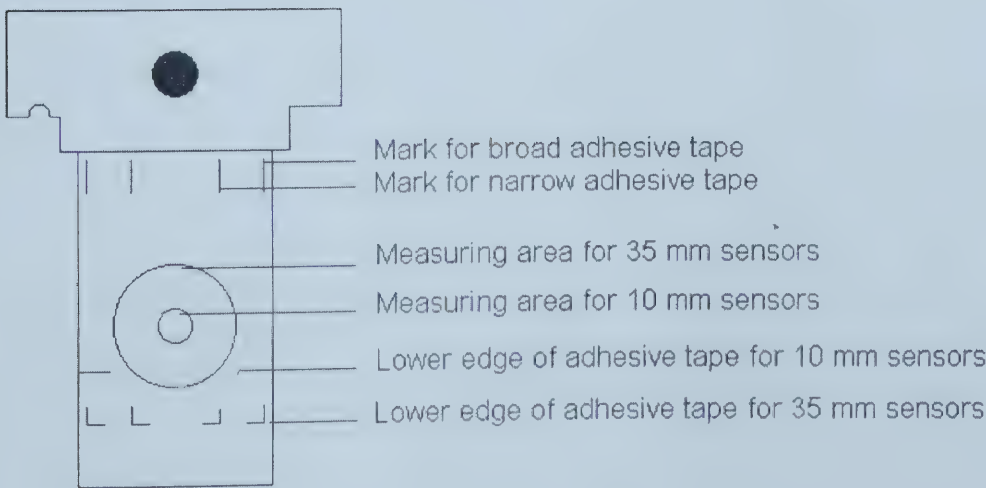


Figure A.2: Type 7 Sample Holder



APPENDIX B

Viscosity measurements for 25% Aq. Polyethylene Glycol

Measurement Data

Instrument - Canon-Fenske Viscometer

Test liquid - 25% PEG 35000 Aqueous solution

Tube No - 725(450)

Viscometer constant = 2.35935 @ 40 °C

Temperature Correction = 1.0009 x Viscometer constant = 2.361473

Density of sample = 1.05 g/cc @ 21.5 °C

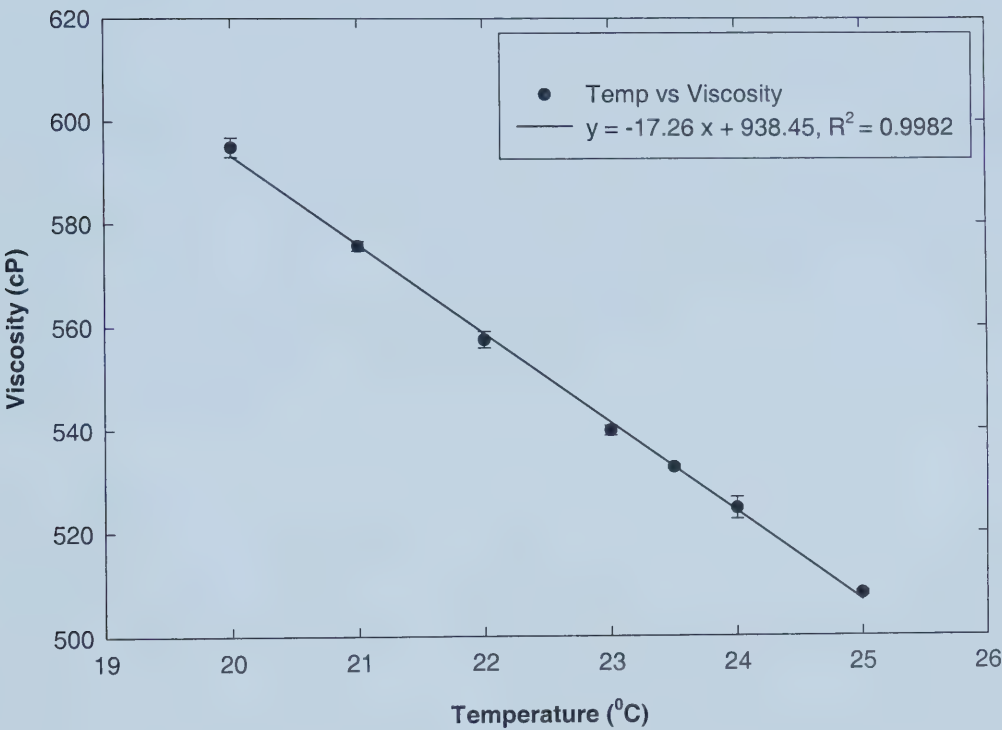
The results obtained are shown in Table B.1 and plotted in Figure B.1

It can be seen that the viscosity has a linear dependence on temperature in the temperature range of 20 - 25 °C. 95% confidence intervals were considered for the error bars and linear regression fit.

Table B.1: Viscosity measurements for 25% Aq. PEG 35000

Temp ° C	Time			Mean	Viscosity mPa-s
	sec	sec	sec		
20	239.82	240.25	239.64	239.90	594.85 ± 0.15%
21	232.03	232.13	232.33	232.16	575.66 ± 0.1%
22	225.13	224.72	224.65	224.83	557.48 ± 0.13%
23	217.55	217.86	217.77	217.73	539.86 ± 0.1%
23.5	214.87	214.88	214.77	214.84	532.71 ± 0.03%
24	211.49	211.99	211.34	211.61	524.69 ± 0.19%
25	204.93	205.04	204.89	204.95	508.19 ± 0.04 %

Figure B.1: Viscosity Plot for 25% Aq. PEG 35000



Appendix C

Table C.1: Permeameter Experimental Data - Nuclepore Membranes

a) 12 Micron (T = 22.5 °C, Viscosity = 0.9437 mPa-s)

h from top (cm)	h _i (cm)	h _f (cm)	ln h _i /h _f	t ₁ (sec)	t ₂ (sec)	t ₃ (sec)	t _{1cal} (sec)	t _{2cal} (sec)	t _{3cal} (sec)
28	70	10	1.95	0.00	0.00	0.00	56.37	56.42	56.58
38	60	10	1.79	5.02	5.18	5.21	51.35	51.24	51.37
48	50	10	1.61	11.39	11.59	11.92	44.98	44.83	44.66
58	40	10	1.39	17.59	17.90	17.75	38.78	38.52	38.83
68	30	10	1.10	26.06	26.89	26.95	30.31	29.53	29.63
78	20	10	0.69	38.48	37.71	38.16	17.89	18.71	18.42
88	10	10	0.00	56.37	56.42	56.58	0.00	0.00	0.00

b) 8 Micron (T = 22.5 °C, Viscosity = 0.9437 mPa-s)

h from top (cm)	h _i (cm)	h _f (cm)	ln h _i /h _f	t ₁ (sec)	t ₂ (sec)	t ₃ (sec)	t _{1cal} (sec)	t _{2cal} (sec)	t _{3cal} (sec)
11	89.2	19.2	1.54	0	0.00	0.00	241.93	243.58	234.33
21	79.2	19.2	1.42	16.02	15.80	15.52	225.91	227.78	218.81
31	69.2	19.2	1.28	34.87	34.33	34.02	207.06	209.25	200.31
41	59.2	19.2	1.13	57.18	56.12	55.30	184.75	187.46	179.03
51	49.2	19.2	0.94	84.71	83.46	81.96	157.22	160.12	152.37
61	39.2	19.2	0.71	120.24	119.15	116.15	121.69	124.43	118.18
71	29.2	19.2	0.42	168.62	167.80	163.08	73.31	75.78	71.25
81	19.2	19.2	0.00	241.93	243.58	234.33	0.00	0.00	0.00

c) 5 Micron (T = 23.5 °C, Viscosity = 0.9219 mPa-s)

h from top cm)	h _i (cm)	h _f (cm)	ln h _i /h _f	t ₁ (sec)	t ₂ (sec)	t ₃ (sec)	t _{1cal} (sec)	t _{2cal} (sec)	t _{3cal} (sec)
10	90	60	0.41	0.00	0.00	0.00	106.46	108.08	107.24
15	85	60	0.35	13.40	13.61	13.05	93.06	94.47	94.19
20	80	60	0.29	28.18	28.80	27.86	78.28	79.28	79.38
25	75	60	0.22	44.52	45.36	44.14	61.94	62.72	63.10
30	70	60	0.15	62.87	63.89	63.50	43.59	44.19	43.74
35	65	60	0.08	83.27	84.70	83.86	23.19	23.38	23.38
40	60	60	0.00	106.46	108.08	107.24	0.00	0.00	0.00

d) 2 Micron (T = 24.0 °C, Viscosity = 0.9111 mPa-s)

h from top (cm)	h _i (cm)	h _f (cm)	ln h _i /h _f	t ₁ (sec)	t ₂ (sec)	t ₃ (sec)	t ₁ cal (sec)	t ₂ cal (sec)	t ₃ cal (sec)
10	80	68	0.16	0.00	0	0.00	267.29	267.8	270.86
12	78	68	0.14	39.48	36.02	39.77	227.81	231.78	231.09
14	76	68	0.11	79.61	76.52	80.77	187.68	191.28	190.09
16	74	68	0.08	121.39	119.76	123.58	145.90	148.04	147.28
18	72	68	0.06	167.42	165.2	170.46	99.87	102.6	100.40
20	70	68	0.03	215.74	214.42	220.02	51.55	53.38	50.84
22	68	68	0.00	267.29	267.8	270.86	0.00	0.00	0.00

Notes:

- 1. t cal is the total time calculated for the liquid level to fall from h_i to h_f
- 2. Fresh sample and freshly filtered water used for each test run

Table C.2: Permeameter Experimental Data - Voith Spectra Meshes

a) Spectra Q (T = 24.0 °C, Viscosity = 524.69 mPa-s)

h from top (cm)	h _i (cm)	h _f (cm)	ln h _i /h _f	t ₁ (sec)	t ₂ (sec)	t ₃ (sec)	t _{1cal} (sec)	t _{2cal} (sec)	t _{3cal} (sec)
20	80	10	2.079	0.00	0.00	0.00	101.02	100.95	100.95
30	70	10	1.946	6.55	6.55	6.49	94.47	94.40	94.46
40	60	10	1.792	13.42	13.98	13.36	87.60	86.97	87.59
50	50	10	1.609	22.12	22.23	22.71	78.90	78.72	78.24
60	40	10	1.386	32.68	33.27	33.52	68.34	67.68	67.43
70	30	10	1.099	46.86	47.91	47.54	54.16	53.04	53.41
80	20	10	0.693	66.92	67.02	66.93	34.10	33.93	34.02
90	10	10	0.000	101.02	100.95	100.49	0.00	0.00	0.46

b) Spectra T (T = 23.0 °C, Viscosity = 539.86 mPa-s)

h from top (cm)	h _i (cm)	h _f (cm)	ln h _i /h _f	t ₁ (sec)	t ₂ (sec)	t ₃ (sec)	t _{1cal} (sec)	t _{2cal} (sec)	t _{3cal} (sec)
20	80	10	2.079	0.00	0.00	0.00	149.21	147.42	148.27
30	70	10	1.946	11.08	11.21	11.24	138.13	136.21	137.03
40	60	10	1.792	24.30	23.80	24.29	124.91	123.62	123.98
50	50	10	1.609	38.27	38.47	38.26	110.94	108.95	110.01
60	40	10	1.386	54.96	54.61	55.15	94.25	92.81	93.12
70	30	10	1.099	75.83	75.61	75.83	73.38	71.81	72.44
80	20	10	0.693	103.52	103.37	103.49	45.69	44.05	44.78
90	10	10	0.000	149.21	147.42	148.27	0.00	0.00	0.00

c) Spectra F (T = 23.0 °C, Viscosity = 539.86 mPa-s)

h from top (cm)	h _i (cm)	h _f (cm)	ln h _i /h _f	t ₁ (sec)	t ₂ (sec)	t ₃ (sec)	t _{1cal} (sec)	t _{2cal} (sec)	t _{3cal} (sec)
10	90	20	2.197	0.00	0.00	0.00	641.96	647.58	641.90
20	80	20	2.079	38.42	38.47	38.74	603.54	609.11	603.16
30	70	20	1.946	81.27	82.06	81.67	560.69	565.52	560.23
40	60	20	1.792	131.15	133.05	131.61	510.81	514.53	510.29
50	50	20	1.609	190.64	190.95	188.61	451.32	456.63	453.29
60	40	20	1.386	257.08	260.98	256.24	384.88	386.60	385.66
70	30	20	1.099	344.22	347.98	344.46	297.74	299.60	297.44
80	20	20	0.693	460.05	464.64	460.02	181.91	182.94	181.88
90	10	20	0.000	641.96	647.58	641.90	0.00	0.00	0.00

Table C.3: Permeameter Experimental Data - Voith Woven Fabrics

a) Voith 1 (T = 24.0 °C, Viscosity = 524.69 mPa-s)

h from top (cm)	h _i (cm)	h _f (cm)	ln h _i /h _f	t ₁ (sec)	t ₂ (sec)	t ₃ (sec)	t _{1cal} (sec)	t _{2cal} (sec)	t _{3cal} (sec)
20	80	20	1.386	0.00	0.00	0.00	844.09	850.61	846.74
30	70	20	1.253	81.65	82.23	82.21	762.44	768.38	764.53
40	60	20	1.099	177.00	177.49	176.86	667.09	673.12	669.88
50	50	20	0.916	286.00	287.29	286.05	558.09	563.32	560.69
60	40	20	0.693	424.92	426.30	423.96	419.17	424.31	422.78
70	30	20	0.405	599.06	604.49	599.12	245.03	246.12	247.62
80	20	20	0.000	844.09	850.61	846.74	0.00	0.00	0.00

b) Voith 2 (T = 24.0 °C, Viscosity = 524.69 mPa-s)

h from top (cm)	h _i (cm)	h _f (cm)	ln h _i /h _f	t ₁ (sec)	t ₂ (sec)	t ₃ (sec)	t _{1cal} (sec)	t _{2cal} (sec)	t _{3cal} (sec)
20	80	10	2.079	0.00	0.00	0.00	596.75	593.91	595.49
30	70	10	1.946	40.89	40.59	40.68	555.86	553.32	554.81
40	60	10	1.792	87.25	86.40	86.05	509.50	507.51	509.44
50	50	10	1.609	141.00	140.06	140.27	455.75	453.85	455.22
60	40	10	1.386	207.67	206.98	206.77	389.08	386.93	388.72
70	30	10	1.099	292.49	291.06	290.15	304.26	302.85	305.34
80	20	10	0.693	407.40	406.09	405.90	189.35	187.82	189.59
90	10	10	0.000	596.75	593.91	595.49	0.00	0.00	0.00

c) Voith 3 (T = 23.5 °C, Viscosity = 532.71 mPa-s)

h from top (cm)	h _i (cm)	h _f (cm)	ln h _i /h _f	t ₁ (sec)	t ₂ (sec)	t ₃ (sec)	t _{1cal} (sec)	t _{2cal} (sec)	t _{3cal} (sec)
20	80	10	2.079	0.00	0.00	0.00	614.26	613.92	612.48
30	70	10	1.946	41.65	41.30	41.59	572.61	572.62	570.89
40	60	10	1.792	89.18	89.17	89.15	525.08	524.75	523.33
50	50	10	1.609	145.26	145.30	144.67	469.00	468.62	467.81
60	40	10	1.386	213.58	212.82	212.79	400.68	401.10	399.69
70	30	10	1.099	300.28	300.17	298.64	313.98	313.75	313.84
80	20	10	0.693	419.69	417.98	416.97	194.57	195.94	195.51
90	10	10	0.000	614.26	613.92	612.48	0.00	0.00	0.00

d) Voith 4 (T = 24.0 °C, Viscosity = 524.69 mPa-s)

h from top (cm)	h _i (cm)	h _f (cm)	ln h _i /h _f	t ₁ (sec)	t ₂ (sec)	t ₃ (sec)	t _{1cal} (sec)	t _{2cal} (sec)	t _{3cal} (sec)
20	80	20	1.386	0.00	0.00	0.00	523.86	536.87	546.25
30	70	20	1.253	58.77	59.24	59.67	465.09	477.63	486.58
40	60	20	1.099	123.96	126.06	128.25	399.90	410.81	418.00
50	50	20	0.916	198.82	203.21	204.74	325.04	333.66	341.51
60	40	20	0.693	286.75	291.93	296.36	237.11	244.94	249.89
70	30	20	0.405	389.55	398.46	404.86	134.31	138.41	141.39
80	20	20	0.000	523.86	536.87	546.25	0.00	0.00	0.00

e) Voith 5 (T = 23.0 °C, Viscosity = 539.86 mPa-s)

h from top (cm)	h _i (cm)	h _f (cm)	ln h _i /h _f	t ₁ (sec)	t ₂ (sec)	t ₃ (sec)	t _{1cal} (sec)	t _{2cal} (sec)	t _{3cal} (sec)
20	80	20	1.386	0.00	0.00	0.00	749.92	753.02	755.40
30	70	20	1.253	72.38	72.56	72.99	677.54	680.46	682.41
40	60	20	1.099	156.89	156.71	157.21	593.03	596.31	598.19
50	50	20	0.916	254.42	255.71	255.69	495.50	497.31	499.71
60	40	20	0.693	376.98	377.86	377.68	372.94	375.16	377.72
70	30	20	0.405	531.46	534.21	534.84	218.46	218.81	220.56
80	20	20	0.000	749.92	753.02	755.40	0.00	0.00	0.00

f) Voith 6 (T = 23.0 °C, Viscosity = 539.86 mPa-s)

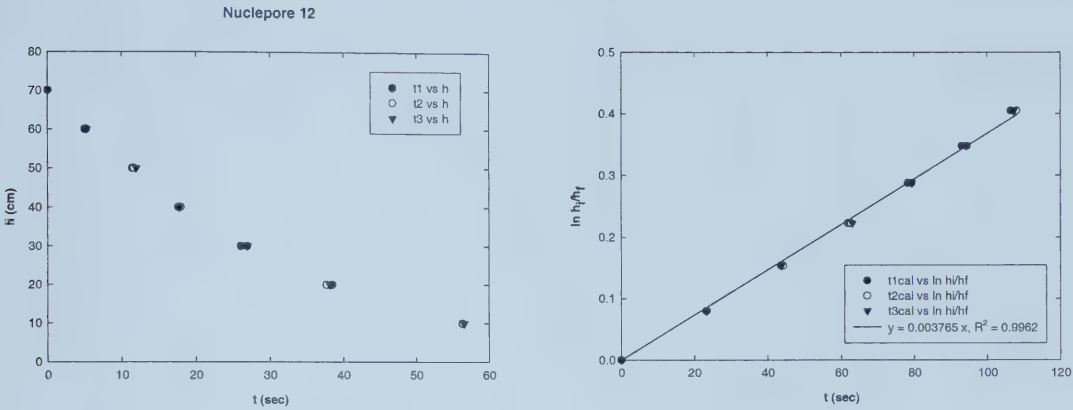
h from top (cm)	h _i (cm)	h _f (cm)	ln h _i /h _f	t ₁ (sec)	t ₂ (sec)	t ₃ (sec)	t _{1cal} (sec)	t _{2cal} (sec)	t _{3cal} (sec)
20	80	10	2.079	0.00	0.00	0.00	743.29	746.53	746.63
30	70	10	1.946	50.52	50.35	50.08	692.77	696.18	696.55
40	60	10	1.792	108.21	107.49	105.36	635.08	639.04	641.27
50	50	10	1.609	176.81	175.88	172.89	566.48	570.65	573.74
60	40	10	1.386	260.24	258.65	255.58	483.05	487.88	491.05
70	30	10	1.099	364.18	363.93	359.14	379.11	382.60	387.49
80	20	10	0.693	508.12	508.49	506.52	235.17	238.04	240.11
90	10	10	0.000	743.29	746.53	746.63	0.00	0.00	0.00

g) Voith 7 (T = 23.75°C, Viscosity = 528.53 mPa-s)

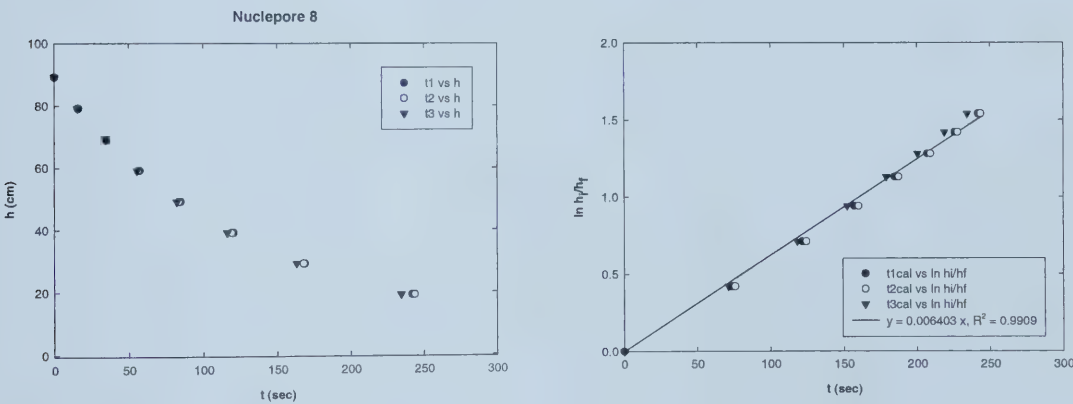
h from top (cm)	h_i (cm)	h_f (cm)	ln h_i/h_f	t₁ (sec)	t₂ (sec)	t₃ (sec)	t₁cal (sec)	t₂cal (sec)	t₃cal (sec)
20	80	10	2.079	0.00	0.00	0.00	630.39	631.16	635.28
30	70	10	1.946	41.52	42.36	42.39	588.87	588.80	592.89
40	60	10	1.792	89.27	89.33	90.21	541.12	541.83	545.07
50	50	10	1.609	145.83	145.21	146.43	484.56	485.95	488.85
60	40	10	1.386	214.27	214.77	216.33	416.12	416.39	418.95
70	30	10	1.099	302.05	303.28	305.26	328.34	327.88	330.02
80	20	10	0.693	425.64	425.08	430.23	204.75	206.08	205.05
90	10	10	0.000	630.39	631.16	635.28	0.00	0.00	0.00

Figure C.1: Nuclepore Membranes

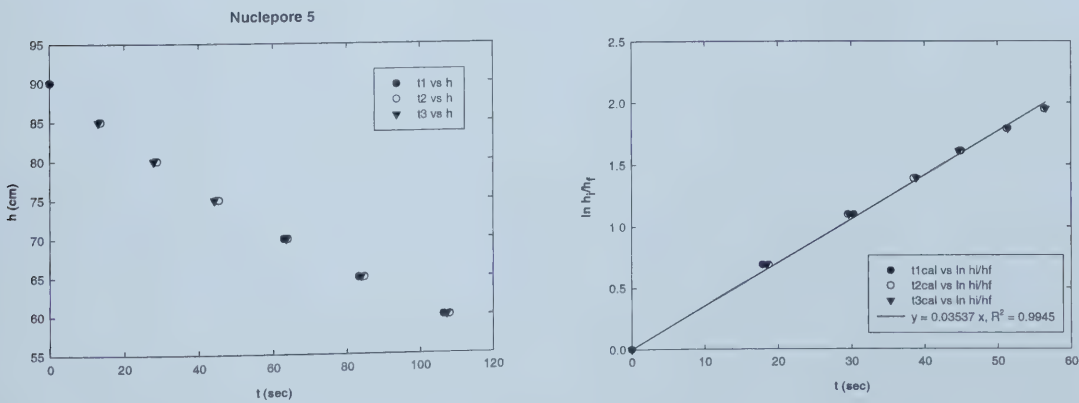
a) 12 Micron



b) 8 Micron



c) 5 Micron



d) 2 Micron

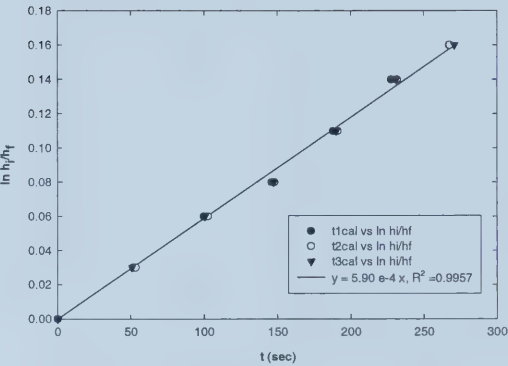
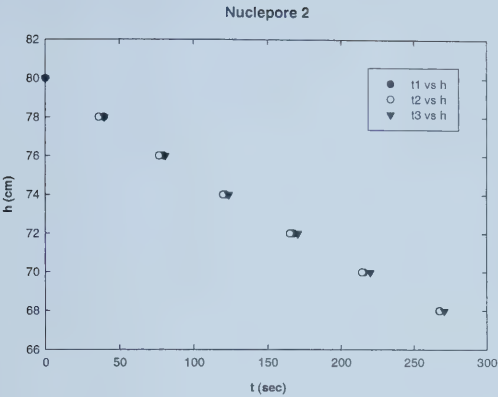
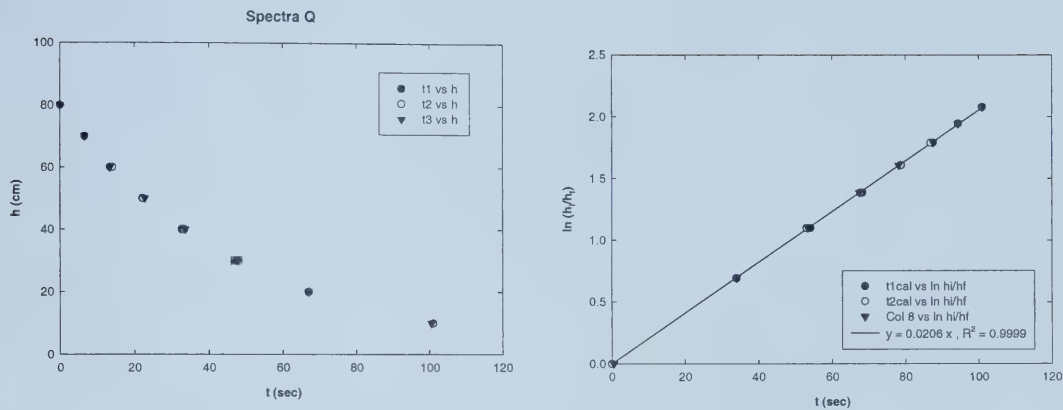
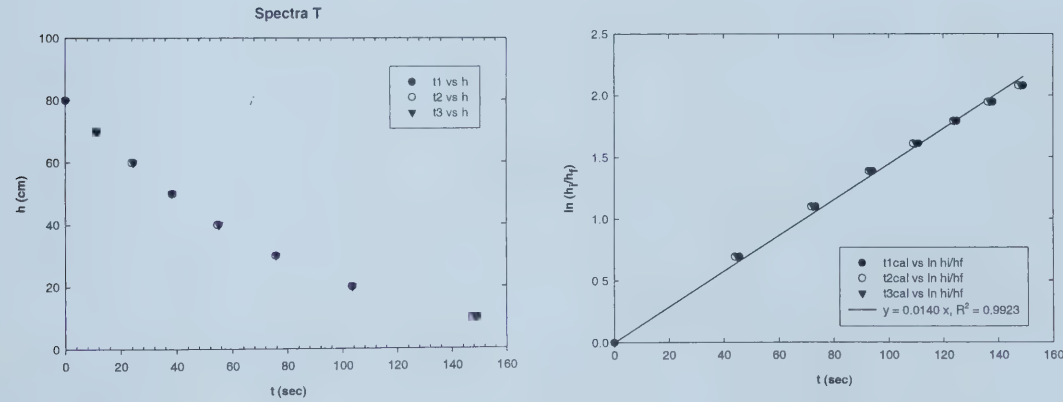


Figure C.2: Voith Spectra Meshes

a) Spectra Q



b) Spectra T



b) Spectra F

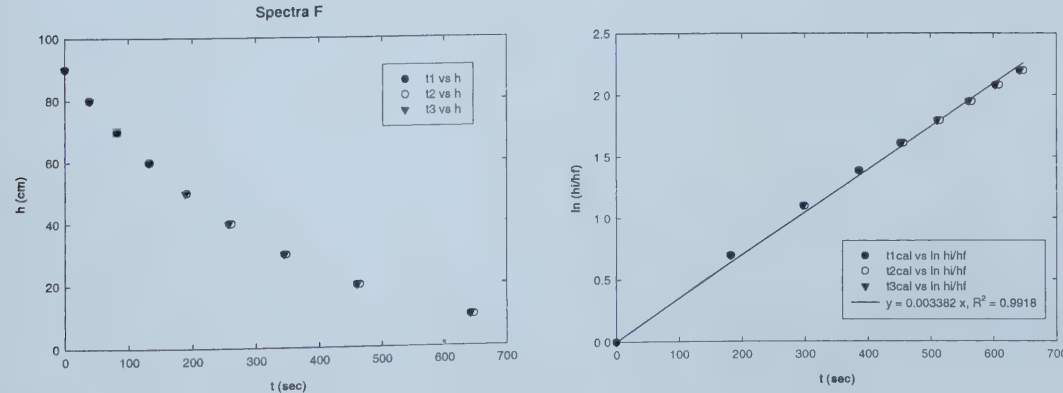
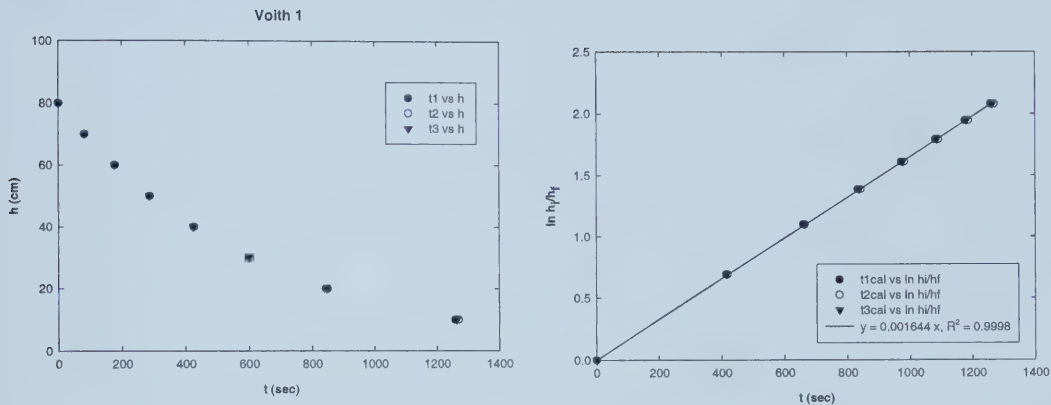
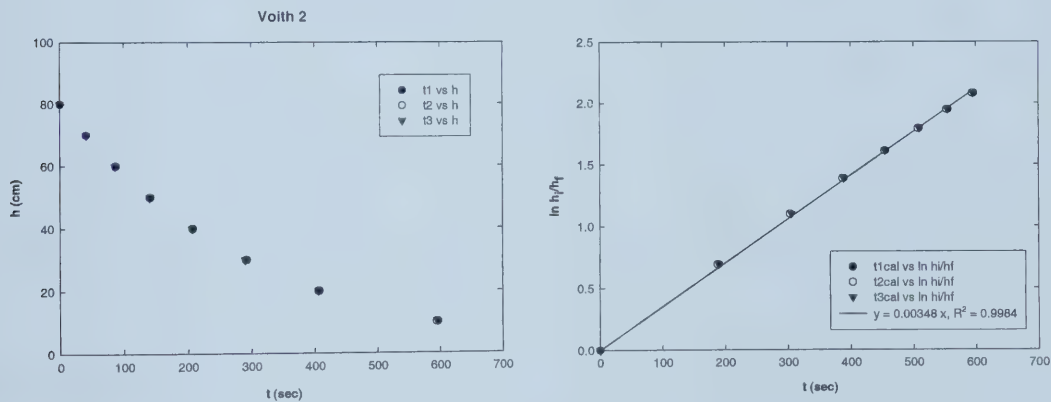


Figure C.3: Voith Woven Fabrics

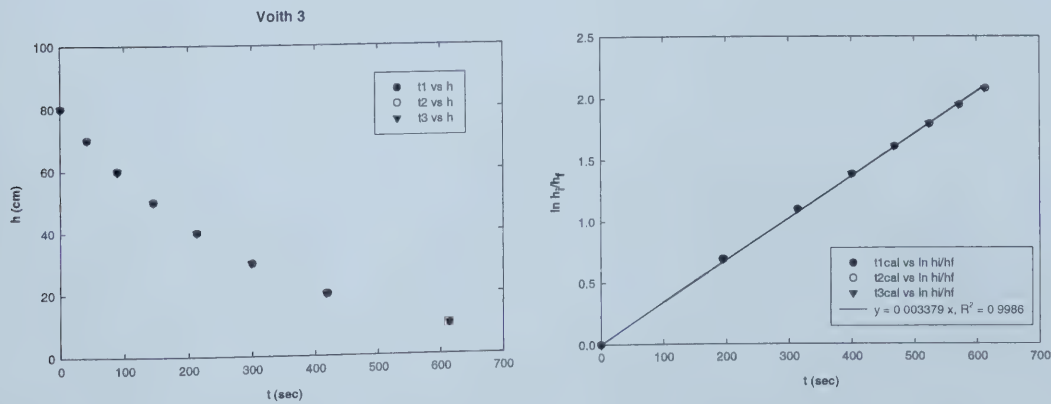
a) Voith 1



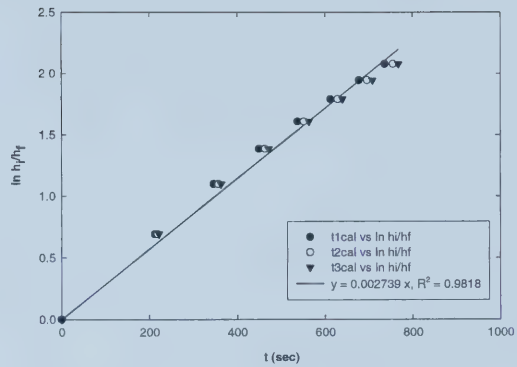
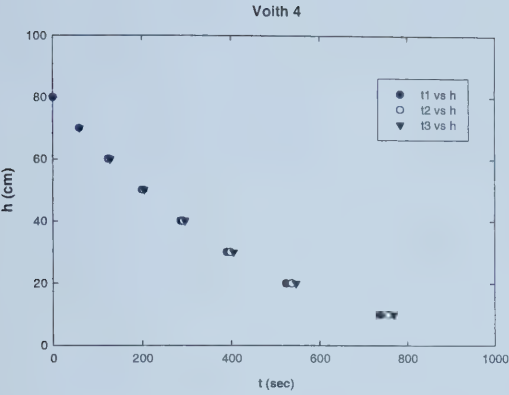
b) Voith 2



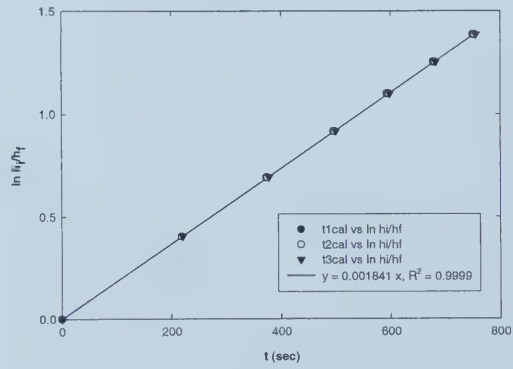
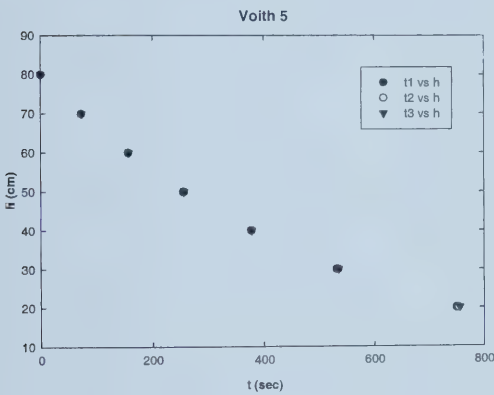
c) Voith 3



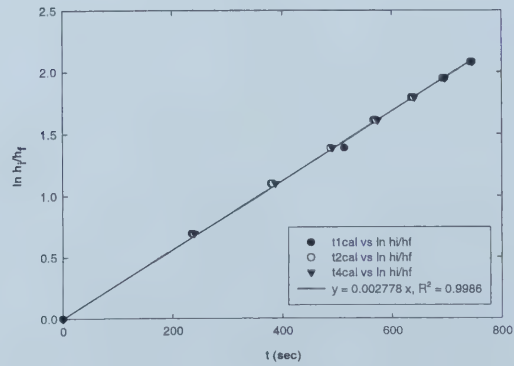
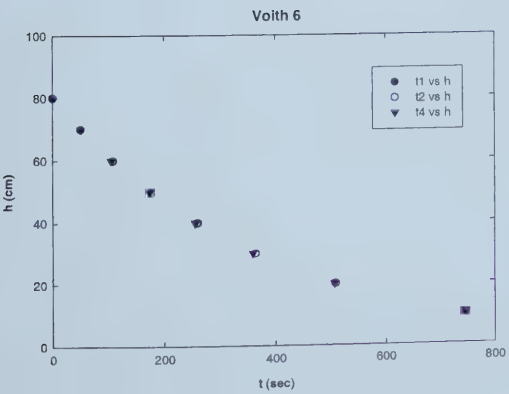
d) Voith 4



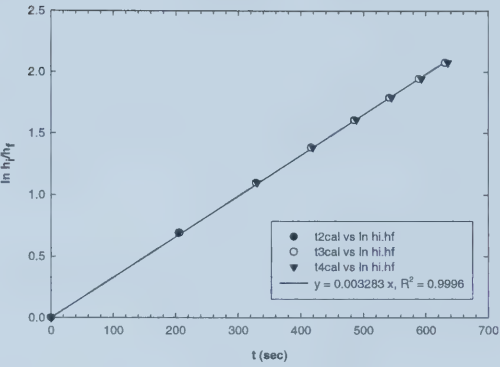
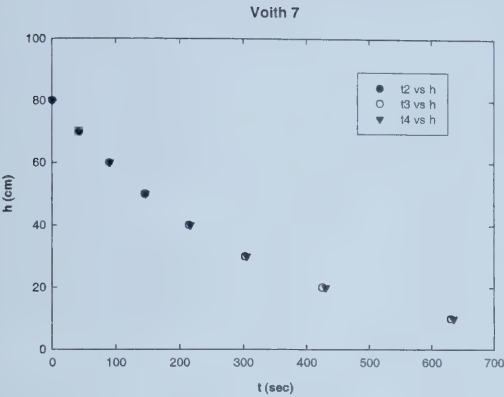
e) Voith 5



f) Voith 6



g) Voith 7



APPENDIX D

Capillary Flow Porometer (PMI Model AF 18) - Specifications

Pore Size Range	: 0.013 - 500 microns
Permeability Range	: 1×10^{-10} - 1×10^{-6} (Microflow in c/sec/m/torr)
Sample Size	: 0.5"- 2.5" diameter
Pressure Range	: 0 - 500 PSIG
Pressurizing Gas	: Clean, dry, compressed air or non-flammable, non-corrosive gas
Pressure Transducer Range	: 0 - 500 PSIG
Resolution	: 1 in 20,000
Accuracy	: 0.15% of reading
Mass Flow Transducer Range	: 10 cc/minute - 500 L/minute
Power Requirements	: 110/120 VAC, 50/60 Hz
Dimensions	: 30" H x 19" W x 18.5" D
Weight	: 100 lbs
Max. pore size detectable	: 600 microns (with water) 200 microns (with Porewick® & Silwick®)

Appendix E

Contact Angle Measurements

Table E.1: -Non-porous Polycarbonate (PC) Membrane

(a) PC-Water

No.	Method	θ (L) [°]	θ (M) [°]	θ (R) [°]	Vol. [μ l]	Height [mm]	BD [mm]
1	T-1	83.5	83.5 \pm 0.09	83.6	197.77	3.643	10.393
2	T-1	83.7	84.2 \pm 0.57	84.8	202.29	3.691	10.422
3	T-1	82.4	82.4	82.4	289.8	3.954	12.102

(b) PC-6% Methanol

No.	Method	θ (L) [°]	θ (M) [°]	θ (R) [°]	Vol. [μ l]	Height [mm]	BD [mm]
1	T-2	72.6	72.1 \pm 0.58	71.5	33.61	1.879	6.179
2	T-1	73.6	75.0 \pm 1.39	76.4	46.19	2.117	6.749
3	T-1	74.8	75.9 \pm 1.12	77	46.13	2.106	6.74

(c) PC-20% Methanol

No.	Method	θ (L) [°]	θ (M) [°]	θ (R) [°]	Vol. [μ l]	Height [mm]	BD [mm]
1	T-1	68.4	67.2 \pm 1.19	66	425.67	4.205	14.826
2	T-1	64.1	64.9 \pm 0.79	65.7	688.85	4.51	18.176
3	T-1	69.5	68.7 \pm 0.85	67.8	713.68	4.65	18.056
4	T-1	69.5	67.7 \pm 1.75	66	608.32	4.462	17.084

(d) PC-40% Methanol

No.	Method	θ (L) [°]	θ (M) [°]	θ (R) [°]	Vol. [μ l]	Height [mm]	BD [mm]
1	T-1	55.6	57.1 \pm 1.48	58.6	58.37	1.808	8.463
2	T-1	48.5	50.7 \pm 2.18	52.9	37.46	1.509	7.536
3	T-1	55.6	53.5 \pm 2.09	51.4	51.88	1.718	8.259

(e) PC-70% Methanol

No.	Method	θ (L) [°]	θ (M) [°]	θ (R) [°]	Vol. [μ l]	Height [mm]	BD [mm]
1	CIR	12.9	12.9	12.9	23.79	0.576	10.231
2	CIR	16.1	16.1	16.1	22.78	0.66	9.345
3	CIR	14.4	14.4	14.4	16.93	0.554	8.796

(f) PC-100% Methanol

No.	Method	θ (L) [°]	θ (M) [°]	θ (R) [°]	Vol. [μ l]	Height [mm]	BD [mm]
1	CIR	7.1	7.1	7.1	17.24	0.349	11.205
2	CIR	6	6	6	11.79	0.275	10.439

Table E.2: Polyvinylpyrrolidone (PVP) coating on a non-porous PC membrane

(a) PVP-Water

No.	Method	θ (L) [°]	θ (M) [°]	θ (R) [°]	Vol. [μ l]	Height [mm]	BD [mm]
1	CIR	11.4	11.4	11.4	11.04	0.412	8.243
2	CIR	12.6	12.6	12.6	11.76	0.451	8.135
3	CIR	11.5	11.5	11.5	10.46	0.406	8.087
4	CIR	11.8	11.8	11.8	8.2	0.382	7.379

(b) PVP-6% Methanol

No.	Method	θ (L) [°]	θ (M) [°]	θ (R) [°]	Vol. [μ l]	Height [mm]	BD [mm]
1	CIR	11.5	11.5	11.5	139.97	0.964	19.197
2	CIR	10.1	10.1	10.1	238.43	1.06	23.901
3	CIR	10	10	10	231.39	1.039	23.781

(c) PVP-20% Methanol

No.	Method	θ (L) [°]	θ (M) [°]	θ (R) [°]	Vol. [μ l]	Height [mm]	BD [mm]
1	CIR	10.3	10.3	10.3	187.64	0.991	21.926
2	CIR	9.9	9.9	9.9	107.13	0.801	18.429
3	CIR	9.5	9.5	9.5	295.54	1.09	26.248

(d) PVP-40% Methanol

No.	Method	θ (L) [°]	θ (M) [°]	θ (R) [°]	Vol. [μ l]	Height [mm]	BD [mm]
1	CIR	7.7	7.7	7.7	21.44	0.394	11.765
2	CIR	9.6	9.6	9.6	31.18	0.52	12.338
3	CIR	8.9	8.9	8.9	15.16	0.388	9.964

Table E.3: Nuclepore® 2 micron membrane

(a) Nuclepore 2 µm -Water

No.	Method	θ (L) [°]	θ (M) [°]	θ (R) [°]	Vol. [µl]	Height [mm]	BD [mm]
1	T-1	65.1	65.4 ± 0.25	65.7	50.64	2.051	7.353
2	T-1	65.8	66.6 ± 0.78	67.4	53.08	2.072	7.459
3	T-1	71.9	72.6 ± 0.62	73.2	65.04	2.291	7.733

(b) Nuclepore 2 µm -6% Methanol

No.	Method	θ (L) [°]	θ (M) [°]	θ (R) [°]	Vol. [µl]	Height [mm]	BD [mm]
1	T-1	56.1	56.1	56.1	422.11	3.68	16.093
2	T-1	55.1	56.6 ± 1.50	58.1	461.38	3.853	16.455
3	T-1	58.7	59.1 ± 0.41	59.5	500.41	3.917	16.84

(c) Nuclepore 2 µm -20% Methanol

No.	Method	θ (L) [°]	θ (M) [°]	θ (R) [°]	Vol. [µl]	Height [mm]	BD [mm]
1	T-1	37.4	37.8 ± 0.48	38.3	372.29	2.542	18.456
2	T-1	40.2	39.4 ± 0.77	38.6	351.72	2.635	17.665
3	T-1	41.7	41.0 ± 0.62	40.4	453.35	2.783	19.319
4	T-1	39.3	40.4 ± 1.15	41.6	382.03	2.627	18.289

(d) Nuclepore 2 µm -40% Methanol

No.	Method	θ (L) [°]	θ (M) [°]	θ (R) [°]	Vol. [µl]	Height [mm]	BD [mm]
1	T-1	32.8	33.1 ± 0.33	33.4	38.96	1.173	8.919
2	T-1	40.2	40.0 ± 0.15	39.8	33.42	1.262	7.909
3	T-1	40.9	41.3 ± 0.35	41.6	49.27	1.417	9.002

Table E.4: Contact Angle Measurements - Nuclepore® 5 micron membrane

(a) Nuclepore 5 µm - Water

No.	Method	θ (L) [°]	θ (M) [°]	θ (R) [°]	Vol. [µl]	Height [mm]	BD [mm]
1	T-1	69.8	69.8	69.9	26.84	1.766	5.724
2	T-1	72.1	72.6 ± 0.45	73	31.9	1.909	5.959
3	T-1	72.7	73.6 ± 0.89	74.5	32.52	1.941	5.95

(b) Nuclepore 5 µm - 6% Methanol

No.	Method	θ (L) [°]	θ (M) [°]	θ (R) [°]	Vol. [µl]	Height [mm]	BD [mm]
1	T-1	66.8	67.4 ± 0.54	67.9	418.61	4.253	14.632
2	T-1	55.1	54.0 ± 1.14	52.9	482.18	3.724	17.145
3	T-1	59.9	59.6 ± 0.30	59.3	492.07	3.965	16.611

(c) Nuclepore 5 µm - 20% Methanol

No.	Method	θ (L) [°]	θ (M) [°]	θ (R) [°]	Vol. [µl]	Height [mm]	BD [mm]
1	T-1	41.7	43.3 ± 1.58	44.9	470.84	2.967	19.064
2	T-1	39.5	43.1 ± 3.60	46.7	522.83	2.975	20.001
3	T-1	39	39.3 ± 0.28	39.6	338.27	2.542	17.58
4	T-1	35.5	39.8 ± 4.30	44.1	525.74	2.919	20.416

(d) Nuclepore 5 µm - 40% Methanol

No.	Method	θ (L) [°]	θ (M) [°]	θ (R) [°]	Vol. [µl]	Height [mm]	BD [mm]
1	T-1	44	43.1 ± 0.96	42.1	49.95	1.457	8.916
2	T-1	40.8	41.4 ± 0.64	42.1	47.63	1.415	8.862
3	T-1	43.9	47.5 ± 3.55	51.1	44.19	1.524	8.18

(e) Nuclepore 5 µm - 70% Methanol

No.	Method	θ (L) [°]	θ (M) [°]	θ (R) [°]	Vol. [µl]	Height [mm]	BD [mm]
1	CIR	12.8	12.8	12.8			
2	CIR	13.4	13.4	13.4			
3	CIR	15.5	15.5	15.5			

(f) Nuclepore 5 µm - 100% Methanol

No.	Method	θ (L) [°]	θ (M) [°]	θ (R) [°]	Vol. [µl]	Height [mm]	BD [mm]
1	CIR	5.6	5.6	5.6	3.45	0.173	7.118
2	CIR	8.1	8.1	8.1	1.53	0.169	4.8

Table E. 5: Nuclepore® 8 micron membrane

(a) Nuclepore 8 µm - Water

No.	Method	θ (L) [°]	θ (M) [°]	θ (R) [°]	Vol. [µl]	Height [mm]	BD [mm]
1	T-1	66.2	66.2	66.2	49.06	1.959	7.363
2	T-1	59.7	61.9 ± 2.19	64.1	56	2.099	7.722
3	T-1	75.7	73.9 ± 1.76	72.2	32.71	2.024	5.856
4	T-1	67.1	68.1 ± 0.96	69	44.26	2.007	6.908

(b) Nuclepore 8 µm - 6% Methanol

No.	Method	θ (L) [°]	θ (M) [°]	θ (R) [°]	Vol. [µl]	Height [mm]	BD [mm]
1	T-1	58.4	59.6 ± 1.16	60.8	370.41	3.724	14.927
2	T-1	65.6	61.9 ± 3.66	58.2	443.28	3.969	15.718
3	T-1	62.9	59.4 ± 3.51	55.9	422.24	3.817	15.724

(c) Nuclepore 8 µm - 20% Methanol

No.	Method	θ (L) [°]	θ (M) [°]	θ (R) [°]	Vol. [µl]	Height [mm]	BD [mm]
1	T-1	45.4	44.2 ± 1.18	43	314.11	2.871	16.015
2	T-1	45.5	46.2 ± 0.66	46.9	307.67	2.907	15.684
3	T-1	50.8	48.2 ± 2.59	45.6	346.4	3.087	16.094
4	T-1	50	53.8 ± 3.77	57.5	517.91	3.412	18.338

(d) Nuclepore 8 µm - 40% Methanol

No.	Method	θ (L) [°]	θ (M) [°]	θ (R) [°]	Vol. [µl]	Height [mm]	BD [mm]
1	T-1	41	40.4 ± 0.66	39.7	34.38	1.241	8.045
2	T-1	39.2	38.7 ± 0.43	38.3	31.03	1.188	7.844
3	T-1	44.3	40.7 ± 3.51	37.2	73.84	1.426	10.821
4	T-1	39.3	38.4 ± 0.95	37.5	47.23	1.286	9.233

(e) Nuclepore 8 µm - 70% Methanol

No.	Method	θ (L) [°]	θ (M) [°]	θ (R) [°]	Vol. [µl]	Height [mm]	BD [mm]
1	CIR	7.1	7.1	7.1	7.91	0.268	8.655
2	CIR	7	7	7	3.42	0.201	6.584
3	CIR	7.3	7.3	7.3	4.77	0.23	7.257

(f) Nuclepore 8 µm - 100% Methanol

No.	Method	θ (L) [°]	θ (M) [°]	θ (R) [°]	Vol. [µl]	Height [mm]	BD [mm]
1	CIR	7.6	7.6	7.6	5.6	0.25	7.539
2	CIR	9.7	9.7	9.7	16.15	0.419	9.891
3	CIR	10.1	10.1	10.1	18.03	0.446	10.134
4	CIR	8.8	8.8	8.8	13.4	0.37	9.593
5	CIR	9.6	9.6	9.6	7.72	0.325	7.766

Table E.6: Contact Angle Measurements - Nuclepore® 12 micron membrane

(a) Nuclepore 12 µm - Water

No.	Method	θ (L) [°]	θ (M) [°]	θ (R) [°]	Vol. [µl]	Height [mm]	BD [mm]
1	T-1	65.7	65.3 ± 0.37	65	28.43	1.719	6.03
2	T-1	68.8	67.6 ± 1.17	66.4	37.68	1.905	6.554
3	T-1	66.8	68.8 ± 2.02	70.8	38.26	1.917	6.559

(b) Nuclepore 12 µm - 6% Methanol

No.	Method	θ (L) [°]	θ (M) [°]	θ (R) [°]	Vol. [µl]	Height [mm]	BD [mm]
1	T-1	62.1	61.2 ± 0.87	60.3	348.57	3.809	14.315
2	T-1	63.8	65.0 ± 1.17	66.2	355.67	3.921	14.116
3	T-1	66.4	64.3 ± 2.02	62.3	317.39	3.853	13.512

(c) Nuclepore 12 µm - 20% Methanol

No.	Method	θ (L) [°]	θ (M) [°]	θ (R) [°]	Vol. [µl]	Height [mm]	BD [mm]
1	T-1	50.4	49.3 ± 1.10	48.2	367.36	3.188	16.278
2	T-1	57.6	57.8 ± 0.18	58	365.79	3.4	15.454
3	T-1	57.2	55.2 ± 2.05	53.1	318.73	3.364	14.682
4	T-1	56.7	56.0 ± 0.75	55.2	215.64	3.039	12.721

(d) Nuclepore 12 µm - 40% Methanol

No.	Method	θ (L) [°]	θ (M) [°]	θ (R) [°]	Vol. [µl]	Height [mm]	BD [mm]
1	T-1	42.6	39.7 ± 2.83	36.9	54.63	1.358	9.631
2	T-1	40.4	37.9 ± 2.52	35.4	57.52	1.315	10.034
3	T-1	42.2	42.4 ± 0.21	42.6	37.48	1.33	8.104

(e) Nuclepore 12 µm - 70% Methanol

No.	Method	θ (L) [°]	θ (M) [°]	θ (R) [°]	Vol. [µl]	Height [mm]	BD [mm]
1	CIR	7.2	7.2	7.2	2.86	0.193	6.135
2	CIR	9.7	9.7	9.7	2.6	0.228	5.381
3	CIR	9	9	9	3.64	0.243	6.177

(f) Nuclepore 12 µm - 100% Methanol

No.	Method	θ (L) [°]	θ (M) [°]	θ (R) [°]	Vol. [µl]	Height [mm]	BD [mm]
1	CIR	8.3	8.3	8.3	6.95	0.286	7.851
2	CIR	6.9	6.9	6.9	5.85	0.238	7.905
3	CIR	7.7	7.7	7.7	14.43	0.348	10.274

Table E.7: Contact Angle Measurements - Spectra F Mesh

(a) Voith - Spectra F - Water

No.	Method	θ (L) [°]	θ (M) [°]	θ (R) [°]	Vol. [μ l]	Height [mm]	BD [mm]
1	T-1	87.7	89.9 ± 2.18	92.1	105.46	2.836	8.433
2	T-1	83	82.1 ± 0.89	81.2	96.82	2.544	8.707
3	T-1	77.7	78.3 ± 0.68	79	84.17	2.554	8.203

(b) Voith - Spectra F - 6% Methanol

No.	Method	θ (L) [°]	θ (M) [°]	θ (R) [°]	Vol. [μ l]	Height [mm]	BD [mm]
1	T-1	81.5	80.8 ± 0.69	80.1	34.53	2.082	5.8
2	T-1	79.3	77.9 ± 1.48	76.4	28.35	2.007	5.417
3	T-1	79	80.9 ± 1.91	82.8	34.31	2.115	5.739

(c) Voith - Spectra F - 20% Methanol

No.	Method	θ (L) [°]	θ (M) [°]	θ (R) [°]	Vol. [μ l]	Height [mm]	BD [mm]
1	T-1	74	72.5 ± 1.46	71.1	482.85	4.502	15.042
2	T-1	73.7	71.7 ± 1.97	69.8	449.21	4.35	14.785
3	T-1	79.2	77.8 ± 1.35	76.5	543.32	4.694	15.389

(d) Voith - Spectra F - 40% Methanol

No.	Method	θ (L) [°]	θ (M) [°]	θ (R) [°]	Vol. [μ l]	Height [mm]	BD [mm]
1	T-2	55.8	56.7 ± 0.89	57.6	359.13	4.137	13.657
2	T-2	54.1	56.4 ± 2.30	58.7	819.62	4.798	19.019
3	T-2	55.7	68.9 ± 13.22	82.2	559.67	4.646	15.614
4	T-2	51.1	61.8 ± 10.72	72.6	341.71	3.626	14.271

(e) Voith - Spectra F - 70% Methanol

No.	Method	θ (L) [°]	θ (M) [°]	θ (R) [°]	Vol. [μ l]	Height [mm]	BD [mm]
1	T-1	63.7	66.4 ± 2.69	69.1	91.05	2.052	9.671
2	T-1	73.5	76.1 ± 2.66	78.8	120.97	2.419	10.082
3	T-1	62.1	61.5 ± 0.67	60.8	115.23	2.264	10.497
4	T-1	61.2	63.5 ± 2.23	65.7	80.01	1.867	9.529

(f) Voith - Spectra F - 100% Methanol

No.	Method	θ (L) [°]	θ (M) [°]	θ (R) [°]	Vol. [μ l]	Height [mm]	BD [mm]
1	CIR	8.8	8.8	8.8	12.43	0.361	9.354
2	CIR	8.1	8.1	8.1	0.58	0.123	3.466
3	CIR	11.1	11.1	11.1	3.36	0.272	5.602

Table E.8: Contact Angle Measurements - Spectra Q Mesh

(a) Voith - Spectra Q - Water

No.	Method	θ (L) [°]	θ (M) [°]	θ (R) [°]	Vol. [μ l]	Height [mm]	BD [mm]
1	T-1	99.2	97.8 ± 1.38	96.4	112.86	3.054	8.196
2	T-1	91.3	91.6 ± 0.28	91.9	141.44	3.107	9.284
4	T-1	101.3	102.0 ± 0.75	102.8	112.07	3.286	7.731
5	T-2	97.1	97.5 ± 0.46	98	112.07	3.286	7.752

(b) Voith - Spectra Q - 6% Methanol

No.	Method	θ (L) [°]	θ (M) [°]	θ (R) [°]	Vol. [μ l]	Height [mm]	BD [mm]
1	T-1	100.4	101.2 ± 0.81	102	28.57	2.294	4.656
2	T-1	96	95.5 ± 0.50	95	70.06	2.729	6.876
3	T-1	101.6	102.4 ± 0.87	103.3	99.86	2.898	7.8

(c) Voith - Spectra Q - 20% Methanol

No.	Method	θ (L) [°]	θ (M) [°]	θ (R) [°]	Vol. [μ l]	Height [mm]	BD [mm]
1	T-1	76.3	79.0 ± 2.69	81.7	387.04	4.562	13.187
2	T-1	79.4	80.4 ± 1.00	81.4	380.12	4.598	12.965
3	T-1	77.8	76.1 ± 1.67	74.5	533.92	4.638	15.418

(d) Voith - Spectra Q - 40% Methanol

No.	Method	θ (L) [°]	θ (M) [°]	θ (R) [°]	Vol. [μ l]	Height [mm]	BD [mm]
1	T-1	70.2	66.6 ± 3.57	63	370.21	3.889	14.358
2	T-1	76.7	70.2 ± 6.45	63.8	422.46	4.095	14.811
3	T-1	75	75.7 ± 0.71	76.4	250.31	3.65	11.926

(e) Voith - Spectra Q - 70% Methanol

No.	Method	θ (L) [°]	θ (M) [°]	θ (R) [°]	Vol. [μ l]	Height [mm]	BD [mm]
1	T-1	49.8	55.4 ± 5.63	61	53.52	1.675	8.424
2	T-1	79.7	72.8 ± 6.91	65.9	68.29	1.987	8.426
3	T-1	67.9	68.1 ± 0.19	68.3	38.56	1.825	6.732
4	T-1	90.1	90.7 ± 0.66	91.4	212.84	2.661	12.347
5	T-1	65.2	68.7 ± 3.58	72.3	60.17	1.869	8.218

Table E.9: Contact Angle Measurements - Spectra T Mesh

(a) Voith - Spectra T - Water

No.	Method	θ (L) [°]	θ (M) [°]	θ (R) [°]	Vol. [μ l]	Height [mm]	BD [mm]
1	T-1	87	86.8 ± 0.18	86.6	75.18	2.471	7.695
2	T-1	92.8	89.7 ± 3.05	86.7	55.75	2.337	6.756
3	T-1	93.1	92.7 ± 0.36	92.3	47.88	2.462	6.039

(b) Voith - Spectra T - 6% Methanol

No.	Method	θ (L) [°]	θ (M) [°]	θ (R) [°]	Vol. [μ l]	Height [mm]	BD [mm]
1	T-1	90.5	91.9 ± 1.41	93.3	55.16	2.299	6.734
2	T-1	90.9	91.9 ± 0.98	92.9	45.97	2.339	6.09
3	T-1	86.3	86.8 ± 0.46	87.2	37.7	2.114	5.898

(c) Voith - Spectra T - 20% Methanol

No.	Method	θ (L) [°]	θ (M) [°]	θ (R) [°]	Vol. [μ l]	Height [mm]	BD [mm]
1	T-1	82.6	83.0 ± 0.45	83.5	293.96	4.309	11.685
2	T-1	89.8	90.5 ± 0.70	91.2	664.02	5.64	14.974
3	T-1	87.8	88.6 ± 0.75	89.3	906.97	5.92	17.187
4	T-1	91.6	91.7	91.7	404.2	5.111	12.219

(d) Voith - Spectra T - 40% Methanol

No.	Method	θ (L) [°]	θ (M) [°]	θ (R) [°]	Vol. [μ l]	Height [mm]	BD [mm]
1	T-1	75.3	77.8 ± 2.47	80.3	332.38	3.938	13.137
2	T-1	89.7	90.0 ± 0.34	90.4	598.73	4.794	15.448
3	T-1	65	62.1 ± 2.87	59.2	366.28	3.968	14.382
4	T-1	58.1	54.9 ± 3.17	51.7	60.85	2.05	8.291
5	T-1	68.1	67.2 ± 0.95	66.2	48.2	1.849	7.458

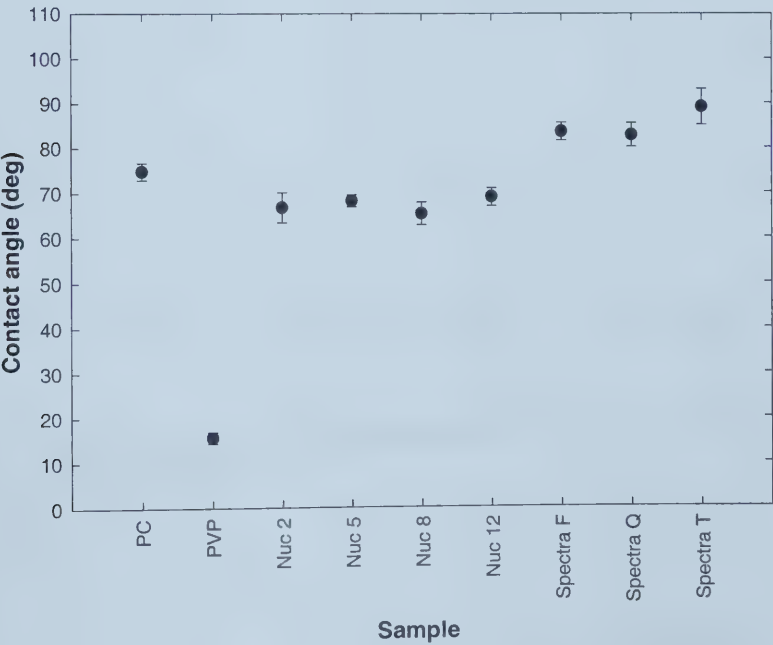
(e) Voith - Spectra T - 70% Methanol

No.	Method	θ (L) [°]	θ (M) [°]	θ (R) [°]	Vol. [μ l]	Height [mm]	BD [mm]
1	T-1	69.3	66.4 ± 2.93	63.5	51.31	1.928	7.566
2	T-1	86.1	104.6 ± 18.46	123.1	122.08	2.009	10.492
3	T-1	56.5	56.7 ± 0.19	56.8	63.35	1.775	8.865

Table E.10: Measurements using manual goniometer with water

Sample	θ (L) [°]	θ (R) [°]	θ (L) [°]	θ (R) [°]	θ (L) [°]	θ (R) [°]	θ (L) [°]	θ (R) [°]	θ (L) [°]	θ (R) [°]	θ (M) [°]
PC	76	73	77	79	73	72	71	74	78	75	74.8
PVP	16	14	17	15	15	17	12	15	17	18	15.6
Nuc 2	63	60	68	69	68	68	65	60	72	74	66.7
Nuc 5	65	70	68	68	69	66	67	68	70	71	68.2
Nuc 8	63	62	63	65	71	68	68	60	69	64	65.3
Nuc 12	70	68	68	65	68	65	72	69	73	72	69.0
Spectra F	80	85	88	80	85	85	80	84	83	86	83.6
Spectra Q	80	78	86	87	85	78	80	87	81	86	82.8
Spectra T	94	91	94	100	83	90	85	83	85	86	89.1

Figure E.1: Contact angle measurements using manual goniometer with water



Appendix F

Emco Results
Nuclepore Membranes

Figure F.1: Nuclepore® 12 micron - water

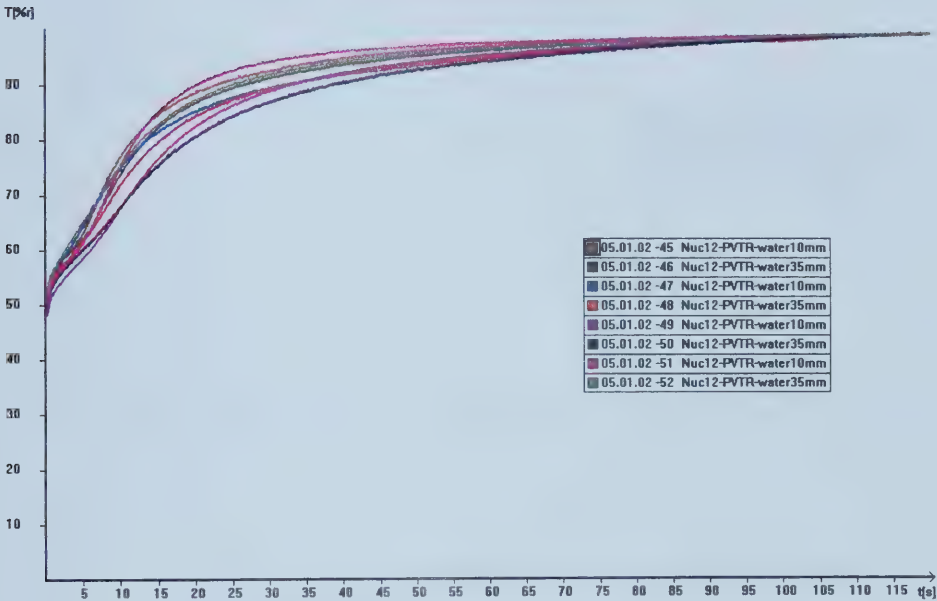


Figure F.2: Nuclepore® 12 micron - 6% methanol

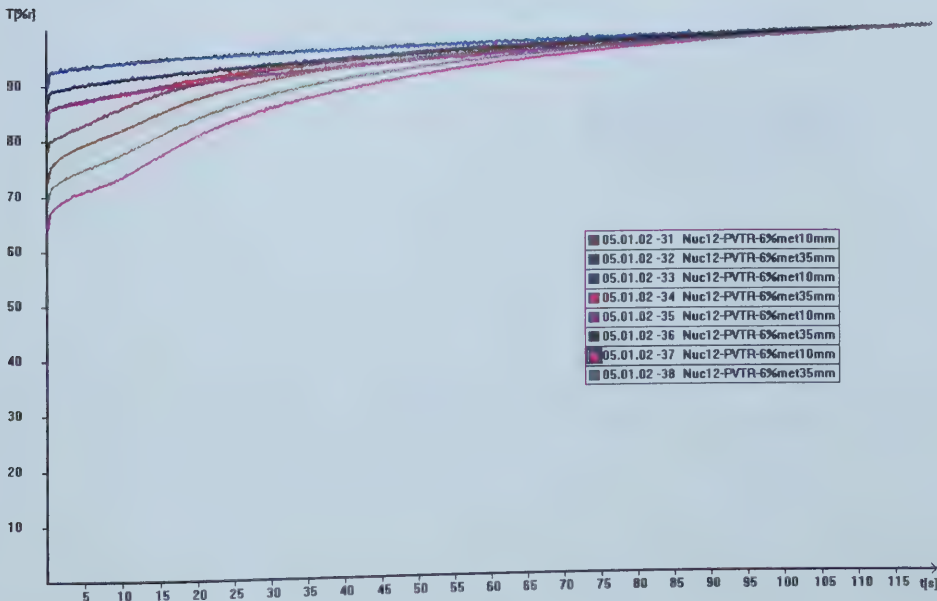


Figure F.3: Nuclepore® 12 micron - 20% methanol

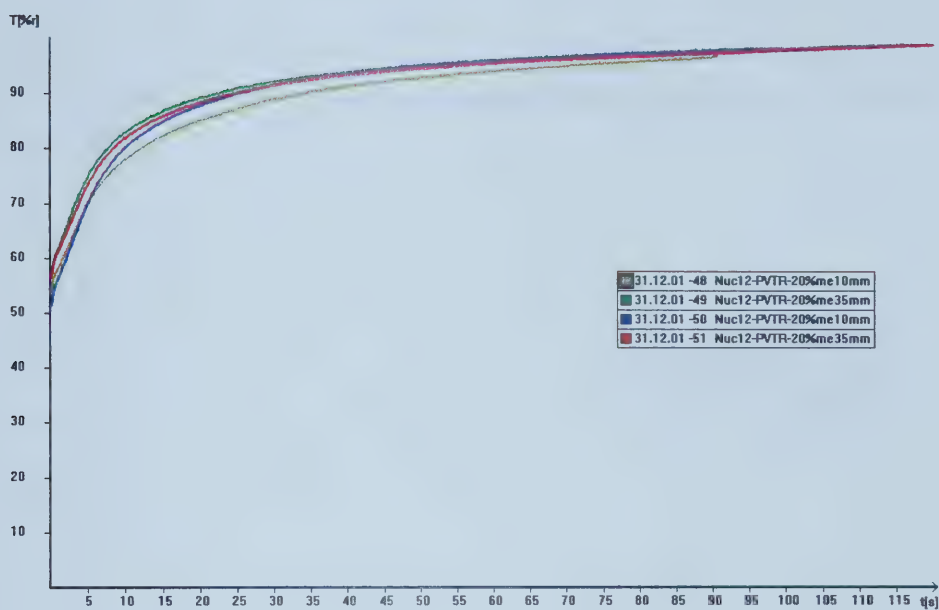


Figure F.4: Nuclepore® 12 micron - 40% methanol

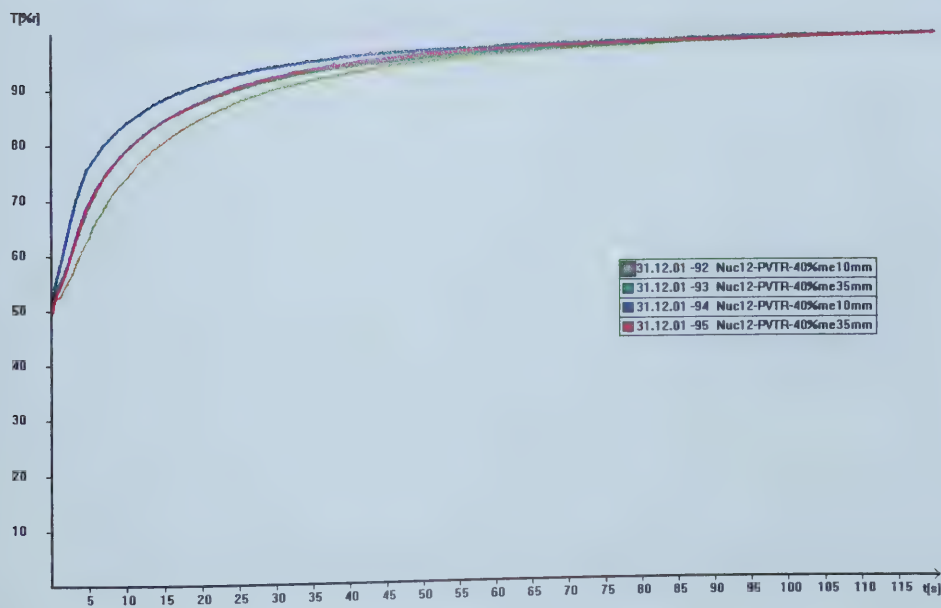


Figure F.5: Nuclepore® 12 micron - 70% methanol

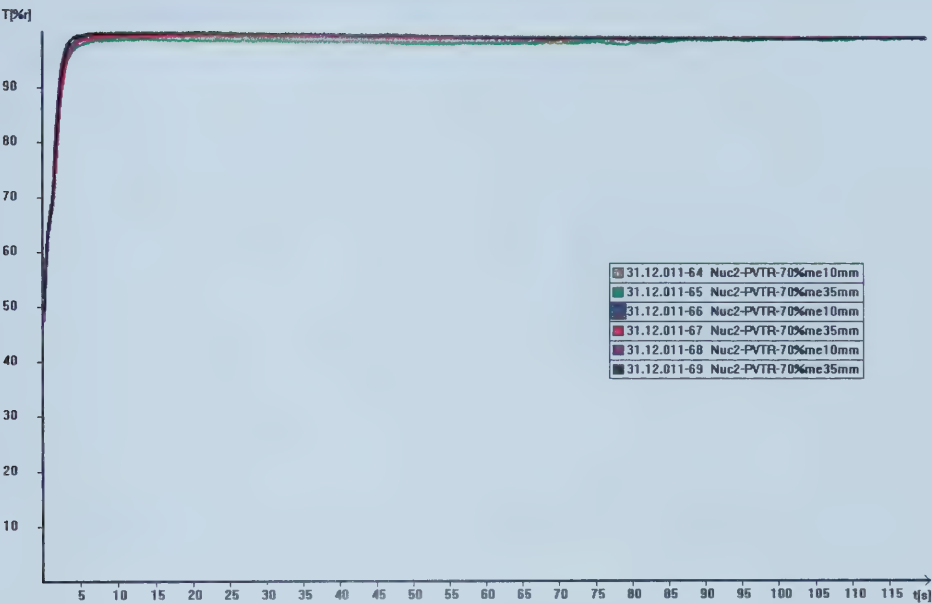


Figure F.6: Nuclepore® 12 micron - 100% methanol

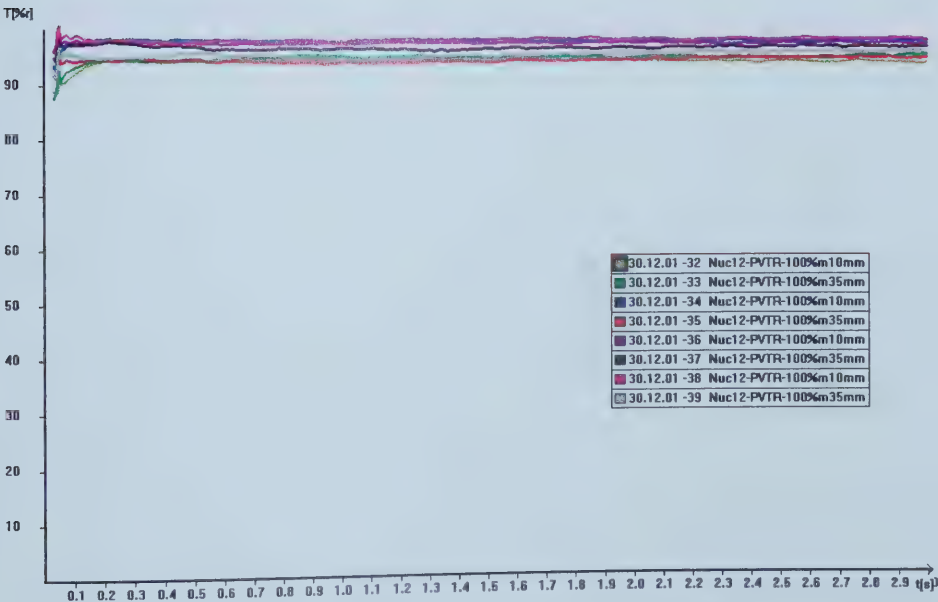


Figure F.7: Nuclepore® 8 micron - water

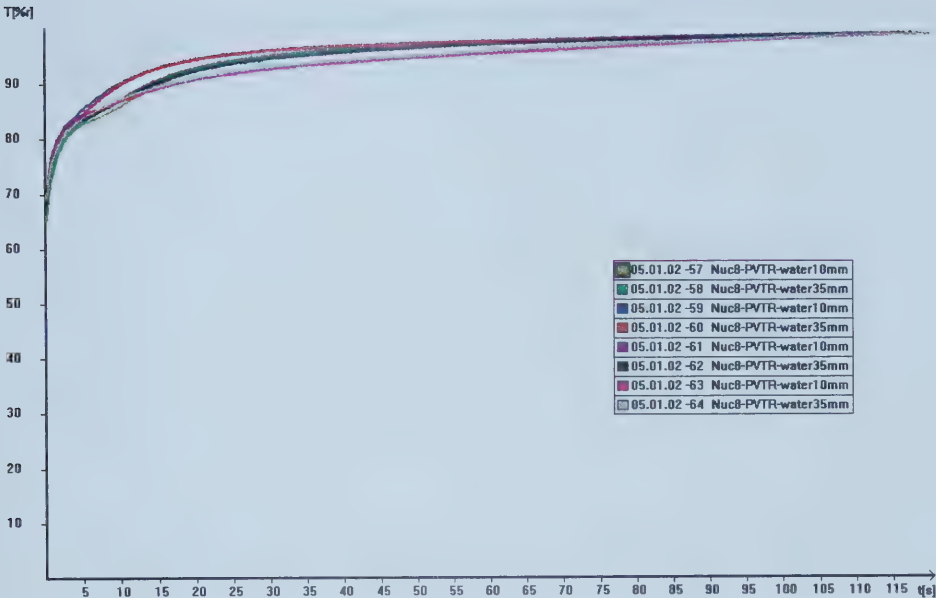


Figure F.8: Nuclepore® 8 micron - 6% methanol

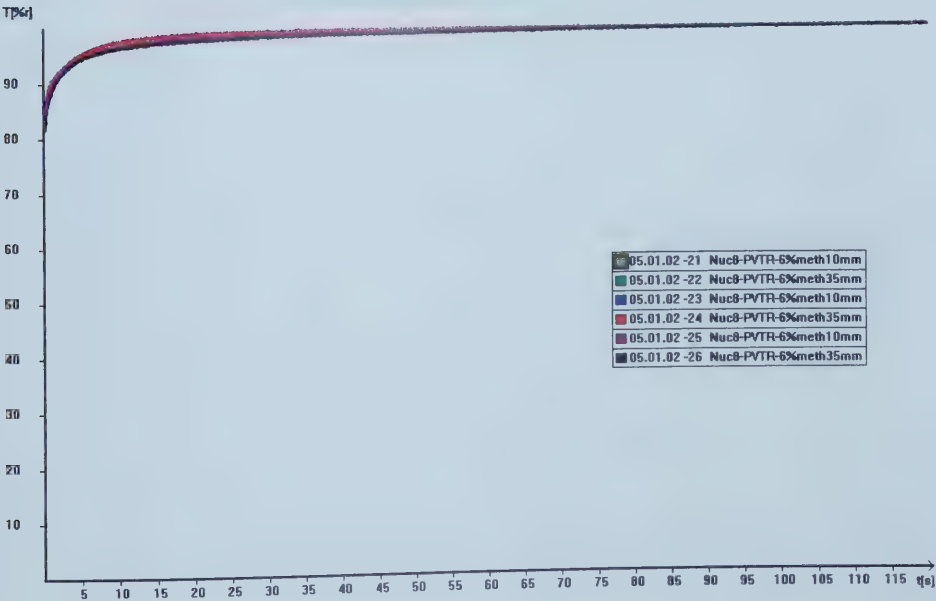


Figure F.9: Nuclepore® 8 micron - 20% methanol

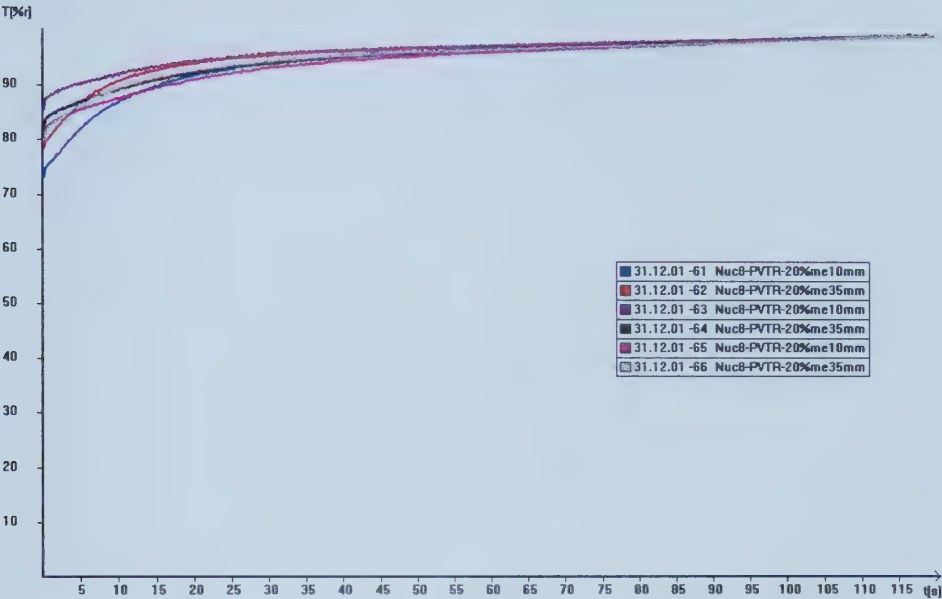


Figure F.10: Nuclepore® 8 micron - 40% methanol

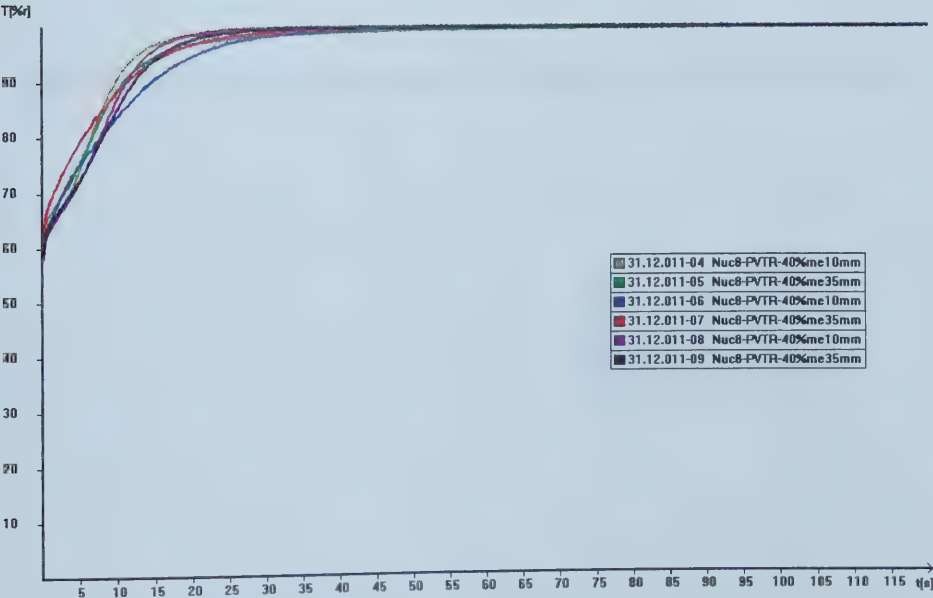


Figure F.11: Nuclepore® 8 micron - 70% methanol

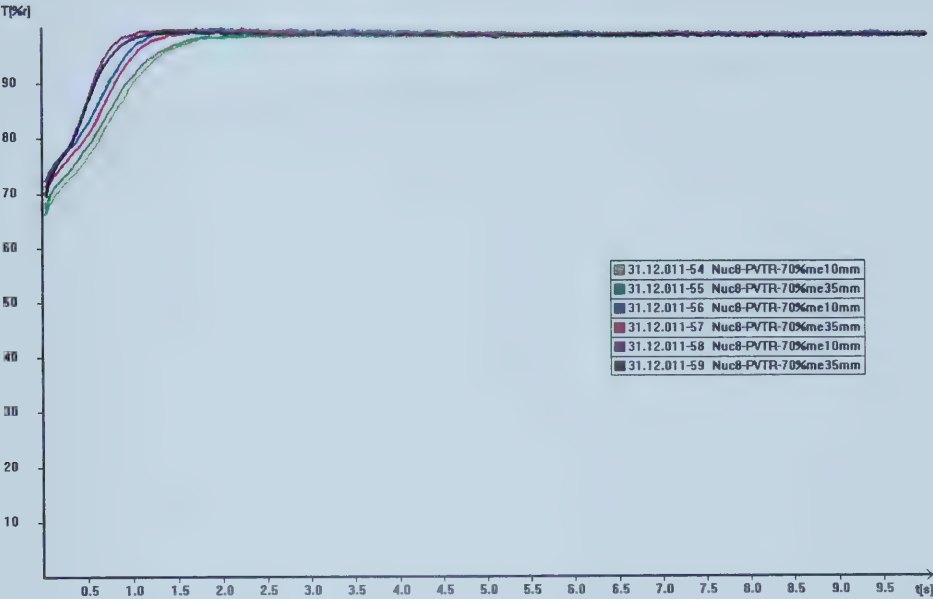


Figure F.12: Nuclepore® 8 micron - 100% methanol

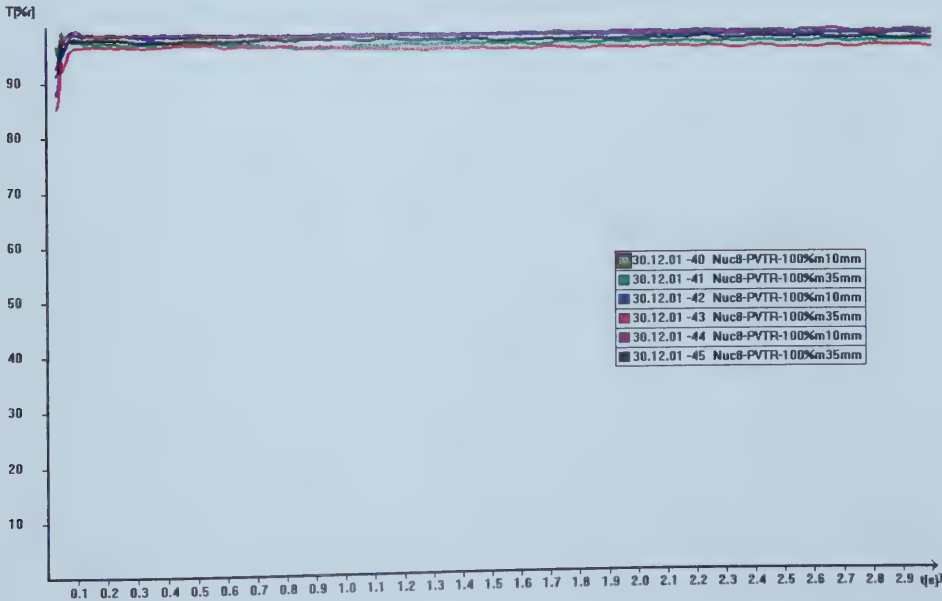


Figure F.13: Nuclepore® 5 micron - water

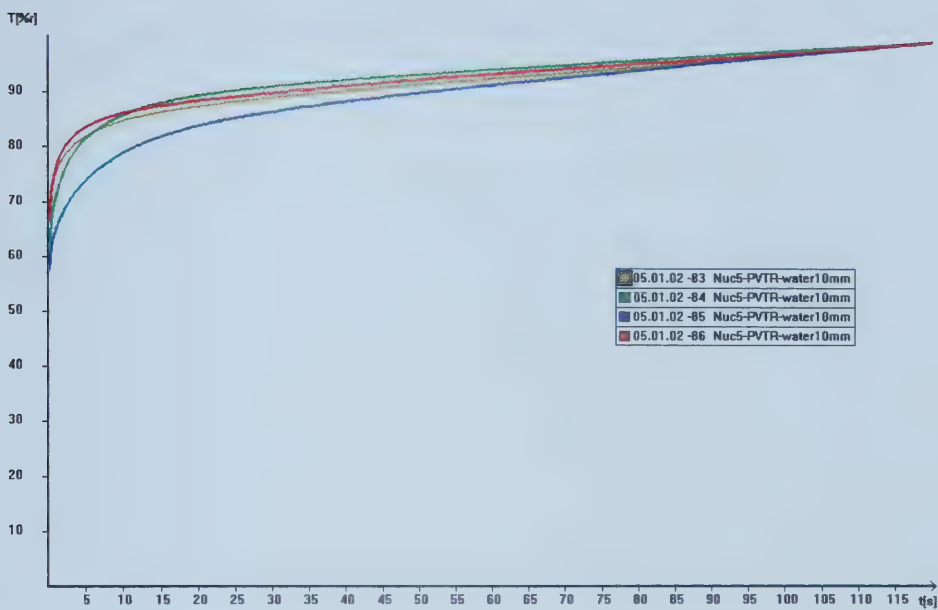


Figure F.14: Nuclepore® 5 micron - 6% methanol

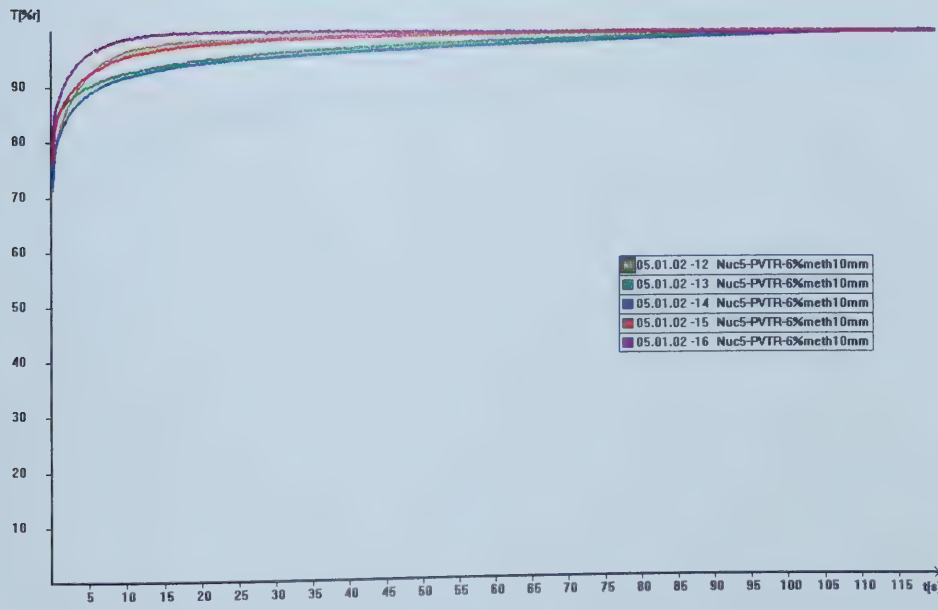


Figure F.15: Nuclepore® 5 micron - 20% methanol

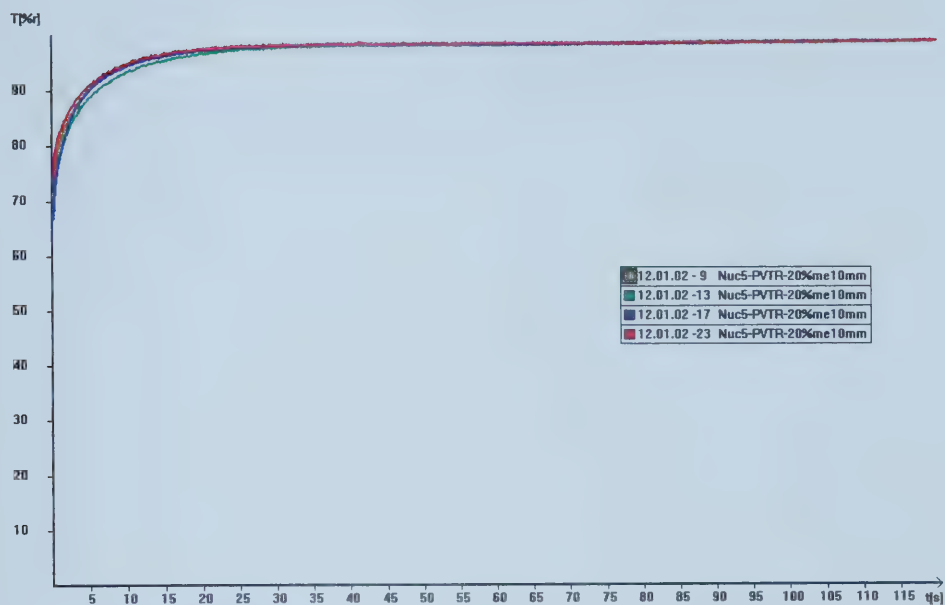


Figure F.16: Nuclepore® 5 micron - 40% methanol

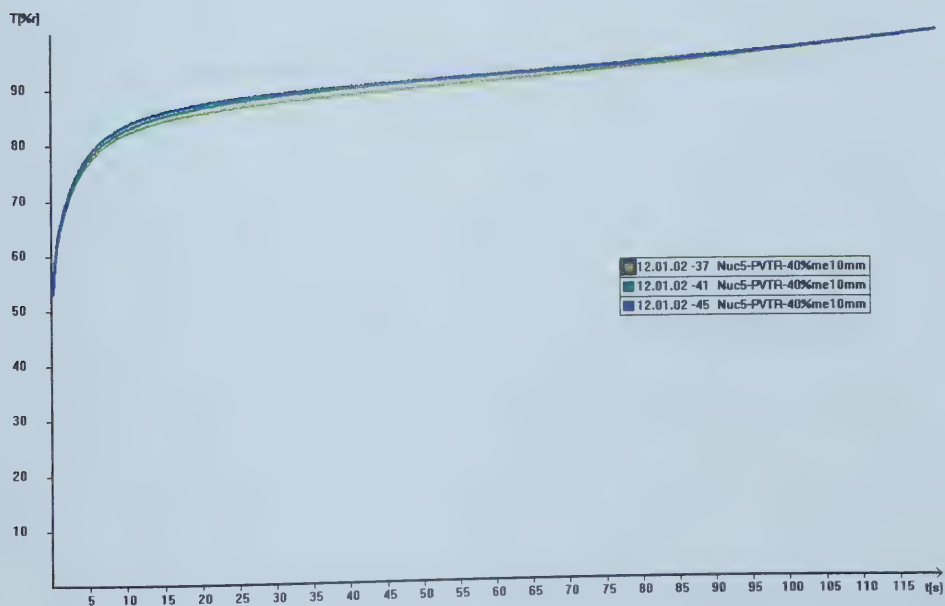


Figure F.17: Nuclepore® 5 micron - 70% methanol

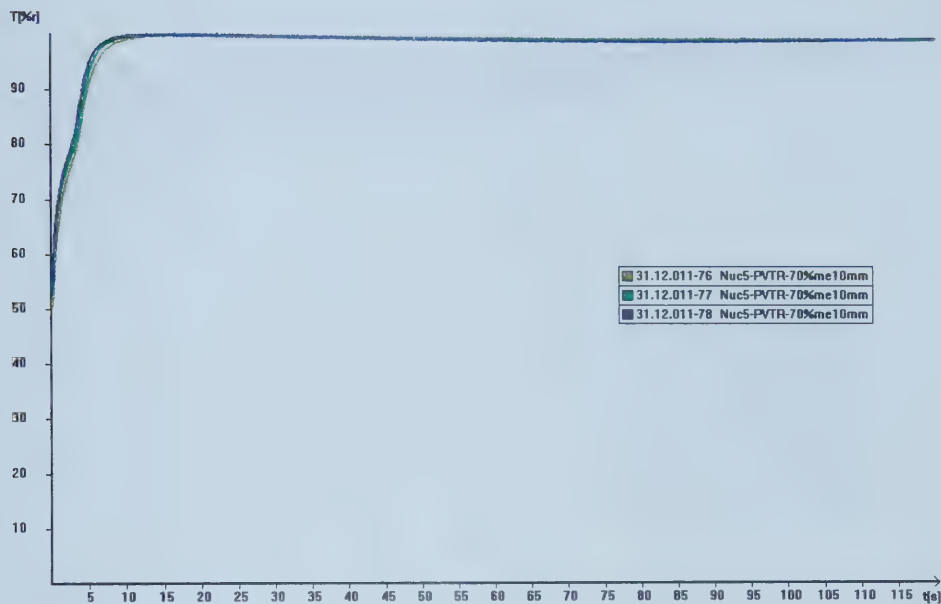


Figure F.18: Nuclepore® 5 micron - 100% methanol

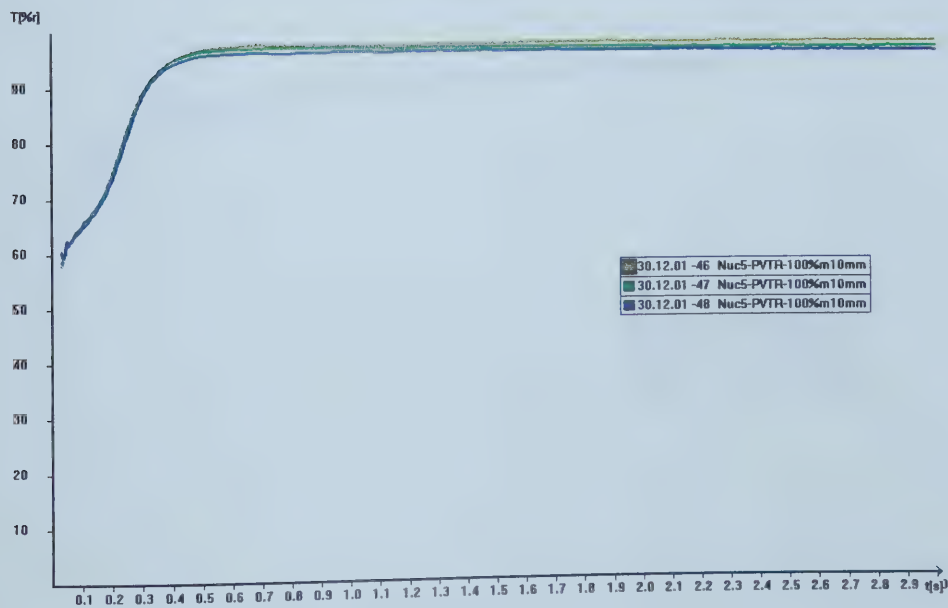


Figure F.19: Nuclepore® 2 micron - water

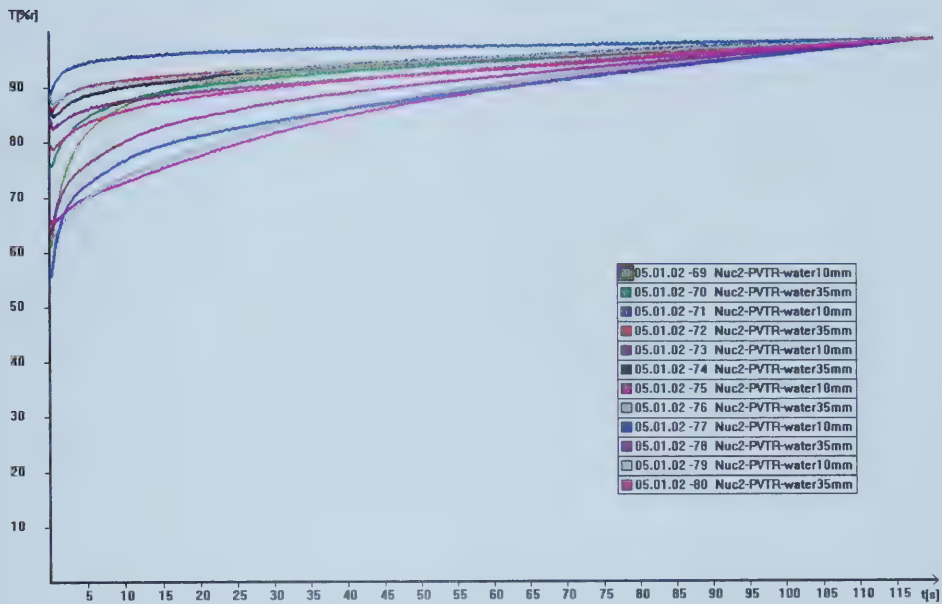


Figure F.20: Nuclepore® 2 micron - 6% methanol

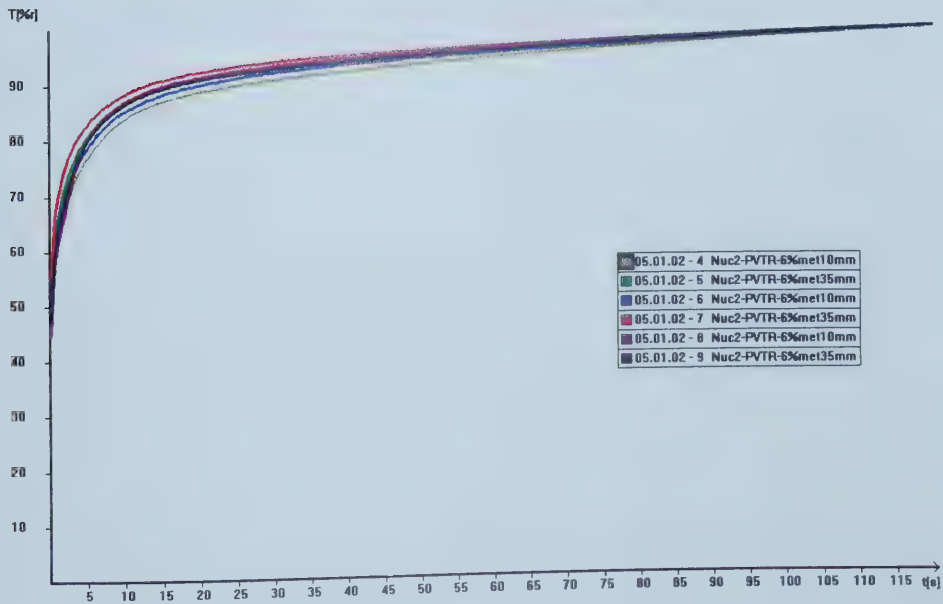


Figure F.21: Nuclepore® 2 micron - 20% methanol

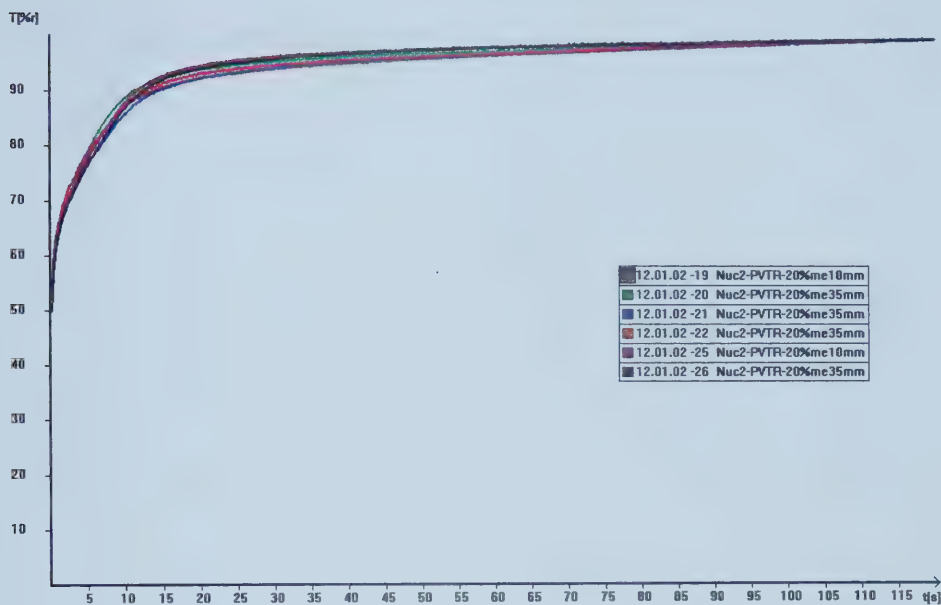


Figure F.22: Nuclepore® 2 micron - 40% methanol

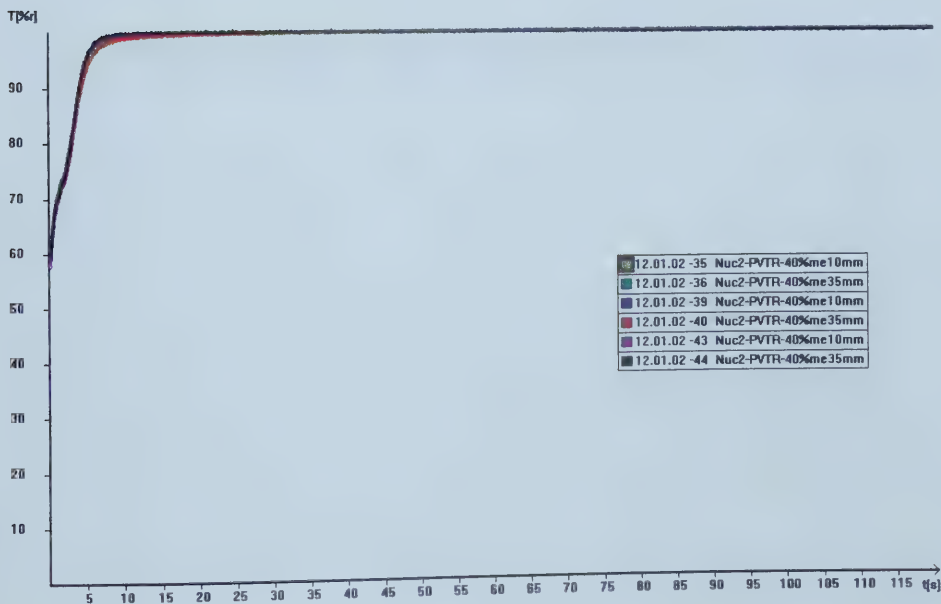


Figure F.23: Nuclepore® 2 micron - 70% methanol

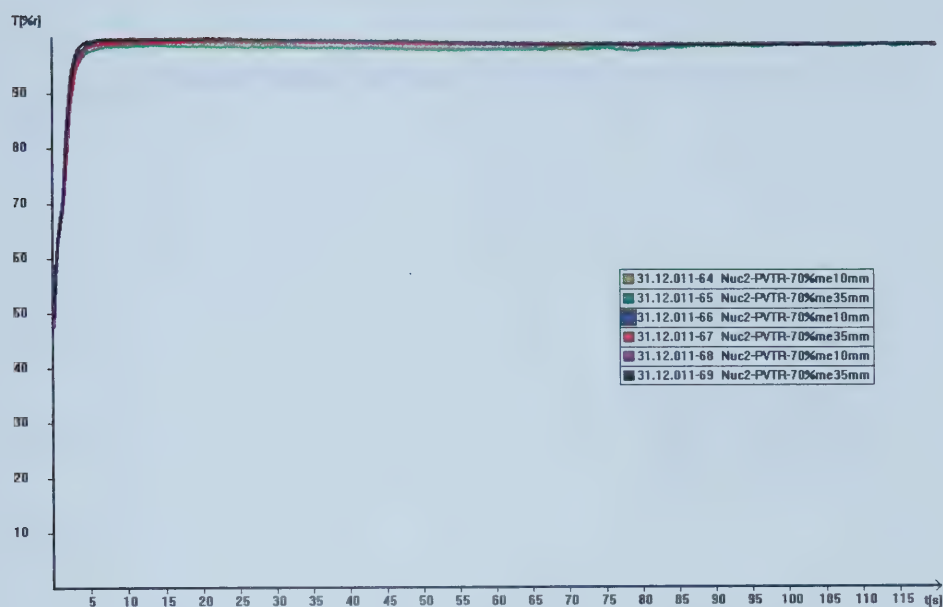


Figure F.24: Nuclepore® 2 micron - 100% methanol

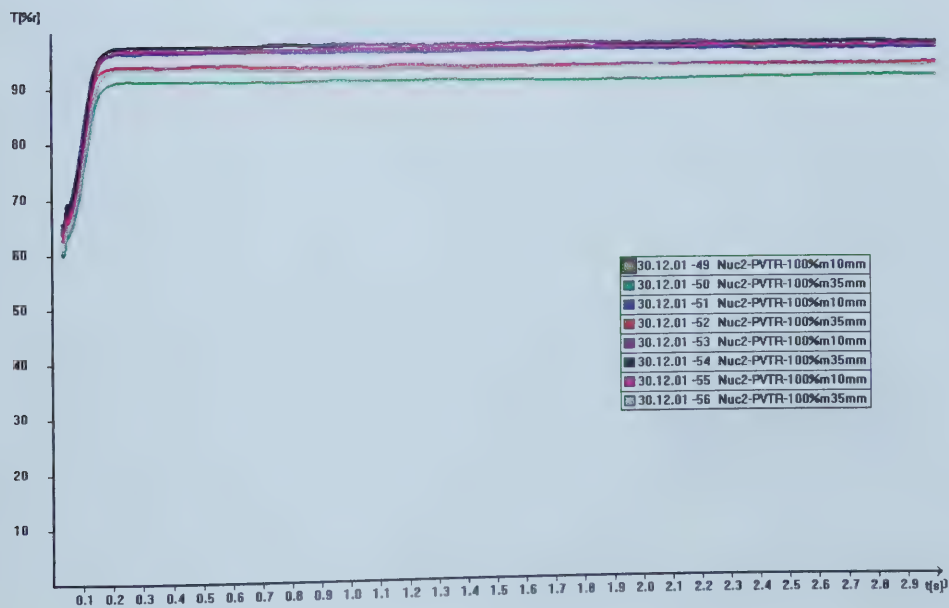


Figure F.25: Spectra F - water

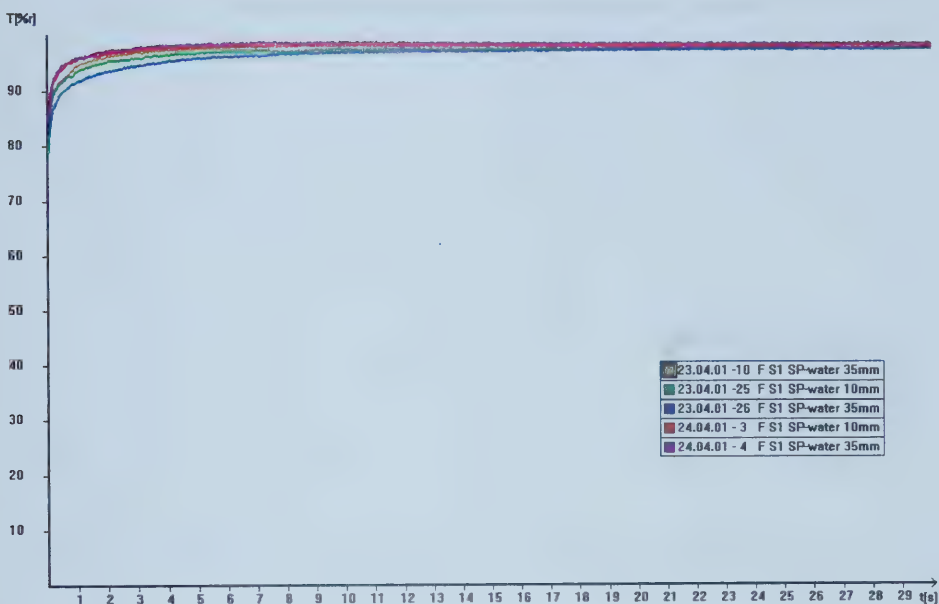


Figure F.26: Spectra F - 6% methanol

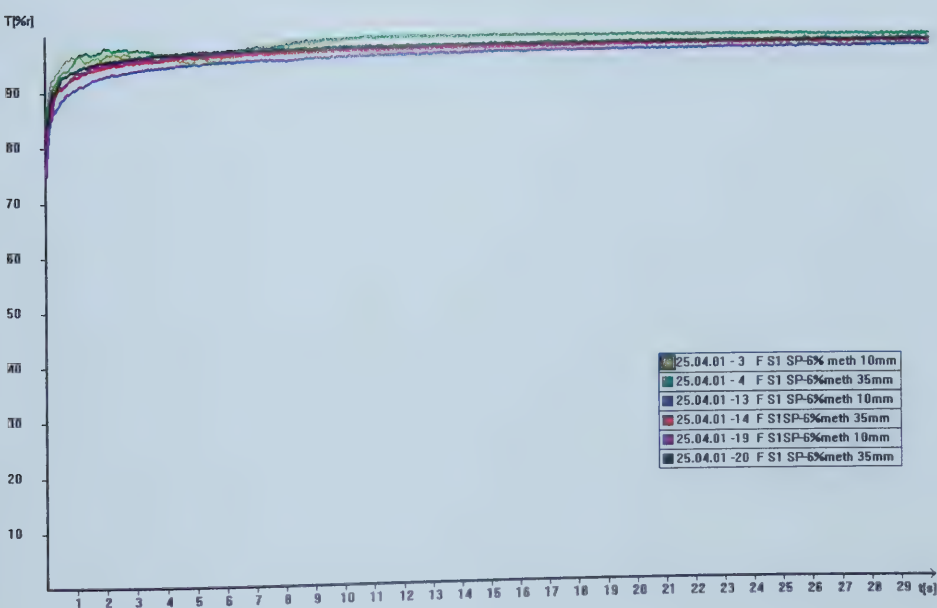


Figure F.27: Spectra F - 20% methanol

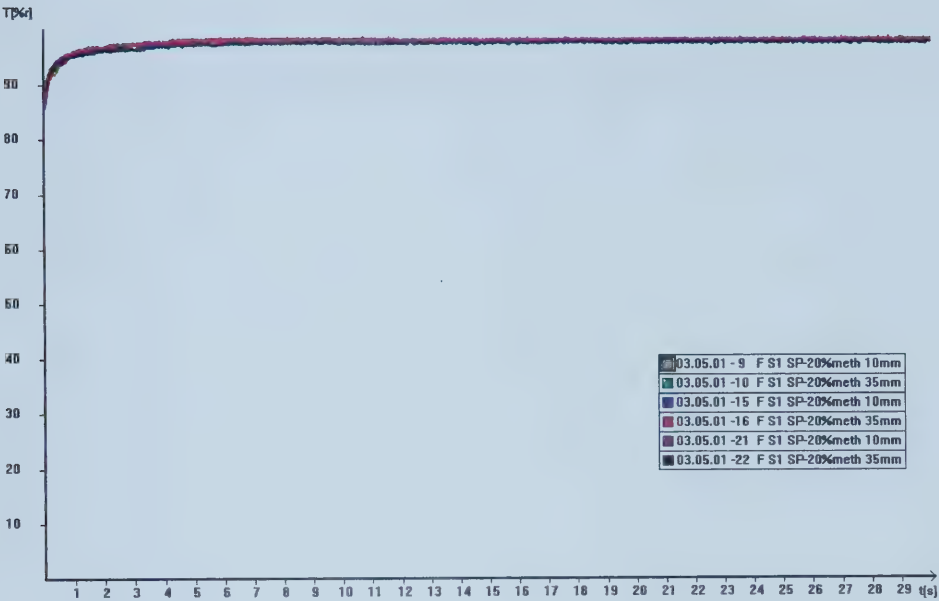


Figure F.28: Spectra F - 40% methanol

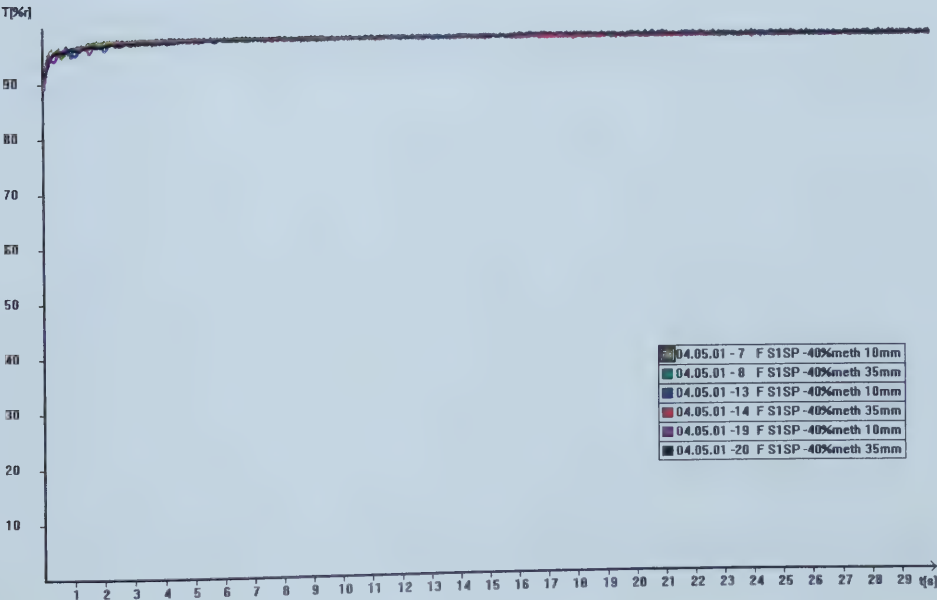


Figure F.29: Spectra F - 70% methanol

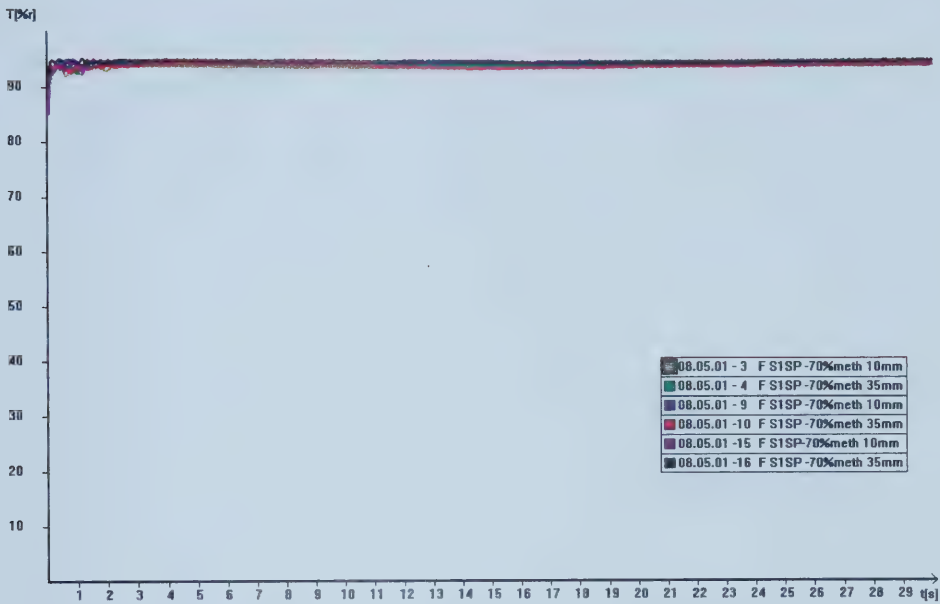


Figure F.30: Spectra F - 100% methanol

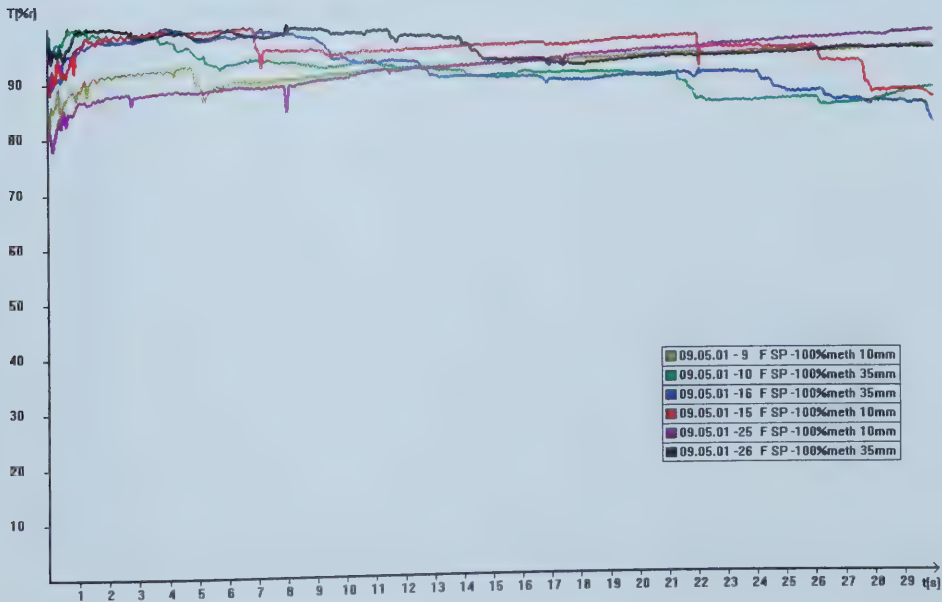


Figure F.31: Spectra Q - water

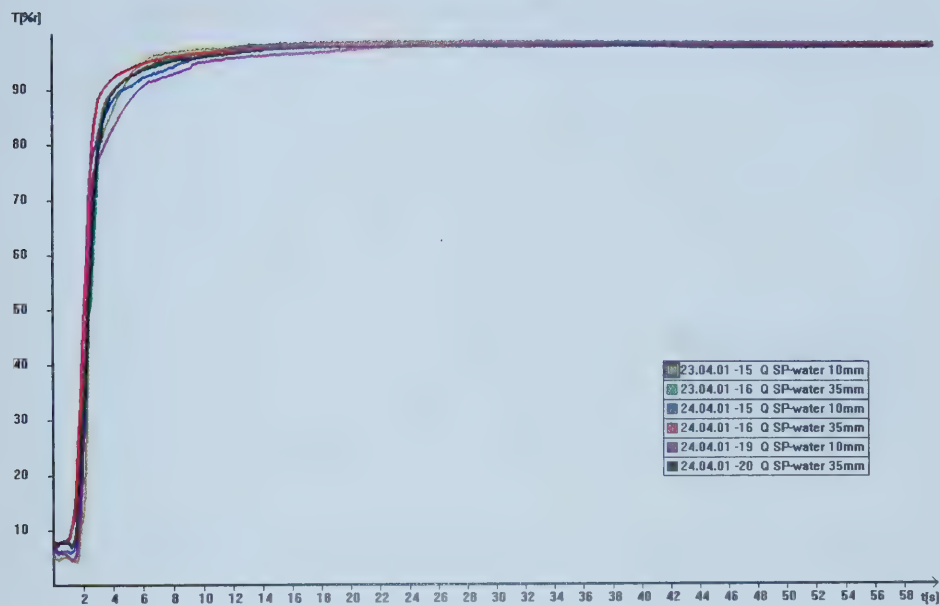


Figure F.32: Spectra Q - 6% methanol

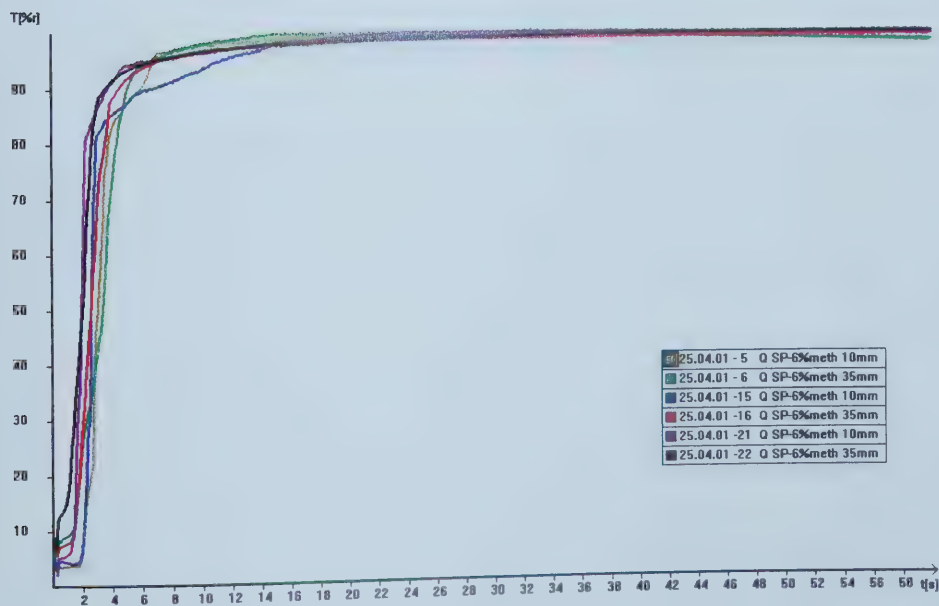


Figure F.33: Spectra Q - 20% methanol

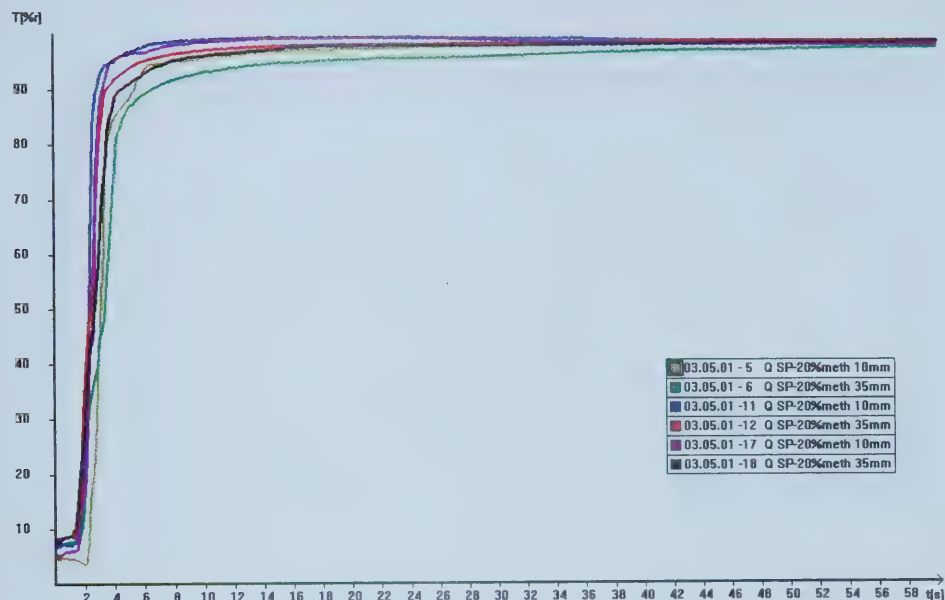


Figure F.34: Spectra Q - 40% methanol

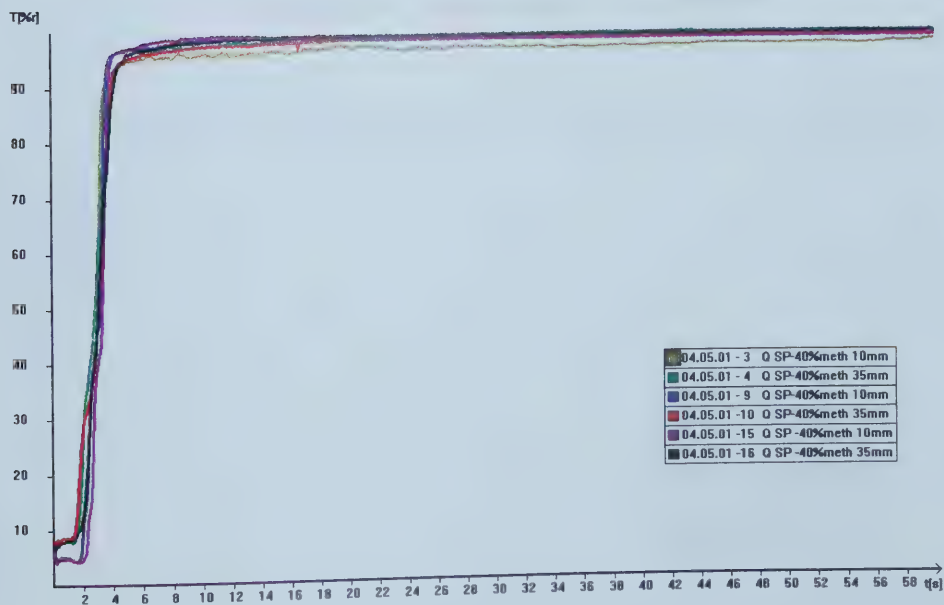


Figure F.35: Spectra Q - 70% methanol

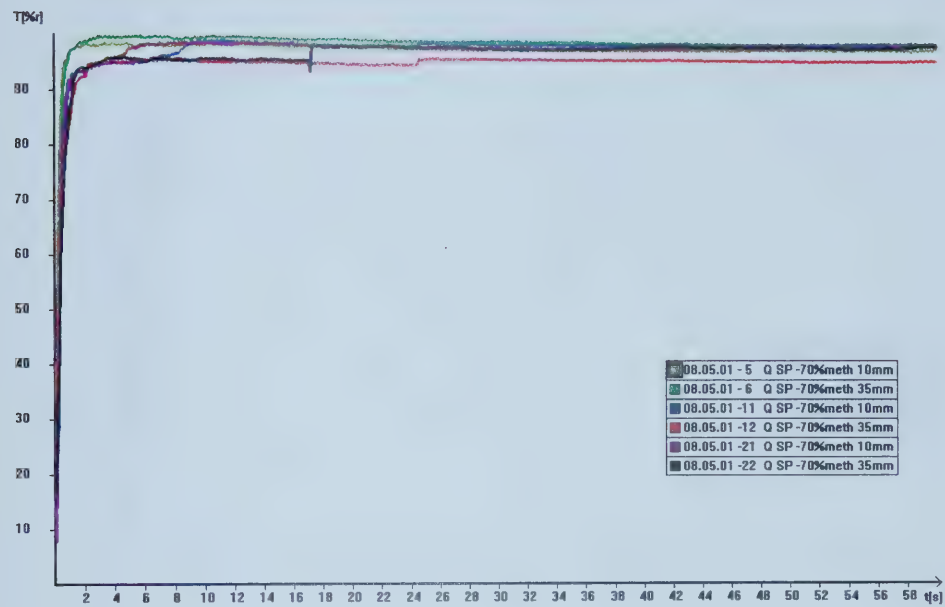


Figure F.36: Spectra Q - 100% methanol

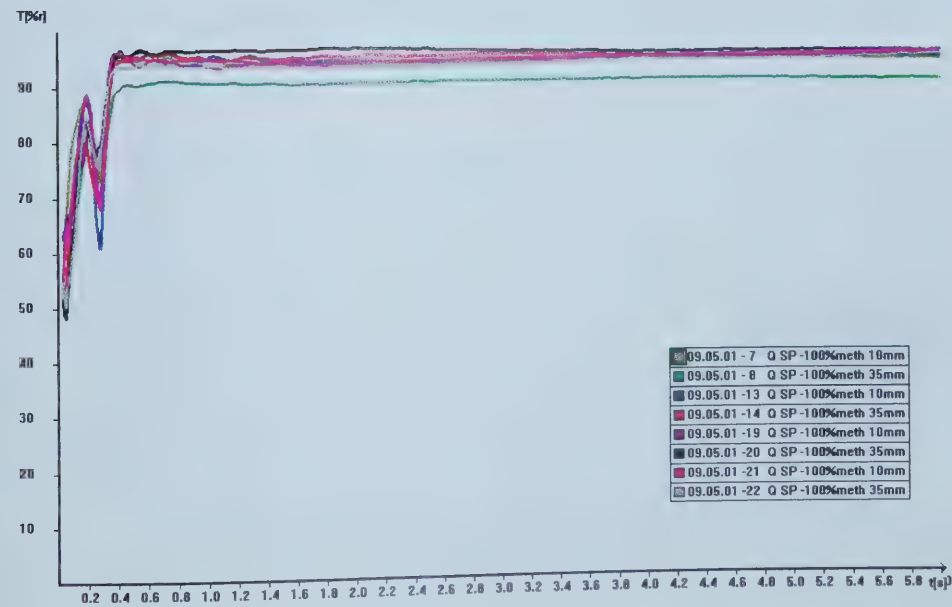


Figure F.37: Spectra T - water

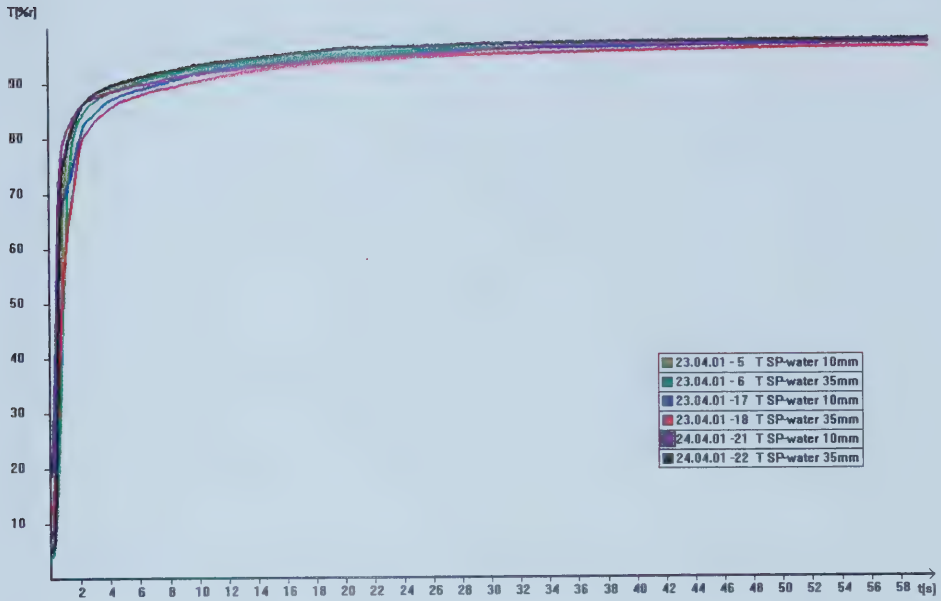


Figure F.38: Spectra T - 6% methanol

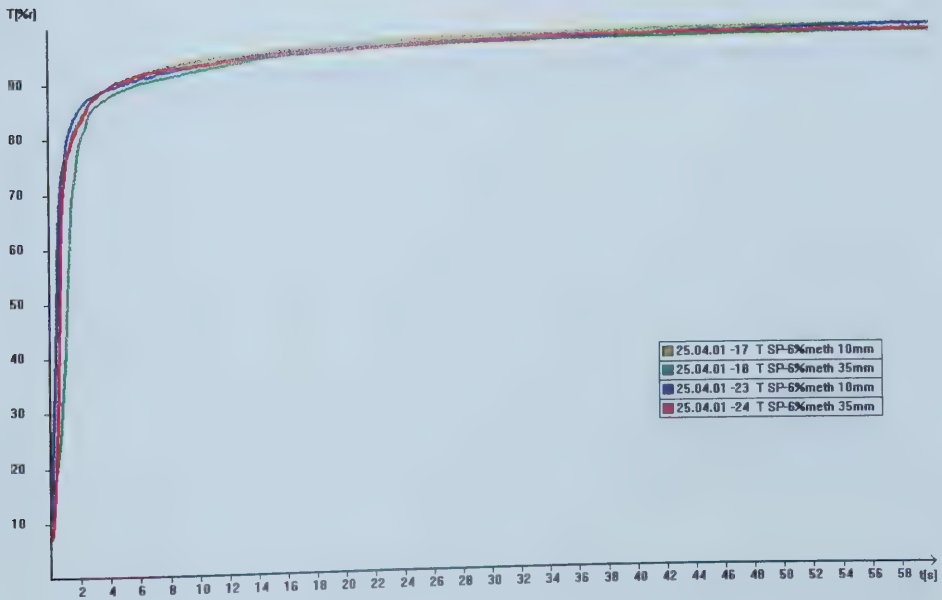


Figure F.39: Spectra T - 20% methanol

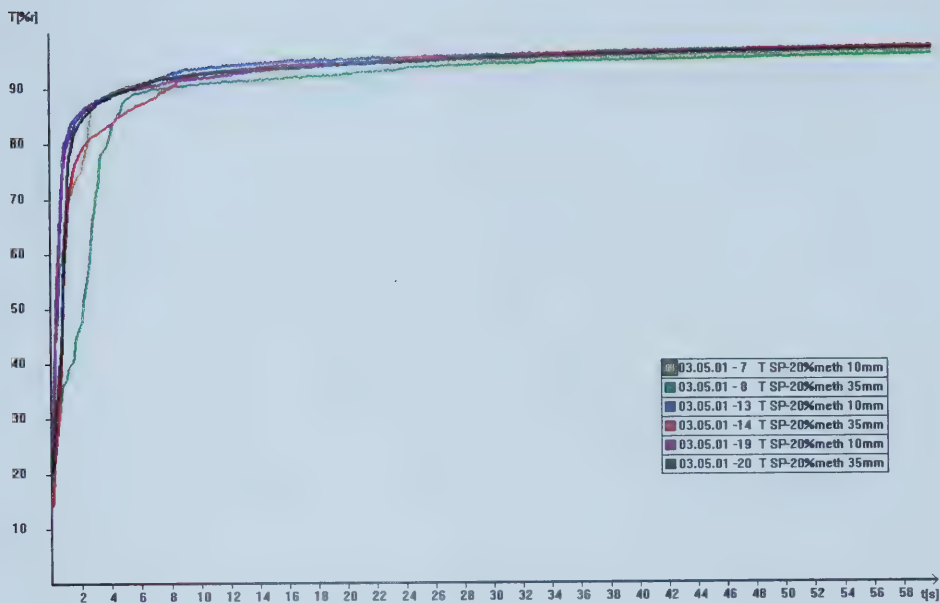


Figure F.40: Spectra T - 40% methanol

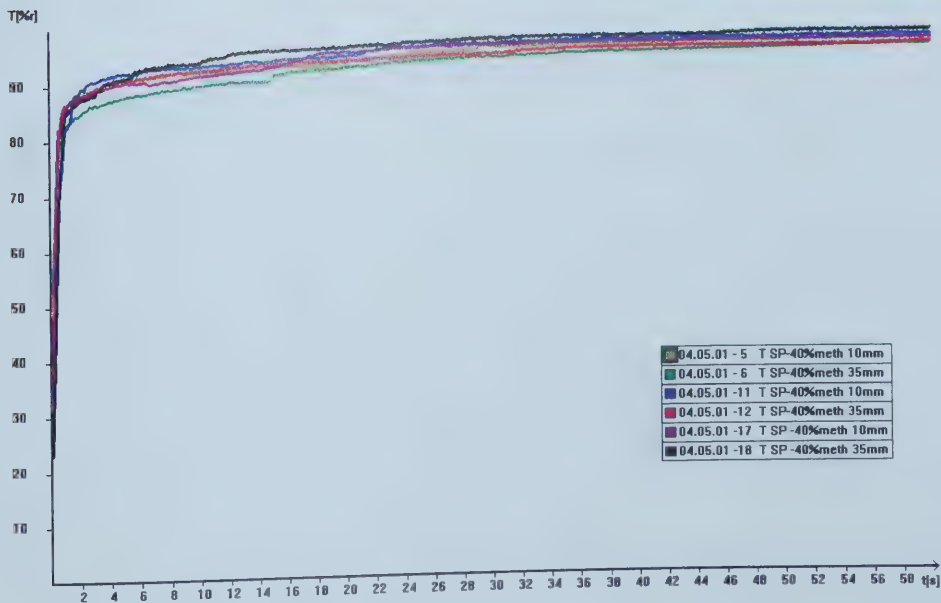


Figure F.41: Spectra T - 70% methanol

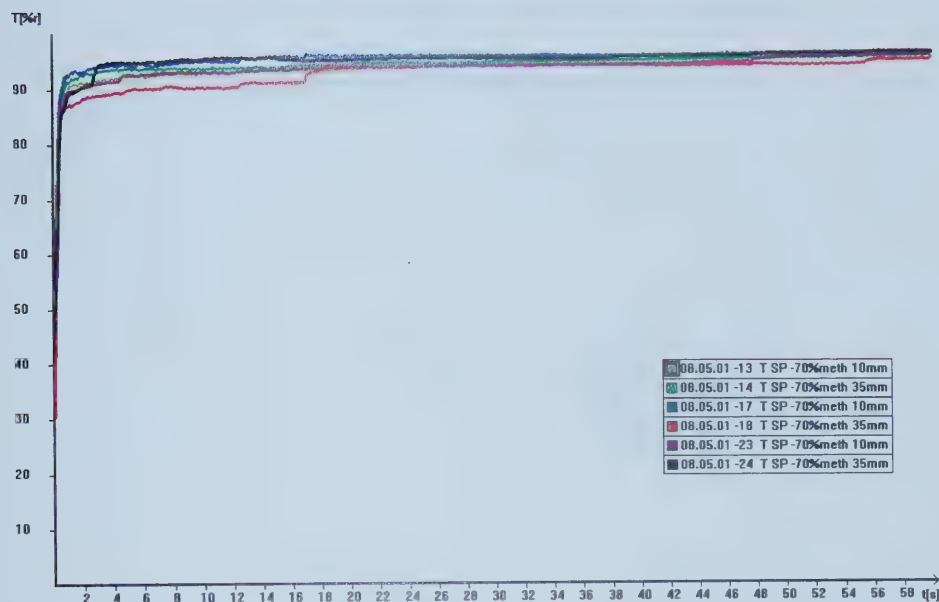


Figure F.42: Spectra T - 100% methanol

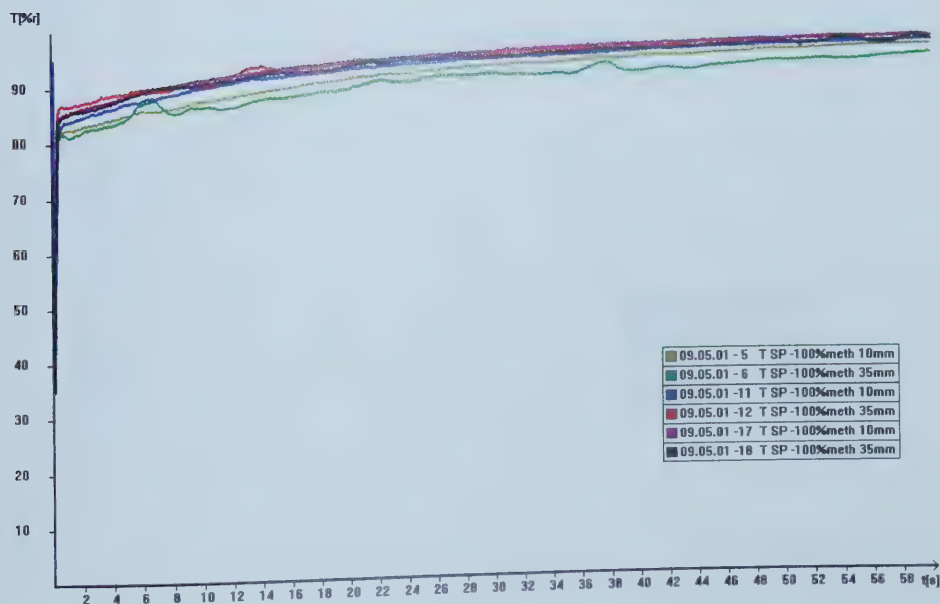


Figure F.43: Voith 1 - 2 sides - water Long time

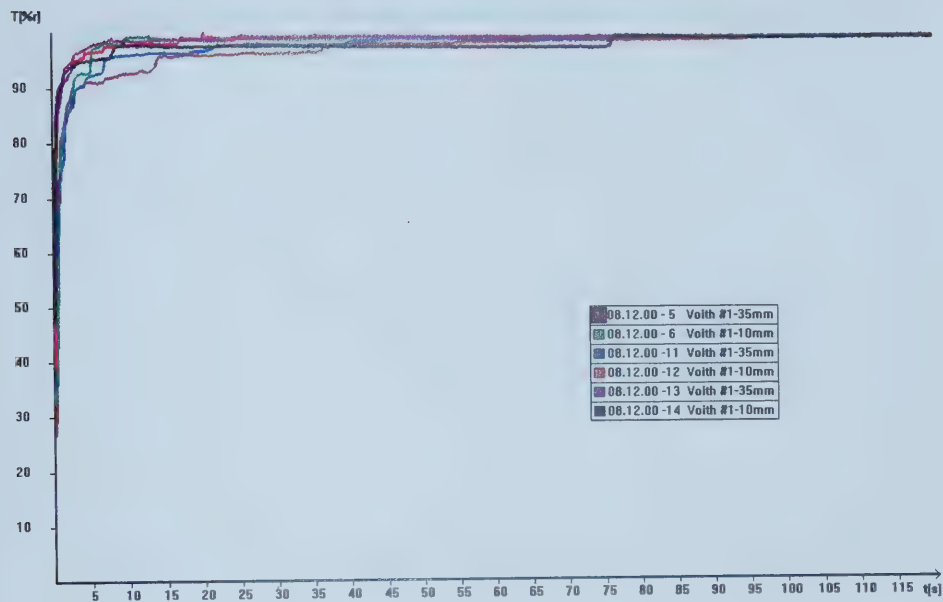


Figure F.44: Voith 1 - 2 sides - water- short time

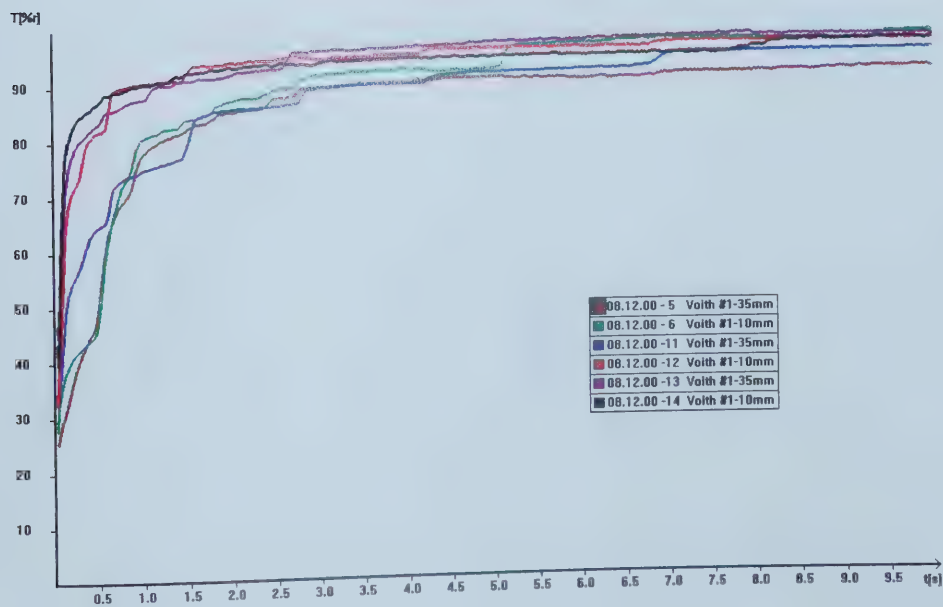


Figure F.45: Voith 1 - 1 sides - water - Long time

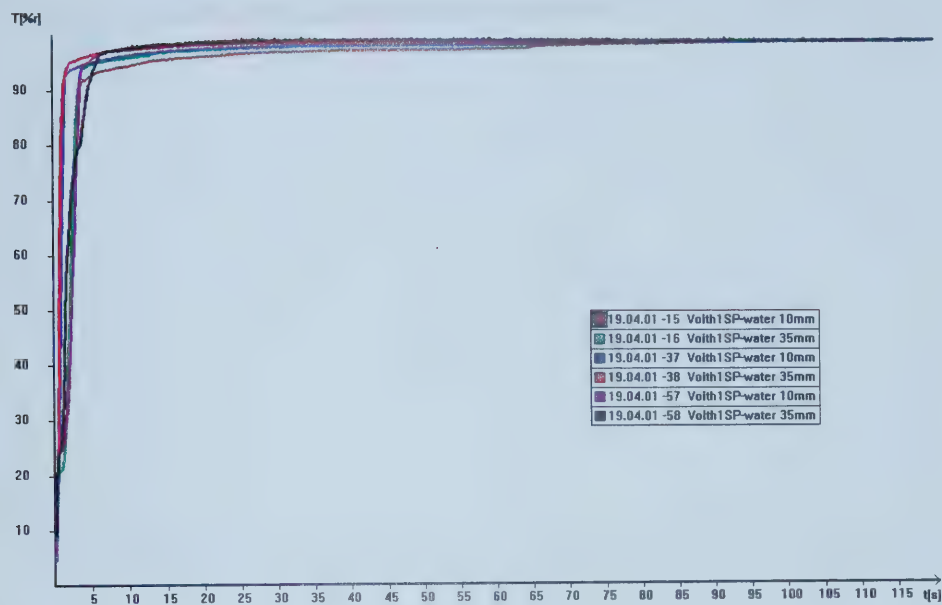


Figure F.46: Voith 1 - 1 side - water- short time

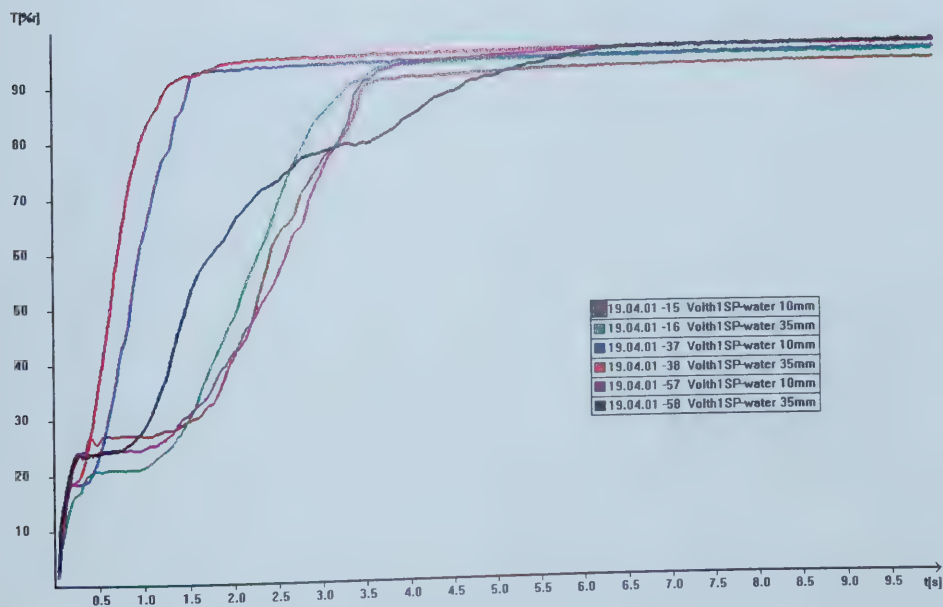


Figure F.47: Voith 2 - 2 sides - water - long time

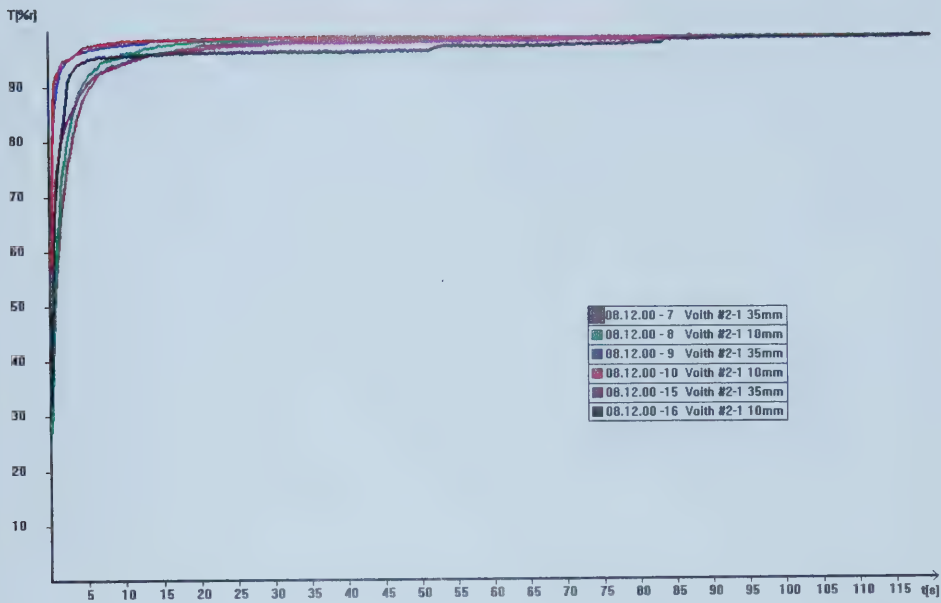


Figure F.48: Voith 2 - 2 side - water-short time

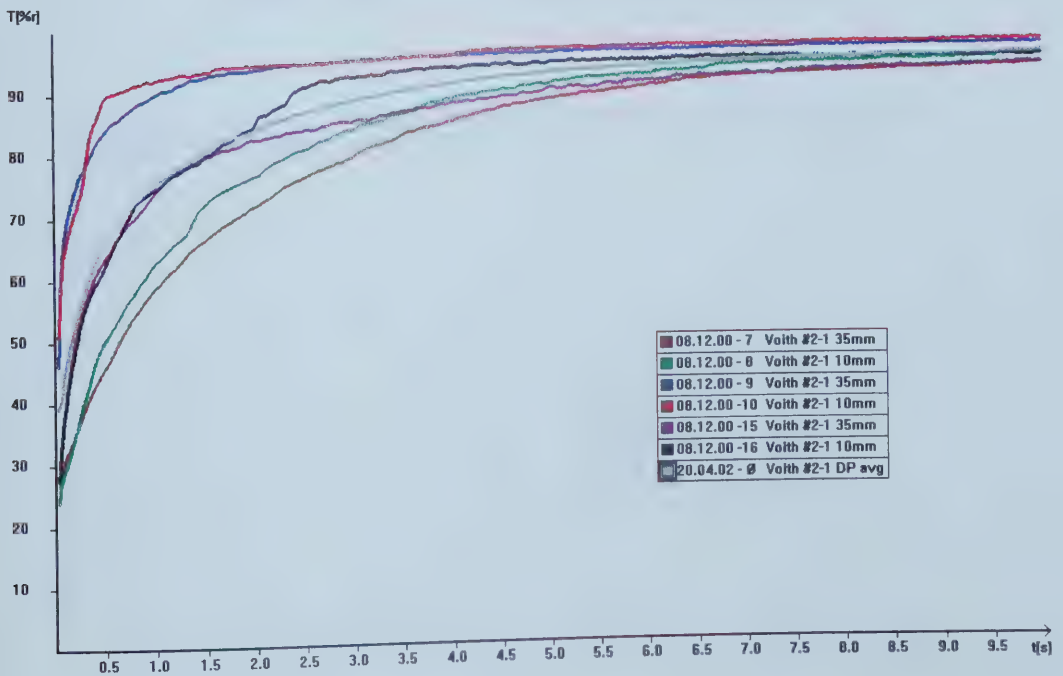


Figure F.49: Voith 2-1 - 1 side - water - long time

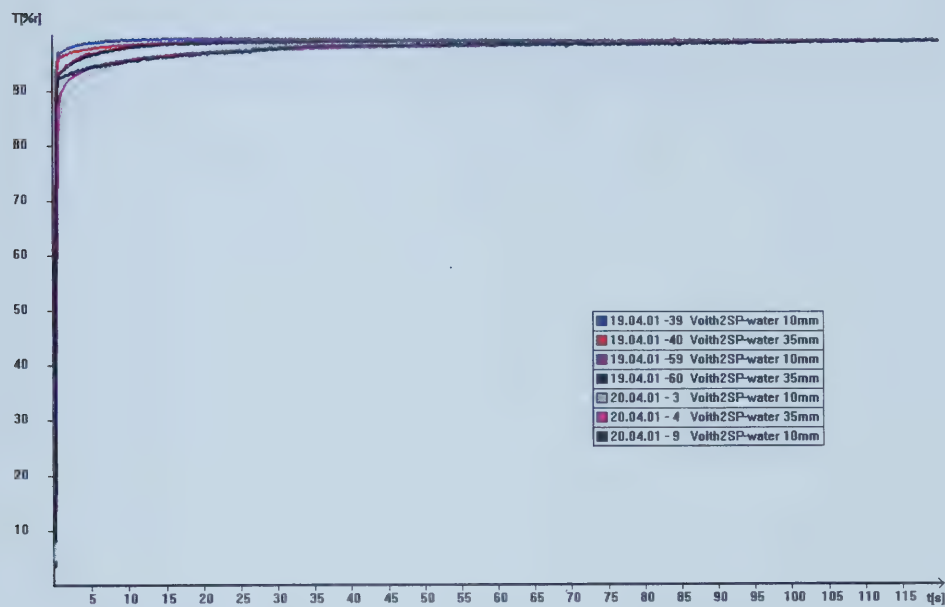


Figure F.50: Voith 2-1 - 1 side - water - short time

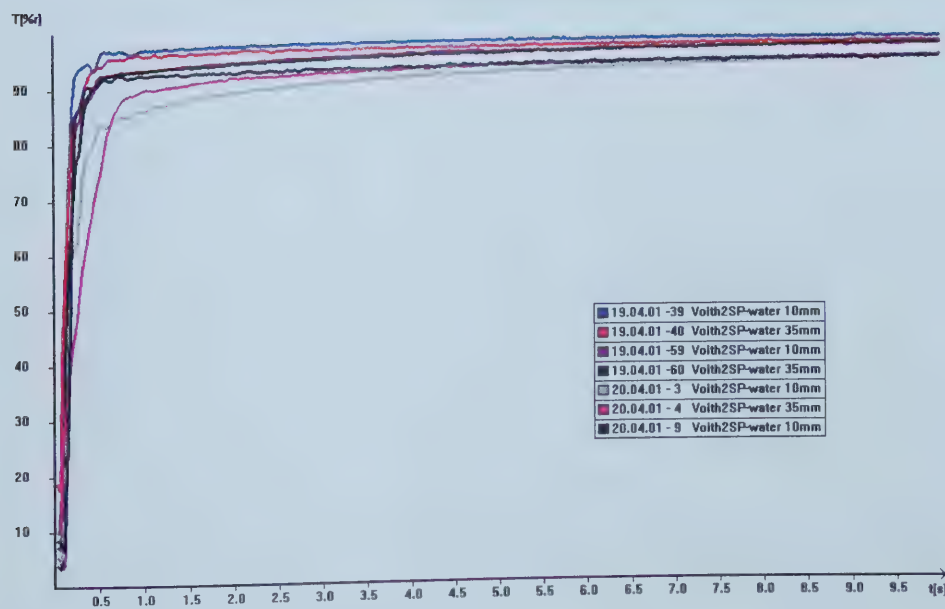


Figure F.51: Voith 2-2 - 1 sides - water - long time

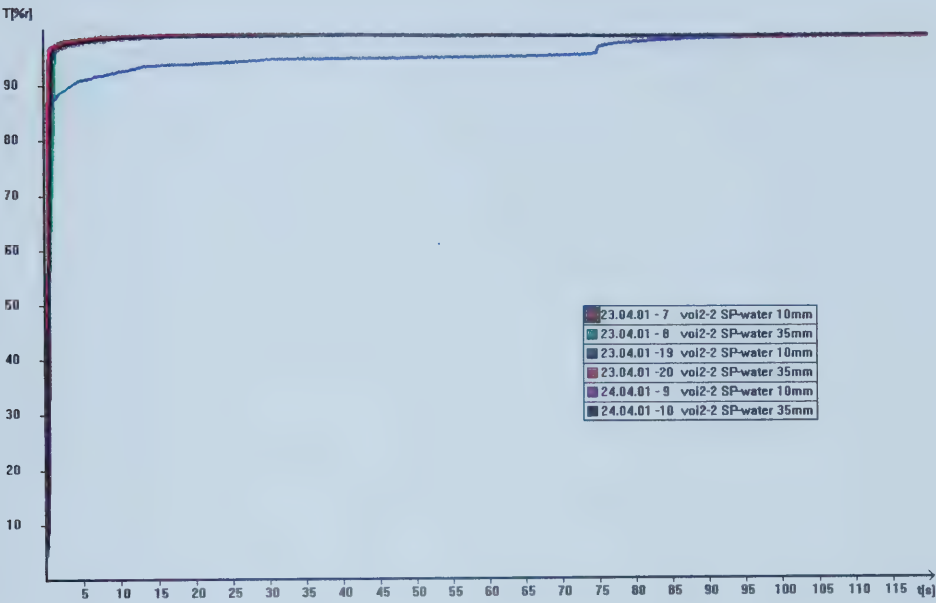


Figure F.52: Voith 2-2 - 1 sides - water - short time

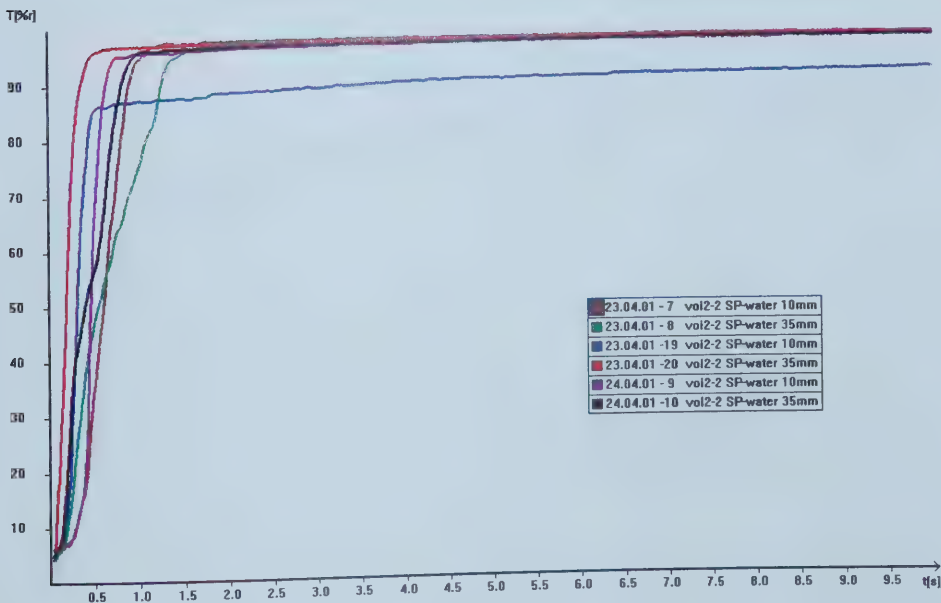


Figure F.53: Voith 3 - 2 sides - water - long time

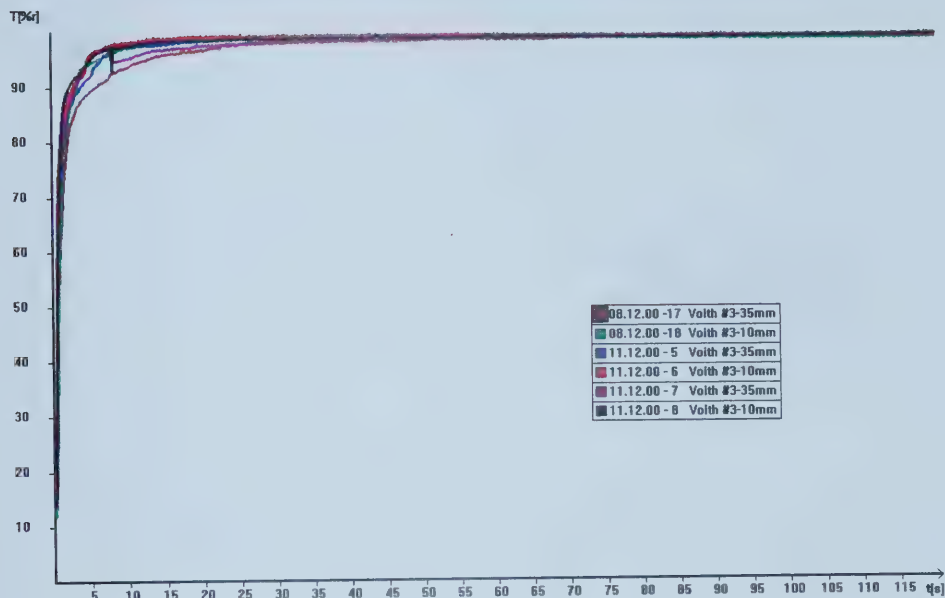


Figure F.54: Voith 3 - 2 sides - water - short time

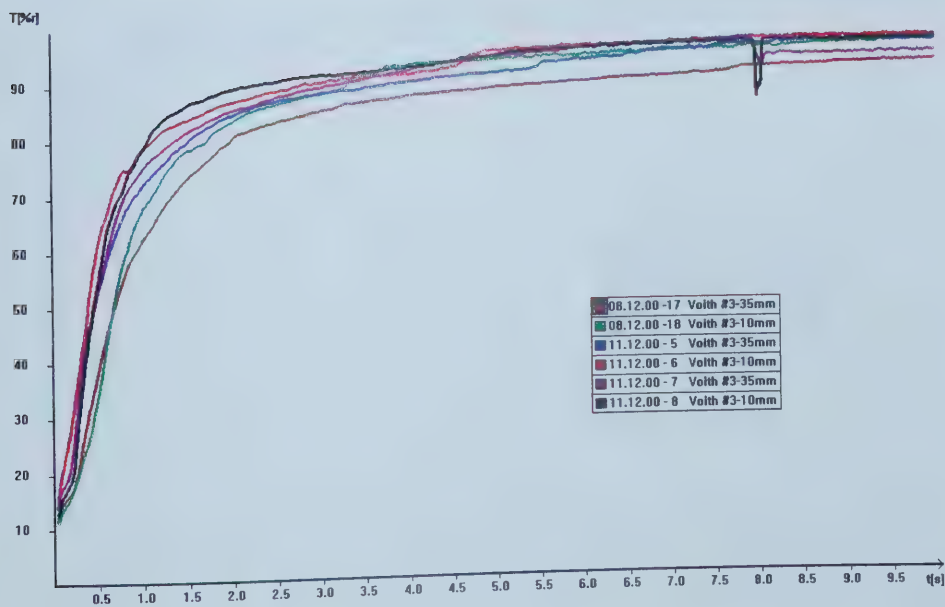


Figure F.55: Voith 3 - 1 sides - water - long time

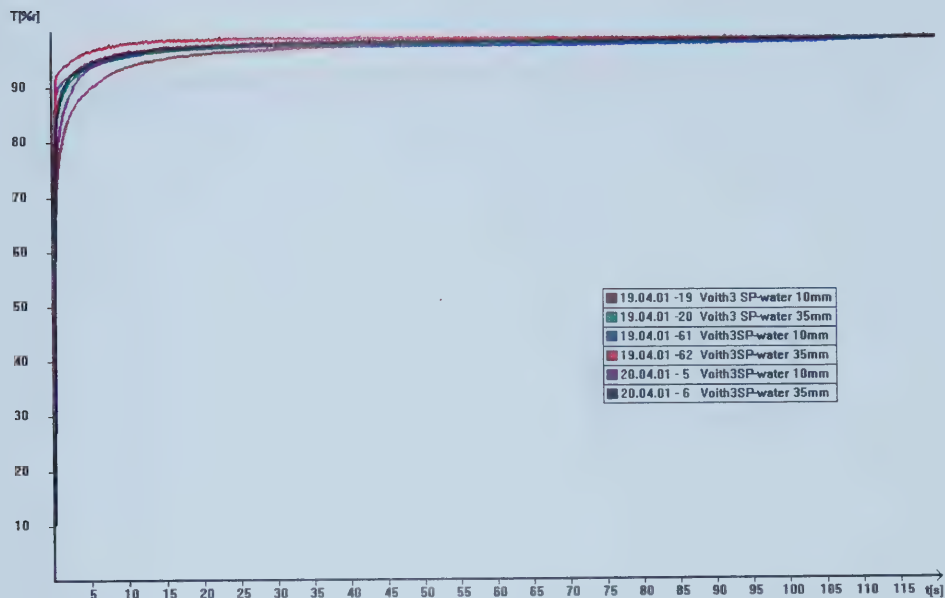


Figure F.56: Voith 3 - 1 sides - water - short time

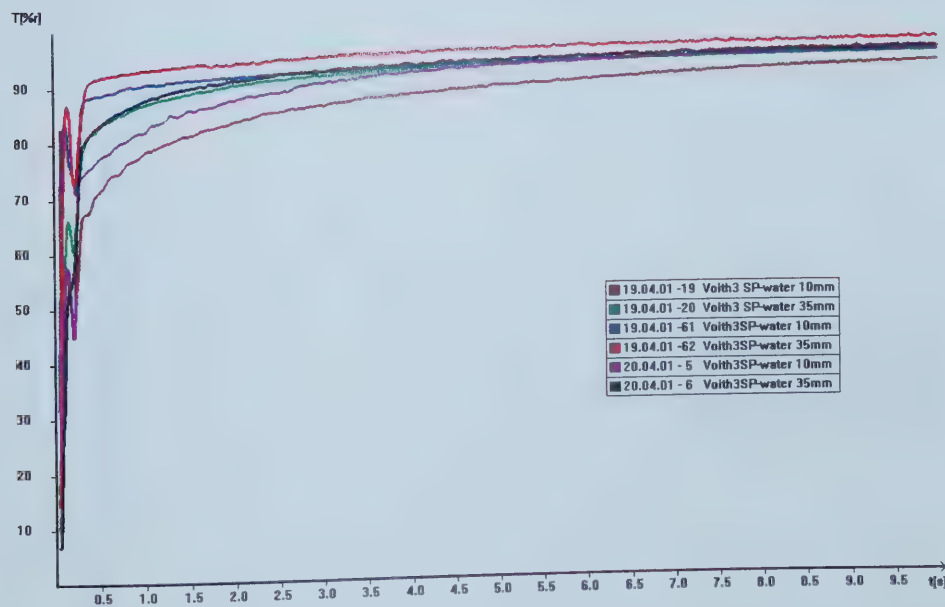


Figure F.57: Voith 3 - 2 sides - water - long time

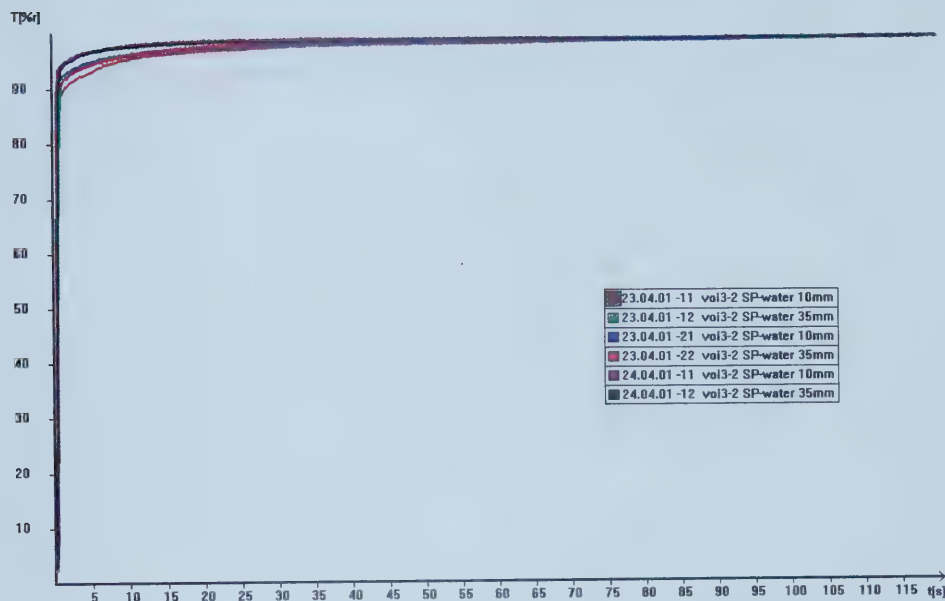


Figure F.58: Voith 3 - 2 sides - water - short time

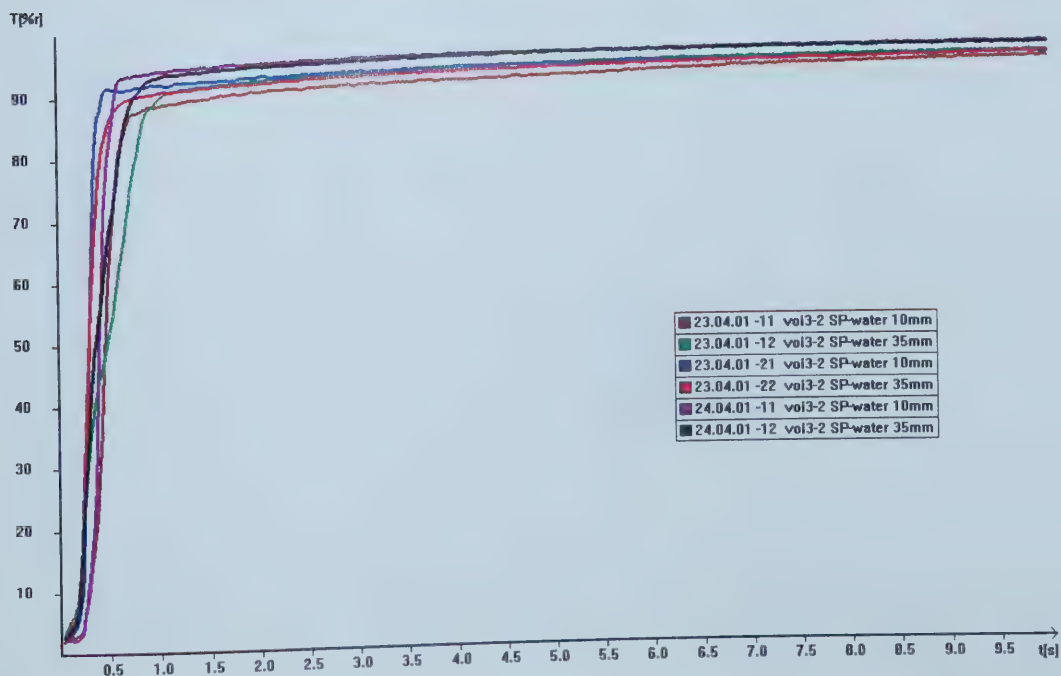


Figure F.59: Voith 4 - 2 sides - water - long time

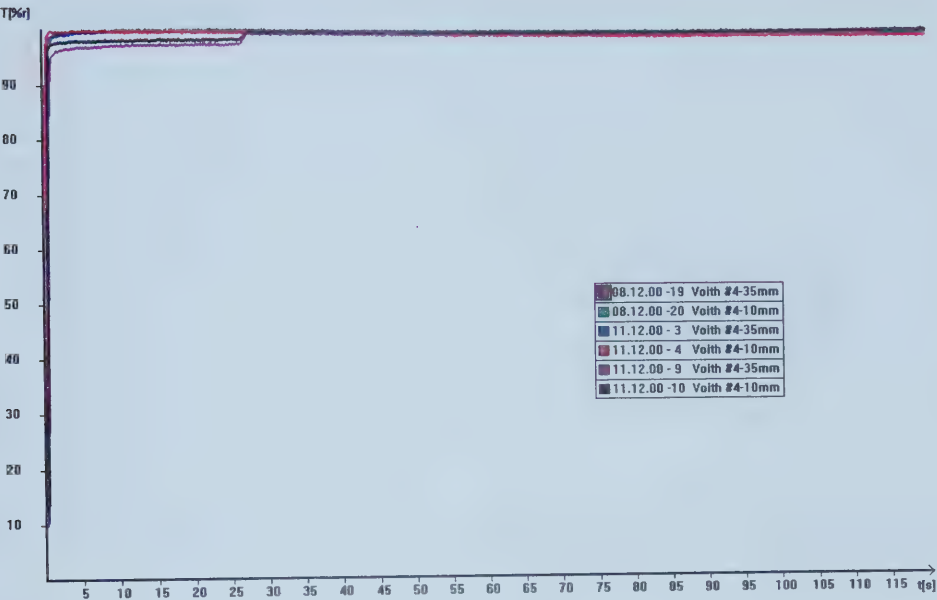


Figure F.60: Voith 4 - 2 sides - water - short time

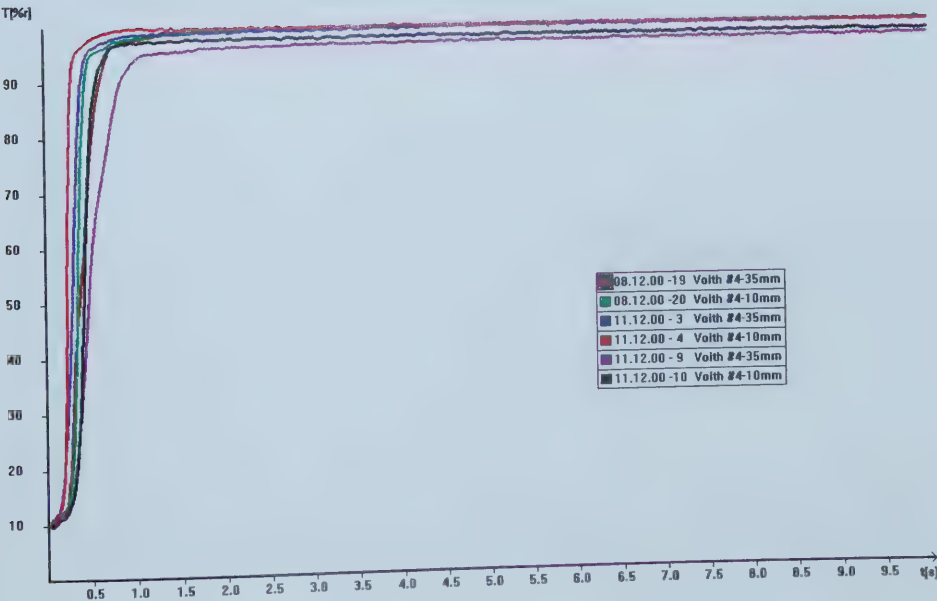


Figure F.61: Voith 4 - 1 sides - water - long time

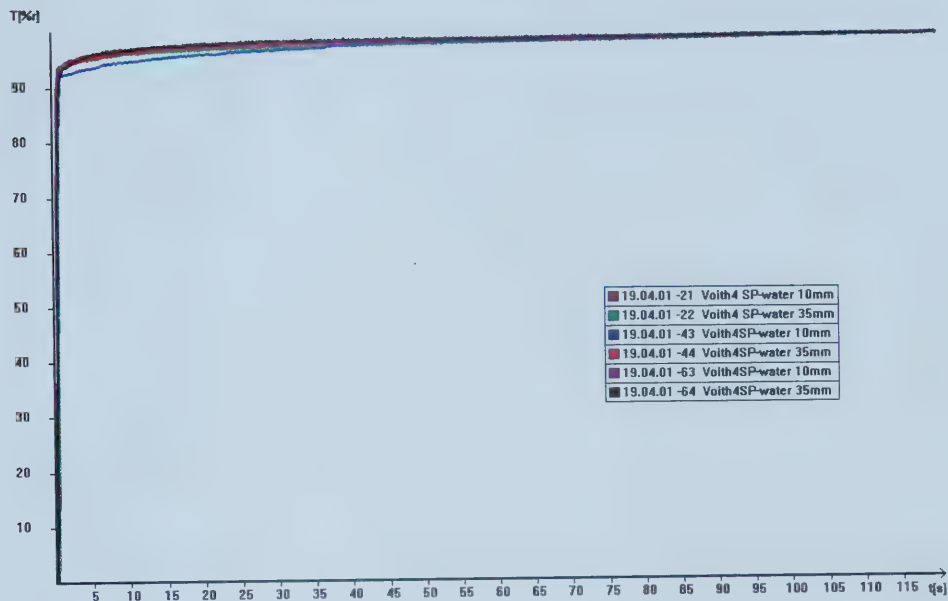


Figure F.62: Voith 5 - 2 sides - water - long time

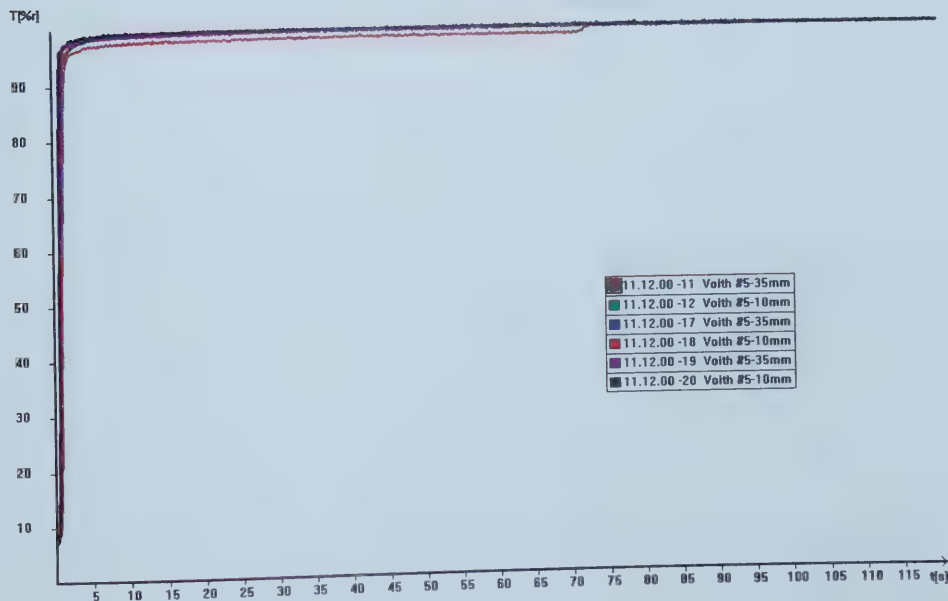


Figure F.63: Voith 5 - 2 sides - water - short time

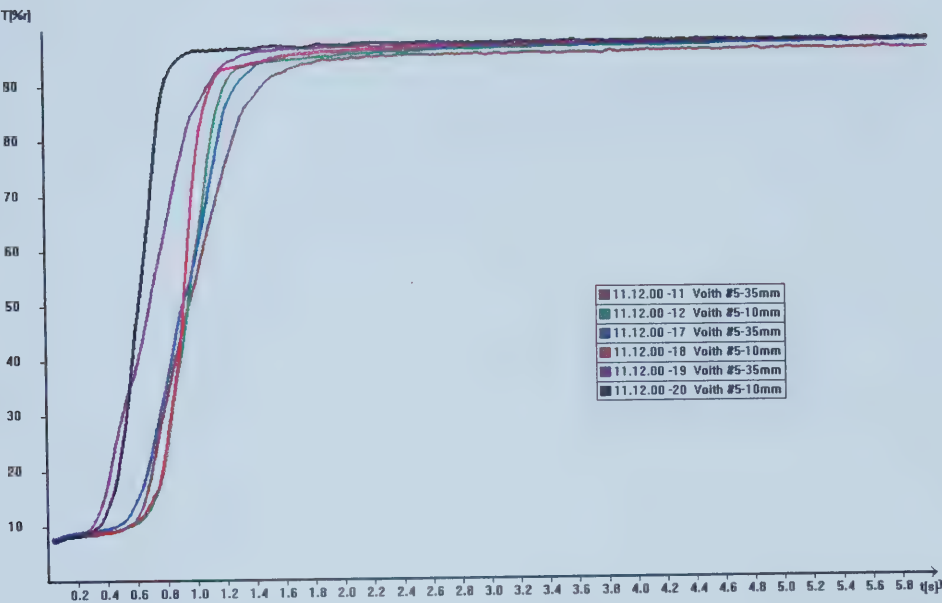


Figure F.64: Voith 5 - 1 sides - water - long time

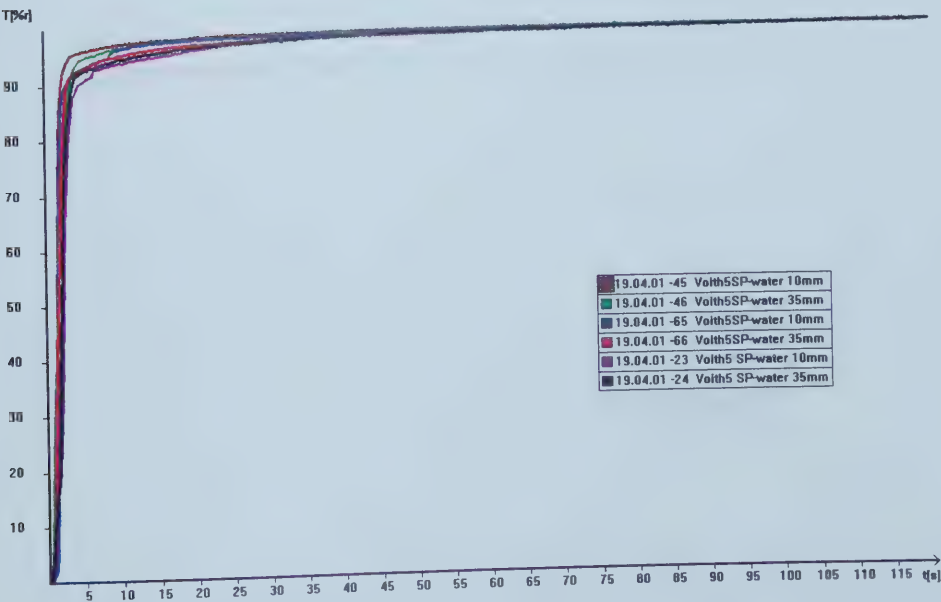


Figure F.65: Voith 5 - 1 sides - water - short time

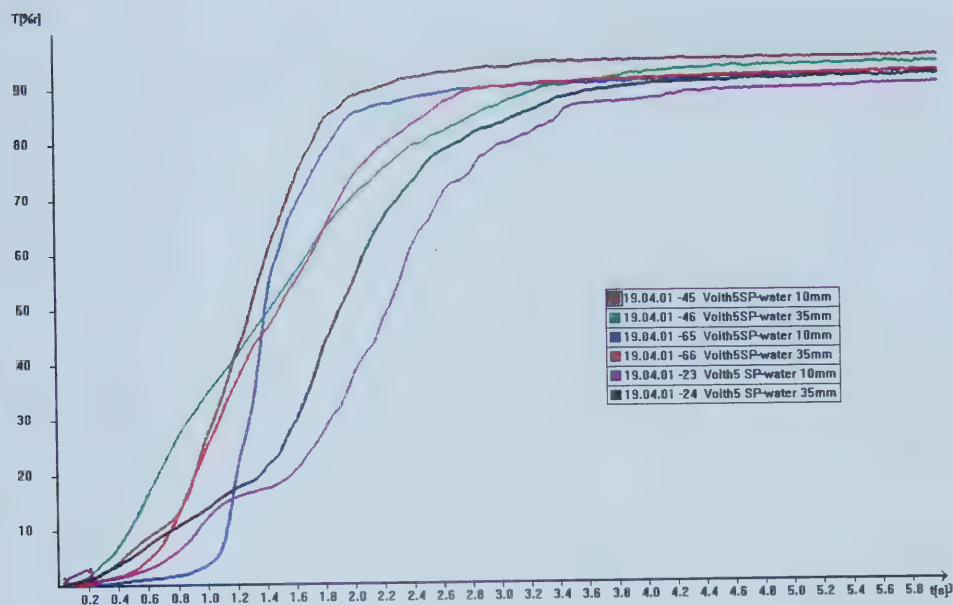


Figure F.66: Voith 6 - 2 sides - water - long time

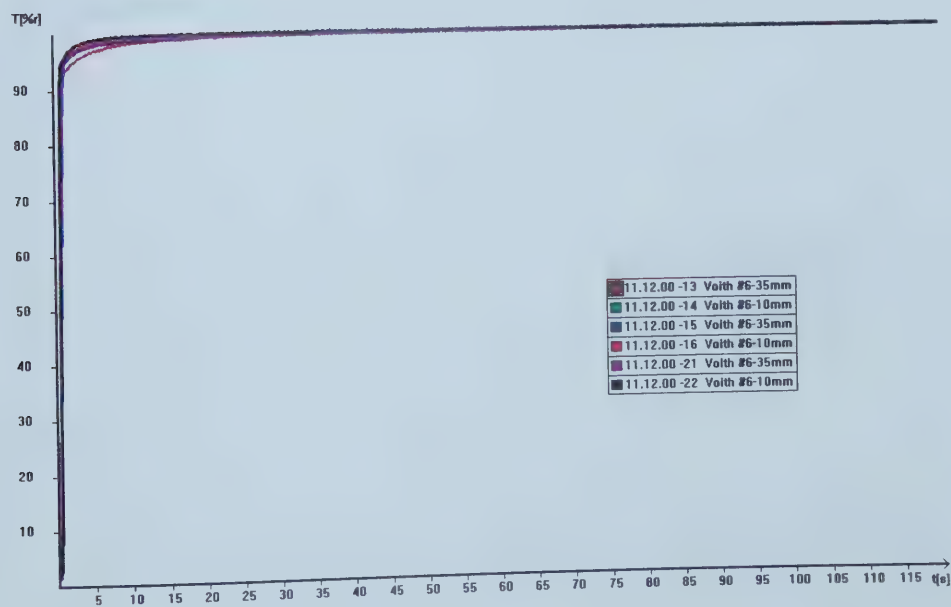


Figure F.67: Voith 6 - 2 sides - water - short time

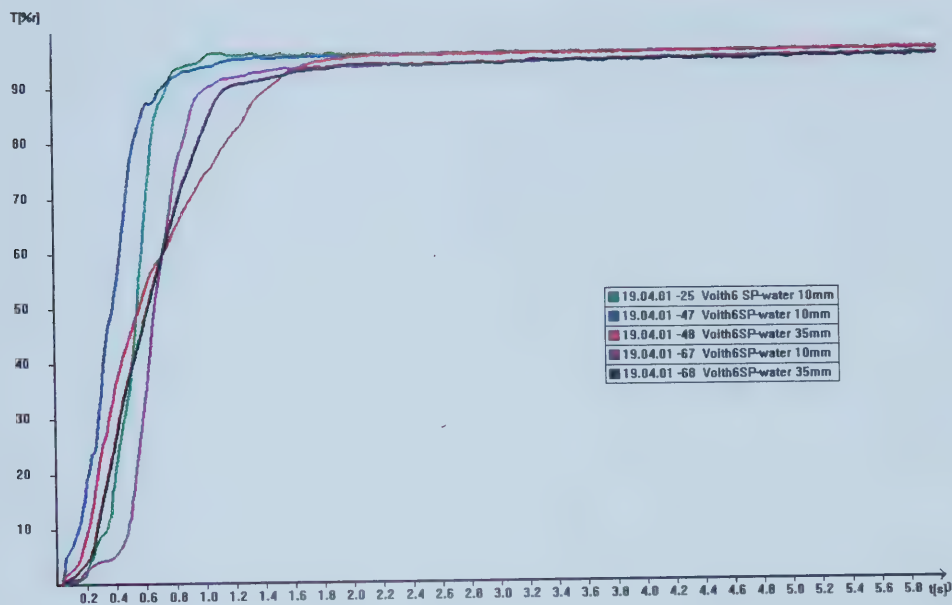


Figure F.68: Voith 6 - 1 sides - water - long time

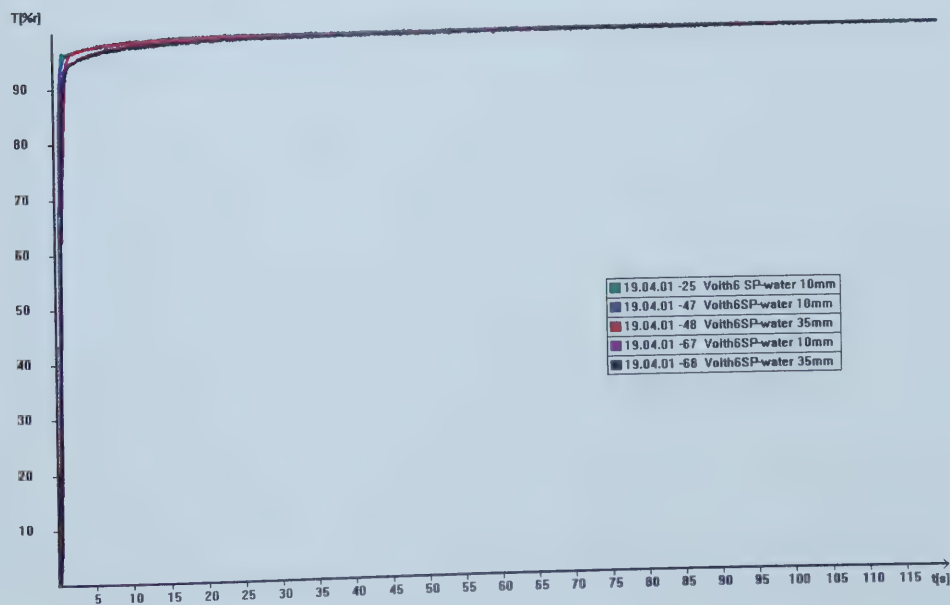


Figure F.69: Voith 6 - 1 sides - water - short time

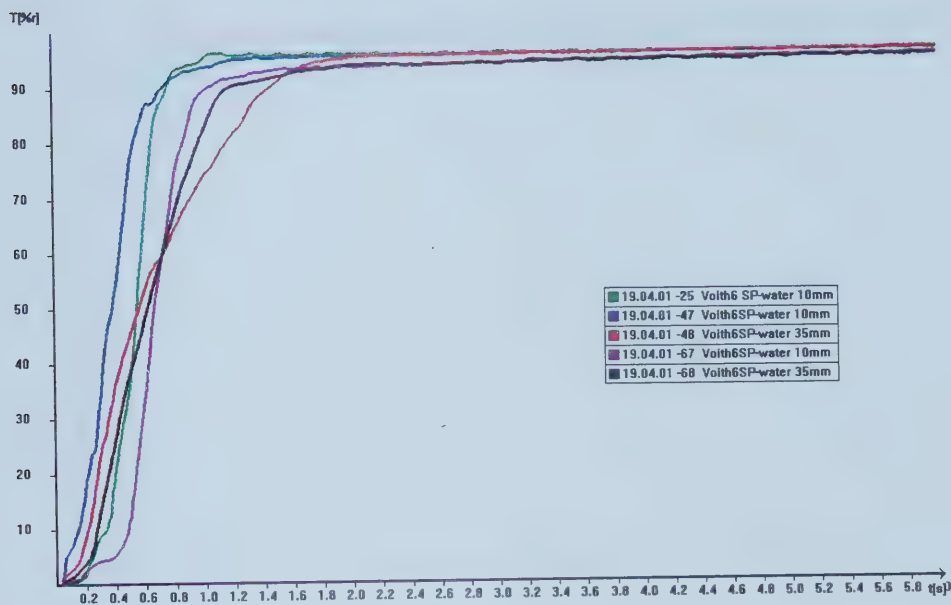


Figure F.70: Voith 7 - 2 sides - water - long time

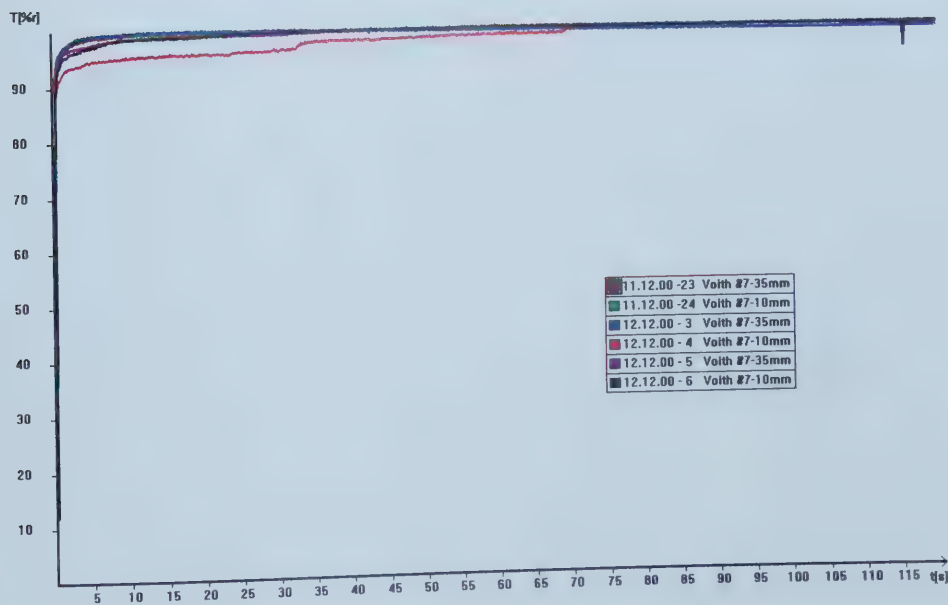


Figure F.71: Voith 7 - 2 sides - water - short time

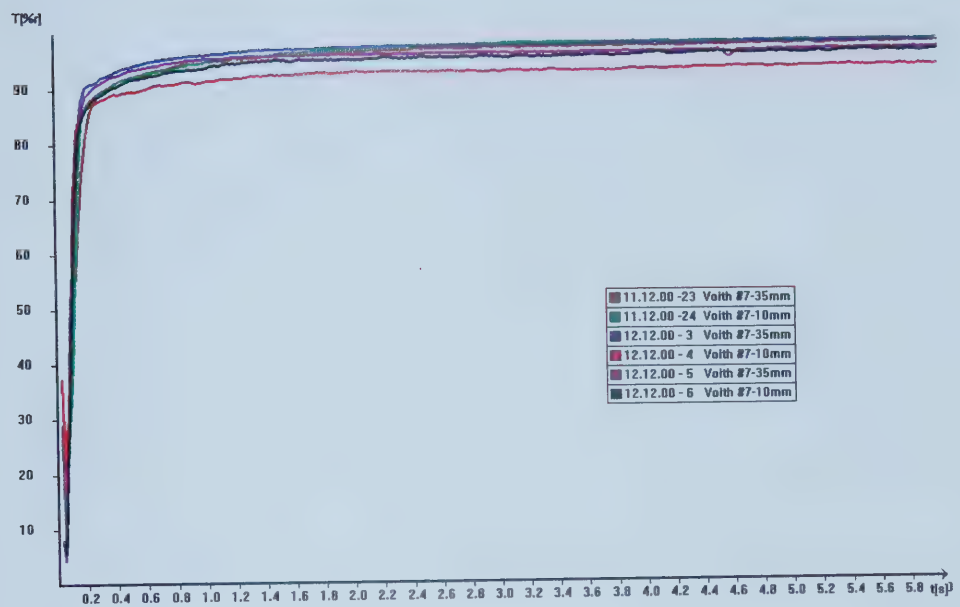


Figure F.72: Voith 7-1 - 1 side - water - long time

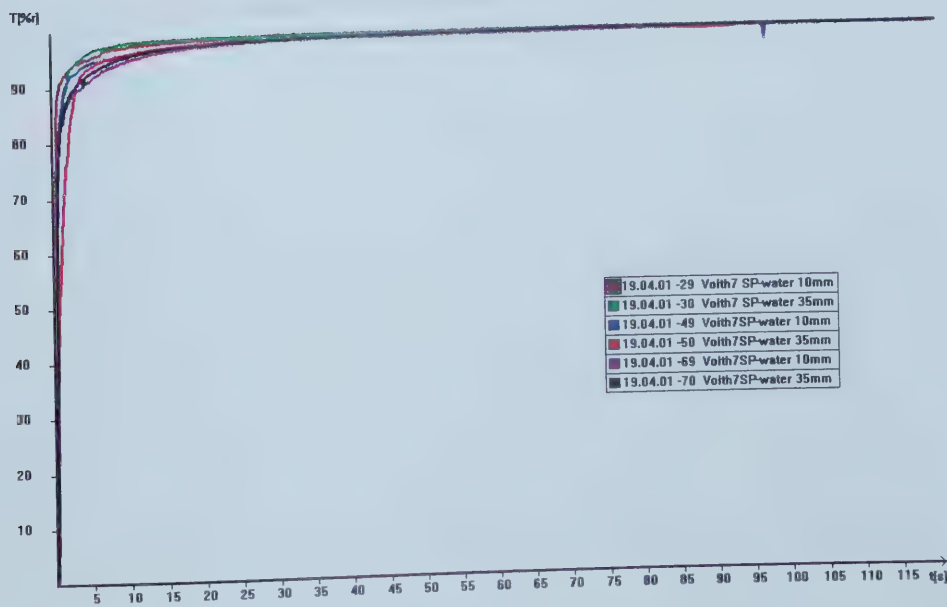


Figure F.73: Voith 7-1 - 1 side - water - short time

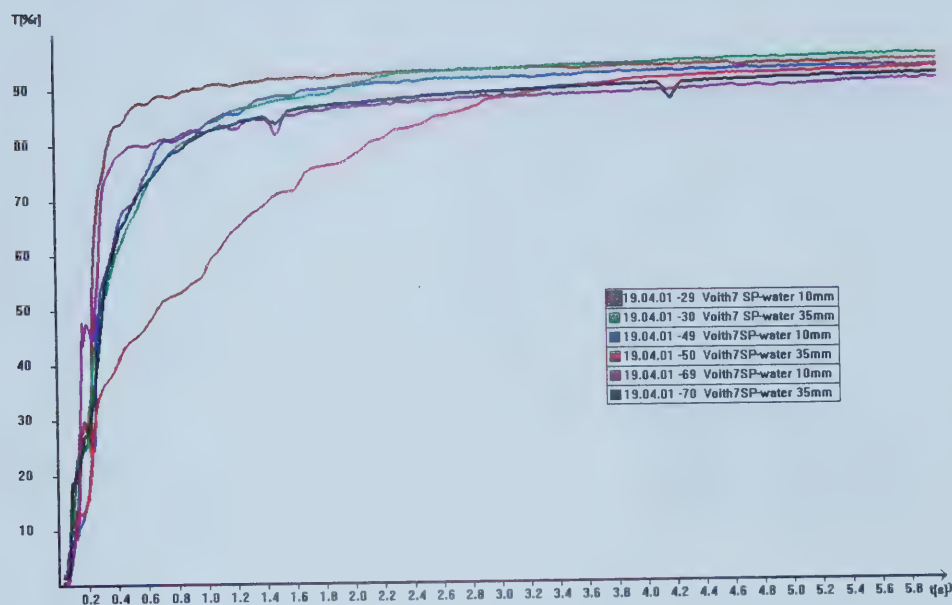


Figure F.74: Voith 7-2 - 1 side - water - long time

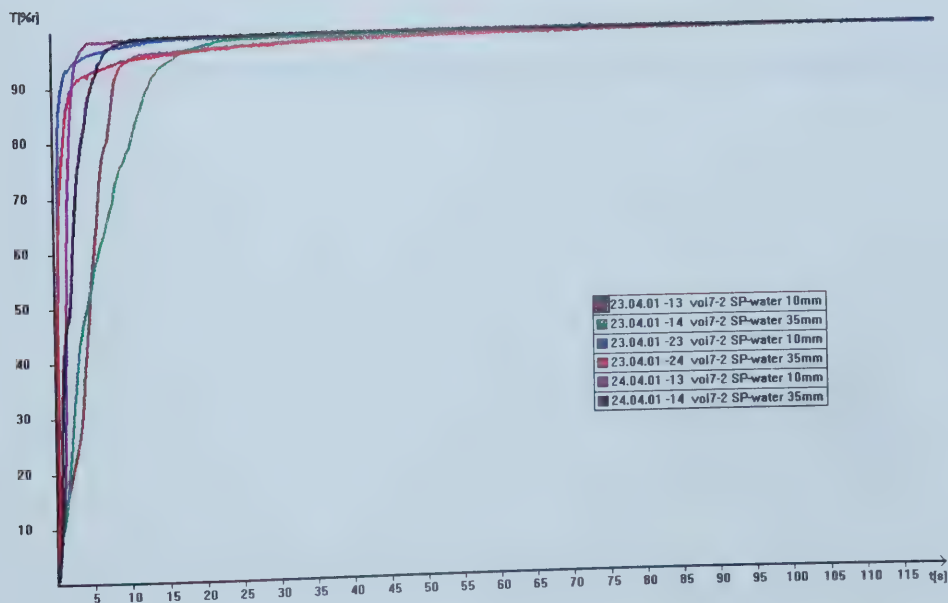


Figure F.75: Voith 7-2 - 1 side - water - short time

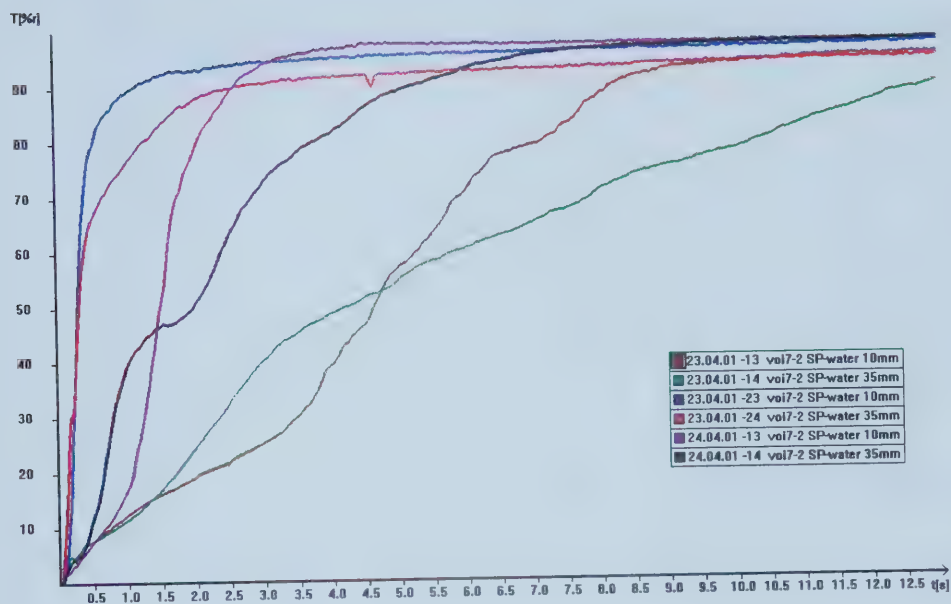
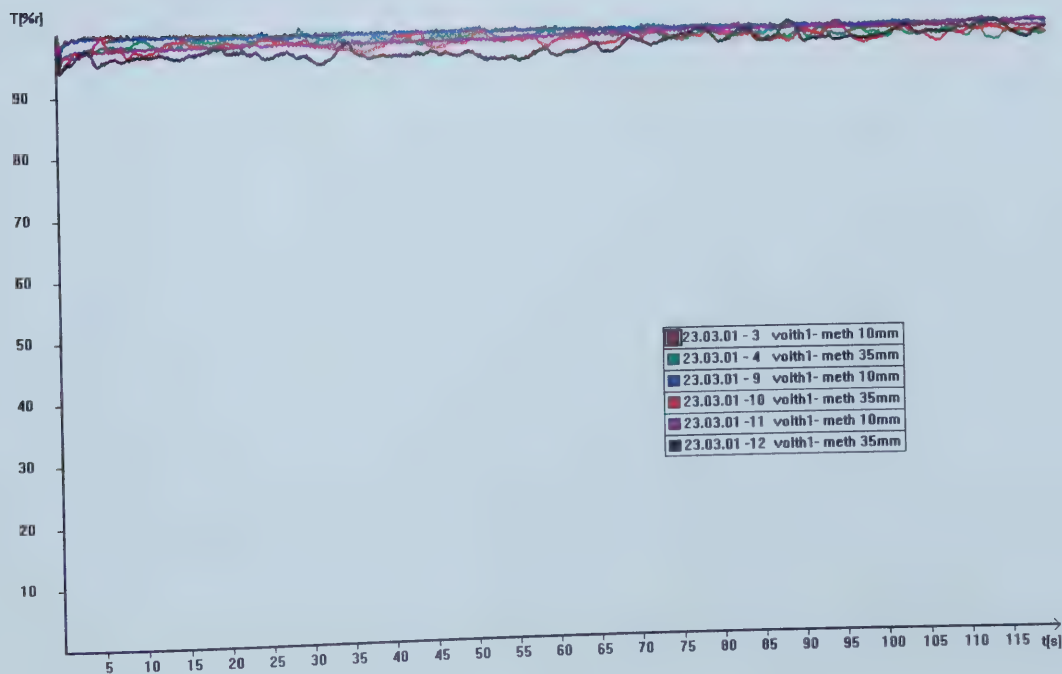


Figure F.76: Voith 1 - 2 sides - methanol



Buckbee Mears

Figure F.77: Buckbee Mears 6-4-4 - water (liquid penetration from both sides)

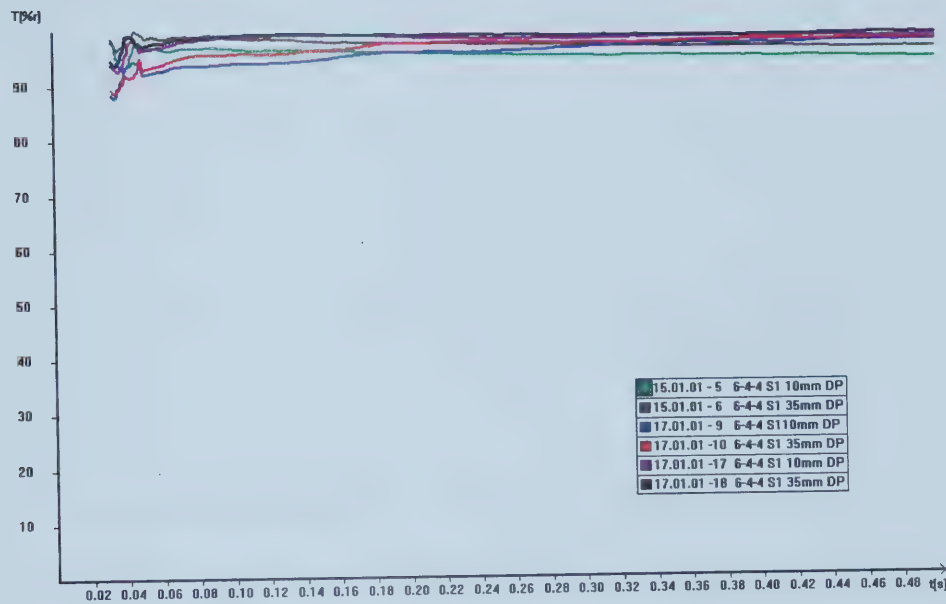


Figure F.78: Buckbee Mears 6-4-4 - water (liquid penetration from one sides)

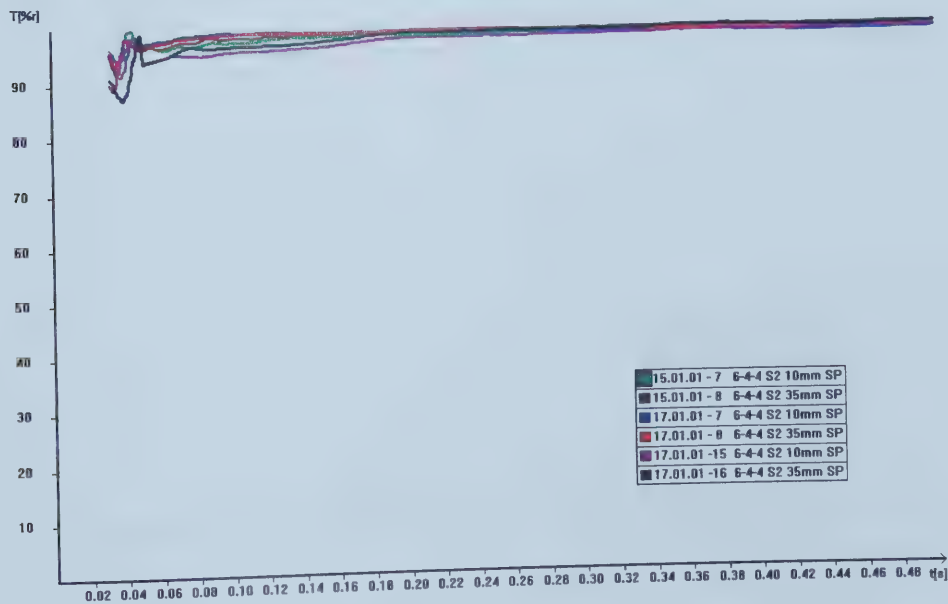


Figure F.79: Buckbee Mears 8-6-2 - water (liquid penetration from one sides)

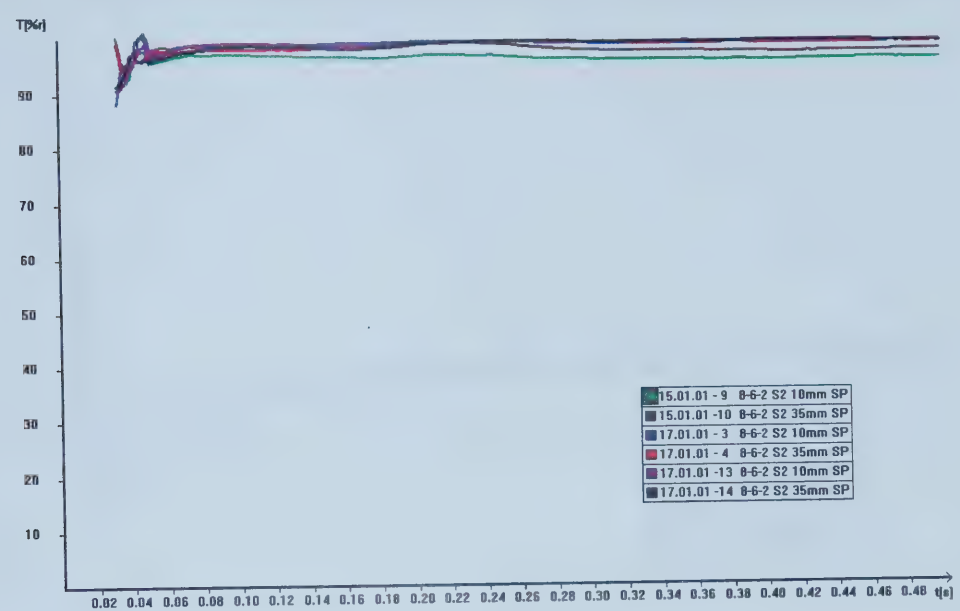


Figure F.80: Buckbee Mears 8-6-2 - water (liquid penetration from both sides)

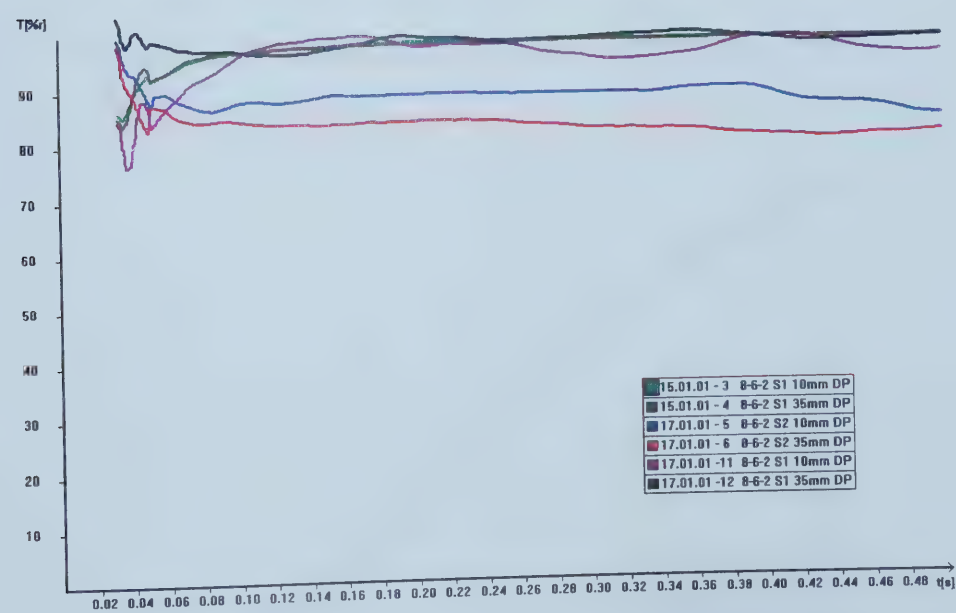


Figure F.81: Alberta Newsprint Company Offset Grade - Water

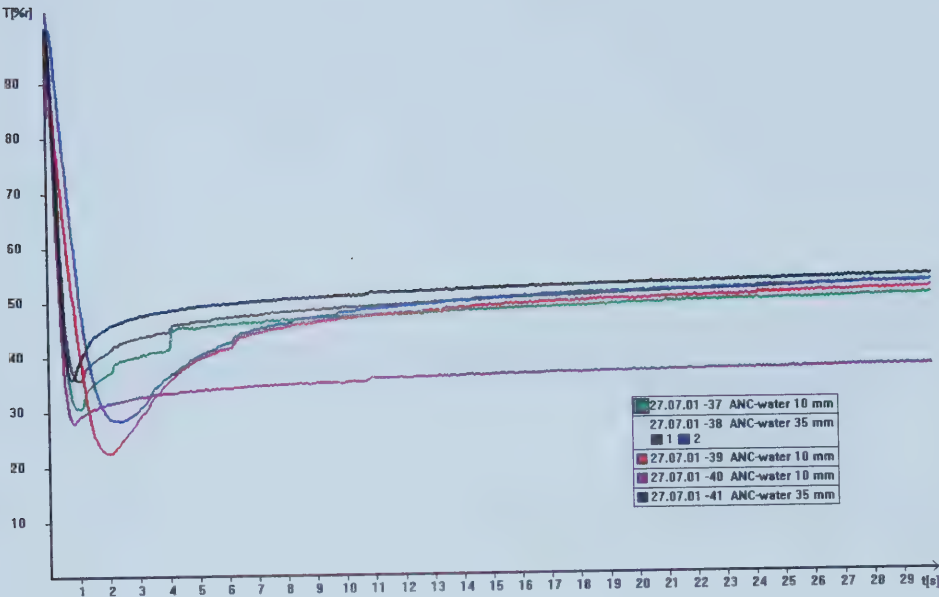


Figure F.82: Alberta Newsprint Company Offset Grade - PDMS

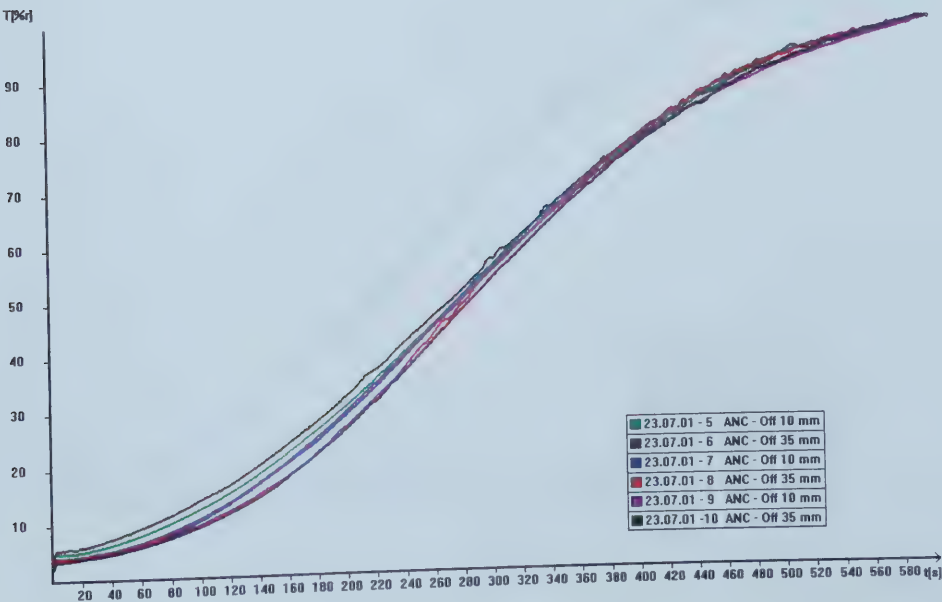


Figure F.83: Alberta Newsprint Company Roto Grade - Water

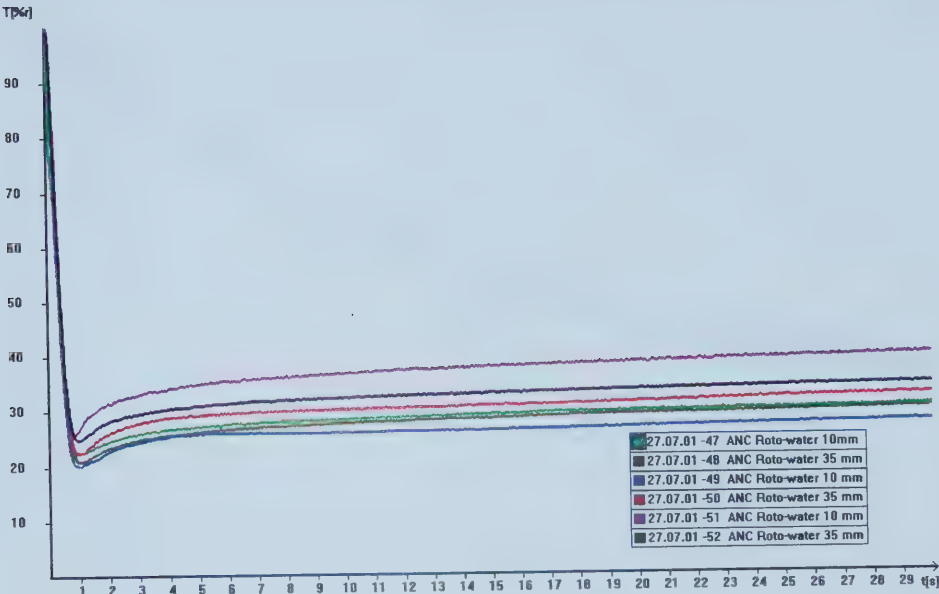


Figure F.84: Alberta Newsprint Company Roto Grade - PDMS

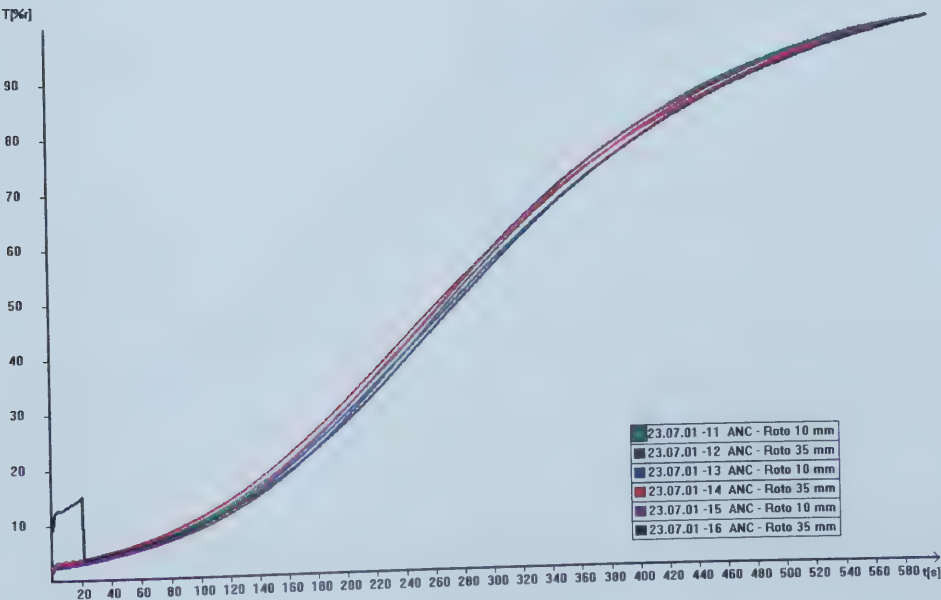


Figure F.85: Champion Ink Jet - Water

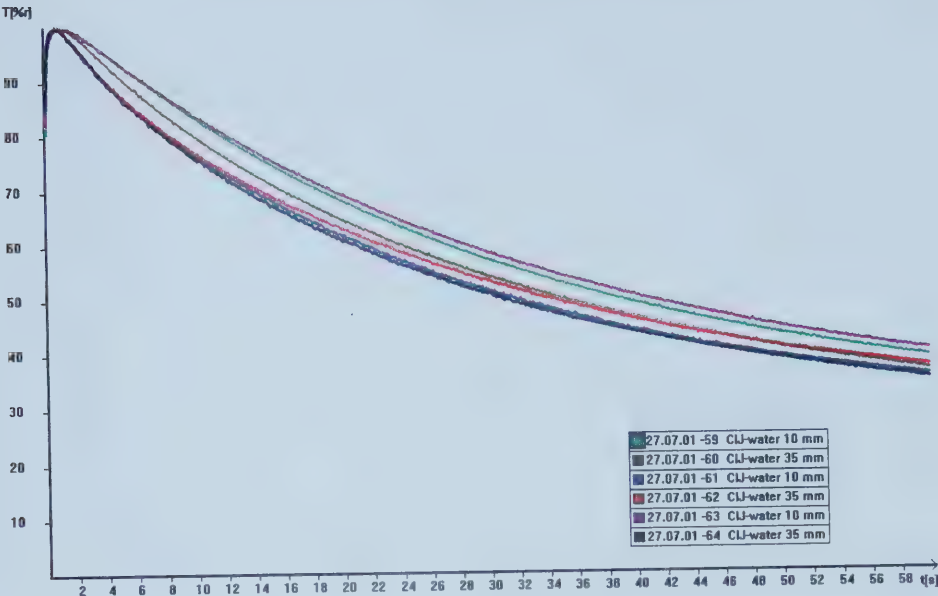


Figure F.86: Champion Ink Jet - PDMS

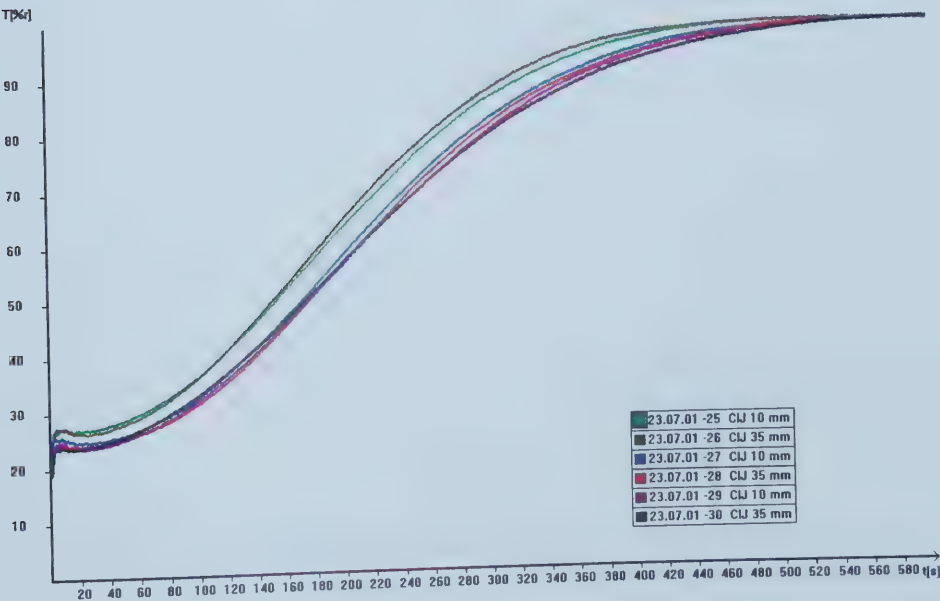


Figure F.87: Hammermill Color - Water

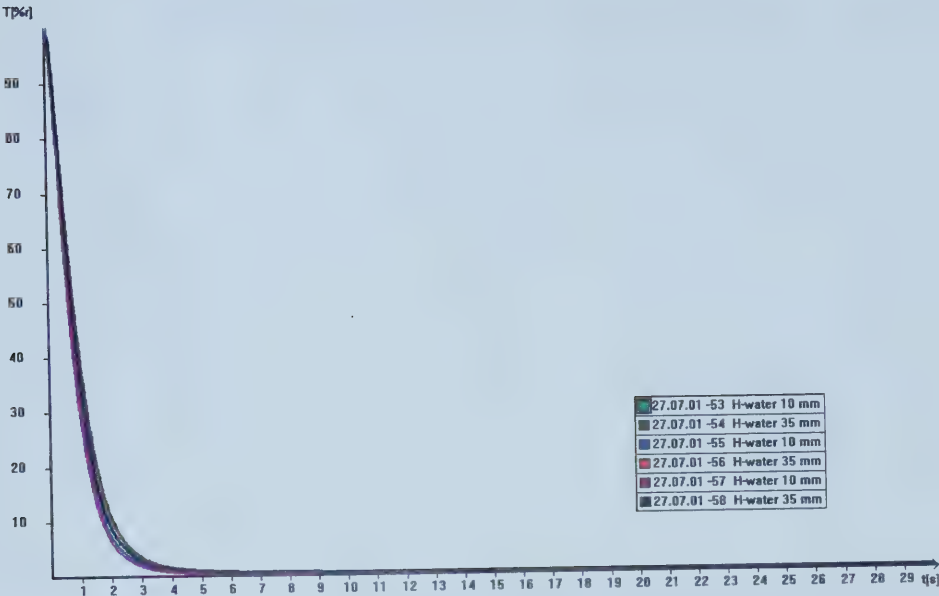


Figure F.88: Hammermill Color - PDMS

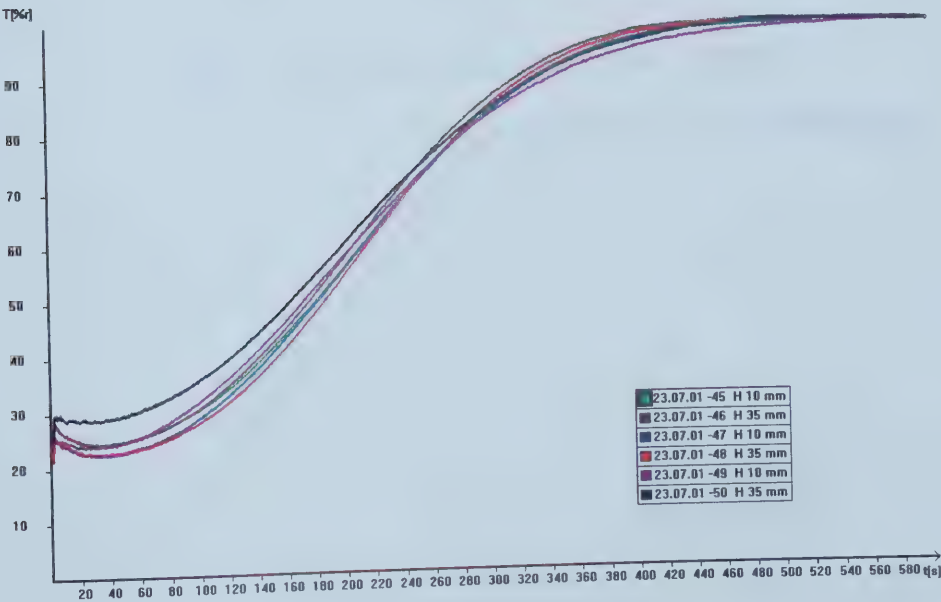


Figure F.89: Weyerhaeuser First Choice - Water

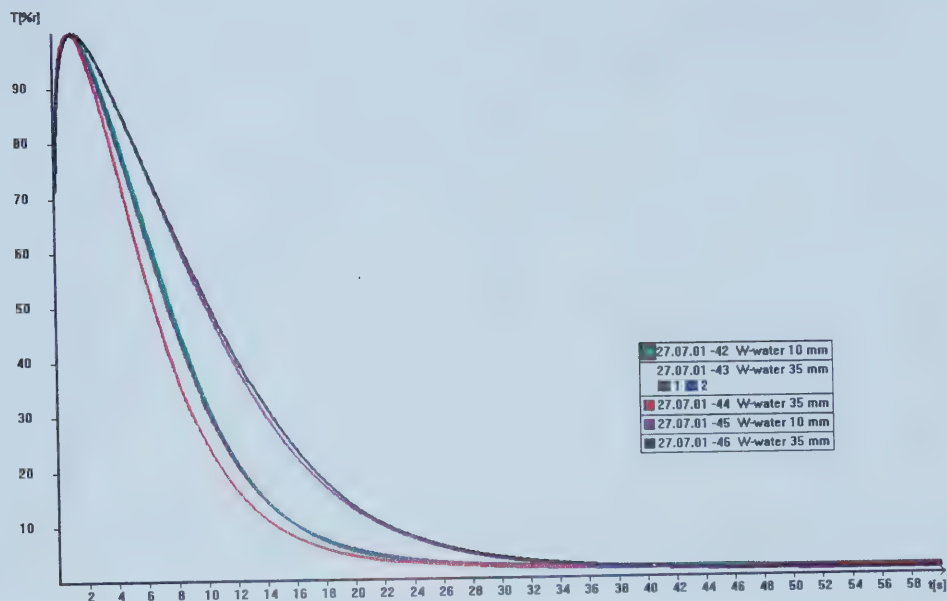


Figure F.90: Weyerhaeuser First Choice - PDMS

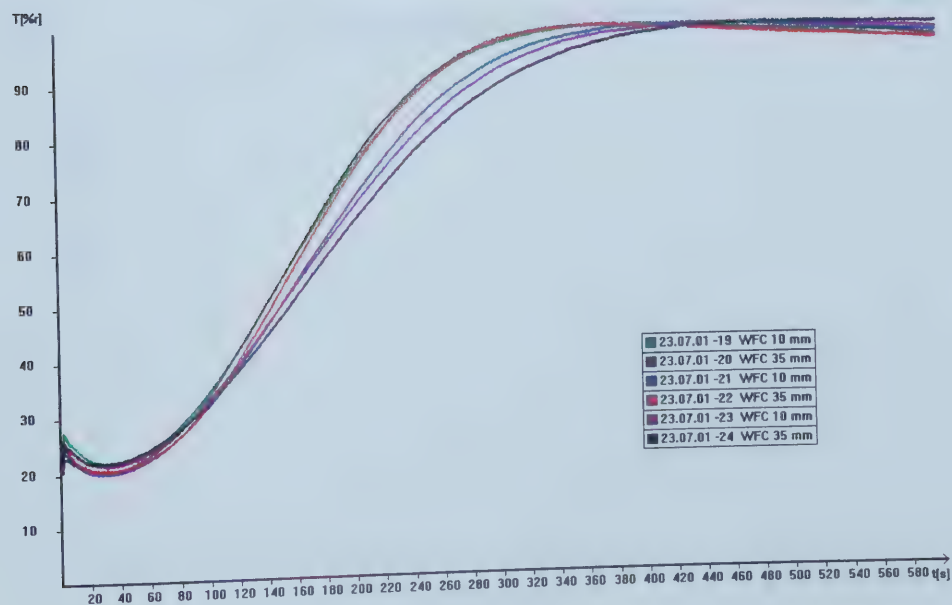


Figure F.91: Glass Fibre Paper (GF/A) - Water

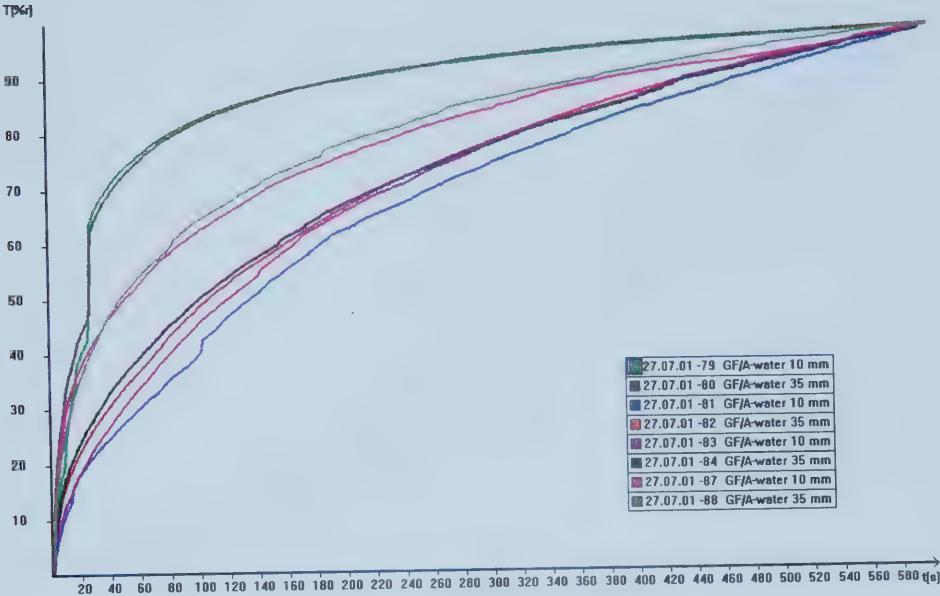


Figure F.92: Glass Fibre Paper (GF/A) - PDMS

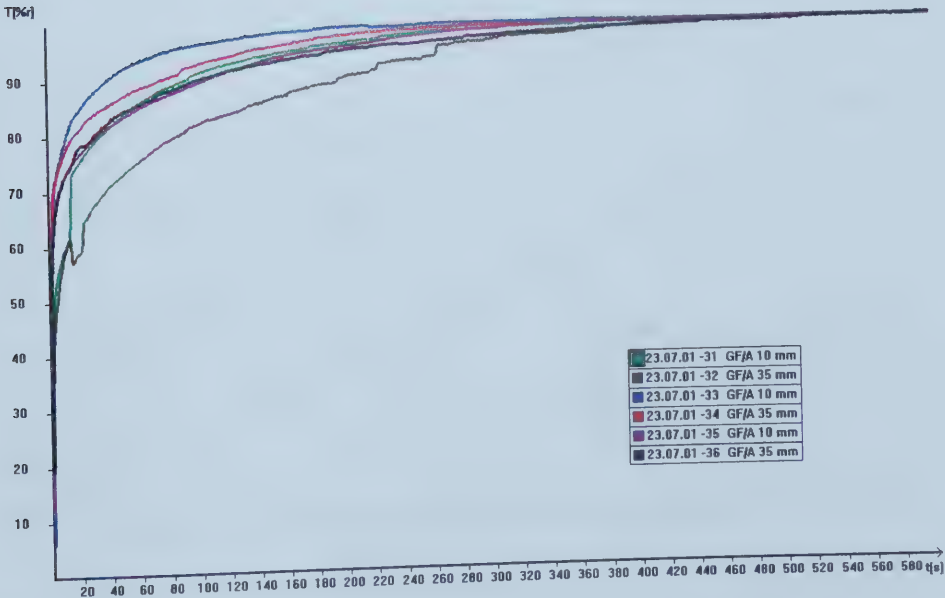


Figure F.93: Glass Fibre Paper (GF/B) - Water

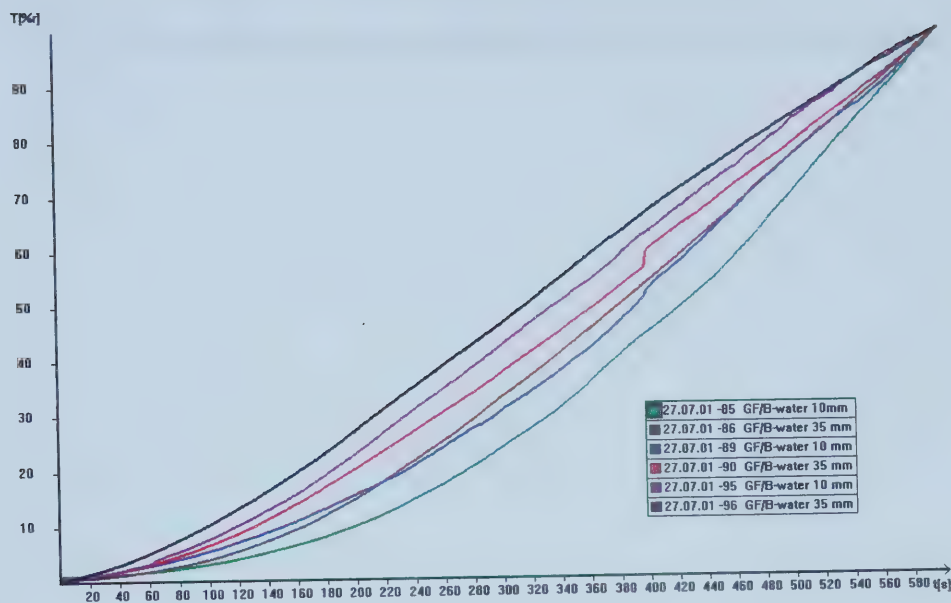


Figure F.94: Glass Fibre Paper (GF/B) - PDMS

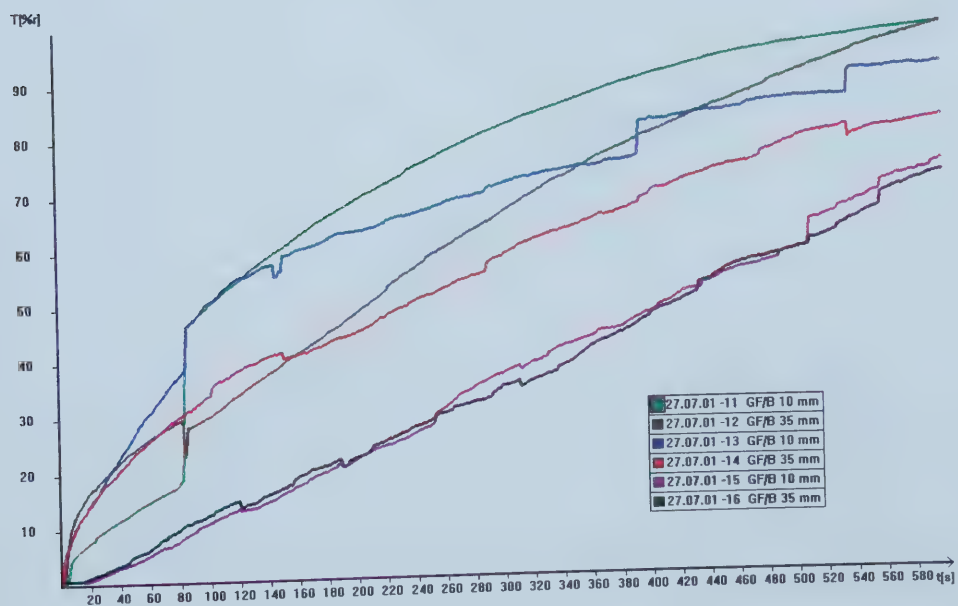


Figure F.95: Glass Fibre Paper (GF/F) - Water

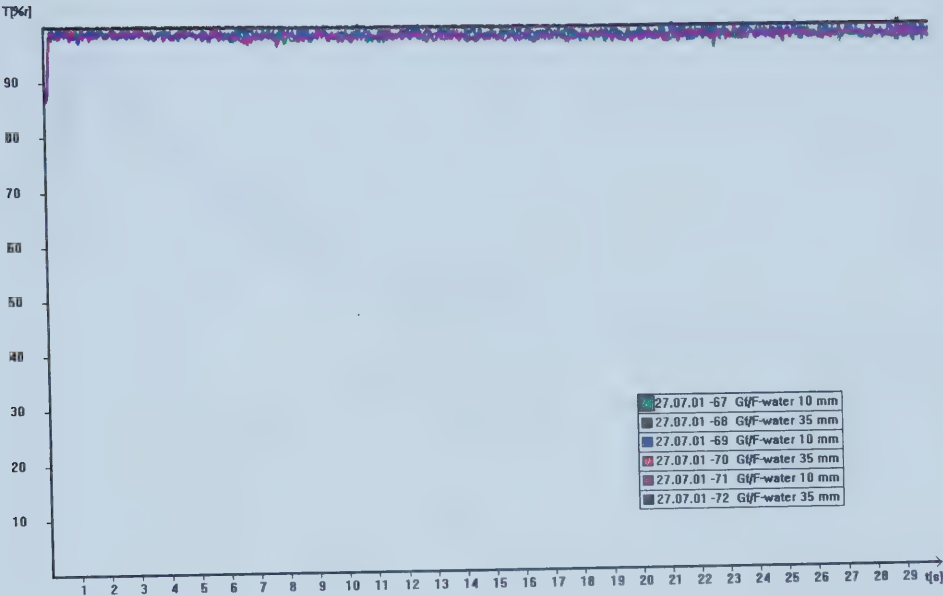


Figure F.96: Glass Fibre Paper (GF/F) - PDMS

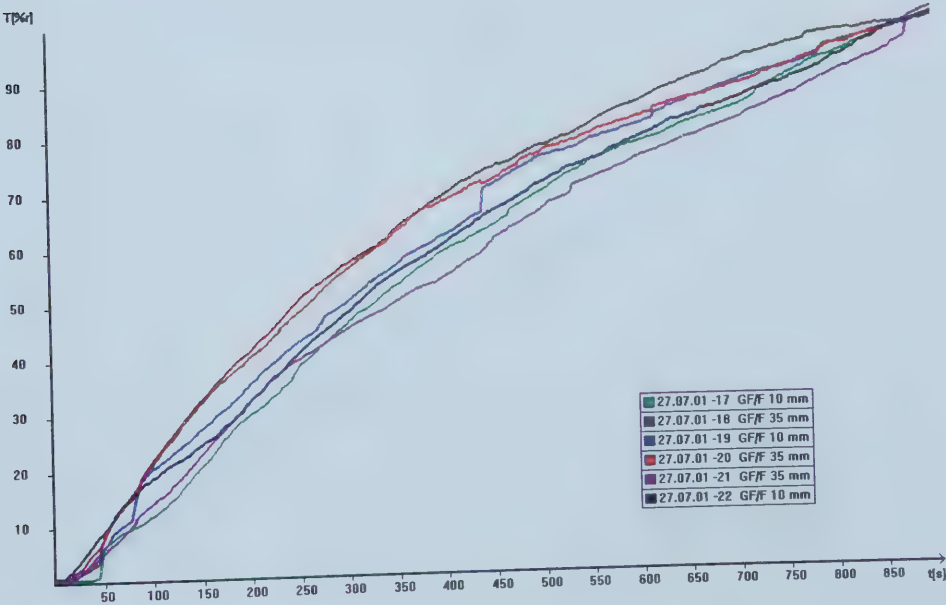


Figure F.97: Phase Separation Filter (1PS) - Water

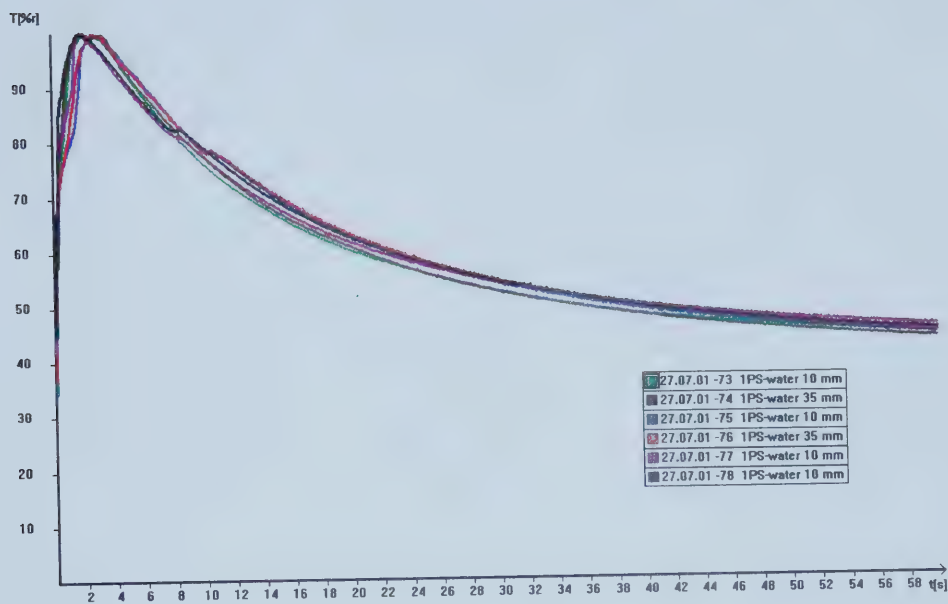
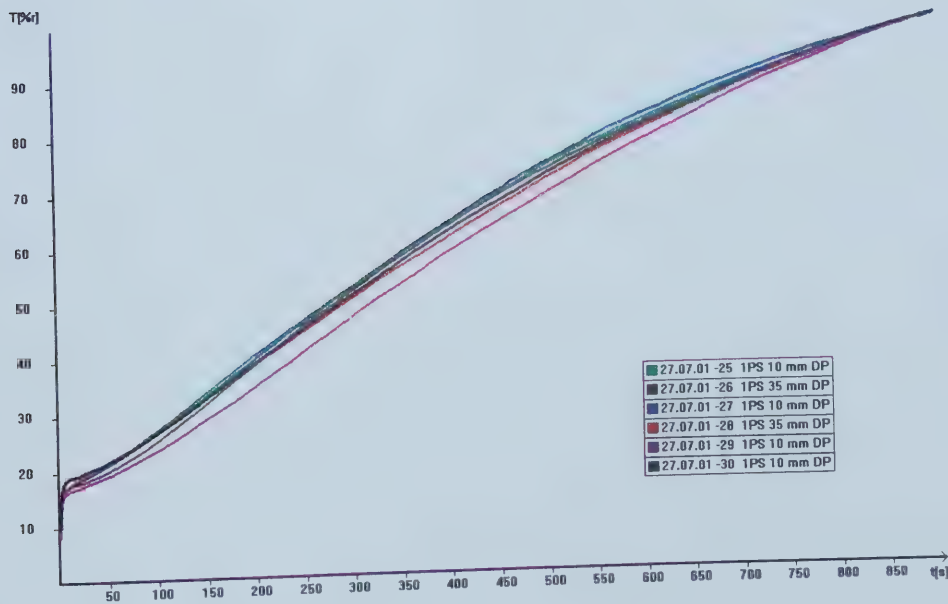


Figure F.98: Phase Separation Filter (1PS) - PDMS



University of Alberta Library



0 1620 1720 2019

B45565